Investigating Defect Topological Quantum Field Theories as Models for Quantum Error-Correction

Isaac Smith
Student Number: 636925
Supervisor: Dr Daniel Murfet

May 22, 2020

Abstract

Quantum error-correcting codes are necessary for realistic quantum computation. Topological quantum error-correcting codes, such as the toric code, represent the primary candidates for physically implementing error-correction. The toric code subspace can be produced by the Turaev-Viro-Barrett-Westbury topological quantum field theory over the spherical fusion category of $\mathbb{Z}_2$-graded vector spaces, however this model fails to adequately treat the projection mapping that is a key component of any quantum error-correction process. It was shown by Carqueville, Runkel and Schaumann that the Turaev-Viro-Barrett-Westbury topological quantum field theory is equivalent to the orbifold of the Reshetikhin-Turaev defect topological quantum field theory over the category of finite-dimensional vector spaces. This defect theory contains richer structure, and we investigate the utility of this structure in representing the projection map for the toric code. The projection map for the toric code can be naturally considered as the composition of two component projections. We show that the morphism defining the orbifold of the defect theory corresponds precisely to one of these projections acting on the image of the other.

Acknowledgements

I would like to acknowledge my family and friends for their constant and unwavering support. I would like to acknowledge Charles Hill for cultivating in me an interest in quantum computing and quantum error correction, Thomas Quella for his accessbility and helpful insights on a range of physically motivated questions, and Nils Carqueville for being a valuable resource from the other side of the world. Most of all I would like to ackowlegde my supervisor Dan Murfet. His incredible guidance as a supervisor and a mentor, coupled with his broad knowlegde base has lead me superbly through what has been my most intellectually fulfilling period at university.

Contents

Chapter 1

Introduction

The physical realisation of quantum computers would make tractable problems believed to be intractable on classical computers. One key example of this is in simulating locally-interacting quantum systems, which is known to take exponential time on a classical computer [Fey99; Llo96]. Such simulations could have immediate and lasting benefit for development of quantum and other technologies.

However, for meaningful simulations and other algorithms to become feasible to implement in reality, quantum computing architectures need to be scaled up in a robust fashion. Inherent to any architecture built from quantum systems is the phenomenon of decoherence: the loss of information stored in the system due to interactions with its environment. Fortunately, a key result commonly known as "the Threshold Theorem" explains how the stored information can be protected provided the rate of error in the quantum architechture is below a specific threshold error rate [AB08]. The information is protected by encoding, via a Quantum Error-Correcting Code (QECC), information distributed across n physical qubits into information stored in k logical qubits where $k < n$. The existence and early examples of such codes were detailed by Calderbank and Shor [CS96], as well as Steane and others [Ste96; Got97].

In a landmark paper [Kit03], Kitaev introduced the toric code, a novel QECC defined for a qubit lattice arrayed on a torus that encodes the information of the logical qubits using the topology of the torus, producing a code robust to local errors. Under certain assumptions, the toric code, or rather its planar cousin the surface code, represents one of the leading choices of quantum error-correcting codes to be implemented in a physical architecture, with error threshold approaching 1% [FSG09]. The invention of the toric code commenced the study of topological quantum computing as a significant area of research within the quantum computing community. Currently, the search for new, high quality error-correcting codes is laborious, a problem that will be exacerbated as quantum architectures continue to get larger, or start to be built from more exotic quantum systems corresponding to non-trivial anyon models (such as those required for universal topological quantum computation [FLW02]). It seems likely that a more general approach will be useful as the numbers, and composition, of qubits in physical hardware progress.

Another significant component of any practical large-scale quantum computer, just as with any classical computer, is a resource-efficient implementation of any program onto the specific architechture of the computer, via a program compiler. Different error-correcting codes have different properties, and as such some may be more suitable for certain aspects of a computation than others. Moreover, different codes require different resources, for example, numbers of physical qubits and physical qubit operations to perform different logical quantum circuit gates. A key feature of any quantum compiler will necessarily be the ability to coherently map between different error-correcting codes on the same physical architecture (Chapters 5 and 6 of [NM+19] provide a thorough overview and list of resources relating to the current state of research on quantum compiler optimisation).

So, does there exist a model for quantum error-correction that is general enough to naturally encapsulate all physical realisations of qubits (or qudits), both topological and otherwise, while maintaining all desired properties of known error-correcting codes and has predictive power for what new codes will look like? This is an open question. The standard circuit model for quantum computation, though widely established, seems to be insufficiently general to treat topological quantum error-correction in a natural way, and other models, such as adiabatic quantum computing or quantum Turing machines, are unsuitable in other ways. One context in which it is known that topological quantum error-correcting codes can be studied, and the approach taken in this thesis, is that of Topological Quantum Field Theories (TQFTs) [Wit89; LW05; FKW02].

There are different methods of formulating TQFTs and the method taken in this thesis is the functorial one: a 3-dimensional TQFT is defined to be a functor

$$\mathcal{Z}^{\mathcal{C}} : \mathbf{Bord}_3^{\mathcal{C}} \to \mathrm{Vect}_{\Bbbk}$$

from some category of 3-bordisms (surfaces and homeomorphism classes of 3-manifolds between them, possibly with extra structure) to the category of (infinite dimensional) $\Bbbk$-vector spaces (we will take $\Bbbk$ to be $\mathbb{C}$ going forward). The superscript $\mathcal{C}$ denotes the dependence of the bordism category $\mathbf{Bord}_3^{\mathcal{C}}$ on a category $\mathcal{C}$, which, in the present context, is usually taken to be a spherical fusion category or a modular tensor category and can be regarded as the choice of anyon model for the quantum system being represented by the TQFT. Due to the categorical nature of TQFTs, they may provide ample machinery for describing maps between error-correcting codes.

It has been shown that the Turaev-Viro-Barrett-Westbury TQFT [TV92; BW96], based on the category of $\mathbb{Z}_2$-graded vector spaces and evaluated on the torus, produces the code space for Kitaev's toric code; see [KKR10; BK12] and references therein. However, the error-correction process requires more than just knowledge of the code space, and depends rather heavily on knowledge of a projection map whose image is the code space. **The aim of this thesis is to reproduce both the code space *and* projection map within a TQFT context**. That is, we aim to identify a surface and morphism in an appropriate bordism category of a given TQFT that evaluate to the code space and projection map of the toric code. Despite some stark similarities between this projection map and the method by which the generalised version of the Turaev-Viro-Barrett-Westbury TQFT, called the Turaev-Viro graph TQFT, evaluates a surface, there seems to be no natural way of producing the projection map from a morphism within $\mathbf{Bord}_3^{\mathrm{col}(\mathbb{Z}_2\text{-}\mathrm{vect}_{\mathbb{C}})}$, the bordism category for the Turaev-Viro graph TQFT over $\mathbb{Z}_2$- $\mathrm{vect}_{\mathbb{C}}$. Thus, the search for an appropriate TQFT must be broadened.

There is in fact a more fundamental TQFT than the Turaev-Viro-Barrett-Westbury TQFT, namely the Reshetikhin-Turaev TQFT. It is known that for a given modular tensor category $\mathcal{C}$, the Turaev-Viro-Barrett-Westbury TQFT over $\mathcal{C}$ evaluated on a bordism M is equivalent to the product of the Reshetikhin-Turaev TQFT also over $\mathcal{C}$ evaluated on M with both possible orientations [Theorem VII.4.1.1, Tur16]. Furthermore, there is another known result that relates the Turaev-Viro graph TQFT over a spherical fusion category $\mathcal{S}$ to the Reshetikhin-Turaev TQFT over the categorical centre of $\mathcal{S}$, $Z(\mathcal{S})$ [Theorem 17.1, TV17]. Both these results indicate that perhaps the Reshetikhin-Turaev TQFT is a more suitable candidate for modelling quantum error-correction. At the very least, the Reshetikhin-Turaev TQFT warrants further investigation in this context.

Our investigation actually proceeds by considering an extension to the Reshetikhin-Turaev TQFT. In a paper due to Carqueville, Runkel and Schaumann [CRS18], it was shown that the Turaev-Viro-Barrett-Westbury TQFT based on any spherical fusion category is equivalent to an orbifold of a different theory: the defect Reshetikhin-Turaev TQFT based on $\mathrm{vect}_{\mathbb{C}}$ (where $\mathrm{vect}_{\mathbb{C}}$ denotes the category of finite-dimensional $\mathbb{C}$-vector spaces). The defect Reshetikhin-Turaev TQFT is a functor that acts on surfaces and (homeomorphism classes of) 3-manifolds that contain specified 0-, 1-, 2-, and 3-dimensional labelled submanifolds, collectively known as defects, in a compatible way. Within this thesis, these defects will be labelled by data internal to the category $\mathrm{vect}_{\mathbb{C}}$. The orbifold of the Reshetikhin-Turaev defect TQFT based on $\mathrm{vect}_{\mathbb{C}}$ proceeds by evaluating an appropriately decorated cylinder over the surface under consideration. Certain elements of the defect data are selected to label each 3-, 2-, 1- and 0-stratum of the Poincaré dual of the cylinder being evaluated. When this orbifold data is selected based on a spherical fusion category, such as $\mathbb{Z}_2$- $\mathrm{vect}_{\mathbb{C}}$, then the orbifold produces the Turaev-Viro-Barrett-Westbury TQFT over $\mathbb{Z}_2$- $\mathrm{vect}_{\mathbb{C}}$.

Just as the evaluation of the Turaev-Viro-Barrett-Westbury TQFT over $\mathbb{Z}_2$- $\mathrm{vect}_{\mathbb{C}}$ is strongly reminiscent of the projection map for the toric code (or part thereof), so too is the orbifold map of the Reshetikhin-Turaev defect TQFT acting on the torus, with orbifold data associated to $\mathbb{Z}_2$- $\mathrm{vect}_{\mathbb{C}}$. This time however, the projection map is actually produced from a valid morphism in the bordism category of the Reshetikhin-Turaev defect TQFT. Furthermore, it is possible to analyse this morphism from the point of view of the component parts that make up the projection map in the toric code, which may prove fruitful for application of the Reshetikhin-Turaev defect TQFT to other topological quantum error-correcting codes. Another advantage of the orbifold construction is its natural ability to handle different orbifold data, corresponding to different spherical fusion categories (and hence different anyon models), in separate localised areas of the surface being evaluated. This ability may also have utility in modelling a map between different error-correcting codes within the same physical architecture.

While this thesis does not fully answer the question posed above regarding a general model for quantum error-correction, it does take a step down what seems to be a viable path towards producing such a model. Any practical implementation of any quantum error-correcting code requires a detailed understanding of both the code space and the projectors associated to the code. A general theoretic approach to constructing these projectors for general anyon models and surfaces could play a key role in the development of topological error-correcting codes. Typically, the literature that develops topological error-correction within a TQFT framework pays little attention to these projectors. This thesis also represents the first use of defect TQFTs and their orbifolds to produce projection maps for quantum error-correcting codes. It would be exciting to see other error-correcting codes, such as the colour code or the surface code, treated similarly within the framework of the Reshetikhin-Turaev defect TQFT.

This thesis is structured as follows. Chapter 2 introduces quantum error-correcting codes in general and the toric code in particular, laying the notational and conceptual foundations for comparison to the Turaev-Viro graph TQFT and Reshetikhin-Turaev defect TQFT in Chapter 5 (which represents the culmination of this thesis). Chapter 3 introduces the Turaev-Viro graph TQFT and Reshetikhin-Turaev defect TQFT via the bordism categories $\mathbf{Bord}_3^{\mathrm{col}(\mathcal{C})}$ and $\mathbf{Bord}_3^{\mathrm{df}}(\mathbb{D})$ respectively, and Chapter 4 introduces the orbifold construction as well as providing intuition behind the use of the terminology 'orbifold' in this case. The full treatment of the content of both these chapters is technical and treated in the existing literature, so many of the details are deferred to the appendices or referenced literature. As mentioned above, Chapter 5 is concerned with translating the toric code subspace and projection map from Chapter 2 into the context of TQFTs. Firstly, the torus is evaluated by the Turaev-Viro graph TQFT over $\mathbb{Z}_2\text{-}\mathrm{vect}_{\mathbb{C}}$ which serves the dual purpose of convincing the reader that this TQFT does indeed produce the code space for the toric code as well as illuminate the similarities to the projection map. Then, essentially the same evaluation occurs for a specific example in the context of the Reshetikhin-Turaev defect TQFT over $\mathrm{vect}_{\mathbb{C}}$ via the orbifold of the torus and the advantages of this model are discussed.

Chapter 2

Quantum Error-Correction

Just as with classical error-correction, there exists an established general theory of quantum error-correction with many useful results such as outlining the conditions that a quantum error-correcting code must satisfy in order to correct a given set of errors (see for example [Chapter 10 NC02] upon which much of the first half of this chapter is based). However, much of this formalism is not relevant to this thesis, and so only the key aspects are presented here. More specifically, this chapter commences by detailing the required definitions and theorems that outline and emphasise the role in the error-correction process played by the projection map onto the code space of a given quantum error-correcting code. Next, a class of quantum error-correcting codes, called stabiliser codes, is quickly introduced since the toric code is a member of this class. The key section of this chapter is Section 2.2 which describes the toric code for a general lattice, as well as through an example for a lattice arising from the dual of a triangulation of the torus. The primary aim of this section is to formalise the toric code in such a way to make as clear as possible the links to the Reshetikhin-Turaev defect TQFT in later chapters.

2.1 Quantum Error-Correcting Codes

For the purposes of the exposition of this thesis, we define quantum error-correcting codes below. Throughout this section, H denotes a finite-dimensional Hilbert space.

Definition 2.1.1. A **quantum error-correcting code** (QECC) is a pair $(H_{\text{code}}, P_{\text{code}})$ where H_{code}, called the **code space**, is a subspace of a Hilbert space H, called the **state space**, and $P_{\text{code}} : H \to H$ is a projector onto H_{code}, that is $P_{\text{code}}(H) \subseteq H_{\text{code}}$.

Remark 2.1.2. (i). Often throughout this thesis, we will not explicitly see the inner product structure on H, and hence H is largely presented simply as a vector space.

(ii). The literature commonly presents the theory of quantum error-correcting codes with the projector

P_{code} not included in the definition of a QECC but mentioned only as a remark. It has been included here to emphasise the role it plays in the encoding procedure of H_{code}, the error-correction procedure (as we shall see shortly), and in later chapters of this thesis.

(iii). The quantum error-correction literature often uses "ket"-notation $|\psi\rangle$ for elements of the state and code spaces, a convention we do not adopt here for the sake of consistency across all chapters. Elements of H and H_{code} will be written as lower-case Latin letters, for example x, y, etc, possibly bold-faced or underlined in the case of basis vectors.

If $x \in H$ is a unit of information that it is desirable to protect against errors in the quantum system, then P_{code} acts as the encoding map, to produce the encoded unit of information $P_{\text{code}}(x) \in H_{\text{code}}$. Due to the properties of quantum mechanics, we thus require P_{code} to be a unitary map $H \to H$. The notion of errors can be made precise via the following definitions.

Definition 2.1.3. A **quantum operation** is a map $\mathcal{E} : H \to H$ such that for all $x \in H$

$$\mathcal{E}(x) = \sum_{i=1}^{n} E_i(x)$$

for some finite set of linear operators $E_i : H \to H$, $1 \leq i \leq n$, called **operation elements**, that satisfy

$$\sum_{i=1}^{n} E_i^\dagger E_i \leq I$$

where I is the identity map. If the above equation is an equality, then the quantum operation is called **trace-preserving**.

A quantum operation $\mathcal{E}$ is called an **error** if

$$\mathcal{E}(x) \notin H_{\text{code}}$$

for at least some $x \in H_{\text{code}}$. For a given error $\mathcal{E}$, an **error-correction procedure** is a trace-preserving quantum operation $\mathcal{R}$ such that

$$(\mathcal{R} \circ \mathcal{E})(x) \propto x \tag{2.1}$$

where the proprtionality here is dependent only on the error $\mathcal{E}$, specifically whether or not it is trace preserving, and no on the specific state x.

The above formulation of an error-correction procedure can be regarded as follows. The quantum operation $\mathcal{E}$ is an error if it "rotates" an element $x \in H_{\text{code}}$ out of H_{code}. Then the quantum operation $\mathcal{R}$ corrects this error if it projects the result of this rotation back to something equivalent to x in the code space. There is the possibility that either $\mathcal{E}(x) = y$ or $(\mathcal{R} \circ \mathcal{E})(x) = y$ where $y \in H_{\text{code}}$ and y is distinct from x (and not proportional to it). In this case, a **logical error** is said to have occurred. Such errors are typically hard to correct.

The following theorem, and in particular its proof, embody the key ideas of how the projector P_{code} and the error-correction process are related.

Theorem 2.1.1. *[Thm 10.1, NC02] Let $(H_{\text{code}}, P_{\text{code}})$ be a QECC and suppose $\mathcal{E}$ is a quantum operation with elements $\{E_i\}_{i=1}^n$. There exists an error-correction procedure $\mathcal{R}$ that satisfies Equation (2.1) if and only if*

$$P_{\text{code}} E_i^\dagger E_j P_{\text{code}} = \alpha_{ij} P_{\text{code}}$$

where (α_{ij}) is a Hermitian matrix over $\mathbb{C}$.

The proof of the theorem makes use of the following lemma and theorem (see the listed reference and page numbers for their proofs):

Lemma 2.1.2. *[Thm 2.3, NC02] Let A be a linear operator on a vector space V. Then there exists a unitary operator U and unique positive operators J and K such that*

$$A = UJ = KU$$

where J and K are defined by $J = \sqrt{A^\dagger A}$ and $K = \sqrt{AA^\dagger}$.

Theorem 2.1.3. *[Thm 8.2, NC02] Suppose $\{E_1, ..., E_m\}$ and $\{F_1, ..., F_n\}$ are operation elements defining quantum operations $\mathcal{E}$ and $\mathcal{F}$ respectively. We can assume that $m = n$ (otherwise append some 0 operators to the smaller of the two sets). Then $\mathcal{E} = \mathcal{F}$ if and only if there exist complex numbers u_{ij} such that $E_i = \sum_j u_{ij} F_j$ and (u_{ij}) is an $m \times m$ unitary matrix.*

Now to the proof of Theorem 2.1.1 (which has been modified slightly from the proof given in [Chapter 10, NC02]). This proof is significant because it illuminates the role that the projector P_{code} plays in the error-correction process, specifically how it relates to the operation elements of the quantum operation $\mathcal{R}$. It is this relationship that justifies the projector for the toric code being the central focus in this thesis.

Proof. For the duration of this proof, the subscript 'code' will be dropped from P_{code} for notational simplicity. Suppose $\{E_i\}$ is a set of operation elements for a quantum operation $\mathcal{E}$ satisfying

$$PE_i^\dagger E_j P = \alpha_{ij} P$$

for some Hermitian matrix $\alpha = (\alpha)_{ij}$. It follows that α can be diagonalised to some diagonal matrix with real entries $d = u^\dagger \alpha u$, with u unitary. Moreover, we can diagonalise α to a positive diagonal matrix d' which is related to d via the following

$$d = d'c$$

where c is the diagonal matrix consisting of -1 and $+1$ entries such that $d_{ii} = d'_{ii}c_{ii}$ and $d'_{ii} \geq 0$ for all i. Thus, we can diagonalise α to d' via

$$d' = u^\dagger \alpha u c^\dagger$$

Let $F_k = \sum_i u_{ik} E_i$. By Theorem 2.1.3, the set $\{F_k\}$ also describes $\mathcal{E}$. We can then write

$$\begin{aligned}
PF_k^\dagger F_l P &= P\big(\sum_i u_{ik} E_i\big)^\dagger \big(\sum_j u_{lj} E_j\big) P \\
&= \sum_{i,j} u_{ik}^\dagger u_{lj} P E_i^\dagger E_j P \\
&= \big(\sum_{i,j} u_{ik}^\dagger \alpha_{ij} u_{lj}\big) P \\
&= d_{kl} P \\
&= d'_{kl} c_{kl} P \\
&= d'_{kl} P
\end{aligned}$$

where the last equality uses the fact that $Pe^{i\theta}x = Px$ for all x in the state space and any phase factor $e^{i\theta}$.

Now let us consider the polar decomposition of the operator $F_k P$. By Lemma 2.1.2 we can write

$$\begin{aligned}
F_k P &= U_k \sqrt{PF_k^\dagger F_k P} \\
&= \sqrt{d'_{kk}} U_k P
\end{aligned}$$

for some unitary U_k (not to be confused with the unitary u). We then define the projectors, for all k such that $d'_{kk} \neq 0$,

$$\begin{aligned}
P_k &= U_k P U_k^\dagger \\
&= \frac{F_k P U_k^\dagger}{\sqrt{d'_{kk}}}
\end{aligned}$$

and note that these projectors define orthogonal subspaces, that is, for $l \neq k$, we see that

$$\begin{aligned}
P_l P_k &= P_l^\dagger P_k \\
&= \frac{U_l P F_l^\dagger F_k P U_k^\dagger}{\sqrt{d'_{ll}}\sqrt{d'_{kk}}} \\
&= \frac{U_l d'_{lk} P U_k^\dagger}{\sqrt{d'_{ll} d'_{kk}}} \\
&= 0
\end{aligned}$$

where the last equality follows from the fact that $d'_{lk} = 0$ for $l \neq k$. Defining the correction procedure $\mathcal{R}$ by the set of operators $\{U_k^\dagger P_k\}$, we see that, for any x in the codespace,

$$\begin{aligned}
\mathcal{R}(\mathcal{E}(x)) &= \sum_{kl} U_k^\dagger P_k F_l x \\
&= \sum_{kl} U_k^\dagger P_k^\dagger F_l P x \quad \text{(since } x \text{ is in the codespace } Px = x) \\
&= \sum_{kl} \frac{U_k^\dagger U_k P F_k^\dagger F_l P x}{\sqrt{d'_{kk}}} \\
&= \sum_{kl} \delta_{kl} \sqrt{d'_{kk}} x \\
&= (\sum_k \sqrt{d'_{kk}}) x \\
&\propto x
\end{aligned}$$

This finishes the first half of the proof, once we note that we can always append additional projectors to the set $\{P_k\}$, in order to have a set of operation elements $\{U_k^\dagger P_k\}$ that satisfies

$$\sum_k P_k U_k U_k^\dagger P_k = \sum_k P_k = I$$

Now, for the other direction, suppose $\{E_i\}$ is a set of errors describing a quantum operation $\mathcal{E}$ that is correctable by a trace-preserving error-correction operation $\mathcal{R}$ described by operation elements $\{R_j\}$. Define a quantum operation $\mathcal{E}'$ such that

$$\mathcal{E}'(x) = \mathcal{E}(Px)$$

Since Px is in the codespace for any x, we get that

$$\mathcal{R}(\mathcal{E}'(x)) \propto Px$$

In fact, we can show that the proportionality is constant and indpendent of x via the following argument. Let x and y in H be arbitrary. Then consider

$$\begin{aligned}
\mathcal{R}(\mathcal{E}'(ax + by)) &= \alpha(ax + by)P(ax + by) \\
&= a\alpha(ax + by)Px + b\alpha(ax + by)Py
\end{aligned}$$

where $\alpha(\cdot)$ denotes the proportionality as a function of vectors. But quantum operations are linear, so

$$\begin{aligned}
\mathcal{R}(\mathcal{E}'(ax + by)) &= a\mathcal{R}(\mathcal{E}'(x)) + b\mathcal{R}(\mathcal{E}'(y)) \\
&= a\alpha(x)Px + b\alpha(y)Py
\end{aligned}$$

Thus, by equating the above two expressions for $\mathcal{R}(\mathcal{E}'(ax + by))$

$$a\alpha(ax + by)Px + b\alpha(ax + by)Py = a\alpha(x)Px + b\alpha(y)Py$$

we find that α must be a constant.

It follows from Theorem 2.1.3 that the operation elements $\{R_j E_i\}$ are equivalent to the quantum operation with the operation elements αP. Thus we have

$$R_j E_i P = \beta_{ji} P$$

for $\beta_{ji} \in \mathbb{C}$. We then get

$$\begin{aligned}
PE_i^\dagger R_k^\dagger R_k E_j^\dagger P &= \beta_{ki}^* \beta_{kj} P \\
\implies \sum_k PE_i^\dagger R_k^\dagger R_k E_j^\dagger P &= \sum_k \beta_{ki}^* \beta_{kj} P \\
\implies PE_i^\dagger (\sum_k R_k^\dagger R_k) E_j^\dagger P &= \sum_k \beta_{ki}^* \beta_{kj} P \\
\implies PE_i^\dagger E_j P &= \gamma_{ij} P
\end{aligned}$$

where the last implication follows by noting that $\sum_k R_k^\dagger R_k = I$ by trace-preservation and where $\gamma_{ij} = \sum_k \beta_{ki}^* \beta_{kj}$ which is a Hermitian matrix. $\square$

Thus, we have seen that the error-correction procedure, if it exists, consists of operation elements $P_{\text{code}} U_k^\dagger$. Hopefully this fact, along with the importance of P_{code} as an encoding map, has successfully justified to the reader the significance of P_{code} in the definition of an error-correcting code.

Discussion of the general theory of quantum error-correction has been useful in establishing the importance of the projector P_{code} in the error-correction process, but the formalism of quantum operations will not be needed for the remainder of this thesis. We do, however, need the formalism of stabiliser codes for treatment of the toric code, and this is the subject of the next section.

2.1.1 Stabiliser Codes

The title 'stabliser codes' implies a relationship between these codes to stabilisers and orbits in group theory. These codes are defined as the invariant subspace H_{stab} of a state space H under the action of a subgroup of the generalised Pauli group (to be defined shortly), along with a projector P_{stab} built out of the generating elements of this subgroup.

Let us consider the following faithful representation of the Pauli group $G_{\text{Pauli}} = \langle \sigma_1, \sigma_2, \sigma_3 \rangle$:

$$\Pi : G_{\text{Pauli}} \to G \subset U(2)$$
$$\sigma_1 \mapsto X = \begin{bmatrix} 0 & 1 \\ 1 & 0 \end{bmatrix}$$
$$\sigma_2 \mapsto Y = \begin{bmatrix} 0 & -i \\ i & 0 \end{bmatrix}$$
$$\sigma_3 \mapsto Z = \begin{bmatrix} 1 & 0 \\ 0 & -1 \end{bmatrix}$$

where G is simply the group generated by X, Y, Z and $U(2)$ is the unitary group of 2×2 complex valued matrices, which can be viewed as the allowed operation on a single qubit. We denote by I the identity matrix in G. We note that X and Z anti-commute, this will be important.

We want to generalise the group G to be able to act on any number of qubits, which we do in the following.

Definition 2.1.4. For any $n \in \mathbb{N}$, the **generalised Pauli group**, G_n, is given by the n-fold tensor product of elements of G

$$G_n := \{\alpha A_1 \otimes A_2 \otimes ... \otimes A_n \mid A_i \in G, \alpha \in \{1, -1, i, -i\}\} \subseteq \mathrm{GL}((\mathbb{C}^2)^{\otimes n})$$

Definition 2.1.5. A **stabiliser subgroup** is a subgroup S of G_n such that $(-1)I^{\otimes n} \notin S$ and all elements of S commute.

Remark 2.1.6. The criterion that $(-1)I^{\otimes n} \notin S$ guarantees that the eigenvalues for any $g \in S$ are precisely ± 1. This can be seen since the eigenvalues of X, Y, Z are ± 1, so the only deviation from these values in an n-fold tensor product must arise from the coefficient α. If there exists a $g \in S$ with coefficient α equal to either i or $-i$, then the product gg is $(-1)I^{\otimes n}$ which is a contradiction. By similar reasoning, for any $g \in S$, the element $-g$ must not be in S, as the product $(-g)g$ would give $(-1)I^{\otimes n}$.

We can now write down the definition of a stabiliser code.

Definition 2.1.7. Let S be a stabiliser subgroup of G_n. The associated **stabiliser code** is the quantum error-correcting code $(H_{\text{stab}}, P_{\text{stab}})$ where

$$H_{\text{stab}} = \{x \in H \mid gx = x, \forall g \in S\}$$
$$P_{\text{stab}} = \frac{1}{2^s} \prod_{i=1}^{s} (I^{\otimes n} + g_i)$$

where $H = \mathbb{C}^{2n}$ is the state space, and s is the size of the set $\{g_1, ..., g_{|S|}\}$ of generators for S.

There is a notion of independent generators for the subgroup S, based upon linear independence of vectors in $\mathbb{Z}_2^{2n}$ corresponding to each $g \in S$ (see [Section 10.5.1, NC02]), which allows one to obtain a minimal set of generators for S. We then define an $[n, k]$**-stabiliser code** as a stabiliser code $(H_{\text{stab}}, P_{\text{stab}})$ based on the stabiliser subgroup S that has $n - k$ independent generating elements. By the following proposition (again see the given reference for the proof), we get that for an $[n, k]$-stabiliser code, H_{stab} is 2^k-dimensional.

Proposition 2.1.4. *[Prop 10.5, NC02] Let a stabiliser subgroup S be generated by $n - k$ independent elements. Then H_{stab} is 2^k-dimensional.*

2.2 The Toric Code

The toric code was introduced by Kitaev ([Kit03]) and marries together lattice models from condensed matter physics with the stabiliser formalism for quantum error-correcting codes. The toric code is so named because its initial presentation was defined via a lattice on a torus, but can be generalised to any closed surface, with certain properties of the code, namely dimension of the code space, varying with the underlying surface. In this section, we will also introduce the toric code via a lattice on a torus, and use the opportunity to set the notational foundations for later chapters, so as to make the relationships between the toric code as presented here, and the construction via TQFTs later, as clear as possible.

Let Σ denote the torus $S^1 \times S^1$, and let t denote a cellular decomposition of Σ, and t^* its Poincaré dual. The toric code can be defined for any cell decomposition, but in order to align more closely with later chapters, we take as an example a triangulation t (in black) of Σ and its dual (in red) as shown in Figure 2.1.

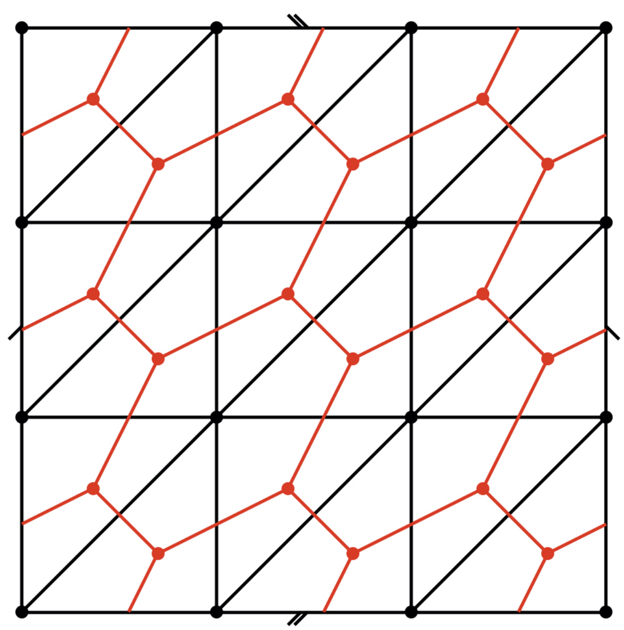

Figure 2.1: Example Triangulation (black) of a torus and its dual (red)

Denote by $t^{(2)}, t^{(1)}, t^{(0)}$ the sets of 2-, 1- and 0-cells of t respectively. The toric code is a stabiliser code, with the elements of the stabiliser subgroup S_{Σ_t} belonging to two types: those related to elements of $t^{(0)}$, called

vertex operators, and those related to elements of $t^{(2)}$, called **plaquette operators**. The notation Σ_t is to denote that the stabiliser subgroup is dependent both on the surface Σ and the chosen triangulation t. Later in this section, we will define these operators equivalently using the dual of the triangulation, via the equivalences $(t^*)^{(0)} \equiv t^{(2)}$, $(t^*)^{(1)} \equiv t^{(1)}$ and $(t^*)^{(2)} \equiv t^{(0)}$. This equivalence is not explictly needed until it is discussed further in Remark 2.2.2 below.

To start to make this more precise, we consider each element of $t^{(1)}$ (and hence also $(t^*)^{(1)}$) as having a qubit "attached", that is, there is a $\mathbb{C}^2$ factor for each element of $t^{(1)}$. Letting $n = |t^{(1)}|$, the state space of Σ with the cell decomposition t is thus

$$H_{\Sigma_t} = \bigotimes_{e \in t^{(1)}} \mathbb{C}^2 \cong (\mathbb{C}^2)^{\otimes n}$$

and the stabiliser subgroup S_{Σ_t}, defined below, will be a subgroup of the generalised Pauli group G_n which acts on $(\mathbb{C}^2)^{\otimes n}$ in the natural way. The vertex operators, denoted A_v where $v \in t^{(0)}$, are defined to be

$$A_v = \bigotimes_{e \in t^{(1)}, v \notin e} I_e \otimes \bigotimes_{e \in t^{(1)}, v \in e} X_e \tag{2.2}$$

where $v \in e$ denotes that v is an endpoint of e, and I_e and X_e denote that the operators I and X act on the $\mathbb{C}^2$ factor associated to edge e. In words, the vertex operator is the tensor product of X operations on all qubits incident to a vertex v and identity elsewhere. Typically, we shall drop the tensor product of identity I over all other edges to write the A_v more concisely as

$$A_v = \bigotimes_{e \in t^{(1)}, v \in e} X_e$$

The plaquette operators are denoted B_p with $p \in t^{(2)}$, and are defined similarly, with the convention of the product of identities on all non-significant edges being implied:

$$B_p = \bigotimes_{e \in t^{(1)}, e \in p} Z_e$$

Here $e \in p$ denotes that e is an edge that bounds a plaquette p.

The vertex and plaquette operators are defined for all $v \in t^{(0)}$ and $p \in t^{(2)}$ respectively (and equivalently for their dual counterparts). The subgroup S_{Σ_t} generated by these operators is clearly a subgroup of G_n, and is in fact a stabiliser subgroup (as per Definition 2.1.5) as can be seen by the following. It has already been noted that X and Z anti-commute, however since any vertex v shares exactly two incident edges with the boundary edges of an adjacent plaquette p, so A_v and B_p have X and Z tensor factors anti-commuting in two locations, and so A_v and B_p commute overall. Any two vertex operators (respectively any two plaquette operators) commute since X (respectively Z) commutes with itself. Any two operators defined with no common edges trivially commute. The other criterion for S_{Σ_t} to be a stabiliser group, that $(-1)I^{\otimes n}$, is also satisfied since all the A_v and all the B_p have coefficient $\alpha = 1$, as does any product of A_v's and B_p's.

We can also ask about a generating set of independent elements of S_{Σ_t} (in the sense mentioned in the previous section). Since $X^2 = Z^2 = 1$, we get the following relations

$$\prod_{v \in t^{(0)}} A_v = I^{\otimes n}$$

and

$$\prod_{p \in t^{(2)}} B_p = I^{\otimes n}$$

since in the product over all v in $t^{(0)}$, every edge e has X applied exactly twice by vertex operators, and similarly for Z's applied by B_p's. Thus, it is possible to write

$$\begin{aligned} A_{v_0} &= \prod_{v \in t^{(0)}, v \neq v_0} A_v \\ B_{p_0} &= \prod_{p \in t^{(2)}, p \neq p_0} B_p \end{aligned}$$

for any choice of $v_0 \in t^{(0)}$ and $p_0 \in t^{(2)}$, meaning that not all A_v's are independent, nor are all the B_p's. However, the sets $\{A_v \,|\, v \in t^{(0)} \setminus v_0\}$ and $\{B_p \,|\, p \in t^{(2)} \setminus p_0\}$ *are* independent, and we can write S_{Σ_t} as being generated by $|t^{(0)}| + |t^{(2)}| - 2$ independent operators:

$$S_{\Sigma_t} = \langle A_v, B_p \,|\, v \in t^{(0)} \setminus v_0,\, p \in t^{(2)} \setminus p_0 \rangle$$

Moreover, by Proposition 2.1.4, this tells us that

$$\begin{aligned} \dim(H_{\text{code}}) &= 2^{|t^{(1)}| - (|t^{(0)}| + |t^{(2)}| - 2)} \\ &= 2^{2 - \chi(\Sigma)} \\ &= 4 \end{aligned}$$

where $\chi(\Sigma)$ denotes the Euler characteristic of Σ, and the above has been written in this way to highlight the dependence of H_{code} on Σ, specifically on its topology.

The topic of diagnosing and correcting errors for the toric code and associated surface code is rich and its research is onging. Despite this topic not being the direct focus of this thesis, some comments should be made on the specific dynamics of how correction is related to the vertex and plaquette operators. The **error syndrome** is defined for a certain state $x \in H_{\Sigma_t}$ by "measuring" all of the operators, which corresponds to determining the eigenvalues of each operator as they act on x. As we know, if $x \in H_{\text{code}}$, then each of these eigenvalues are $+1$, but if $x \in H_{\Sigma_t} \setminus H_{\text{code}}$, one or more of the eigenvalues of operators will be -1 (in fact (-1)-eigenvalues always occur in pairs). The "locations" of these (-1)-eigenvalues (i.e. the vertices or plaquettes defining the operators that produce (-1)-eigenvalues) provide knowledge of how $x \in H_{\Sigma_t}$ differs from the elements of H_{code} and what operations are required to project x into H_{code}. It is this projection,

$P_{\text{stab}(\Sigma_t)}$, that is of interest for this thesis, and that we turn to next, using the theory seen in the previous section.

Recall from Definition 2.1.7 that we can write P_{stab} from a choice of a set of independent generators of the stabiliser group $S \subset G_m$ as follows:

$$P_{\text{stab}} = \prod_{g \in \text{Gen}(S)} \frac{I^{\otimes m} + g}{2}$$

where Gen(S) denotes the given set of independent generators for S. Thus, for the toric code, we have

$$P_{\text{stab}(\Sigma_t)} = \prod_{v \in t^{(0)} \setminus v_0} \frac{(I^{\otimes n} + A_v)}{2} \cdot \prod_{p \in t^{(2)} \setminus p_0} \frac{(I^{\otimes n} + B_p)}{2}$$

for a given $v_0 \in t^{(0)}$ and $p_0 \in t^{(2)}$. In fact, the projector P_{stab} is equivalent to

$$P'_{\text{stab}} = \Big(\prod_{g \in \text{Gen}(S)} \frac{I^{\otimes m} + g}{2} \Big) \Big(\frac{I^{\otimes m} + g'}{2} \Big)$$

where $g' = \prod_{g \in \text{Gen}\, S} g$ (simply expanding the products shows P_{stab} and P'_{stab} are equivalent). It will be more beneficial for Chapter 5 to take $P_{\text{stab}(\Sigma_t)}$ to also be defined over a not fully independent set of generators (we use the same notation for the equivalent projector):

$$P_{\text{stab}(\Sigma_t)} = \prod_{v \in t^{(0)}} \frac{(I^{\otimes n} + A_v)}{2} \cdot \prod_{p \in t^{(2)}} \frac{(I^{\otimes n} + B_p)}{2}$$

The order of the products does not matter due to the commuting properties of the operators. For ease of notation, we will write

$$P_v = \frac{I^{\otimes n} + A_v}{2} \tag{2.3}$$

$$P_p = \frac{I^{\otimes n} + B_p}{2} \tag{2.4}$$

It will also be useful to make the following definition:

Definition 2.2.1. Let $\mathfrak{A} \subset G_{|t^{(1)}|}$ denote the group

$$\mathfrak{A} = \langle A_v \,|\, v \in t^{(0)} \rangle$$

We write

$$P_{\text{vert}} = \prod_{v \in t^{(0)}} P_v = \frac{1}{|\mathfrak{A}} \sum_{g \in \mathfrak{A}} g \tag{2.5}$$

$$P_{\text{plaq}} = \prod_{p \in t^{(2)}} P_p \tag{2.6}$$

where $|\mathfrak{A}| = 2^{|t^{(0)}|}$ by definition of the A_v. The aim is to investigate the nature of $P_{\text{stab}(\Sigma_t)}$ by investigating P_v and P_p. Both P_v and P_p have eigenvalues 0 and 1 only, with a 0 eigenvalue corresponding to a -1 eigenvalue for the A_v or B_p, and hence an error by the informal discussion above.

Let us fix a basis for H_{Σ_t} as follows. Let $\underline{e}_0^i$ and $\underline{e}_1^i$ be the vectors

$$\underline{e}_0^i = \begin{bmatrix} 1 \\ 0 \end{bmatrix}$$
$$\underline{e}_1^i = \begin{bmatrix} 0 \\ 1 \end{bmatrix}$$

in the ith tensor factor of $H_{\Sigma_t} = (\mathbb{C}^2)^{\otimes n}$ (this choice of basis corresponds to the "computational basis" of $\{|0\rangle, |1\rangle\}$ in ket notation). Let us then denote a basis of H_{Σ_t} as

$$\mathcal{B}_{\Sigma_t} = \{\mathbf{e}_j \mid j \in \{0,1\}^n\}$$

where $\mathbf{e}_j = \underline{e}_{j_1}^1 \otimes \underline{e}_{j_2}^2 \otimes ... \otimes \underline{e}_{j_n}^n$. We then write an $x \in H_{\Sigma_t}$ as

$$x = \sum_{j=(j_1,\ldots,j_n)\in\{0,1\}^n} c_j \mathbf{e}_j$$

where the c_j are scalars in $\mathbb{C}$ and are properly normalised as appropriate for a quantum state (that is, $\sum_j |c_j|^2 = 1$). Now, let us establish some notation regarding the action of the A_v and B_p on some basis vector $\mathbf{e}_j$ that will simplify the discussion below regarding the projections P_v, P_p, P_{vert} and P_{plaq}. Let v be a vertex incident to edges corresponding to the $k_1, ..., k_s$ tensor factors of $H_{\Sigma(t)}$. Writing k_v for the vector in $\{0,1\}^n$ that has 1's in the entries corresponding to $k_1, ..., k_s$ and 0's elsewhere, we can then define the action of A_v on $\mathbf{e}_j$ as

$$A_v \cdot \mathbf{e}_j = \mathbf{e}_{j+k_v} \tag{2.7}$$

where the entry-wise sum of j and k_v is modulo 2. For the plaquette operators, let p be bounded by edges corresponding to the $l_1, ..., l_r$ tensor factors of $H_{\Sigma(t)}$. Similarly to k_v, we write l_p for the vector in $\{0,1\}^n$ with 1's in the entries corresponding to $l_1, ..., l_r$ and 0's elsewhere. Then the action of B_p on $\mathbf{e}_j$ is

$$B_p \cdot \mathbf{e}_j = (-1)^{j \cdot l_p} \mathbf{e}_j$$

where $j \cdot l_p$ is the dot product with addition modulo 2 (i.e. the bitwise dot product). This dot product can be viewed as counting (modulo two) how many of the entries of j corresponding to the $l_1, ..., l_s$ are 1.

The action of P_v on $x = \sum_{j=(j_1,\dots,j_n)\in\{0,1\}^n} c_j \mathbf{e}_j$ for some vertex v is then

$$\begin{aligned}P_v x &= P_v\Big(\sum_j c_j \mathbf{e}_j\Big)\\ &= \frac{1}{2}\Big(\sum_j c_j \mathbf{e}_j + \sum_j c_{j+k_v}\mathbf{e}_{j+k_v}\Big)\\ &= \sum_j \frac{c_{j+k_v}+c_j}{2}\mathbf{e}_{j+k_v}\end{aligned}$$

The action of P_p on x for some plaquette p is

$$P_p x = \sum_j \frac{c_j + (-1)^{j\cdot l_p} c_j}{2}\mathbf{e}_j \tag{2.8}$$

It is then clear that for $P_v x = x$, we require $c_{j+k_v} = c_j$ for all j, and for $P_p x = x$, we need $j \cdot l_p = 0 \mod 2$. Extending this reasoning to P_{plaq}, we get that $P_{\text{plaq}} x = x$ precisely when $x = \sum_{j=(j_1,\dots,j_n)\in\{0,1\}^n} c_j \mathbf{e}_j$ such that for each j with $c_j \neq 0$, $j \cdot l_p = 0 \mod 2$ for all $p \in t^{(2)}$. We write this more succinctly as

$$\mathrm{Im}(P_{\text{plaq}}) = \mathrm{span}\Big\{\mathbf{e}_j \mid j\cdot l_p = 0 \mod 2,\, \forall p \in t^{(2)}\Big\}$$

To make a similar comment about P_{vert} recall that the operators A_v for $v \in t^{(0)}$ generate a subgroup of S_{Σ_t}, $\mathfrak{A}$. Then for $P_{\text{vert}} x = x$, x must satisfy the following condition: for every $\mathbf{e}_j$ such that c_j is non-zero in x, then every element of the orbit $\mathfrak{A}\cdot\mathbf{e}_j$ appears in x with a non-zero scalar and moreover all of these scalars, including c_j, are equal. We write

$$\mathrm{Im}(P_{\text{vert}}) = \mathrm{span}\Big\{\frac{1}{\sqrt{|\mathfrak{A}|}}\sum_{\mathbf{e}\in\mathfrak{A}\cdot\mathbf{e}_j}\mathbf{e} \mid \mathbf{e}_j \in \mathcal{B}_{\Sigma_t}\Big\}$$

It is important to note for later chapters, that $\mathrm{Im}(P_{\text{plaq}})$ and $\mathrm{Im}(P_{\text{vert}})$ can be seen as "intermediate" spaces between the state space H_{Σ_t} and the codespace. We can in general write the codespace $H_{\text{code}} = \mathrm{Im}(P_{\text{stab}(\Sigma_t)}) = \mathrm{Im}(P_{\text{plaq}}) \cap \mathrm{Im}(P_{\text{vert}})$, however to write down a specific basis and to get a full intuition of this codespace, it is prudent to restrict ourselves to an example, namely of the toric code defined on a triangulation of the torus as in Figure 2.1. Before we do, we reformulate the operators A_v and B_p, and consequently $P_v, P_p, P_{\text{vert}}, P_{\text{plaq}}$ and $P_{\text{stab}(\Sigma_t)}$, in a different but equivalent way using the dual t^* of the triangulation t.

Remark 2.2.2. The reasoning behind this reformulation is due to the fact that the operators P_{vert} and P_{plaq} under this reformulation more closely resemble those operators constructed during the evaluation of the Turaev-Viro graph TQFT and Reshetikhin-Turaev defect TQFT in Chapter 5. Ultimately, the operators are equivalent in either formulation but a judgement was made to recast the operators here in order to make the exposition in Chapter 5 as clear as possible. We also note that this reformulation could also be performed by considering each of the generators A_v and B_p as being multiplied by a specific unitary matrix (namely a tensor product of Hadamards), but again this was deemed less optimal than the following discussion (for more details about the equivalence of error-correction procedures under the multiplication by a unitary see Theorem 2.1.3 or more appropriately, the corresponding theorem in [NC02]).

This reformulation writes down the generators A_v and B_p in terms of elements of the dual t^*. As mentioned earlier, the nature of the Poincaré dual provides the following equivalences: $(t^*)^{(0)} \equiv t^{(2)}$, $(t^*)^{(1)} \equiv t^{(1)}$ and $(t^*)^{(2)} \equiv t^{(0)}$. So we can consider the vertex operators A_v defined for some $v \in t^{(0)}$ as equivalently being defined by some $v \in (t^*)^{(2)}$, and similarly for B_p with $p \in t^{(2)}$. At the risk of causing confusion, despite the element in the dual t^* corresponding to the vertex $v \in t^{(0)}$, which is a "plaquette" in the dual cell decomposition, we will still refer to the A_v operators as "vertex operators" and similarly for the plaquette operators B_p. The edges incident to a vertex $v \in t^{(0)}$ correspond to the edges bounding the plaquette $v \in (t^*)^{(2)}$, and vice versa for the edges bounding $p \in t^{(2)}$ and the edges incident to the vertex $p \in (t^*)^{(0)}$. Essentially, this reformulation just replaced $t^{(0)}$ with $(t^*)^{(2)}$, $t^{(1)}$ with $(t^*)^{(1)}$ and $t^{(2)}$ with $(t^*)^{(0)}$ in the above discussion of the A_v and B_p operators, and the projections $P_{\mathrm{stab}(\Sigma_t)}, P_{\mathrm{vert}}, P_{\mathrm{plaq}}, P_p$ and P_v.

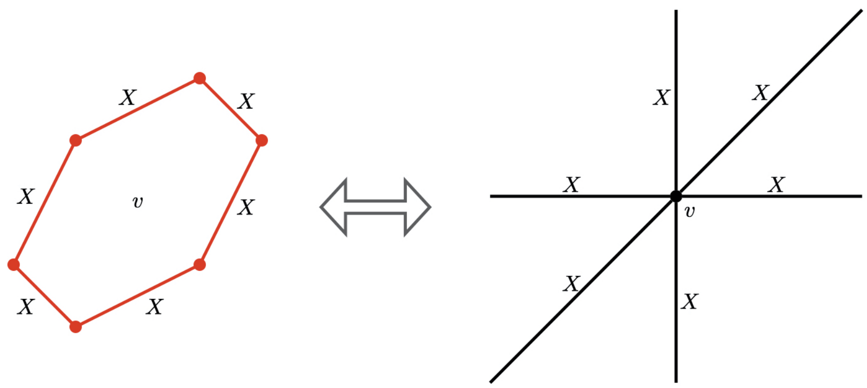

Figure 2.2: The transformation of a vertex operator from being defined by the triangulation to being defined by the dual.

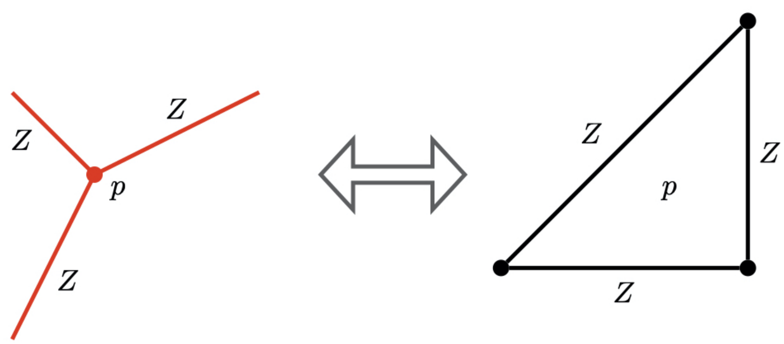

Figure 2.3: The transformation of a plaquette operator from being defined by the triangulation to being defined by the dual.

We now commence a specific example in this reformulation.

Example 2.2.3. Let us consider the triangulation t of the torus as given in Figure 2.1 (repeated below in Figure 2.4 for convenience), or rather its dual t^*.

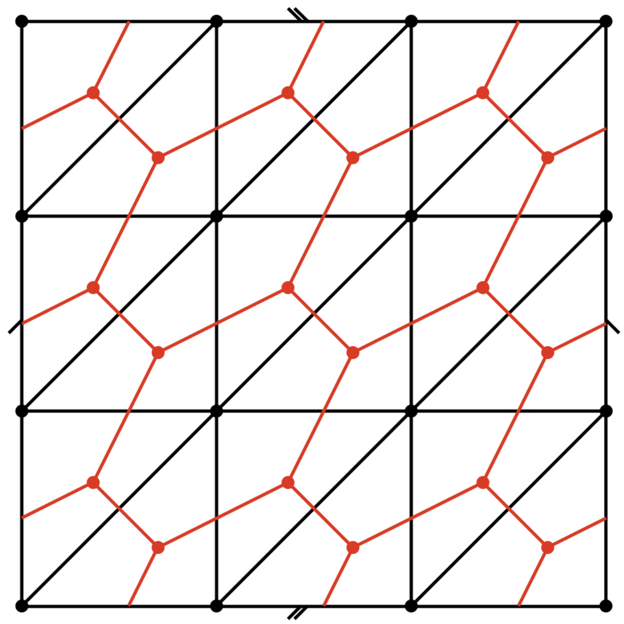

Figure 2.4: A triangulation, and its dual, of a torus.

Throughout this example we will represent all vectors x graphically, for example an arbitrary $x \in H_{\Sigma_t}$ is shown in Figure 2.5 where the c_j are such that $\sum_j |c_j|^2 = 1$ and the picture stands for $\mathbf{e}_j$.

$$x = \sum_{j\in\{0,1\}^{27}} c_j$$

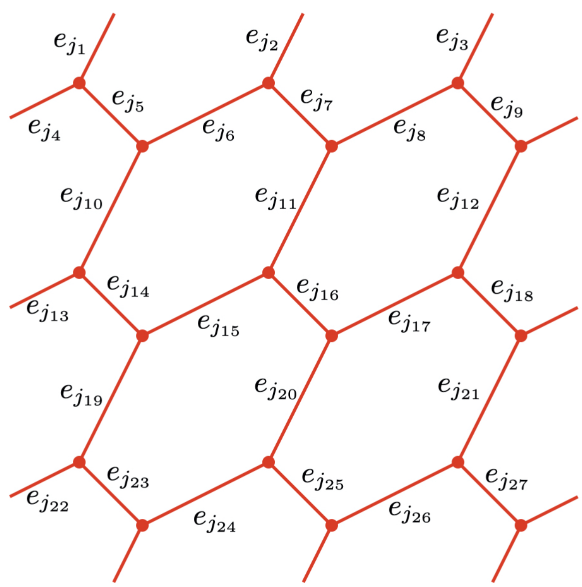

Figure 2.5: An arbitrary vector in the state space.

An example of a vector x that satisfies $P_v x = x$ is shown in Figure 2.6 since the action of A_v on the first factor produces the second factor (and vice versa), and the coefficients of each factor are the same (Figure 2.6 and the figures that follow denote $\underline{e}_0$ and $\underline{e}_1$ by 0 and 1 for simplicity, and edges labelled by 1's are also coloured blue to emphasise the link between the basis vectors of H_{code} and the non-trivial cycles of the torus in later figures).

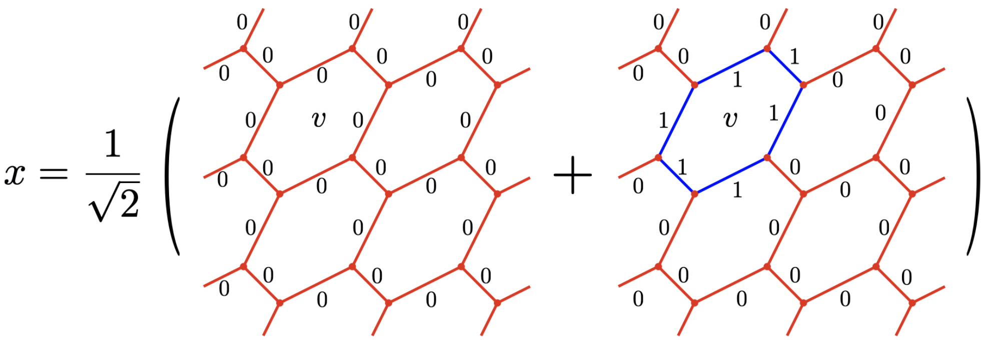

Figure 2.6: A vector invariant under P_v

Similarly, an example of a vector x that satisfies $P_p x = x$ is shown in Figure 2.7

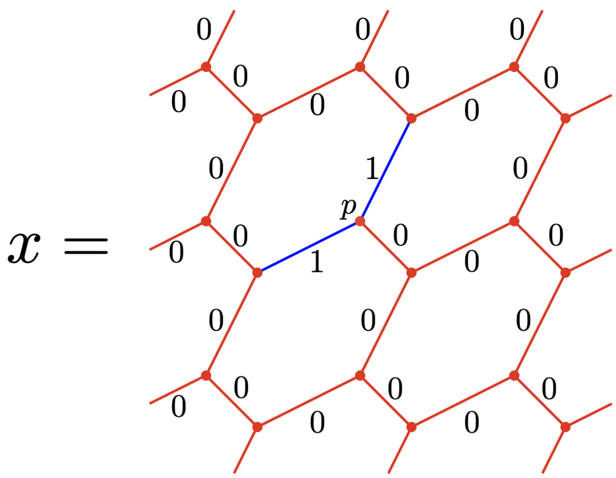

Figure 2.7: An vector invariant under P_p

Now we make the following observation which follows from the commuting properties of the A_v and B_p. For any given x that satisfies $P_p x = x$, the resulting vector from the action of any A_v on x still satisfies this property: $P_p(A_v \cdot x) = A_v \cdot x$. This extends also to P_{plaq}: for any x such that $P_{\text{plaq}} x = x$, then for any A_v (or product of A_v's), $P_{\text{plaq}}(A_v \cdot x) = A_v \cdot x$. This provides a method for producing vectors of the codespace H_{code} as follows. Select an $\mathbf{e}_j$ such that $P_{\text{plaq}} \mathbf{e}_j = \mathbf{e}_j$, then produce the following vector x:

$$x = \sum_{x_j \in \mathfrak{A} \cdot \mathbf{e}_j} \frac{1}{\sqrt{|\mathfrak{A}|}} x_j \tag{2.9}$$

where $\mathfrak{A}$ is defined in Definition 2.2.1, and so $|\mathfrak{A}| = 2^8$ in this case (recall that the number of independent A_v

operators is 8). By the comments above, we know that $P_{\text{plaq}}x = x$, and moreover we can see that $P_{\text{vert}}x = x$ since the coefficients are all equal to $\frac{1}{\sqrt{|\mathfrak{A}|}}$ (which satisfies the conditions of squares summing to 1) and since it is the sum over the orbit $\mathfrak{A} \cdot \mathbf{e}_j$. Thus, $x \in H_{\text{code}}$. It is possible to produce a basis of H_{code} by selecting $\mathbf{e}_a, \mathbf{e}_b, \mathbf{e}_c$ and $\mathbf{e}_d$ such that each $P_{\text{plaq}}\mathbf{e}_i = \mathbf{e}_i$ for $i = a, b, c, d$ and such that $\mathbf{e}_i \notin \mathfrak{A} \cdot \mathbf{e}_j$ for all $j \neq i$, and then proceeding as above by defining the basis elements as the sum over each of the orbits with equal coefficients. In particular, we define $\mathbf{e}_a, \mathbf{e}_b, \mathbf{e}_c$ and $\mathbf{e}_d$ as in Figure 2.8.

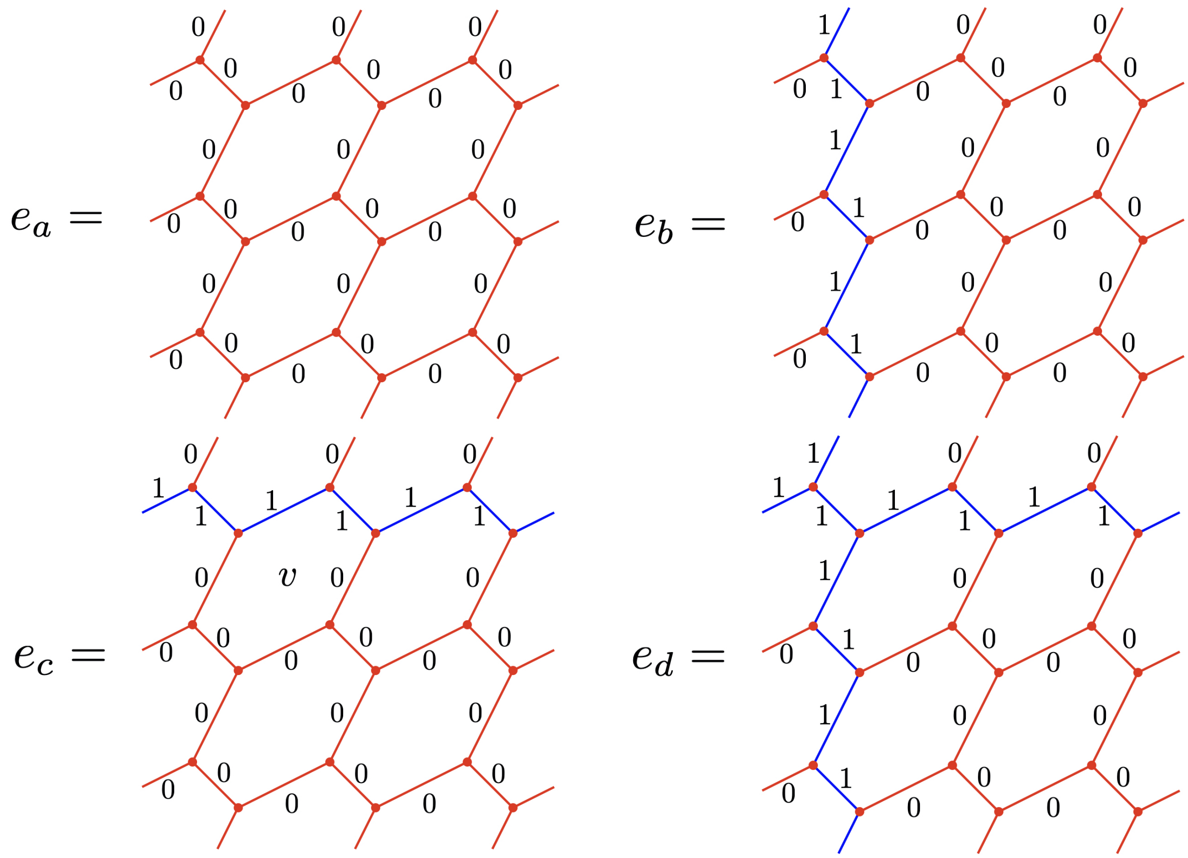

Figure 2.8: The vectors of $\text{Im}(P_{\text{plaq}})$ that induce the basis vectors x_a, x_b, x_c and x_d of H_{code}.

It can be shown that each of these vectors are indeed invariant under P_{plaq} and have disjoint orbits. It is interesting to note that we start to see the topological influence here: each of the above vectors is related to a homology class of the the torus. More explictly, $\mathbf{e}_b$ and $\mathbf{e}_c$ each have edges labelled by $\underline{e}_1$ that form a non-trivial loop of the torus, while $\mathbf{e}_d$ has edges labelled by $\underline{e}_1$ corresponding to the presence of both non-trivial loops, and $\mathbf{e}_a$ represents the absence of non-trivial loops. Denote by x_a, x_b, x_c and x_d the vectors produced by the process of summing over the orbits of $\mathbf{e}_a, \mathbf{e}_b, \mathbf{e}_c$ and $\mathbf{e}_d$ respectively as in Equation (2.9), then a basis for H_{code} is $\{x_a, x_b, x_c, x_d\}$ (this can be identified with the computational basis $\{|00\rangle, |01\rangle, |10\rangle, |11\rangle\}$.

Of course, it is possible to arrive at the same basis vectors by considering vectors invariant under P_{vert}

first, and then filtering out by the P_{plaq} projection, but as shall be seen in Chapter 5, when computing the Turaev-Viro graph TQFT the equivalent of P_{plaq} is applied first, followed by the equivalent of P_{vert}.

Chapter 3

Topological Quantum Field Theories

This chapter is devoted to setting up the foundations required to describe the two key topological quantum field theories (TQFTs) considered in later chapters. The two TQFTs are the defect TQFT, due to Carqueville, Runkel and Schaumann [CRS18; CRS17; CRS19], which extends the Reshetikhin-Turaev TQFT [Tur16], and the graph TQFT, which is an extension of the Turaev-Viro TQFT (in the form of Barrett and Westbury) [TV92; BW96] and is due to Turaev and Virelizier [TV17].

An **n-dimensional topological quantum field theory** is a symmetric strong monoidal functor

$$\mathcal{Z}^{\mathcal{C}} : \mathbf{Bord}_n^{\mathcal{C}} \to \mathrm{Vect}_{\Bbbk}$$

where $\mathbf{Bord}_n$ is a bordism category of dimension n, $\mathcal{C}$ is the category on which the definition of the bordism category, and hence the functor $\mathcal{Z}^{\mathcal{C}}$, depends, and $\mathrm{Vect}_{\Bbbk}$ is the category of (infinite-dimensional) vector spaces over field $\Bbbk$. Throughout this thesis, the notation $\mathrm{Vect}_{\Bbbk}$ (i.e. with capital 'V') denotes the category of all vector spaces over $\Bbbk$ and $\mathrm{vect}_{\Bbbk}$ denotes the category of finite-dimensional $\Bbbk$-vector spaces. We will typically only consider the case $\Bbbk = \mathbb{C}$ in any concrete examples.

This thesis primarily deals with 3-dimensional TQFTs (with the exception of Section 4.2 which briefly discusses 2-dimensional defect TQFTs in order to aid a conceptual discussion) and their corresponding 3-dimensional bordism categories will either be based on a modular tensor or spherical fusion category $\mathcal{C}$. These 3-dimensional TQFTs all essentially evaluate surfaces and bordisms by evaluating graphs, often extended in some way such as in the case of ribbon graphs, that have objects and morphisms of $\mathcal{C}$ assigned to edges and vertices (or coupons in the case of ribbon graphs; see Section 3.2.1) respectively. These evaluations largely proceed by manipulating a graphical calculus (see Appendix A) and either produce a vector space homomorphism, or the vector space corresponding to the image of such a homomorphism, as a result.

Section 3.1 establishes the required theory for this thesis related to modular tensor and spherical fusion categories, and introduces the categories $\mathrm{vect}_{\mathbb{C}}$ of finite dimensional $\mathbb{C}$-vector spaces and $\mathbb{Z}_2$- $\mathrm{vect}_{\mathbb{C}}$ of $\mathbb{Z}_2$-graded finite dimensional $\mathbb{C}$-vector spaces, upon which the TQFTs under consideration will be based. Section 3.2 introduces the bordism categories for the Turaev-Viro graph TQFT and the Reshetikhin-Turaev defect TQFT, and the final two sections, Section 3.3 and Section 3.4, introduce the theories themselves. The Turaev-Viro graph TQFT and the Reshetikhin-Turaev defect TQFT (including the Reshetikhin-Turaev TQFT upon which it is based) are rather technical to treat in full generality, so many of the details are omitted from this chapter and left to the appendices (and some are omitted from this thesis entirely). For a fuller understanding of the Turaev-Viro graph TQFT that may be useful for Chapter 5, one should consult Appendix B alongside Section 3.3 (or better yet consult [TV17] and [Tur16]), and for a fuller understanding of the Reshetikhin-Turaev defect TQFT one should consult Appendix C alongside Section 3.4 (or the literature [CRS18; CRS17; CRS19] and [Tur16]).

3.1 Requisite Category Theory

3.1.1 Spherical Fusion and Modular Tensor Categories

The two primary types of categories that are relevant to later discussion are spherical fusion categories and modular tensor categories. Below we highlight the key components of each of these types of categories that are pertinent to the construction of the two TQFTs in later sections. A theorem due to Müger [Theorem 1.2, Müg03] provides machinery to produce modular tensor categories from spherical fusion categories, a result that can be leveraged to produce an equivalence between the Turaev-Viro graph TQFT and the Reshetikhin-Turaev TQFT (see Theorem 3.3.1). The two main categories utilised in later TQFT calculations, $\mathrm{vect}_{\mathbb{C}}$ and $\mathbb{Z}_2$-$\mathrm{vect}_{\mathbb{C}}$, are introduced in a subsequent subsection and are shown to be modular and spherical fusion respectively.

Unless otherwise stated, throughout this section let $\mathcal{C}$ denote a tensor category, and let α and λ and ρ denote the associator and unital natural isomorphisms respectively:

$$\alpha_{X,Y,Z} : (X \otimes Y) \otimes Z \to X \otimes (Y \otimes Z)$$
$$\lambda_X : \mathbb{1} \otimes X \to X$$
$$\rho_X : X \otimes \mathbb{1} \to X$$

where $X, Y, Z \in \mathcal{C}$ and $\mathbb{1}$ is the unit object. The isomorphisms are assumed to satisfy the coherence conditions required for $\mathcal{C}$ to be a tensor category (these coherence conditions are listed in any standard category theory textbook, such as [Mac]). The theory presented in this subsection is largely drawn from [Chapters 1 to 3, TV17] with the exception of that regarding fusion categories which is drawn from [ENO05].

Definition 3.1.1. A **rigid category** is a tensor category $\mathcal{C}$ such that for every object X in $\mathcal{C}$ there is an assignment, called a **left duality**, $X \mapsto (X^*, \mathrm{coev}_X : \mathbb{1} \to X \otimes X^*, \mathrm{ev}_X : X^* \otimes X \to \mathbb{1})$ and an assignment called a **right duality**, $X \mapsto ({}^*X, \widetilde{\mathrm{coev}}_X : \mathbb{1} \to {}^*X \otimes X, \widetilde{\mathrm{ev}}_X : X \otimes {}^*X \to \mathbb{1})$, where X^* and ${}^*X$ are objects of $\mathcal{C}$ and the maps coev_X, ev_X, $\widetilde{\mathrm{coev}}_X$ and $\widetilde{\mathrm{ev}}_X$ satisfy the following for all objects X:

$$\rho_X \circ (\mathrm{id}_X \otimes \mathrm{ev}_X) \circ \alpha_{X,X^*,X}(\mathrm{coev}_X \otimes \mathrm{id}_X) \circ \lambda_X^{-1} = \mathrm{id}_X \tag{3.1}$$

$$\lambda_X \circ (\mathrm{ev}_X \otimes \mathrm{id}_{X^*}) \circ \alpha^{-1}_{X^*,X,X^*}(\mathrm{id}_{X^*} \otimes \mathrm{coev}_X) \circ \rho^{-1}_{X^*} = \mathrm{id}_{X^*} \tag{3.2}$$

$$\lambda_X \circ (\widetilde{\mathrm{ev}}_X \otimes \mathrm{id}_X) \circ \alpha_{X,^*X,X}(\mathrm{id}_X \otimes \widetilde{\mathrm{coev}}_X) \circ \rho_X^{-1} = \mathrm{id}_X \tag{3.3}$$

$$\rho_{^*X} \circ (\mathrm{id}_{^*X} \otimes \widetilde{\mathrm{ev}}_X) \circ \alpha_{^*X,X,^*X} \circ (\widetilde{\mathrm{coev}}_X \otimes \mathrm{id}_{^*X}) \circ \lambda^{-1}_{^*X} = \mathrm{id}_{^*X} \tag{3.4}$$

Definition 3.1.2. A **pivotal category** is a rigid tensor category $\mathcal{C}$ with a natural isomorphism $\gamma_X : {}^*X \to X^*$ for all objects X in $\mathcal{C}$.

Definition 3.1.3. A **spherical category** is a pivotal category $(\mathcal{C}, \{\gamma_X\}_{X \in \mathrm{Ob}(\mathcal{C})})$ such that for all $X \in \mathcal{C}$ and $f \in \mathrm{Hom}_{\mathcal{C}}(X, X)$ the following holds:

$$\mathrm{ev}_X \circ (\mathrm{id}_{X^*} \otimes (f \circ \gamma^{-1}_{X^*})) \circ \mathrm{coev}_{X^*} =: \mathrm{tr}^L_X(f) = \mathrm{tr}^R_X(f) := \mathrm{ev}_{X^*} \circ ((\gamma_{X^*} \circ f) \otimes \mathrm{id}_{X^*}) \circ \mathrm{coev}_X \tag{3.5}$$

The maps tr^L_X and tr^R_X are called the **left trace** and **right trace** respectively. Taking $\mathrm{tr} = \mathrm{tr}^L = \mathrm{tr}^R$, we can define the **dimension** of an object $X \in \mathcal{C}$ by

$$\dim(X) = \mathrm{tr}(\mathrm{id}_X)$$

Definition 3.1.4. A **fusion category** is an abelian, $\Bbbk$-linear, semisimple, rigid tensor category $\mathcal{C}$ with simple unit object $\mathbb{1}$, finite-dimensional morphism spaces and finitely many isomorphism classes of simple objects. We take $\Bbbk$ to be a field and I to be a representative set of simple objects of $\mathcal{C}$. Thus, a **spherical fusion category** is a fusion category $\mathcal{C}$ where the left and right duals of every object X are isomorphic, and the left and right traces of each endomorphism f coincide.

Definition 3.1.5. The **dimension** of a spherical fusion category $\mathcal{C}$ is

$$\dim(\mathcal{C}) = \sum_{i \in I} \dim(i)^2$$

where $\dim(i)$ is the dimension of the object $i \in I$.

Remark 3.1.6. There are a couple of things worth highlighting about the above definitions. Firstly, $\Bbbk$-linearity coupled with the fact that $\Bbbk$ is a field provides a natural way of producing finite-dimensional $\Bbbk$-vector spaces from hom-sets. In particular, $\mathrm{End}_{\mathcal{C}}(\mathbb{1}) = \mathrm{Hom}_{\mathcal{C}}(\mathbb{1}, \mathbb{1}) = \Bbbk$. This property is a key feature in evaluating graphs labelled by objects (specifically the simple objects in I) and morphisms, and hence, as elaborated upon in Appendix A, is ubiquitous in the Turaev-Viro graph TQFT and Reshetikhin-Turaev defect TQFT. Semisimplicity is also used, in particular to split idempotents between objects in $\mathcal{C}$ and in considering the isomorphism arising from the composition map

$$\mathrm{Hom}_{\mathcal{C}}(X, Y_i) \otimes \mathrm{Hom}_{\mathcal{C}}(Y_i, W) \to \mathrm{Hom}_{\mathcal{C}}(X, W)$$

for any two objects X, W in $\mathcal{C}$, and the Y_i are in I. A consequence of sphericity that does not show itself until later on, is the ability to take as equivalent the evaluation of a graph on a 2-sphere labelled by objects in I with the evaluation of the projection of the same graph to the plane $\mathbb{R}^2$ (see Theorem A.2.2).

In order to define a modular category, we also require knowledge of ribbon categories, as described in the following sequence of definitions.

Definition 3.1.7. A **braiding** in a tensor category $\mathcal{C}$ is a natural family of isomorphisms

$$b = \{b_{X,Y} : X \otimes Y \to Y \otimes X\}_{X,Y \in \mathrm{Ob}(\mathcal{C})}$$

such that the following conditions hold for all $X, Y, Z \in \mathrm{Ob}(\mathcal{C})$

$$b_{X,Y\otimes Z} = \alpha^{-1}_{Y,Z,X} \circ (\mathrm{id}_Y \otimes b_{X,Z}) \circ \alpha_{Y,X,Z} \circ (b_{X,Y} \otimes \mathrm{id}_Z) \circ \alpha^{-1}_{X,Y,Z} \tag{3.6}$$

$$b_{X\otimes Y,Z} = \alpha_{Z,X,Y} \circ (b_{X,Z} \otimes \mathrm{id}_Y) \circ \alpha^{-1}_{X,Z,Y} (\mathrm{id}_X \otimes b_{Y,Z}) \circ \alpha_{X,Y,Z} \tag{3.7}$$

A **braided category** is a tensor category $\mathcal{C}$ equipped with a braiding b. A braiding b is **symmetric** if, for all $X, Y \in \mathrm{Ob}(\mathcal{C})$,

$$b_{Y\otimes X} \circ b_{X\otimes Y} = \mathrm{id}_{X\otimes Y} : X \otimes Y \to X \otimes Y$$

A braided category with a symmetric braiding is called a **symmetric tensor category**.

Definition 3.1.8. For a braided pivotal category $\mathcal{C}$, a **left twist** of $\mathcal{C}$ is a family of morphisms

$$\theta^l = \{\theta^l_X\}_{X\in\mathrm{Ob}(\mathcal{C})}$$

where

$$\theta^l_X := \lambda_X \circ (\mathrm{ev}_X \otimes \mathrm{id}_X) \circ \alpha^{-1}_{X^*,X,X} \circ (\mathrm{id}_{X^*} \otimes b_{X,X}) \circ \alpha_{X^*,X,X} \circ (\widetilde{\mathrm{coev}}_X \otimes \mathrm{id}_X) \circ \lambda^{-1}_X : X \to X \tag{3.8}$$

A **right twist** of $\mathcal{C}$ is a family of morphisms $\theta^r = \{\theta^r_X\}_{X\in\mathrm{Ob}(\mathcal{C})}$ defined similarly by

$$\theta^r_X := \rho_X \circ (\mathrm{id}_X \otimes \widetilde{\mathrm{ev}}_X) \circ \alpha_{X,X,X^*} \circ (b_{X,X} \otimes \mathrm{id}_{X^*}) \circ \alpha^{-1}_{X,X,X^*} (\mathrm{id}_X \otimes \mathrm{coev}_X) \circ \rho^{-1}_X : X \to X \tag{3.9}$$

Definition 3.1.9. A **ribbon category** $\mathcal{C}$ is a braided pivotal category with twists, where the left twist and right twist are equal and is denoted by θ, and the twist, braiding and rigid structure are compatible. A twist θ, braiding b and rigid structure are **compatible** if the following equations are satisfied for all objects $X, Y \in \mathcal{C}$

$$\theta_{X\otimes Y} = b_{Y,X} \circ b_{X,Y} \circ (\theta_X \otimes \theta_Y) \tag{3.10}$$

$$(\theta_X \otimes \mathrm{id}_{X^*}) \circ \mathrm{coev}_X = (\mathrm{id}_X \otimes \theta_{X^*}) \circ \mathrm{coev}_X \tag{3.11}$$

A consequence of the left and right twist coinciding is that for all $X \in \mathrm{Ob}(\mathcal{C})$, is

$$(\theta_X)^* = \theta_{X^*}$$

Remark 3.1.10. It can be shown that all ribbon categories are spherical [Corollary 3.4, TV17].

Definition 3.1.11. For a ribbon fusion $\Bbbk$-category $\mathcal{C}$ with twist θ, the **S-matrix** is defined as follows. Letting I denote a representative set of simple objects of $\mathcal{C}$, the matrix elements $S_{i,j}$ are defined as

$$S_{i,j} := \operatorname{tr}(b_{j,i} \circ b_{i,j}) \in \operatorname{End}_{\mathcal{C}}(\mathbb{1})$$

where $i, j \in I$.

Remark 3.1.12. Recall that in a spherical category $\mathcal{C}$ the left and right traces are equal, so we denote by tr *the* trace of $\mathcal{C}$. Also recall from the previous remark that any ribbon category is spherical, so it is valid to talk about the trace in the above scenario. Some useful shortcuts for computing the S-matrix arise from the symmetry of the trace, so that $S_{i,j} = S_{j,i}$ for all $i, j \in I$, and we can also use

$$S_{\mathbb{1},i} = \operatorname{tr}(\mathrm{id}_{\mathbb{1}}) = \dim(i)$$

for all $i \in I$. Up to bijection the S-matrix does not depend on the set I.

Definition 3.1.13. A ribbon fusion $\Bbbk$-category $\mathcal{C}$ is **modular** if its S-matrix is invertible over $\Bbbk$.

The following theorem provides insight into how to produce modular tensor categories from spherical fusion ones (see reference for proof):

Theorem 3.1.1. *[Thm 1.2, Müg03] Let $\Bbbk$ be an algebraically closed field and $\mathcal{C}$ be a spherical $\Bbbk$-linear tensor category with* $\operatorname{End}(\mathbb{1}) \cong \Bbbk$. *Assume that $\mathcal{C}$ is semisimple with finitely many simple objects and* $\dim \mathcal{C} \neq 0$. *Then also the centre $Z(\mathcal{C})$ has all these properties and is a modular category.*

The consequences of this application for the Turaev-Viro and Reshetikhin-Turaev TQFTs is discussed in Section 3.3.

3.1.2 The Categories $\mathrm{vect}_{\mathbb{C}}$ and $\mathbb{Z}_2\text{-}\mathrm{vect}_{\mathbb{C}}$

The categories that will feature most prominently in the definition of the bordism categories in Section 3.2 are $\mathrm{vect}_{\mathbb{C}}$, the category of finite dimensional complex vector spaces, and $\mathbb{Z}_2\text{-}\mathrm{vect}_{\mathbb{C}}$, $\mathbb{Z}_2$-graded finite dimensional complex vector spaces. We shall shortly see that $\mathrm{vect}_{\mathbb{C}}$ is a modular tensor category but $\mathbb{Z}_2\text{-}\mathrm{vect}_{\mathbb{C}}$ is not, due to having a singular S-matrix, but does satisfy the criteria for being a spherical fusion category. Both categories have fairly trivial structure, but provide relevant perspectives for quantum computing, in particular with regard to representing qubits. The category $\mathrm{vect}_{\mathbb{C}}$ also plays an important role in the orbifolding of the Reshetikhin-Turaev defect TQFT associated to an arbitrary spherical fusion category (see Theorem 4.3.1), so despite having trivial structure, is highly non-trivial in application.

Example 3.1.14. The category $\mathrm{vect}_{\mathbb{C}}$ is defined to have finite-dimensional complex vector spaces X, X' as objects and vector space homomorphisms $f : X \to X'$ as morphisms. It is equipped with a tensor product $\otimes : \mathrm{vect}_{\mathbb{C}} \times \mathrm{vect}_{\mathbb{C}} \to \mathrm{vect}_{\mathbb{C}}$ that is defined to be the usual tensor product of vector spaces and of vector space homomorphisms. The unit object of $\text{vect}_{\mathbb{C}}$ is $\mathbb{C}$ as a vector space. The tensor structure on $\text{vect}_{\mathbb{C}}$ is trivial, so throughout this example we will drop the notation α, λ and ρ from any equations in which they feature.

Let us define a left duality for each object X to be the assignment $X \mapsto (X^*, \text{coev}_X, \text{ev}_X)$ where X^* is the vector space dual to X, that is $X^* = \text{Hom}_{\text{vect}_{\mathbb{C}}}(X, \mathbb{C})$, and coev_X and ev_X are defined as follows. Let the basis vectors of X be denoted by e_i for $i = 1, ..., n = \dim(X)$, with $\dim(X)$ here being the usual complex vector space dimension, and similarly, the basis for X^* be $\{e_i^*\}_{i=1}^n$ such that $e_i^*(e_j) = \delta_{i,j}$. Let $x = \sum_{i=1}^n x_i e_i \in X$ and $f = \sum_{i=1}^n f_i e_i^* \in X^*$, where $x_i, f_i \in \mathbb{C}$. Then

$$\text{coev}_X : \mathbb{C} \to X \otimes_{\mathbb{C}} X^*$$
$$1_{\mathbb{C}} \mapsto \sum_{i=1}^n e_i \otimes_{\mathbb{C}} e_i^*$$
$$\text{ev}_X : X^* \otimes_{\mathbb{C}} X \to \mathbb{C}$$
$$\Big(\sum_{i=1}^n f_i e_i^*\Big) \otimes_{\mathbb{C}} \Big(\sum_{i=1}^n x_i e_i\Big) \mapsto \sum_{i=1}^n f_i e_i^*(x_i e_i) = \sum_{i=1}^n f_i x_i$$

where it is understood that the definition of coev_X above is extended by linearity. We define the right duality to be the assignment $X \mapsto ({}^*X, \widetilde{\text{coev}}_X, \widetilde{\text{ev}}_X)$ where we take ${}^*X$ to also be $\text{Hom}_{\text{vect}_{\mathbb{C}}}(X, \mathbb{C})$ (and hence has the same basis as X^* above) and $\widetilde{\text{coev}}_X$ and $\widetilde{\text{ev}}_X$ are defined as

$$\widetilde{\text{coev}}_X : \mathbb{C} \to {}^*X \otimes X$$
$$1_{\mathbb{C}} \mapsto \sum_{i=1}^n e_i^* \otimes_{\mathbb{C}} e_i$$
$$\widetilde{\text{ev}}_X : X \otimes {}^*X \to \mathbb{C}$$
$$\Big(\sum_{i=1}^n x_i e_i\Big) \otimes_{\mathbb{C}} \Big(\sum_{i=1}^n f_i e_i^*\Big) \mapsto \sum_{i=1}^n f_i x_i e_i^*(e_i)$$

The maps $\text{coev}_X, \text{ev}_X, \widetilde{\text{coev}}_X$ and $\widetilde{\text{ev}}_X$ can be shown to satisfy Equations (3.1) to (3.4) essentially just by following an arbitrary element through the required compositions and using linearity of the tensor product. In doing so, we prove that $\text{vect}_{\mathbb{C}}$ is a rigid category. Pivotality is immediate since $X^* = {}^*X$, so we take γ_X to be the identity natural transformation for each X.

Sphericity is also easily shown since we identify, for all objects $X \in \text{vect}_{\mathbb{C}}$, X^{**} and X via the identity γ_{X^*}, which in particular means that $\{e_i\}_{i=1,...,n}$ is a basis for X^{**}, and moreover, this basis is dual to that of X^*. Thus, the required criterion regarding the left and right traces maps, namely Equation (3.5), holds in $\text{vect}_{\mathbb{C}}$.

Moreover, $\text{vect}_{\mathbb{C}}$ is spherical fusion since it is $\mathbb{C}$-linear and rigid, and has a single simple object $\mathbb{C}$. We get that $\text{vect}_{\mathbb{C}}$ is semisimple since every object is isomorphic to $\mathbb{C}^n$ for some finite $n \in \mathbb{N}$, and hence can be written as the direct sum of the unit object. There is only one isomorphism class of simple objects, and for each $X, Y \in \text{vect}_{\mathbb{C}}$, $\text{Hom}_{\text{vect}_{\mathbb{C}}}(X, Y)$ has finite dimension nm where the dimension of X is $n < \infty$ and that of Y is $m < \infty$. We have that $\text{vect}_{\mathbb{C}}$ is abelian since it is pre-additive and satisfies the required criteria (i.e. $\text{vect}_{\mathbb{C}}$ admits a zero object, biproducts, kernels and cokernels, etc).

We now attach a compatible ribbon structure to $\mathrm{vect}_{\mathbb{C}}$ by defining the braiding map and left and right twist to all be identity maps. This ribbon structure is compatible with the rigid structure outlined earlier, and so vect_c is a ribbon fusion category. Finally, $\mathrm{vect}_{\mathbb{C}}$ has the non-singular S-matrix

$$\begin{aligned} S &= \begin{bmatrix} \mathrm{tr}(b_{\mathbb{C},\mathbb{C}} \circ b_{\mathbb{C},\mathbb{C}}) \end{bmatrix} \\ &= \begin{bmatrix} 1 \end{bmatrix} \end{aligned}$$

since $b_{\mathbb{C},\mathbb{C}} \circ b_{\mathbb{C},\mathbb{C}} = \mathrm{id}_{\mathbb{C}}$ and $\mathrm{tr}(\mathrm{id}_{\mathbb{C}}) = 1$ as per the definition of the trace. This proves that $\mathrm{vect}_{\mathbb{C}}$ is a modular tensor category.

The category $\mathbb{Z}_2$- $\mathrm{vect}_{\mathbb{C}}$ of $\mathbb{Z}_2$-graded vector spaces is understandably very similar to $\mathrm{vect}_{\mathbb{C}}$, with slightly more interesting rigid and ribbon structures, but fails to satisfy the conditions on the S-matrix to be modular, as we shall see below. This category is sometimes called the category of super vector spaces, and it is worth working through its structure more carefully since this structure plays a more overt role in Chapter 5 than that of $\mathrm{vect}_{\mathbb{C}}$.

Example 3.1.15. The category $\mathbb{Z}_2$- $\mathrm{vect}_{\mathbb{C}}$ has as objects finite-dimensional complex vector spaces X together with a direct sum decomposition

$$X = X_0 \oplus X_1$$

where X_0, X_1 are called the degree 0 and degree 1 parts of X respectively. The (non-zero) elements of X_0 and X_1 are called homogeneous, and we define the notation $|\cdot|$ to denote the parity of homogeneous elements, that is $|x_i| = i$, where $i = 0, 1$. Much of the structure defined below is done so for homogeneous elements and makes use of the parity function, and then extended to the non-homogenous case by linearity. For any objects $X, Y \in \mathbb{Z}_2$- $\mathrm{vect}_{\mathbb{C}}$, the morphisms are degree 0 vector space homomorphisms $f : X \to Y$, meaning that $f(X_i) \subseteq Y_i$ for $i = 0, 1$. In particular, this means we can write $f = f_0 \oplus f_1$ where $f_i : X_i \to Y_i$.

The category $\mathbb{Z}_2$- $\mathrm{vect}_{\mathbb{C}}$ is given the structure of a tensor category by defining the tensor product as follows. For $X, Y \in \mathbb{Z}_2$- $\mathrm{vect}_{\mathbb{C}}$, we have

$$\begin{aligned} X \otimes Y &= (X_0 \oplus X_1) \otimes (Y_0 \otimes Y_1) \\ &= (X_0 \otimes Y_0 \oplus X_1 \otimes Y_1)_0 \oplus (X_0 \otimes Y_1 \oplus X_1 \otimes Y_0)_1 \end{aligned}$$

where the subscripts 0 and 1 on the brackets help identify which factors are degree 0 and which are degree 1. Similarly, for morphisms $f = f_0 \oplus f_1 : X \to X'$ and $g = g_0 \oplus g_1 : Y \to Y'$, we have

$$\begin{aligned} f \otimes g &= (f_0 \oplus f_1) \otimes (g_0 \oplus g_1) \\ &= (f_0 \otimes g_0 \oplus f_1 \otimes g_1)_0 \oplus (f_0 \otimes g_1 \oplus f_1 \otimes g_0)_1 \end{aligned}$$

where $f_i \otimes g_j : X_i \otimes Y_j \to X'_i \otimes Y'_j$ is defined by $x_i \otimes y_j \mapsto f_i(x_i) \otimes g_j(y_j)$. The unit object of $\mathbb{Z}_2$- $\mathrm{vect}_{\mathbb{C}}$ is $\mathbb{1} = \mathbb{C}$ in degree 0, and $\alpha_{X,Y,Z}$, $\lambda_X : \mathbb{1} \otimes X \to X$ and $\rho_X : X \otimes \mathbb{1} \to X$ are again trivial so will be dropped from any equations in which they feature throughout this example.

For the rigid structure on $\mathbb{Z}_2\text{-}\mathrm{vect}_{\mathbb{C}}$ we will define the left and right duals of an object $X \in \mathbb{Z}_2\text{-}\mathrm{vect}_{\mathbb{C}}$ to be the same, by noting that for any two objects $W, Z \in \mathrm{vect}_{\mathbb{C}}$, $\mathrm{Hom}_{\mathrm{vect}_{\mathbb{C}}}(W, Z)$ is a $\mathbb{C}$-vector space and making the following definition. We define the internal-hom, denoted by $\mathrm{hom}_{\mathbb{Z}_2\text{-}\mathrm{vect}_{\mathbb{C}}}(X, Y)$, as

$$\mathrm{hom}_{\mathbb{Z}_2\text{-}\mathrm{vect}_{\mathbb{C}}}(X, Y) := \mathrm{Hom}_{\mathrm{vect}_{\mathbb{C}}}(X, Y)$$

that is, $\mathrm{hom}_{\mathbb{Z}_2\text{-}\mathrm{vect}_{\mathbb{C}}}(X, Y)$ is the space of all $\mathbb{C}$-linear maps between X and Y. This is not a hom-set of $\mathbb{Z}_2\text{-}\mathrm{vect}_{\mathbb{C}}$ since it contains more than just degree 0 maps, but can be shown to be an object of it, as follows:

$$\begin{aligned}\mathrm{hom}_{\mathbb{Z}_2\text{-}\mathrm{vect}_{\mathbb{C}}}(X, Y) &= \mathrm{Hom}_{\mathrm{vect}_{\mathbb{C}}}(X_0 \oplus X_1, Y_0 \oplus Y_1)\\ &= \big(\mathrm{Hom}_{\mathrm{vect}_{\mathbb{C}}}(X_0, Y_0) \oplus \mathrm{Hom}_{\mathrm{vect}_{\mathbb{C}}}(X_1, Y_1)\big) \oplus \big(\mathrm{Hom}_{\mathrm{vect}_{\mathbb{C}}}(X_0, Y_1) \oplus \mathrm{Hom}_{\mathrm{vect}_{\mathbb{C}}}(X_1, Y_0)\big)\end{aligned}$$

Taking

$$(\mathrm{hom}_{\mathbb{Z}_2\text{-}\mathrm{vect}_{\mathbb{C}}}(X, Y))_0 = \mathrm{Hom}_{\mathrm{vect}_{\mathbb{C}}}(X_0, Y_0) \oplus \mathrm{Hom}_{\mathrm{vect}_{\mathbb{C}}}(X_1, Y_1)$$

and

$$(\mathrm{hom}_{\mathbb{Z}_2\text{-}\mathrm{vect}_{\mathbb{C}}}(X, Y))_1 = \mathrm{Hom}_{\mathrm{vect}_{\mathbb{C}}}(X_0, Y_1) \oplus \mathrm{Hom}_{\mathrm{vect}_{\mathbb{C}}}(X_1, Y_0)$$

we can clearly see that $\mathrm{hom}_{\mathbb{Z}_2\text{-}\mathrm{vect}_{\mathbb{C}}}(X, Y)$ is $\mathbb{Z}_2$-graded. So, for any $X \in \mathbb{Z}_2\text{-}\mathrm{vect}_{\mathbb{C}}$, we define ${}^*X = X^* = \mathrm{hom}_{\mathbb{Z}_2\text{-}\mathrm{vect}_{\mathbb{C}}}(X, \mathbb{1})$. Since we view $\mathbb{C}$ as a degree 0 vector space, we get that for any $X = X_0 \oplus X_1$, we have $X^* = X_0^* \oplus X_1^*$ where X_0^* and X_1^* are the usual duals in $\mathrm{vect}_{\mathbb{C}}$. Let $\{e_i^0\}_{i=1}^{n+m}$ be a basis for X, where $\{e_i\}_{i=1}^{n=\dim(X_0)}$ is a basis for X_0 and $\{e_i\}_{i=n+1}^{n+m}$ is a basis for X_1 ($m = \dim(X_1)$). The dual basis for X is again denoted $\{e_i^*\}_{i=1}^{n+m}$. Denoting homogenous elements of X and X^* by x and f respectively, the maps coev_X, $\widetilde{\mathrm{coev}}_X$, ev_X and $\widetilde{\mathrm{ev}}_X$ as required to stipulate a rigid structure are defined by

$$\begin{gathered}\mathrm{coev}_X : \mathbb{1} \to X \otimes X^*\\ 1_{\mathbb{C}} \mapsto \sum_{i=1}^{n+m} e_i \otimes e_i^*\\ \widetilde{\mathrm{coev}}_X : \mathbb{C} \to X^* \otimes X\\ 1_{\mathbb{C}} \mapsto \sum_{i=1}^{n+m} (-1)^{|e_i|} e_i^* \otimes e_i\\ \mathrm{ev}_X : X^* \otimes X \to \mathbb{C}\\ f \otimes x \mapsto f(x)\\ \widetilde{\mathrm{ev}}_X : X \otimes X^* \to \mathbb{C}\\ x \otimes f \mapsto (-1)^{|x||f|} f(x)\end{gathered}$$

Before outlining how the above maps satisfy the necessary equations to be a valid rigid structure (Equation (3.1) through Equation (3.4)), we make an observation regarding the coevaluation and evaluation maps that will be used in Chapter 5: if X is degree 0, for example if $X = \mathbb{C}_0$ which is the case most often seen in Section 5.1.2, then both coevaluation maps and both evaluation maps are essentially the same since there is no influence from the minus sign. Since coev_X and ev_X are the same as the corresponding maps in $\mathrm{vect}_{\mathbb{C}}$, they satisfy Equation (3.1) and Equation (3.2) by the same reasoning. This reasoning also applies in the case of $\widetilde{\mathrm{coev}}_X$ and $\widetilde{\mathrm{ev}}_X$ and Equation (3.3) and Equation (3.4), but we check these details more explicitly in order to show that the minus sign behaves nicely. By writing $x = \sum_{j=1}^{n+m} x_j e_j \in X$, we follow x through the composition of the left hand side of Equation (3.3):

$$\begin{aligned}
\sum_{j=1}^{n+m} x_j e_j &\mapsto \sum_{j=1}^{n+m} x_j e_j \otimes 1_{\mathbb{C}} \\
&\mapsto \sum_{j=1}^{n+m} x_j e_j \otimes \sum_{i=1}^{n+m} (-1)^{|e_i|} e_i^* \otimes e_i \\
&= \sum_{i,j=1}^{n+m} (-1)^{|e_i|} x_j e_j \otimes e_i^* \otimes e_i \\
&\mapsto \sum_{i,j=1}^{n+m} (-1)^{|e_j||e_i|} (-1)^{|e_i|} x_j e_i^*(e_j) \otimes e_i \\
&= \sum_{i,j=1}^{n+m} (-1)^{|e_j||e_i|} (-1)^{|e_i|} x_j \delta_{i,j} \otimes e_i \\
&= \sum_{i=1}^{n+m} (-1)^{|e_i||e_i|} (-1)^{|e_i|} x_i 1_{\mathbb{C}} \otimes e_i \\
&= \sum_{i=1}^{n+m} x_i e_i
\end{aligned}$$

The term $\delta_{i,j}$ in the third last line arises from the term $e_i^*(e_j)$ and the nature of the dual bases. The condition $j = i$ then removes any chance of a minus sign occuring and so x is recovered. The same reasoning follows for Equation (3.4) by defining $f = \sum_{j=1}^{n+m} f_j e_j^* \in X^*$, and so $\mathbb{Z}_2\text{-}\mathrm{vect}_{\mathbb{C}}$ is rigid. Since we once again have defined the left and right duals of an object to be equal, $\mathbb{Z}_2\text{-}\mathrm{vect}_{\mathbb{C}}$ is automatically pivotal. Instead of showing that $\mathbb{Z}_2\text{-}\mathrm{vect}_{\mathbb{C}}$ is spherical directly, we instead describe its ribbon structure and invoke the result in Remark 3.1.10.

Define the braiding b for $\mathbb{Z}_2\text{-}\mathrm{vect}_{\mathbb{C}}$, for all objects X, Y, by

$$\begin{aligned}
b_{X,Y} &: X \otimes Y \to Y \otimes X \\
x \otimes y &\mapsto (-1)^{|x||y|} y \otimes x
\end{aligned}$$

where again, we are taking $x \in X$ and $y \in Y$ to be homogeneous elements. We notice that this is a symmetric braiding. The left and right twists of $\mathbb{Z}_2\text{-}\mathrm{vect}_{\mathbb{C}}$ are defined to be the identity on all objects, and so Equation (3.10) and Equation (3.11) are immediately satisfied and thus $\mathbb{Z}_2\text{-}\mathrm{vect}_{\mathbb{C}}$ is a ribbon category (and hence also spherical). Moreover, it is a fusion category by the same arguments as for $\mathrm{vect}_{\mathbb{C}}$, instead now there are two isomorphism classes of simple objects, which we take to be represented by $\mathbb{C}$ in degree 0 and 1, denoted $\mathbb{C}_0$ and $\mathbb{C}_1$ respectively. We have the following

$$\begin{aligned}\dim(\mathbb{C}_0) &= 1\\ \dim(\mathbb{C}_1) &= 1\\ \dim(\mathbb{Z}_2\text{-}\,\mathrm{vect}_{\mathbb{C}}) &= 2\end{aligned}$$

However, $\mathbb{Z}_2\text{-}\,\mathrm{vect}_{\mathbb{C}}$ fails to be modular, since it has S-matrix

$$S = \begin{bmatrix} 1 & 1 \\ 1 & 1 \end{bmatrix}$$

which is clearly singular. We conclude this discussin of $\mathbb{Z}_2\text{-}\,\mathrm{vect}_{\mathbb{C}}$ by writing down the so-called fusion rules and F-tensor that are used extensively throughout calculation in Chapter 5. The fusion rules describe the behaviour of the simple objects under the tensor product:

$$\begin{aligned}\mathbb{C}_0 \otimes \mathbb{C}_0 &= \mathbb{C}_0\\ \mathbb{C}_0 \otimes \mathbb{C}_1 &= \mathbb{C}_1\\ \mathbb{C}_1 \otimes \mathbb{C}_0 &= \mathbb{C}_1\\ \mathbb{C}_1 \otimes \mathbb{C}_1 &= \mathbb{C}_0\end{aligned}$$

These conditions can be written more succintly in one equation by considering simple objects $\mathbb{C}_i$, $\mathbb{C}_j$ and $\mathbb{C}_k$, where $i, j, k \in \{0, 1\}$:

$$i + j = k \mod 2 \tag{3.12}$$

The F-tensor describes how to treat a change in the ordering of fusion of multiple simple objects. A typical picture used to define the F-tensor is shown in Figure 3.1. By a slight abuse of notation, we identify a simple object $\mathbb{C}_i$ with its subscript i, and in doing so the left side of the diagram is to be interpreted as $i \otimes j = m$ and $m \otimes k = l$, or more succinctly $(i \otimes j) \otimes k = l$. If we want to change the order to consider $i \otimes (j \otimes k)$ and still produce l, we need to consider all possible simple objects n such that $j \otimes k = n$ and $i \otimes n = l$ are valid. The F-tensor, currently denoted F^{ijk}_{lmn}, enforces when each individual fusion is valid, so for the present case of $\mathbb{Z}_2\text{-}\,\mathrm{vect}_{\mathbb{C}}$ we can use Equation (3.12) above to write

$$F^{ijk}_{lmn} = \delta_{(i+j=m \mod 2)}\, \delta_{(m+k=l \mod 2)}\, \delta_{(i+n=l \mod 2)}\, \delta_{(j+k=n \mod 2)}$$

Furthermore, because the fusion rules are relatively trivial in this case, we can see that the sum disappears since for any simple objects i, j, k, l and m for which $i + j = m \mod 2$ and $m + k = l \mod 2$, there is only one simple n for which $F^{ijk}_{lmn} \neq 0$. It will be useful for Chapter 5 to write this F-tensor slightly differently using hom-spaces. Still considering Figure 3.1, let us note that $\mathrm{Hom}_{\mathbb{Z}_2\text{-}\,\mathrm{vect}_{\mathbb{C}}}(i \otimes j, m)$ is non-zero precisely when $i + j = m \mod 2$ by definition (and similarly for the other fusions). In fact, these hom-spaces

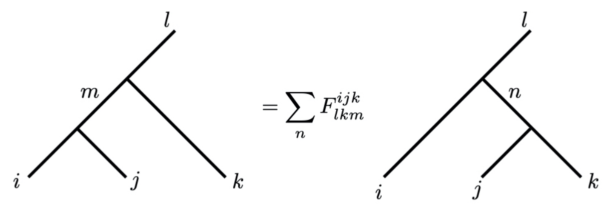

Figure 3.1: A change of basis via the F-tensor.

are 1-dimensional in this case, so we can identify them with a basis element, which we denote by λ_{ijm} for $\mathrm{Hom}_{\mathbb{Z}_2\text{-}\mathrm{vect}_{\mathbb{C}}}(i \otimes j, m)$. We then define

$$\mathbf{F}^{\lambda_{ijm},\lambda_{mkl}}_{\lambda_{inl},\lambda_{jkn}} := F^{ijk}_{lkm}$$

This change of notation is in order to be consistent with Section 5.2.2 which uses a slightly modified version of the notation of the referenced work relevant to that subsection.

So we have seen one example each of a modular tensor category and a spherical fusion category but there are many others and there is research being done to classify them, in particular unitary modular tensor categories which are most commonly associated with the TQFT perspective of quantum computation [RW18]. The Reshetikhin-Turaev TQFT and the defect TQFT are based on modular tensor categories, and every calculation made with the defect TQFT in this thesis will be using $\mathrm{vect}_{\mathbb{C}}$. The Turaev-Viro graph TQFT is based on spherical fusion categories, and all main calculations with this TQFT will be made both over $\mathbb{Z}_2\text{-}\mathrm{vect}_{\mathbb{C}}$. A key point that is discussed later in this chapter is the equivalence between the Turaev-Viro graph TQFT based on a spherical fusion category $\mathcal{C}$, and the Reshetikhin-Turaev TQFT based on the centre of $\mathcal{C}$, $Z(\mathcal{C})$.

3.2 3-dimensional Bordism Categories

We can now commence the process of describing the TQFTs of interest for this thesis: the Turaev-Viro graph TQFT and the defect Reshetikhin-Turaev TQFT. Each of these two TQFTs have slightly different source bordism categories, respectively $\mathbf{Bord}_3^{\mathrm{col}(\mathcal{C})}$, which is based on a spherical fusion category $\mathcal{C}$, and $\mathbf{Bord}_3^{\mathrm{df}}(\mathbb{D})$, which is defined using defect data $\mathbb{D}$ arising from a modular tensor category $\mathcal{D}$. Before we introduce these specific bordism categories, let us discuss in more generality the notion of a bordism category.

An **n-dimensional bordism category** is a tensor category whose objects X, Y are $(n-1)$-manifolds, possibly with extra structure, and whose morphisms are homeomorphism classes of bordisms between objects. Loosely speaking, a bordism is an n-dimensional manifold M, again possibly with extra structure, where the boundary of M is $X \sqcup Y$ and where the notion of homeomorphism is such that any extra structure present is preserved by the homeomorphism. The composition of bordisms is by gluing of n-manifolds via a homeomorphism between boundaries in a compatible way, such that any extra structure is composed compatibly and that passing to the homeomorphism class of the resultant manifold does not depend on the specific details of the gluing (more comments on this in the 3-dimensional case below). The tensor structure for the bordism category arises from the disjoint union of objects and bordisms, and the tensor unit is defined to be the empty $(n-1)$-manifold.

3.2.1 $\mathbf{Bord}_3^{\mathrm{col}(\mathcal{C})}$

The bordism category $\mathbf{Bord}_3^{\mathrm{col}(\mathcal{C})}$, which is the topic of this subsection, is the source category for the functor for the Turaev-Viro graph TQFT, which is denoted by $|\cdot|_{\mathcal{C}}$. The Turaev-Viro graph TQFT generalises the Turaev-Viro-Barrett-Westbury TQFT (which was the TQFT originally shown to produce the toric code subspace) and correspondingly, $\mathbf{Bord}_3^{\mathrm{col}(\mathcal{C})}$ is a more general bordism categoery than that for the Turaev-Viro-Barrett-Westbury TQFT (which won't be formally defined in this thesis). The main difference between the two bordism categories is regarding specified sets of points labelled with objects of $Z(\mathcal{C})$ in surfaces, and ribbon graphs extending these points in 3-manifolds (the bordism category for the Turaev-Viro-Barrett-Westbury TQFT does not include these points or ribbons). The difference between the functors for the Turaev-Viro graph TQFT and the Turaev-Viro-Barrett-Westbury TQFT are greater than just the difference between their bordism categories; these differences will be discussed in Section 3.3. Throughout this subsection, let $\mathcal{C}$ be a spherical fusion category (in fact, a pivotal category would suffice).

Definition 3.2.1. A **$\mathcal{C}$-coloured surface** is a pair (Σ, A) such that Σ is a closed, oriented 2-manifold and $A \subset \Sigma$ is finite (and possibly empty) set where each element of A is labelled with an object of $Z(\mathcal{C})$ (the centre of $\mathcal{C}$, as per the previous section), a non-zero tangent direction in Σ and a sign in $\{+,-\}$.

A simple example of a coloured sphere is shown in Figure 3.2.

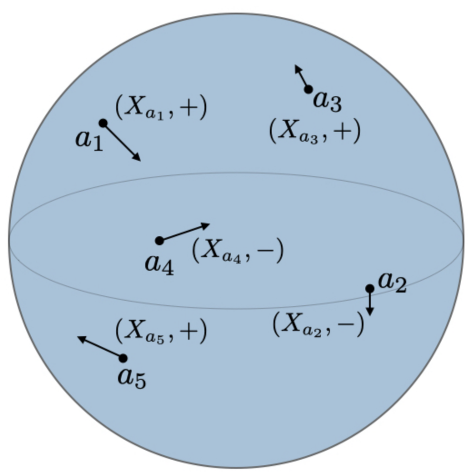

Figure 3.2: A simple coloured sphere with five coloured points.

Remark 3.2.2. (i). The reasoning behind the definition of $\mathcal{C}$-coloured surface having points labelled by objects in $Z(\mathcal{C})$ rather than in $\mathcal{C}$ ultimately has to do with the correspondence of the Turaev-Viro graph

TQFT that is based off $\mathbf{Bord}_3^{\mathrm{col}(\mathcal{C})}$ and the Reshetikhin-Turaev TQFT based on a bordism category over $Z(\mathcal{C})$. When evaluating a surface with points labelled by objects in $Z(\mathcal{C})$, these points are typically passed through the forgetful functor $F : Z(\mathcal{C}) \to \mathcal{C}$ and are treated as objects in $\mathcal{C}$.

(ii). Despite its prevalence in this chapter so far, the centre $Z(\mathcal{C})$ of a spherical fusion category hasn't actually been explicitly described. This is because we won't actually have any need for it, other than perhaps for the case where $\mathcal{C}$ is $\mathrm{vect}_{\mathbb{C}}$ in which case we know how to handle $Z(\mathcal{C})$, since our calculations with the Turaev-Viro graph TQFT over $\mathbb{Z}_2$-$\mathrm{vect}_{\mathbb{C}}$ will be on a coloured surface where A is empty. In terms of being able to understand the forgetful functor $F : Z(\mathcal{C}) \to \mathcal{C}$ above, it suffices to say that the objects of $Z(\mathcal{C})$ are the objects of $\mathcal{C}$ equipped with a half-braiding, and that the forgetful functor outputs the object of $\mathcal{C}$ without the half-braiding (see [Section 5.1.2, TV17]).

The following definition requires knowlegde of ribbon graphs, which are extensions of the usual notion of graph to allow edges to contain twists by thickening each edge into a ribbon. Vertices also become 2-dimensional by becoming rectangles (called coupons) where edges join either the top or bottom horizontal edges of the rectangle. A $\mathcal{C}$-coloured ribbon graph is a ribbon graph where each edge (ribbon) is assigned an object of $\mathcal{C}$ and each vertex (coupon) is assigned a morphism of $\mathcal{C}$. See Appendix A and the references therein for more details.

Definition 3.2.3. A **homeomorphism of $\mathcal{C}$-coloured surfaces** $f : (\Sigma_0, A_0) \to (\Sigma_1, A_1)$ is an orientation preserving homeomorphism of the uncoloured surfaces $f' : \Sigma_0 \to \Sigma_1$ such that A_0 is mapped to A_1, and each tangent direction, sign and object labelling an element in A_0 is preserved under the mapping.

Definition 3.2.4. A **bordism between $\mathcal{C}$-coloured surfaces** (Σ_0, A_0) and (Σ_1, A_1) is a triple (M, R, h) where M is a compact oriented 3-manifold, R is a $\mathcal{C}$-coloured ribbon graph in M, and $h : (-\Sigma_0) \sqcup \Sigma_1 \to (\partial M, \partial R)$ is a homeomorphism of $\mathcal{C}$-coloured surfaces, where ∂R is the set of points of $R \cup \partial M$ with non-zero tangent direction and colour determined by the framing and colours of R.

Figure 3.3 shows an example of a bordism over the coloured surface from Figure 3.2, specifically the identity bordism.

Definition 3.2.5. A **homeomorphism of bordisms between $\mathcal{C}$-coloured surfaces** (M, R, h) and (M', R', h') is an orientation preserving homeomorphism $f : M \to M'$ such that $f \circ h = h'$ and $f(R) = R'$ (up to isotopy).

Definition 3.2.6. The category $\mathbf{Bord}_3^{\mathrm{col}(\mathcal{C})}$ has $\mathcal{C}$-coloured surfaces for objects and homeomorphism classes of bordisms between $\mathcal{C}$-coloured surfaces for morphisms. The composition of morphisms is given by gluing of bordisms between $\mathcal{C}$-coloured surfaces. If (M_0, R_0, h_0) and (M_1, R_1, h_1) are bordisms that represent morphisms $(\Sigma_0, A_0) \to (\Sigma', A')$ and $(\Sigma', A') \to (\Sigma_1, A_1)$ respectively, then the **gluing** of M_0 to M_1 along $h_1 h_0^{-1} : h_0(\Sigma') \to h_1(\Sigma_1)$ is a bordism (M, R, h) where R is the union of the images R_0 and R_1 under the embeddings $M_0 \to M$ and $M_1 \to M$, and $h = h_0|_{\Sigma_0} \sqcup h_1|_{\Sigma_1}$.

Pursuant to the general comments made in the preamble at the beginning of this section, $\mathbf{Bord}_3^{\mathrm{col}(\mathcal{C})}$ can be given the structure of a symmetric tensor category where the tensor product is given by the disjoint union of

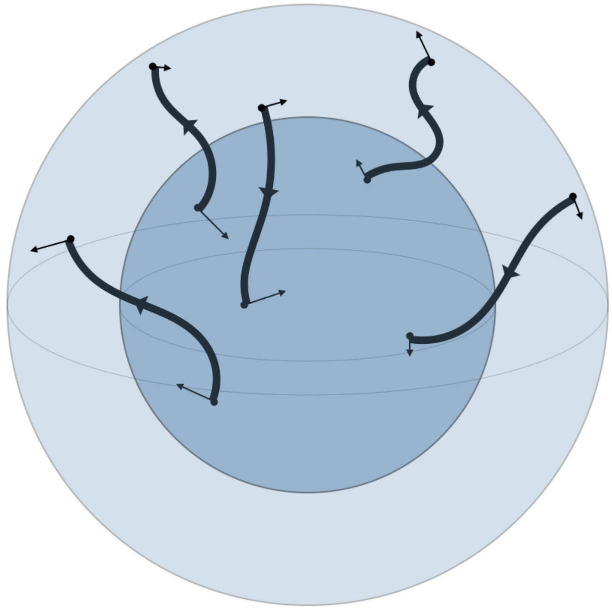

Figure 3.3: The identity bordism on a coloured sphere

surfaces and bordisms. For full details of the composition of morphisms and the symmetric tensor structure of $\mathbf{Bord}_3^{\mathrm{col}(\mathcal{C})}$ see [Section 15.2, TV17] (the bordism category there is denoted differently).

Remark 3.2.7. The main calculations using the Turaev-Viro graph TQFT in Chapter 5 are over coloured surfaces where A is empty. As shall be seen below in Section 3.3, the evaluation of the Turaev-Viro graph TQFT on a surface proceeds via consideration of a cylinder over that surface, which represents a morphism in $\mathbf{Bord}_3^{\mathrm{col}(\mathcal{C})}$. Since these surfaces all have empty sets A, these cylinders have no ribbon graphs in their interior. Moreover, the evaluations of the Turaev-Viro graph TQFT and the Turaev-Viro-Barrett-Westbury TQFT on these surfaces are precisely the same ([Section 13.1.2 TV17]). It is then reasonable to ask why the Turaev-Viro graph TQFT is being introduced in this chapter rather than the Turaev-Viro-Barrett-Westbury TQFT. The answer is simply that the evaluation of the Turaev-Viro graph TQFT on the torus in Chapter 5 provides a much clearer link to the projection map for the toric code from Section 2.2 than the corresponding evaluation in the Turaev-Viro-Barrett-Westbury TQFT.

3.2.2 $\mathbf{Bord}_3^{\mathrm{df}}(\mathbb{D})$

Just as in the previous section with the Turaev-Viro graph TQFT and $\mathbf{Bord}_3^{\mathrm{col}(\mathcal{C})}$, the Reshetikhin-Turaev defect TQFT generalises the Reshetikhin-Turaev TQFT and so the bordism category $\mathbf{Bord}_3^{\mathrm{df}}(\mathbb{D})$ for the former accomodates much more structure than the bordism category for the latter. The bordism category for the Reshetikhin-Turaev TQFT is essentially the same as that for the Turaev-Viro graph TQFT above, that is with objects as surfaces with points labelled with objects of a modular tensor category, and morphisms as homeomorphism classes of 3-manifolds with internal coloured ribbons. The category $\mathbf{Bord}_3^{\mathrm{df}}(\mathbb{D})$

is defined using stratified surfaces and stratified 3-manifolds where each stratum is labelled with specific data from modular tensor category $\mathcal{C}$, collectively known as defect data. The Reshetikhin-Turaev defect TQFT ultimately evaluates these stratified surfaces and 3-manifolds by systematically transforming them into surfaces with labelled points and bordisms with internal ribbon graphs respectively, and then evaluating via the pure Reshetikhin-Turaev TQFT (more on this in Section 3.4).

Definition 3.2.8. An **n-dimensional stratified manifold** M is an n-dimensional topological manifold with a filtration $M = M_n \supset M_{n-1} \supset M_{n-2} \supset ... \supset M_0 \supset \emptyset$ where for each $j \in \{0, ..., n\}$, $M_j \setminus M_{j-1}$ is a j-dimensional submanifold of M. The connected components of $M_j \setminus M_{j-1}$ are called j-strata of which there are finitely many. An **oriented stratified n-dimensional manifold** is an n-dimensional stratified manifold M such that the underlying n-dimensional manifold is oriented, each n-stratum has the same orientation as M, and a choice of orientation has been made for each j-stratum for $j < n$. An **n-dimensional stratified manifold with boundary** is an n-dimensional stratified manifold M where the underlying manifold M has boundary such that each j-stratum either has empty boundary, or whose boundary lies entirely in the boundary of M.

An example of a stratified surface is shown in Figure 3.4a and a simple stratified 3-manifold in Figure 3.4b.

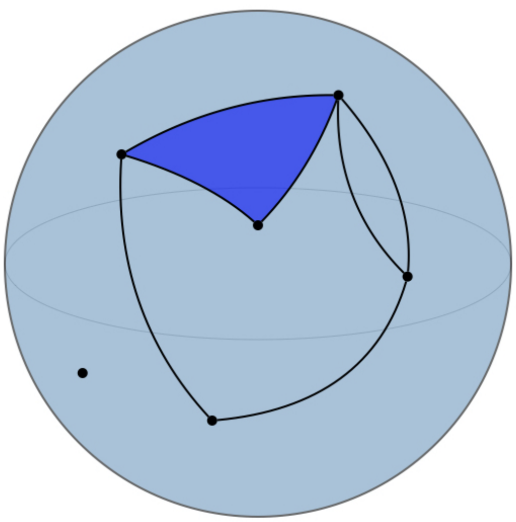

(a) A stratified surface with a 2-stratum in blue, and 1- and 0-strata in black.

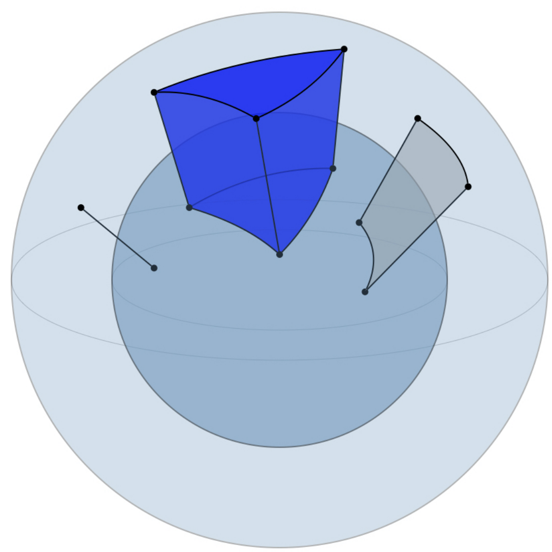

(b) A stratified 3-manifold.

Figure 3.4: Some examples of stratified manifolds.

Definition 3.2.9. A set of **defect data** $\mathbb{D}$ is a tuple $\mathbb{D} = (D_3, D_2, D_1; s, t, j)$ where D_3, D_2, D_1 are sets, the elements of which label 3-, 2- and 1-strata respectively, and s, t, j are maps that impose compatibility criteria on labellings (see [Section 3, CRS17]).

Definition 3.2.10. A **$\mathbb{D}$-decorated surface** Σ is a stratified surface where each j-stratum for $j \in \{0, 1, 2\}$ is labelled by an element from D_{j+1}.

By labelling the strata for the stratified manifold in Figure 3.4a by elements of $\mathbb{D}$, specifically the 2-strata by elements of D_3, the 1-strata by elements of D_2 and the 0-strata by D_1, the stratified sphere shown would become a $\mathbb{D}$-decorated surface.

Remark 3.2.11. The index is shifted by one so when a cylinder over a surface is considered, the 1-, 2- and 3-strata are labelled with corresponding indices. There is also a set D_0 that is lurking behind the scenes, the elements of which label 0-strata in the interior of a stratified 3-manifold. However, this set is not explicitly listed in the defect data, as the set D_0 can be constructed by evaluating the defect TQFT on a sphere surrounding the 0-strata in question. This process is called **D_0-completion** and is discussed in Appendix C but a more rigorous account is found in [Section 2.4, CRS19].

Definition 3.2.12. A **Lagrangian subspace** $\mathcal{L}$ of a symplectic vector space (H, ω) is a maximal isotropic subspace of H. That is, the maximal linear subspace $B \subset H$ such that $B \subset \mathrm{Ann}(B)$ where the annihilator is with respect to the anti-symmetric bilinear form ω on H.

For more on isotropic and Lagrangian subspaces, see Appendix C.

Definition 3.2.13. A **$\mathbb{D}$-defect bordism between $\mathbb{D}$-decorated surfaces** Σ_0 and Σ_1 is a pair (N, ϕ) where $N : \Sigma_0 \to \Sigma_1$ is a compact, decorated stratified 3-bordism and $\phi : (-\Sigma_0) \sqcup \Sigma_1 \to \partial N$ is a homeomorphism of $\mathbb{D}$-decorated surfaces.

Definition 3.2.14. The category $\mathbf{Bord}_3^{\mathrm{df}}(\mathbb{D})$ has objects as pairs $(\Sigma, \mathcal{L})$ where Σ is a $\mathbb{D}$-decorated surface and $\mathcal{L} \subset H_1(\Sigma; \mathbb{R})$ is a Lagrangian subspace of first homology group of the unstratified 2-manifold underyling Σ. The morphisms of $\mathbf{Bord}_3^{\mathrm{df}}(\mathbb{D})$ are pairs $([N], m)$ where N is a $\mathbb{D}$-defect bordism between $\mathbb{D}$-decorated surfaces where $[N]$ denotes its homeomorphism class, and $m \in \mathbb{Z}$ is an integer satisfying the condition that if $N \cong \emptyset$ then $m = 0$. The composition of morphisms is again by gluing.

Remark 3.2.15. The inclusion of the Lagrangian subspace $\mathcal{L}$ and the weight m in the above definition is required in order to make the definition of the defect Reshetikhin-Turaev TQFT anomaly-free (this is elaborated upon in Appendix C). For more details on this, and on the symmetric structure of the category $\mathbf{Bord}_3^{\mathrm{df}}(\mathbb{D})$ (where tensor product is again by disjoint union), see [Chapter IV, Tur16] and [Section 2.2.2, CRS19]

3.3 The Turaev-Viro Graph TQFT

Finally we arrive at the first substantial introduction of the Turaev-Viro graph TQFT seen in this thesis. As noted a number of times, this TQFT generalises the Turaev-Viro-Barrett-Westbury TQFT which historically precedes it. The Turaev-Viro-Barrett-Westbury TQFT is a state sum TQFT whereby the manifold being evaluated is triangulated, with each simplex having an associated set of states, and the evaluation proceeds by "averaging" over all these states. The evaluation does not depend on the specifics of the triangulation in the interior of the manifold, only on the information that resides on the boundary.

The Turaev-Viro graph TQFT, sometimes called simply the graph TQFT, will be denoted

$$|\cdot|_{\mathcal{C}} : \mathbf{Bord}_3^{\mathrm{col}(\mathcal{C})} \to \mathrm{Vect}_{\Bbbk}$$

where $\mathcal{C}$ is a spherical fusion category over base field $\Bbbk$ (in practice we will take $\Bbbk$ to be $\mathbb{C}$). This TQFT differs from the Turaev-Viro-Barrett-Westbury TQFT insofar as that instead of taking a triangulation of a manifold, a more general decomposition can be taken. In Chapter 5 it will be seen that the calculation using a specific choice of cell decomposition of the cylinder over the torus provides a clearer picture, and much neater computation, than the corresponding calculation done in using the Reshetikhin-Turaev defect TQFT (which is based on a triangulation).

A proper treatment of the graph TQFT is rather lengthy due to the amount of technical detail required to rigorously describe its evaluation on objects and morphisms of $\mathbf{Bord}_3^{\mathrm{col}(\mathcal{C})}$. The present section will not concern itself with providing all this detail, but rather give an outline and intuition of how $|\cdot|_{\mathcal{C}}$ behaves (more detail is provided in Appendix B, but still falls short of the full story, for which one should refer to [TV17]). In particular, for Chapter 5 we only really require an understanding of the behaviour of $|\cdot|_{\mathcal{C}}$ on $Z(\mathcal{C})$-coloured surfaces, which by definition basically requires knowledge of the behaviour of $|\cdot|_{\mathcal{C}}$ on the cylinder over these surfaces. The full details of the evaluation of the graph TQFT on objects and morphisms of $\mathbf{Bord}_3^{\mathrm{col}(\mathcal{C})}$ don't differ too much from those presented below and in the appendices, however, they are still deferred to references such as [TV17].

So, how does the Turaev-Viro graph TQFT actually work? In a sentence, the graph TQFT evaluates a coloured surface Σ by first assigning a preliminary vector space to Σ via the use of homspaces, typically involving the objects colouring the points of Σ, and then considering the image of the morphism represented by the cylinder over Σ as a subspace of the preliminary vector space. It is this subspace that is the evaluation of $|\cdot|_{\mathcal{C}}$ on the surface. The description of the graph TQFT below consequently mirrors these two steps, by first describing the assignment of the vector space to Σ, then describing the evaluation of the cylinder C_{Σ}.

Throughout this section, let $\mathcal{C}$ denote a spherical fusion category, I a representative set of simple objects of $\mathcal{C}$ and $Z(\mathcal{C})$ denote the centre of $\mathcal{C}$.

3.3.1 Vector Spaces for Coloured Surfaces

As outlined above, the first step in understanding the evaluation of the graph TQFT on coloured surfaces is the construction of the "naive" vector space assigned to a coloured surface (Σ, A). This assignment leans heavily on the use of coloured graphs and their evaluations (see Appendix A).

Definition 3.3.1. Let G be a graph and let $G^{(0)}$ and $G^{(1)}$ denote the set of vertices and edges of G respectively. A **colouring** of G is a map $c : G^{(1)} \to I$ and a **coloured graph** is a pair (G, c) where c is a colouring, often denoted G^c. A graph G is **oriented** if each element of $G^{(1)}$ is given an orientation.

Recalling that the points of A are labelled with a simple object of $Z(\mathcal{C})$, a sign $\{+, -\}$ and a tangent direction in Σ, we define a skeleton of (Σ, A) as follows.

Definition 3.3.2. A **skeleton** of the $Z(\mathcal{C})$-coloured surface (Σ, A) is an oriented graph G embedded in Σ that satisfies the following:

1. each element $a \in A$ lies in the interior of an edge $e_a \in G^{(1)}$ such that the tangent direction at a is transversal to the edge e_a;
2. for each $a \in A$, the orientation of e_a followed by the tangent direction of a determine the positive orientation of Σ (that is, locally at a, the orientation of e_a followed by the tangent direction of a looks like the standard orientation of $\mathbb{R}^2$);
3. each $v \in G^{(0)}$ has valence greater than or equal to two;
4. each component of $\Sigma \setminus G$ is an open disk.

Let G_A denote the oriented graph induced by G and the elements of A where the points a in e_a are considered as new vertices (and consequently, each edge e_a is split into two edges), and these vertices are labelled by $F(X_a)$ where X_a is the object of $Z(\mathcal{C})$ and $F : Z(\mathcal{C}) \to \mathcal{C}$ is the forgetful functor (recall the comments from Remark 3.2.2). These new vertices are called **distinguished vertices**, and denote the set of distinguished vertices by $G_A^{(0)} \setminus G^{(0)}$.

A choice of skeleton for the coloured surface in Figure 3.2 is shown in Figure 3.5. The points of A are now shown in red, and by considering these points as new vertices on the black lines (not including the black arrows), the graph G_A is produced.

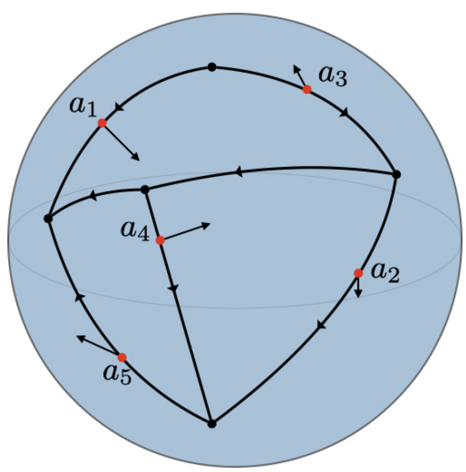

Figure 3.5: A choice of skeleton for a coloured sphere.

Definition 3.3.3. A **colouring** of the graph G_A is a map $c : G_A^{(1)} \cup (G_A^{(0)} \setminus G^{(0)}) \to \mathrm{Ob}(\mathcal{C})$ such that c assigns to any $e \in G_A^{(1)}$ an object in I, and to every distinguished vertex $v_a \in G_A^{(0)} \setminus G^{(0)}$ the object $F(X_a)$ where F and X_a are as above. Denote a coloured graph by G_A^c and the set of colourings of G_A by $\mathrm{col}(G_A)$.

We can now define the vector space assigned to the coloured surface (Σ, A) with embedded graph G_A based on a skeleton G:

$$|G;(\Sigma,A)|^\circ := \bigoplus_{c\in \mathrm{col}(G_A)} \mathcal{H}(G_A^c)$$

where $\mathcal{H}(G_A^c)$ is defined as a tensor product of hom-spaces over the vertices, both distinguished and otherwise, of G_A, that is

$$\mathcal{H}(G_A^c) = \bigotimes_{v\in G_A^{(0)}} H_v \tag{3.13}$$

The rigorous definition of the H_v relies on taking an inverse limit of a projective system (as outlined in the Appendix B), but for all intents and purposes we can take

$$H_v = \mathrm{Hom}_{\mathcal{C}}(\mathbb{1}, c(e_1^v)^{\epsilon(e_1^v)} \otimes c(e_2^v)^{\epsilon(e_2^v)} \otimes ... \otimes c(e_n^v)^{\epsilon(e_n^v)})$$

for all $v \in G^{(0)}$ (i.e non-distinguished vertices) and

$$H_v = \mathrm{Hom}_{\mathcal{C}}(\mathbb{1}, c(e_{\mathrm{out}}^a) \otimes F(X_a)^{\epsilon(a)} \otimes c(e_{\mathrm{in}}^a)^*)$$

for all distinguished vertices a. In the above, $e_1^v, ..., e_n^v$ are the edges incident to v with the numbering relative to a chosen anti-clockwise cyclic ordering, the orientation of the edges with regard to v are encoded by the map ϵ where $\epsilon(e_i^v)$ evaluates to $+$ (respectively $-$) if e_i^v is oriented away from (respectively towards) the vertex v and similarly $\epsilon(a)$ is the given sign for the point a. An object X^- is interpreted as X^* while $X^+ = X$. The edges e_{out}^a and e_{in}^a are the outgoing and incoming edges to the distinguished vertex e_a respectively. Recall that since $\mathcal{C}$ is spherical fusion, all hom-spaces are finite-dimensional $\mathbb{C}$-vector spaces (see Definition 3.1.4).

Remark 3.3.4. **(i)**. As seen in Appendix B, the inverse limit essentially allows one to remove any dependence on a choice of cyclic ordering of edges incident to a vertex. The system over which the limit is taken consists of isomorphisms, which is why, for any practical calculation, we can make a choice of ordering and produce vector spaces as above.

(ii). It shall be seen that taking inverse limits is fairly ubiquitous in the evaluation of TQFTs, at least in those considered in this thesis. A very similar procedure for producing vector spaces from hom-spaces related to 2-cells incident to edges will be seen later (again, in Appendix B). This procedure also takes an inverse limit to excise the dependence on a choice of cyclic ordering of 2-cells around the given edge.

Thus we are able to assign this “naive” vector space $|G;(\Sigma,A)|^\circ$ to a coloured surface Σ, which completes the first step of understanding the graph TQFT. We next turn to the similarly naive assignment of a vector space homomorphism to the cylinder C_Σ between two copies of the coloured surface (Σ, A). The continued use of the word “naive” here is to help distinguish these preliminary vector spaces and vector space homomorphisms used to define the graph TQFT from those produced as the end product. It also alludes to the fact that certain criteria for being a TQFT are not met by the construction above, and by the construction in the next section (see [Section 15.7.3, TV17]).

3.3.2 Vector Space Homomorphism Assigned to $\mathrm{id}_{(\Sigma,A)}$

Clearly, a major problem with the vector space $|G;(\Sigma,A)|^\circ$ as a candidate for what the graph TQFT $|\cdot|_{\mathcal{C}}$ assigns to a coloured surface (Σ, A), is the dependence on the choice of skeleton G. The dependence on this choice will once again be removed by way of an inverse limit. We state first the final definition of $|\cdot|_{\mathcal{C}}$ evaluated on (Σ, A) in terms of this limit, then subsequently pick apart the pieces:

$$|(\Sigma,A)|_{\mathcal{C}} := \lim_{\leftarrow} \mathrm{Im}(|\,\mathrm{id}_{(\Sigma,A)}, G_A, G_A|^\circ : |G;(\Sigma,A)|^\circ \to |G;(\Sigma,A)|^\circ)$$

Once again, all discussion of the inverse limit is relegated to Appendix B since, by the nature of the system over which the limit is taken, we have

$$|(\Sigma,A)|_{\mathcal{C}} \cong \mathrm{Im}(|\,\mathrm{id}_{(\Sigma,A)}, G_A, G_A|^\circ)$$

for any valid choice of skeleton G of (Σ, A) and so can in practice proceed without knowledge of the specifics of the limit. Thus, let us focus on the vector space homomorphism $|\,\mathrm{id}_{(\Sigma,A)}, G_A, G_A|^\circ$. The construction of this homomorphism is the most technical part of understanding the graph TQFT, and consequently, the following discussion has the highest proportion of detail pushed to Appendix B.

We are considering $\mathrm{id}_{(\Sigma,A)} : (\Sigma, A) \to (\Sigma, A)$ as a morphism in $\mathbf{Bord}_3^{\mathrm{col}(\mathcal{C})}$, in particular, the morphism represented by the ribbon triple (C_Σ, R, h) where C_Σ is the cylinder over Σ, R is the ribbon graph defined by $A \times [0,1]$ where the framing for each strand is given by the tangent direction of each element a, and h is the obvious homeomorphism of $Z(\mathcal{C})$-coloured surfaces

$$h : (-\Sigma, -A) \sqcup (\Sigma, A) \to (\partial C_\Sigma, \partial R)$$

Here, $(-\Sigma, -A)$ is the coloured surface induced by (Σ, A) with opposite orientation to Σ and each element $a \in -A$ has opposite sign to the correpsonding element in A, with all other information kept the same. Let G be a skeleton (Σ, A) which induces a skeleton G^{op} of $(-\Sigma, -A)$. Note that if A is empty, then there is no ribbon graph within C_Σ (as will be the case in Chapter 5). Recalling that

$$|G;(\Sigma,A)|^\circ = \bigoplus_{c \in \mathrm{col}(G_A)} \mathcal{H}(G_A^c)$$

we construct $|\,\mathrm{id}_{(\Sigma,A)}, G_A, G_A|^\circ$ via

$$|\,\mathrm{id}_{(\Sigma,A)}, G_A, G_A|^\circ = \sum_{c_0, c_1 \in \mathrm{col}(G_A)} |\,\mathrm{id}_{(\Sigma,A)}, G_A^{c_0}, G_A^{c_1}|^\circ$$

The construction of $|\,\mathrm{id}_{(\Sigma,A)}, G^{c_0}, G^{c_1}|^\circ$ draws some parallels to the construction of $|G;(\Sigma,A)|^\circ$ by considering the underlying space C_Σ with extra structure, which we call a 3-skeleton to distinguish it from the skeleton G, and can essentially be thought of as "almost" a cellular decomposition of C_Σ. A 3-skeleton P of C_Σ is required to satisfy a number of conditions that will not be fully set out here, but in particular is required to be compatible with the skeletons of the boundary surfaces, that is, $P|_{\partial C_\Sigma} = G_A \sqcup G_A^{\mathrm{op}}$.

If A is empty, and hence so too is the ribbon graph R, this definition is sufficient to evaluate $|\operatorname{id}_{(\Sigma,A)}, G_A, G_A|^\circ$, however when A is non-empty, we need to consider more structure on C_Σ. A **neat, positive diagram** (P, d) is an extension of the definition of 3-skeleton in such a way as to encode how the 3-skeleton P of C_Σ and the ribbon graph R interact. The formal definition of this structure is delayed until Appendix B, but in essence, a neat positive diagram is a 3-skeleton P with a (non-ribbon) graph embedded in its 2-cells that corresponds to the ribbon graph R. This embedded graph d is required to satisfy certain criteria, for example that edges of the graph d must meet 1-cells of P transversally and that d avoids all 0-cells of P. The crossings of edges of d and 1-cells of P are called **switches**.

We then define the set of **faces** of (P, d), denoted $(P, d)^{(2)}$, to be the set of 2-dimensional connected componenets of $P\backslash(P^{(1)}\cup d^{(1)})$, the set of **nodes** to be the set consisting of 0-cells of P, vertices of d and switches, and finally the set of **edges** to be the set of closures of any connected component of the complement of nodes in $P^{(1)} \cup d^{(1)}$. A node is **internal** if it lies in the interior of C_Σ. A **colouring** of the neat positive diagram (P, d) is a map from the set of faces to I the set of representative simple objects of $\mathcal{C}$, such that the colours of the faces adjacent to edges of $(G_A^{\text{op}})^{c_0}$ and $G_A^{c_1}$ (of which there is precisely one face adjacent to each edge by the conditions of P being a 3-skeleton) are consistent with the colours of the edges of G_A and G_A^{op}. The set of colours of (P, d) is denoted $\operatorname{col}(P, d)$.

It again seems prudent to write down the full expression for $|\operatorname{id}_{(\Sigma,A)}, G^{c_0}, G^{c_1}|^\circ$ and then discuss each component:

$$|\operatorname{id}_{(\Sigma,A)}, G_A^{c_0}, G_A^{(c_1)}|^\circ := \frac{\dim(\mathcal{C})^{\#(\Sigma\backslash G)-\#(C_\Sigma\backslash P)}}{\dim(c_1)} \sum_{c\in\operatorname{col}(P,d)} \dim(c)(V_c \otimes \operatorname{id}_{\mathcal{H}(G_R)})(*_c)$$

Firstly, all the components related to dimension are as follows:

- $\dim \mathcal{C}$ is the categorical dimension, that is $\sum_{i\in I} \dim(i)^2$;
- $\dim(c_1)$ is defined to be the product over the dimension of all objects assigned to each edge of G_A under the colouring c_1:

$$\dim(c_1) := \prod_{e\in G_A^{c_1}} \dim(c_1(e));$$

- and similarly, $\dim(c)$ is the product over all objects assigned to each face of (P, d) by the colouring c also taking into account the Euler characteristic of the face:

$$\dim(c) := \prod_{r\in(P,d)^{(2)}} \dim(c(r))^{\chi(r)}.$$

Next, the notation $\#(\cdot)$ denotes the number of connected components of the argument, that is, the number of 2-dimensional connected components of $\Sigma \setminus G$ and the number of the 3-dimensional connected components of $C_\Sigma \setminus P$.

Finally, consider the term $(V_c \otimes \mathrm{id}_{\mathcal{H}(G_R)})(*_c)$. Here $G_R = h((G_A^{\mathrm{op}})^{c_0} \sqcup G_A^{c_1})$. Once again, the formal details of the map V_c and the so-called **contraction vector** $*_c$ are left to Appendix B and presently we undertake a more heuristic discussion. In essence, the map $V_c \otimes \mathrm{id}_{\mathcal{H}(G_R)}$ acting on $*_c$ enforces a notion of compatibility in building the bordism C_Σ from the elements of $(P, d)^{(2)}$. The map V_c acts by evaluating graphs on spheres around each internal node of (P, d), where each graph is formed from the intersection of the faces adjacent to the given node with the sphere around the node. Evaluation is by the Penrose calculus (see Appendix A), and since each node-graph has no "free ends", it evaluates to an element in $\mathrm{End}_{\mathcal{C}}(\mathbb{1}, \mathbb{1}) = \Bbbk$.

Now the contraction vector $*_c$ is basically just the vector that consists of unit elements of the objects associated to each face, and hence each edge of the graph being evaluated. The evaluation then outputs either 0 or 1 in $\Bbbk$ depending on whether the labelling of the edges of the graph (or equivalently the labelling of the faces of (P, d)) are compatible in terms of the fusion rules for $\mathcal{C}$.

We can take the perspective that

$$(V_c \otimes \mathrm{id}_{\mathcal{H}(G_R)})(*_c) \in \Bbbk \otimes \mathcal{H}(G_R) \cong \mathcal{H}(G_R) \cong \mathcal{H}(G_A^{c_0})^* \otimes \mathcal{H}(G_A^{c_1}) \cong \mathrm{Hom}_{\Bbbk}(\mathcal{H}(G_A^{c_0}), \mathcal{H}(G_A^{c_1})) \tag{3.14}$$

and so $(V_c \otimes \mathrm{id}_{\mathcal{H}(G_R)})(*_c)$ is a vector space homomorphism from $\mathcal{H}(G_A^{c_0})$ to $\mathcal{H}(G_A^{c_1})$, and it is the image of this map that $|\cdot|_{\mathcal{C}}$ assigns to Σ. More details are provided in Appendix B and more completely in [Chapter 15, TV17].

Remark 3.3.5. The $6j$-symbols which are used to calculate the Turaev-Viro-Barrett-Westbury TQFT can be recovered in the Turaev-Viro graph TQFT context from the graphs obtained from spheres around internal nodes in a specific choice of skeleton (see [Section 13.1.2, TV17]).

This section is concluded with some comments regarding the links to the toric code and why it is necessary to consider other topological field theories in order to model error-correction properly. The dimension of the code space of the toric code does not depend on the specifics of the lattice used to define it, that is, the dimension is independent of the number of physical qubits in the state space. However, there are other properties of the code, such as code distance (basically the number of errors the code can correct for) that *do* depend on the specifics of the lattice. Many of these properties can be obtained from knowledge of the projection map onto the code space, especially when the code is a stabiliser code and hence the projection map is written as a product of operators defined from the lattice.

As will be seen in Chapter 5, the Turaev-Viro graph TQFT produces the correct code space for the toric code, but doesn't really retain any other information about the code. One could argue that by taking $|\Sigma|_{\mathcal{C}} \cong \mathrm{Im}(|\,\mathrm{id}_{(\Sigma,A)}, G_A, G_A|^\circ)$, we can regard the skeleton G as the lattice defining the code, but this perspective isn't quite correct for the following reasons. Firstly, the presence of a qubit (or qudit or more generally an anyon) is modelled by the labelled points of A with the type of particle corresponding to the simple object that label these points. However, there are no marked points in the evaluation of the torus that produces the toric code subspace. Secondly, we aren't really "allowed" to consider the skeleton G because it only really exists as a tool in defining the Turaev-Viro graph TQFT. For example, if we wanted to express a logical operation on the code space by a morphism in $\mathbf{Bord}_3^{\mathrm{col}(\mathcal{C})}$, then this is a morphism with boundary components as two copies of the unlabelled torus; there is no skeleton G involved at all.

So it seems like what we need is a TQFT whose bordism category can handle this extra required structure. Fortunately, we have seen that the category $\mathbf{Bord}_3^{\mathrm{df}}(\mathbb{D})$ for the Reshetikhin-Turaev defect TQFT does precisely this, and so this seems like a prudent avenue to explore. This is only bolstered by the following theorem and subsequent comments:

Theorem 3.3.1. *[Thm 17.1, TV17] The graph TQFT over spherical fusion category $\mathcal{C}$ and the Reshetikhin-Turaev TQFT over $Z(\mathcal{C})$ are isomorphic (as TQFTs).*

In the next section, the Reshetikhin-Turaev defect TQFT is defined, and it will be seen that it evaluates defect surface and bordisms by reducing to bordisms with ribbon graphs and labelled points, and then passing to the original Reshetikhin-Turaev TQFT. In light of the above theorem, it seems plausible that we would be able to manufacture a $Z(\mathbb{Z}_2\text{-}\,\mathrm{vect}_{\mathbb{C}})$-coloured surface whose evaluation by the Reshetikhin-Turaev TQFT produces precisely the toric code subspace, and also has an interpretation in terms of a defect surface in $\mathbf{Bord}_3^{\mathrm{df}}(\mathbb{D}')$ where $\mathbb{D}'$ is defect data arising from $Z(\mathbb{Z}_2\text{-}\,\mathrm{vect}_{\mathbb{C}})$. In actual fact, we will consider a defect surface in $\mathbf{Bord}_3^{\mathrm{df}}(\mathbb{D})$ where $\mathbb{D}$ is defect data from $\mathrm{vect}_{\mathbb{C}}$, that replicates the Turaev-Viro-Barrett-Westbury TQFT on the underlying non-defect surface by orbifolding (see the next section and also Chapter 4).

3.4 The Defect Reshetikhin-Turaev TQFT

The discussion at the end of the previous section provides the motivation for seeking 3-dimensional TQFTs that are powerful enough to be able to evaluate manifolds with extra structure. There are a couple of different ways to modify existing TQFTs in order to accomodate this extra structure: one can appeal to higher category theory and consider the improved TQFTs as higher functors, or one can modify the bordism category and functor of the original TQFT and stay within the 1-categorical setting. The Reshetikhin-Turaev defect TQFT of Carqueville, Runkel and Schaumann takes the second approach, although ultimately there are equivalences between the two approaches and the higher categorical setting plays a role in Chapter 4. It is necessary to introduce the Reshetikhin-Turaev TQFT first before turning our attention to the defect TQFT.

The evaluation of the Reshetikhin-Turaev TQFT (and hence of the Reshetikhin-Turaev defect TQFT) differs to that of the Turaev-Viro graph TQFT, since instead of summing over a decomposition of a manifold, the Reshetikhin-Turaev TQFT appeals to surgery theory to produce an invariant. To each surface and each 3-manifold, a ribbon graph in $\mathbb{R}^3$ can be assigned, and it is the evaluation of coloured versions of these graphs that the Reshetikhin-Turaev TQFT outputs. Consequently, the Reshetikhin-Turaev TQFT and Reshetikhin-Turaev defect TQFT are based on modular tensor categories in order for the ribbon graphs to be well-defined and able to be evaluated. Again, the full treatment of the Reshetikhin-Turaev TQFT and defect TQFT requires more technical detail than is appropriate in this chapter, so much is left to Appendix C and references such as [Chapter IV, Tur16]. Let $\mathcal{C}$ be a modular tensor category throughout this section, and I a representative set of simple objects.

3.4.1 The Reshetkhin-Turaev TQFT

The form of the Reshetikhin-Turaev TQFT presented here is the anomaly-free version, but there are other somewhat preliminary versions of this TQFT that aren't anomaly-free (the reference [Chapter IV, Tur16] defines the Reshetikhin-Turaev TQFT by first introducing the most basic form, which represents the largest conceptual element of the TQFT, then makes small successive modifications to arive at the anomaly-free version). It was mentioned during the discussion of the bordism category for the Reshetikhin-Turaev defect TQFT that certain aspects of definitions of objects and morphisms of that category exist precisely to deal with the occurrence of anomalies; the same goes for the bordism category $\mathbf{Bord}^{\mathcal{C}}_{\mathrm{wt}}$ for the anomaly-free Reshetikhin-Turaev TQFT here. We write the Reshetikhin-Turaev TQFT as

$$\mathcal{Z}_{RT,\mathcal{C}} : \mathbf{Bord}^{\mathcal{C}}_{\mathrm{wt}} \to \mathrm{Vect}_{\Bbbk}$$

where the category $\mathbf{Bord}^{\mathcal{C}}_{\mathrm{wt}}$ is the bordism category with objects as extended surfaces and morphisms (bordisms) as homeomorphism classes of weighted extended 3-manifolds between extended surfaces. Similarly to the objects of the bordism category for the Reshetikhin-Turaev defect TQFT an **extended surface** is a pair $(\Sigma, \mathcal{L})$ where Σ is a closed oriented surface with a finite family of disjoint marked arcs and $\mathcal{L}$ is a Lagrangian space $\mathcal{L} \subset H_1(\Sigma; \mathbb{R})$. A **marked arc** is a simple oriented arc in Σ labelled by an object of $\mathcal{C}$ and a sign. By taking the perspective that a marked arc signifies a tangent direction to a point (the source of the oriented arc) in Σ, we basically regain the definition of $\mathcal{C}$-coloured surface in the previous subsection. A **homeomorphism of extended surfaces** is a homeomorphism of the underlying surfaces that preserves the arcs, their orientations, their objects and signs, and induces an isomorphism of 1-homologies that preserves the Lagrangian subspace.

A **weighted extended 3-manifold** is a pair (M, m) where M is an extended 3-manifold and $m \in \mathbb{Z}$ satisfies only the criterion that if $M = \emptyset$ then $m = 0$. An **extended 3-manifold** is a compact oriented 3-manifold with extended surfaces as boundary and a $\mathcal{C}$-coloured ribbon graph in the interior, that meets the boundary in a compatible way (i.e. along the arcs with the colours of strands consistent with the objects of the arcs). A **homeomorphism of weighted extended 3-manifolds** is a map $(M, m) \to (M', m')$ where $m = m'$ and the map is a homeomorphism of the underlying 3-manifolds that sends the coloured ribbon in M to the coloured ribbon in M' and restricts to a homeomorphism of extended surfaces on the boundary.

In order to define how $\mathcal{Z}_{RT,\mathcal{C}}$ evaluates an extended surface $(\Sigma, \mathcal{L})$ we need to quickly introduce the notion of a standard surface Σ^{std}, which is an extended surface without the Lagrangian subspace (that is an extended surface that hasn't been extended), and the corresponding preliminary version of the Reshetikhin-Turaev TQFT, which will be denoted $\overline{\mathcal{Z}}^{\mathcal{C}}_{RT}$, that evalautes standard surfaces. An extended surface $(\Sigma, \mathcal{L})$ is said to be parametrised by a standard surface Σ^{std} if a homeomorphism $f : \Sigma^{\mathrm{std}} \to \Sigma$ that preserves marked arcs is given (the pair $(\Sigma^{\mathrm{std}}, f)$ is called a parametrisation). Ultimately, $\mathcal{Z}_{RT,\mathcal{C}}$ evaluates $(\Sigma, \mathcal{L})$ via an inverse limit over parametrisations of $(\Sigma, \mathcal{L})$, but before we make any further comments on that, let us denote what $\overline{\mathcal{Z}}^{\mathcal{C}}_{RT}$ assigns to standard surfaces.

We consider a standard surface Σ^{std} as a canonical marked surface of a certain type $t = (g; (X_1, \epsilon_1), ..., (X_n, \epsilon_n))$ where g is the genus of Σ^{std} and the (X_i, ϵ_i) denote the objects and signs associated to the marked arcs in some order. We then consider a bordism from $\emptyset$ to Σ^{std} with an internal ribbon graph consisting of one coupon and $n+g$ strands. An example for a standard surface of type $t = (1; (X_{a_1}, -), (X_{a_2}, +), (X_{a_3}, +))$ is shown in Figure 3.6.

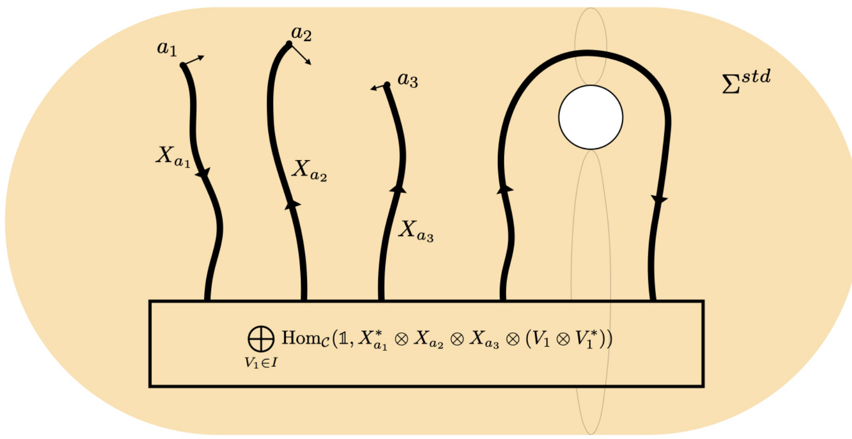

Figure 3.6: An example of the ribbon graph used to compute $\overline{\mathcal{Z}}^{\mathcal{C}}_{RT}(\Sigma^{\mathrm{std}})$.

The strands that encode the genus of Σ^{std} and the single coupon are uncoloured, and so by summing over the colourings by simple objects, $\overline{\mathcal{Z}}^{\mathcal{C}}_{RT}$ assigns the following vector space to Σ^{std}:

$$\overline{\mathcal{Z}}^{\mathcal{C}}_{RT}(\Sigma^{\mathrm{std}}) = \bigoplus_{(V_1, ..., V_g) \in I^g} \mathrm{Hom}_{\mathcal{C}}(\mathbb{1}, X_1^{\epsilon_1} \otimes ... \otimes X_n^{\epsilon_1} \otimes \bigotimes_{r=1}^{g} (V_r \otimes V_r^*))$$

The projective system by which $\mathcal{Z}_{RT,\mathcal{C}}$ is defined is constructed as follows. Let $f_0 : \Sigma_0^{\mathrm{std}} \to \Sigma$ and $f_1 : \Sigma_1^{\mathrm{std}} \to \Sigma$ be two homeomorphisms from parametrisations of $(\Sigma, \mathcal{L})$. Then there is a homeomorphism $f_1^{-1} f_0 : \Sigma_0^{\mathrm{std}} \to \Sigma_1^{\mathrm{std}}$ which induces an isomorphism

$$\phi(f_0, f_1) : \overline{\mathcal{Z}}_{RT,\mathcal{C}}(\Sigma_0^{\mathrm{std}}) \to \overline{\mathcal{Z}}_{RT,\mathcal{C}}(\Sigma_1^{\mathrm{std}})$$

This isomorphism involves some factors that require more theory than can be presented here and depend on $\mathcal{C}$, Σ, Σ_0^{std} and Σ_1^{std} in non-trivial ways in general (for the case of $\mathrm{vect}_{\mathbb{C}}$ these isomorphisms are somewhat simpler; see Appendix C.1.3). We then set $\mathcal{Z}_{RT,\mathcal{C}}(\Sigma, \mathcal{L})$ to be the inverse limit over the $\mathcal{Z}_{RT,\mathcal{C}}(\Sigma^{\mathrm{std}})$ along the 'intertwiners' $\phi(f_0, f_1)$ over all parametrisations of Σ. Similarly to the inverse limit mentioned for the Turaev-Viro graph TQFT, for any parametrisation $(\Sigma^{\mathrm{std}}, f)$ there is an isomorphism $\mathcal{Z}_{RT,\mathcal{C}}(\Sigma, \mathcal{L}) \to \mathcal{Z}_{RT,\mathcal{C}}(\Sigma^{\mathrm{std}})$, and this is how $\mathcal{Z}_{RT,\mathcal{C}}$ is computed in practice.

Defining the evaluation of $\mathcal{Z}_{RT,\mathcal{C}}$ on a weighted extended 3-manifold (M, m) also requires some non-trivial groundwork which has been relegated to the Appendix C (and references therein). The evaluation of morphisms is where the appeal to a result from surgery theory comes into play, and the general gist is as follows. First consider a closed 3-manifold with internal ribbon graph. A known result states that every closed, connected and oriented 3-manifold can be obtained from a 3-sphere via surgery on a link. A intimate knowledge of what 'surgery on a link' means is not necessary for this thesis; it suffices to know that we can evaluate the ribbon graph in the original closed 3-manifold by considering the same ribbon graph, with an extra uncoloured link corresponding to the surgery, as residing in the 3-sphere, and equivalently in $\mathbb{R}^3$. This graph is evaluated via the usual method (see Appendix A) by summing over simple objects of $\mathcal{C}$ for the uncoloured link.

Remark 3.4.1. The calculations done with the Reshetikhin-Turaev defect TQFT in the next chapter are more or less reduced to this point at some stage. However, since we are considering the defect TQFT over vect_c, the only simple object is $\mathbb{C}$. Furthermore, the braiding on $\mathrm{vect}_{\mathbb{C}}$ is trivial, so we can in fact, by subsequent applications of the braiding, "pull" the link corresponding to the surgery out of the ribbon graph so the two are disjoint. At this point, since $\mathbb{C}$ is the ground field as well as the simple object, this tensor product (disjoint union) of the ribbon graph and the link coloured by $\mathbb{C}$, evaluates to something that is equivalent to the evaluation of the ribbon graph on its own. Thus, we are able to largely ignore the effects of the surgery in the next chapter, and basically consider the ribbon graph in the 3-manifold as a ribbon graph in $\mathbb{R}^3$.

To get an idea of how a 3-manifold with boundary is evaluated by $\mathcal{Z}_{RT,\mathcal{C}}$, we note that any such 3-manifold can be transformed into a closed 3-manifold by gluing a 3-manifold of a similar form to that in Figure 3.6 to each component of the boundary, and then proceeding as above. This produces a morphism between the vector spaces assigned to the boundaries surfaces via $\overline{\mathcal{Z}}^{\mathcal{C}}_{RT}$ (and hence $\mathcal{Z}_{RT,\mathcal{C}}$).

For a proof that $\mathcal{Z}_{RT,\mathcal{C}}$ as per (the more rigorous version of) the discussion above is an anomaly-free, non-degenerate TQFT see [Theorem IV.9.2.1 Tur16].

3.4.2 The Defect TQFT

It has already been mentioned that the defect Reshetikhin-Turaev TQFT, denoted $\mathcal{Z}^{\mathrm{df}}_{RT,\mathcal{C}}$ evaluates objects and morphisms in $\mathbf{Bord}_3^{\mathrm{df}}(\mathbb{D})$ by transforming them so that they can be evalauted by the original Reshetikhin-Turaev TQFT from the previous subsection. By comparing the bordism category $\mathbf{Bord}^3_{\mathrm{wt}}$ above with the bordism category $\mathbf{Bord}_3^{\mathrm{df}}(\mathbb{D})$ in Section 3.2.2, the similarities between objects and morphisms are stark. In fact, the defect TQFT transforms both $\mathbb{D}$-decorated surfaces and $\mathbb{D}$-decorated bordisms into weighted extended 3-manifolds, before passing to the anomaly-free Reshetikhin-Turaev TQFT.

Before we look at the details of this reduction process, we need to look more closely at what information is packed into the defect data $\mathbb{D}$ [Section 2.1, CR12]. Again, throughout $\mathcal{C}$ denotes a modular tensor category over a field $\Bbbk$.

Definition 3.4.2. The set of **defect data** $\mathbb{D} = (D_3^{\mathcal{C}}, D_2^{\mathcal{C}}, D_1^{\mathcal{C}}, s, t, j)$ associated to a modular tensor category

$\mathcal{C}$ is as follows

- $D_3^{\mathcal{C}}$ is the one element set $\{\mathcal{C}\}$;
- $D_2^{\mathcal{C}}$ is the set of Δ-separable symmetric Frobenius algebras in $\mathcal{C}$;
- $D_1^{\mathcal{C}}$ is defined to be the disjoint union

  $$D_1^{\mathcal{C}} := \sqcup_{n\in\mathbb{Z}_{\geq 0}} L_n$$

  where $L_0 = \{X \in \mathcal{C} | \theta_X = \mathrm{id}_X\}$ and for $n > 0$

  $$L_n = \{((A_1, \epsilon_1), (A_2, \epsilon_2), ..., (A_n, \epsilon_n), M)\}$$

  with the $A_i \in D_2^{\mathcal{C}}$, the $\epsilon_i \in \{+, =\}$ and M is a cyclic $(A_1^{\epsilon_1}, ..., A_n^{\epsilon_n})$-multi-module;
- $s(A, \pm) = t(A, \pm) = \mathcal{C}$ for all $A \in D_2^{\mathcal{C}}$;
- $j(M) = \mathcal{C}$ for $n = 0$ and for $n > 0$,

  $$j((A_1, \epsilon_1), ..., (A_n, \epsilon_n), M) = ((A_1, \epsilon_1), ..., (A_n, \epsilon_n))/C_n$$

  where C_n denotes the cyclic group.

Pursuant to Remark 3.2.11, there is also the set D_0 that is relevant to the evaluation of $\mathcal{Z}^{\mathrm{df}}_{RT,\mathcal{C}}$ on bordisms with internal 0-strata, which is commented upon below, but most of the details are again suppressed until the appendices.

For the set $D_2^{\mathcal{C}}$, we need the following definition:

Definition 3.4.3. A **Frobenius algebra** in $\mathcal{C}$ is a tuple $(A, \nabla, \eta, \Delta, \delta)$ where A is an object of $\mathcal{C}$, (A, ∇, η) is an associative unital algebra, (A, Δ, δ) is a coassociative counital coalgebra, and

$$(\nabla \otimes \mathrm{id}_A) \circ (\mathrm{id}_A \otimes \Delta) = \Delta \circ \nabla = (\mathrm{id}_A \otimes \nabla) \circ (\Delta \otimes \mathrm{id}_A)$$

A Frobenius algebra is **symmetric** if $\delta \circ \nabla = \delta \circ \nabla \circ c_{A,A} \circ (\mathrm{id}_A \otimes \theta_A)$ and is **Δ-separable** if $\nabla \circ \Delta = \mathrm{id}_A$.

By describing how the defect TQFT evaluates surfaces $(\Sigma, \mathcal{L}) \in \mathbf{Bord}_3^{\mathrm{df}}(\mathbb{D})$, we gain insight on how to produce the set of defect data D_0. This evaluation proceeds as follows. Consider the cylinder $C_\Sigma = \Sigma \times [0, 1]$ where any 1- and 0-strata of Σ are extended to 2- and 1-strata respectively of C_Σ. To each 1-strata labelled by $((A_1, \epsilon_1), ..., (A_n, \epsilon_n), M)$, associate a ribbon labelled by M (where the framing of the strand is compatible with the cyclicity of the module M - this is made precise in [CRS17] but doesn't feature heavily in this thesis). For each 2-strata labelled with Frobenius algebra A_i, triangulate the 2-strata, then decorate the (oriented) Poincaré dual of this triangulation with A_i for each edge, and either ∇ or Δ to each point depending on the orientations of the incoming and outgoing edges. Thicken these lines to ribbons. Note that the triangulation of the 2-strata of C_Σ induces a triangulation t of the 1-strata in Σ and turn C_Σ into a bordism between two surfaces with marked points. To the intersections where the A-ribbons connect with an adjacent M-ribbon, associate the action $\rho : A_i \otimes M \to M$ or $\rho : M \otimes A_i \to M$ depending on the orientations.

In this way, C_Σ has become a weighted extended 3-manifold (we can just assign a 0 weight to the cylinder) and hence can be evaluated by $\mathcal{Z}_{RT,\mathcal{C}}$ to produce a morphism $\psi^{\Sigma}_{t,t'} : \mathcal{Z}_{RT,\mathcal{C}}(\Sigma_t, \mathcal{L}) \to \mathcal{Z}_{RT,\mathcal{C}}(\Sigma_{t'}, \mathcal{L})$, where Σ_t and $\Sigma_{t'}$ are the extended surfaces in the boundary of C_Σ with coloured points induced by the triangulations above. Once again an inverse limit construction over the $\mathcal{Z}_{RT,\mathcal{C}}(\Sigma_t)$ and $\psi^{\Sigma}_{t,t'}$ defines $\mathcal{Z}^{\mathrm{df}}_{RT,\mathcal{C}}$, and again we can take

$$\mathcal{Z}^{\mathrm{df}}_{RT,\mathcal{C}}(\Sigma) \cong \mathrm{Im}(\psi^{\Sigma}_{t,t})$$

for any triangulation t.

The defect data set D_0 can be produced by evaluating defect spheres around internal 0-strata using the above method. That is, by inserting a sphere around a 0-stratum in the interior of a defect bordism, one can consider the intersection of the 2- and 1-strata incident to this 0-stratum as 1- and 0-strata on the sphere, turning it into a defect surface ready to be evaluated (see Appendix C.2.2 or [Section 2.4, CRS19] for more details). The elements of D_0 seen in this thesis (as part of the orbifold data introduced in the next chapter) can typically be viewed as morphisms between tensor products of multi-modules, or simply as elements of the ground vector space (that is, an element of the evaluation of $\mathcal{Z}^{\mathrm{df}}_{RT,\mathcal{C}}$ on the undecorated sphere).

The evaluation on an arbitrary bordism in $\mathbf{Bord}^{\mathrm{df}}_3(\mathbb{D})$ proceeds in a similar fashion, just now with the added data for 0-strata. By the same construction regarding labelling the Poincaré dual of triangulations of 2-strata and by thickening lines into ribbons, a weighted extended manifold with a $\mathcal{C}$-coloured ribbon graph inside it is produced which can then be passed to $\mathcal{Z}_{RT,\mathcal{C}}$. This construction can be shown to be independent of triangulations of the 2-strata that don't meet the boundary, and the effect of the triangulation on the boundary surfaces can be removed by an inverse limit.

Remark 3.4.4. One may have noted that the Lagrangian space $\mathcal{L}$ that makes up part of the definition of an object of $\mathbf{Bord}^{\mathrm{df}}_3(\mathbb{D})$ doesn't make its presence felt in the above discussion. The role of the Langragian space resides entirely in the realm of the original Reshetikhin-Turaev TQFT and plays no further part with respect to defects and the evaluation of $\mathcal{Z}^{\mathrm{df}}_{RT,\mathcal{C}}$ other than when this is reduced to $\mathcal{Z}_{RT,\mathcal{C}}$. As a result, $\mathcal{L}$ will largely be dropped from consideration, especially in the calculations of Chapter 5.

Chapter 4

Orbifolds of TQFTs

The aim of this chapter is to introduce the orbifold construction of the defect Reshetikhin-Turaev TQFT mentioned briefly in the previous chapter and required for the next (the best references to become acquainted with the orbifold construction are [CRS19; CRS17; CRS18]). This orbifold construction produces an equivalence between the defect TQFT evaluated over $\mathrm{vect}_{\mathbb{C}}$ and the Turaev-Viro graph TQFT evaluated over $\mathbb{Z}_2$- $\mathrm{vect}_{\mathbb{C}}$ and represents the key motivation for considering the Reshetikhin-Turaev defect TQFT as a potential model for quantum error-correcion. Before detailing the orbifold construction in the context of TQFTs, we take a moment to introduce orbifolds in their initial context in order to generate some intuition as to why the term 'orbifold' is appropriate in the TQFT setting, and why an orbifold of a defect TQFT might output something that is similar to a state sum TQFT like the Turaev-Viro-Barrett-Westbury TQFT. Orbifolds of 2-dimensional TQFTs are marginally easier to understand than the 3-dimensional case, so they are examined first as a stepping stone to the 3-dimensional case. For a more rigorous approach to the usual notion of orbifolds generally, see [Thu79], and for orbifolds of defect TQFTs specifically, see [CRS19; CR12].

4.1 Orbifolds

The concept of an orbifold, first introduced in a slightly different form by Satake [Sat57] and then by Thurston [Thu79] in a closer form to the following, is a generalisation of the concept of a manifold to include a group acting on the underlying topological space. Let G be a finite group that acts faithfully and properly discontinuously on $\mathbb{R}^n$ such that for all $g \in G$ and $U \subset \mathbb{R}^n$, $g(U) \subset U$. Let U/G denote the topological space defined as the space of orbits of U under G and given the quotient topology. Paralleling the definition of manifold, an **orbifold** is a topological Hausdorff space X such that for each element U of a set of open sets $\mathcal{U}$ that cover X, there is a homeomorphism $\phi_U : U \to U/G$, such that all U and ϕ_U satisfy certain compatibility conditions ([Thu79]).

Instead of considering G acting on $\mathbb{R}^n$, if we considered G acting (properly discontinuously) on the manifold

X directly, then X/G has the structure of an orbifold ([Proposition 13.2.1, Thu79]). Denote by $\rho : X \to X/G$ the quotient map (which is continuous). Let Y be another topological space, and denote by $C(X, Y)$ the set of all continuous maps from X to Y. Consider the following map:

$$H : C(X/G, Y) \to C(X, Y)$$
$$f \mapsto f \circ \rho$$

In particular, this means that for $f \in C(X, Y)$ and all $g \in G$ and $x \in X$, $f(x) = f(gx)$, or in other words, f is constant on orbits.

Now since G acts continuously on X, each $g \in G$ defines a homeomorphism $g : X \to X$. We can then define a right G-action on $C(X, Y)$ as follows:

$$C(X, Y) \times G \to C(X, Y)$$
$$(f, g) \mapsto f \circ g$$

Since $f \in C(X, Y)$ is constant on orbits if and only if $f \circ g = f$, we can identify

$$\mathrm{Im}(H) = C(X, Y)^G$$

where $C(X, Y)^G$ denotes the G-invariant subset of $C(X, Y)$. This induces a bijection natural in Y:

$$C(X/G, Y) \cong C(X, Y)^G. \tag{4.1}$$

We now take the first step in the process that will allow us to generalise this perspective of orbifolds. Recall a functor $F' : \mathcal{C} \to \mathbf{Set}$ is **representable** if there exists an object $R \in \mathcal{C}$, called the **representing object** such that F is naturally isomorphic to $\mathrm{Hom}_{\mathcal{C}}(R, \cdot)$. Let us denote the category of topological spaces, that is, the category with objects as topological spaces and morphism as continuous maps between them, by **Top**, and the category of sets by **Set**. Let us consider the following functor

$$F : \mathbf{Top} \to \mathbf{Set}$$
$$Y \mapsto C(X, Y)^G$$

The orbifold X/G is a representing object for this functor by Equation (4.1)

More generally, if $\mathcal{C}$ is a category, G is a finite group and $X \in \mathcal{C}$ is an object with a G-action

$$\alpha : G \to \mathrm{Aut}_{\mathcal{C}}(X)$$

an **orbifold** of $X \in \mathcal{C}$ by the action of G is a pair $(X/G, \rho)$ consisting of a representing object X/G of the functor

$$\mathrm{Hom}_{\mathcal{C}}(X, \cdot)^G : \mathcal{C} \to \mathbf{Set}$$
$$Y \mapsto \mathrm{Hom}_{\mathcal{C}}(X, Y)^G$$

where $\mathrm{Hom}_{\mathcal{C}}(X,Y)^G$ is the subset of G-invariant maps $f : X \to Y$, and $\rho : X \to X/G$ corresponds under the bijection $\mathrm{Hom}_{\mathcal{C}}(X/G, X/G) \cong \mathrm{Hom}_{\mathcal{C}}(X, X/G)^G$ to $1_{X/G}$.

The representing object X/G need not exist in $\mathcal{C}$ but it is possible to embed $\mathcal{C}$ in a "bigger" category $\hat{\mathcal{C}}$ that does contain X/G as an object (and ρ as a morphism), which leads to the notion of the orbifold completion of a category $\mathcal{C}$.

We discuss one more abstraction in the present context as preparation for the next two sections. The group G and its action on an object $X \in \mathcal{C}$ can be reformulated as follows. We can consider G as a catgeory $\underline{G}$ that has a single object $*$, and morphisms such that $\mathrm{Hom}_{\mathcal{C}}(*, *) = G$. The group homomorphism α above is then viewed as a functor A:

$$\begin{aligned} A : \underline{G} &\to \mathcal{C} \\ * &\mapsto X \\ g &\mapsto A(g) = \alpha(g) \in \mathrm{Aut}_{\mathcal{C}}(X) \end{aligned}$$

This abstraction doesn't buy us anything in the present context, but generalises in a useful way, as we shall shortly see.

4.2 Orbifolds of 2-dimensional Defect TQFTs

Up until now, 2-dimensional defect TQFTs have not made an appearance within this thesis, nor are they pertinent to any other section than the current one. The reason that they have been included here is to conceptually bridge the gap between orbifolds as presented earlier and orbifolds of 3-dimensional defect TQFTs in the next section. The finer details of 2-dimensional defect TQFTs $\mathcal{Z}^{\mathrm{df}}$ are not explictly needed beyond a few comments regarding 2-dimensional defect data $\mathbb{D}$ and the corresponding defect bordism category $\mathbf{Bord}_2^{\mathrm{df}}(\mathbb{D})$, which are the 2-dimensional analogues of those introduced in the preceding chapter.

A set of **defect data** for a 2-dimensional defect TQFT is a tuple $(D_2, D_1; s, t)$ where D_2, D_1 are sets whose elements label 2- and 1-strata respectively, and s, t are maps that enforce compatibility of adjacent labellings. For the present discussion, we need only know a little more about the set D_2, which is a set of "phases" or "theories". Just as for the defect data associated to the Reshetikhin-Turaev defect TQFT outlined in the previous chapter, there is a set D_0 for labels on 0-strata, which can be computed directly from the TQFT $\mathcal{Z}^{\mathrm{df}}$ and the tuple given above (see Appendix C).

This entices us to consider the orbifold of a theory $\mathcal{Z}_{\mathcal{C}}^{\mathrm{df}}$ as the orbifold of the element $\mathcal{C} \in D_2$ viewed as an object in some category, just as in the end of the previous section. However, the defect TQFT $\mathcal{Z}_{\mathcal{C}}^{\mathrm{df}}$ encodes much more information than just the category upon which it is based, so it is not enough to consider $\mathcal{C}$ as an object in a 1-category, but rather we need a formulation in a higher category, namely a strictly pivotal bicategory [Section 3.2, CR12]. Let us quickly introduce bicategories before discussing their equivalence to 2-dimensional defect TQFTs.

A **bicategory** $\mathcal{B}$ consists of the following data:

- a class of objects $a \in \mathcal{B}$;
- for each $a, b \in \mathcal{B}$, there is a category $\mathcal{B}(a,b)$ whose objects are 1-morphisms $f, g : a \to B$ and whose morphisms are called 2-morphisms $\phi : f \to g$;
- 1-morphisms are composed via the family of functors

$$\kappa_{abc} : \mathcal{B}(b,c) \times \mathcal{B}(a,b) \to \mathcal{B}(a,c)$$

  where a, b, c run over the objects of $\mathcal{B}$. For $a, b, c \in \mathcal{B}$, 1-morphisms $f, f' : a \to b$ and $g, g' : b \to c$, and 2-morphisms $\phi : f \to f'$ and $\psi : g \to g'$, we write $f \otimes g = \kappa_{abc}(f,g)$ and $\psi \otimes \phi = \kappa_{abc}(\psi, \phi)$;
- for any triple of composable 1-morphisms f, g, h, there is a 2-isomorphism $\alpha_{f,g,h} : (f \otimes g) \otimes h \to f \otimes (g \otimes h)$, called the **associator**, and for every $a \in \mathcal{B}$ there is a unit 1-morphism $1_a \in \mathcal{B}(a,a)$ along with natural 2-isomorphisms

$$\lambda_f : 1_b \otimes f \to f$$
$$\rho_f : f \otimes 1_a \to f$$

  for every $f \in \mathcal{B}(a,b)$. The 2-isomorphisms satisfy coherence conditions that are not currently important, and are deferred to [Chapter 7, Bor94].

An **adjunction** $f \vdash g$ in a bicategory $\mathcal{B}$ is a pair of 1-morphisms $f \in \mathcal{B}(a,b)$ and $g \in \mathcal{B}(b,a)$ together with 2-morphisms $\epsilon : f \otimes g \to 1_b$ and $\eta : 1_a \to g \otimes f$ that satisfy certain conditions (see [Section 2.1, CR12]). $\mathcal{B}$ is a **bicategory with left adjoints** if for every $f \in \mathcal{B}(a,b)$ there is a ${}^\dagger f \in \mathcal{B}(b,a)$ and a choice of adjunction ${}^\dagger f \vdash f$, and similarly for a bicategory with right adjoints. $\mathcal{B}$ is a **bicategory with adjoints** if it has left and right adjoints. Analogously to the 1-categorical case, $\mathcal{B}$ is **pivotal** if the left and right adjoints coincide for every 1-morphism, and the chosen adjunctions satisfy certain conditions (again see [CR12]). The adjective 'strict' in the case of 2-categories is also analogous to that of 1-categories, in that the associator α and the left and right unit maps λ and ρ are identity in strict 2-categories, as opposed to simply isomorphism as with general bicategories.

According to Theorem 3.2 in [CR12], every 2-dimensional defect TQFT $\mathcal{Z}_{\mathcal{C}}^{\mathrm{df}} : \mathbf{Bord}_2^{\mathrm{df}}(\mathbb{D}) \to \mathrm{vect}_{\mathbb{C}}$ gives rise to a strictly pivotal 2-category $\mathcal{D}_{\mathcal{Z}}$. This pivotal 2-category is defined roughly as follows. The set of objects of $\mathcal{D}_{\mathcal{Z}}$ is the set D_2 from the defect data, which we take to consist of a single element $\mathcal{C}$. The 1-morphisms are defined to be finite formal sums of sequences of composable elements of D_1 with associated signs, where composable has a formal definition (not presented here) in terms of compatibility via the source and target maps s and t. The identity 1-morphism is the empty sequence and the product '$\otimes$' is concatenation of sequences. The 2-morphism spaces, compositions and adjunction maps are all defined by evaluating $\mathcal{Z}_{\mathcal{C}}^{\mathrm{df}}$ on specific objects of $\mathbf{Bord}_2^{\mathrm{df}}(\mathbb{D})$, namely the circle S^1 with marked points of various particular labellings (again see [CR12] for more details).

We now have a way of expressing our to-be-orbifolded TQFT $\mathcal{Z}_{\mathcal{C}}^{\mathrm{df}}$ in terms of a bicategory, but we still need to detail what is meant by the action of a finite group G on this bicategory, which we do via the bicategorical version of the construction at the end the previous section. Before doing so, let us introduce the concept of orbifold data, which is simply a choice of elements from each set of the defect data $\mathbb{D}$ such that the evaluation of a specific defect bordism labelled solely by this choice of data is equivalent to the evaluation of a related bordism by a different TQFT (more comments on this are made below). We will then discuss how this orbifold data arises from a specific type of 2-functor from the bicategory associated to a finite group G to the bicategory associated to $\mathcal{Z}_{\mathcal{C}}^{\mathrm{df}}$.

Definition 4.2.1. An **orbifold datum** for a 2-dimensional defect TQFT $\mathcal{Z}^{\mathrm{df}} : \mathbf{Bord}_2^{\mathrm{df}}(\mathbb{D}) \to \mathrm{Vect}_{\Bbbk}$ is a tuple $\mathcal{A} = (\mathcal{C}, A, \nabla, \Delta)$ where $\mathcal{C}$ is the single element in D_2, $A \in D_1$ is a Δ-seperable symmetric Frobenius algebra (see Definition 3.4.3), and $\nabla, \Delta \in D_0$ are the multiplication and comultiplication maps of A respectively. The unit and counit maps can be produced by evaluating $\mathcal{Z}^{\mathrm{df}}$ on appropriately decorated surfaces (see [CR12]).

Remark 4.2.2. In the literature regarding orbifolds of TQFTs (e.g. [CR12; CRS19; CRS18]) the orbifold datum above is called special as a more general definition of orbifold datum can be given.

The condition that A be a Δ-separable symmetric Frobenius algebra is equivalent to imposing the condition that $\mathcal{Z}^{\mathrm{df}}$ evaluated on the Poincaré dual of a triangulation of a 2-manifold labelled by A, ∇ and Δ is invariant under the (dual of the) Pachner moves [Proposition 3.4, CR12]. This pre-empts how the orbifold theory is computed, by labelling the Poincaré dual of a triangulation by the orbifold datum $\mathcal{A}$.

Returning to the action of a finite group G on the bicategory $\mathcal{D}_{\mathcal{Z}}$, let us define the bicategory $\underline{\underline{G}}$ similarly to the category $\underline{G}$: let $\underline{\underline{G}}$ be the bicategory with a single object $*$, the space of 1-morphisms $\mathrm{Hom}(*, *)$ is the group G, and all 2-morphisms are identity. Due to the richer structure of bicategories, there is a more varied class of 2-functors between them. In particular, we want to define the action of G on $\mathcal{D}_Z$ by considering a **lax-oplax functor** from $\underline{\underline{G}}$ to $\mathcal{D}_{\mathcal{Z}}$, which will be denoted by $\mathcal{A}$ in order to emphasise the relation to the orbifold datum above. The precise definition of a lax-oplax functor is not given here (see instead [Bor94]) but in essence a lax-oplax functor $\Phi : \mathcal{B} \to \mathcal{D}$ is a type of 2-categorical analogue of a functor with some equalities relaxed to hold up to isomorphism or more generally, and consists of the following data:

- a function from the objects of $\mathcal{B}$ to those of $\mathcal{D}$;
- a functor from the category $\mathcal{B}(a, b)$ to $\mathcal{D}(\Phi(a), \Phi(b))$ for all objects a and b in $\mathcal{B}$;
- 2-morphisms relating $1_{\phi(a)}$ and $\phi(1_a)$ for all objects a in $\mathcal{B}$;
- a family of natural transformations;

all of which is required to satisfy certain coherence relations.

In particular, a lax-oplax functor $\mathcal{A} : \underline{\underline{G}} \to \mathcal{D}_{\mathcal{Z}}$ specifies an object of $\mathcal{D}_{\mathcal{Z}}$, of which there is only one choice $\mathcal{C}$, an object A of $\mathcal{D}_{\mathcal{Z}}(\mathcal{C}, \mathcal{C})$, 2-morphisms η and δ, and natural transformations ∇ and Δ. The coherence relations precisely correspond to the conditions making $(A, \nabla, \eta, \Delta, \delta)$ into a Frobenius algebra.

Remark 4.2.3. It seems as though the extra conditions of symmetry and Δ-separability that are placed on the Frobenius algebra A are additional to those conditions enforced by the lax-oplax functor. More work is required to investigate the origins of these conditions within this functorial framework, however this is beyond the scope of this thesis.

The action of G on an object x of $\mathcal{D}_{\mathcal{Z}}$ is then defined similarly to the end of the previous section as $\mathcal{A}$ where $\mathcal{A}(g) \in \mathcal{D}_{\mathcal{Z}}(x, x)$. The orbifold of x by G is also defined similarly to above, this time as a representing object of a pesudofunctor from $\mathcal{D}_{\mathcal{Z}}$ to the bicategory **Cat**. Once again, this representing object may not be contained in the bicategory $\mathcal{D}_Z$, but rather in a related category $\mathcal{D}_{\mathcal{Z}}^{\mathrm{orb}}$.

4.3 Orbifolds of 3-dimensional Defect TQFTs

In this final section, we comment briefly upon the analogous situation to the previous section on 2-dimensional TQFTS for the 3-dimensional defect TQFT of interest: the Reshetikhin-Turaev defect TQFT. A rigorous treatment of the details presented here is beyond the scope of this thesis. This section does, however, provide a perfect opportunity to introduce the orbifold data for the Reshetikhin-Turaev defect TQFT based on $\mathrm{vect}_{\mathbb{C}}$ required for the next chapter, as well as the equivalence between this defect TQFT and the Turaev-Viro-Barrett-Westbury TQFT for a given spherical fusion category.

Recall from Definition 3.4.2, that the defect data for the Reshetikhin-Turaev defect TQFT is a tuple $\mathbb{D} = (D_3, D_2, D_1, D_0, s, t, j)$ where D_3, D_2 and D_1 are the sets $\{\mathcal{C}\}$, the set of Δ-separable symmetric Frobenius algebras in $\mathcal{C}$, and a set of tuples based on multi-modules resepctively, and where s, t and j are maps that enforce compatibility of labellings of strata by elements of D_3, D_2 and D_1. The set D_0 consists of maps between tensor products of multi-modules (see [CRS18]).

In the following chapter, we consider the Reshetikhin-Turaev defect TQFT over $\mathrm{vect}_{\mathbb{C}}$, so we are taking $\mathcal{C} = \mathrm{vect}_{\mathbb{C}}$ in the above defect data. For a given spherical fusion category $\mathcal{S}$, we can write down the orbifold datum internal to $\mathrm{vect}_{\mathbb{C}}$ and associated to $\mathcal{S}$. Let I be a representative set of simple objects for $\mathcal{S}$.

Definition 4.3.1. The **orbifold datum** $\mathcal{A}_{\mathcal{S}}$ of $\mathcal{Z}^{\mathrm{df}}_{RT,\mathrm{vect}_{\mathbb{C}}}$ associated to $\mathcal{S}$ is

- $\mathcal{A}_3 = \mathrm{vect}_{\mathbb{C}}$;
- $\mathcal{A}_2 = \bigoplus_{i \in I} \mathbb{C}$, where $\mathbb{C}$ is considered as a (Δ-separable symmetric) Frobenius algebra;
- $\mathcal{A}_1 = \bigoplus_{i,j,k \in I} \mathrm{Hom}_{\mathcal{S}}(i \otimes j, k)$ considered as a multi-module and where $\mathcal{A}_2$ acts on each factor by the kth factor $\mathbb{C}$ on the left and by the tensor product of the ith and jth factors $\mathbb{C} \otimes \mathbb{C}$ on the right;
- $A_0^+, \mathcal{A}_0^- : \mathcal{A}_1 \otimes_{\mathcal{A}_2} \mathcal{A}_1 \to A_1 \otimes_{\mathcal{A}_2} A_1$ are maps based on the fusion rules of $\mathcal{S}$ (see below) that label 0-strata at the intersection of 1-strata; and
- ψ^2 and ϕ in D_0 label 0-strata in the interior of 2- and 3-strata respectively, and where ψ^2 is an $|I| \times |I|$ diagonal matrix with entries the dimensions of the elements $i \in I$, and where $\phi = \dim(\mathcal{S})$.

To define the maps $\mathcal{A}_0^{\pm}$, let us denote basis elements of the first tensor factor T of the domain by λ and λ' and basis elements of the second factor by μ and μ'. Then

$$\mathcal{A}_0^{+} : \lambda \otimes \mu \mapsto \sum_{i \in I, \lambda', \mu'} (\dim i)^{-1} F_{\mu\mu'}^{\lambda\lambda'} \cdot \lambda' \otimes \mu'$$

where the sum is over all elements of I and basis elements of each factor T. Similarly, the map $\mathcal{A}_0^{-}$ is defined by

$$\lambda \otimes \mu \mapsto \sum_{i \in I, \lambda', \mu'} (\dim i)^{-1} (F^{-1})_{\mu\mu'}^{\lambda\lambda'} \cdot \lambda' \otimes \mu'$$

Remark 4.3.2. In the above two equations, the factor F is the F-tensor associated to fusion rules (an example is given in Example 3.1.15), and is not to be confused with say the functor also labelled F earlier in this chapter.

From the point of view of generalised orbifolds taken in this chapter, we want to be able to consider the Reshetikhin-Turaev defect TQFT in some categorical sense, and then consider an object corresponding to invariance under the action of a finite group, just as in the 2-dimensional case above. It turns out that every 3-dimensional defect TQFT gives rise to a variation of a tricategory, namely a Gray category with duals [Theorem 1.1, CMS16]. It is also possible to define a Gray category $\overline{\underline{\underline{G}}}$ from the finite group G in a parallel fashion to the bicategory $\underline{\underline{G}}$ from the previous section, where all 3-morphisms are also taken to be identity.

Here we become most conjectural, and, to reiterate the comments made at the start of this chapter, the following paragraph is simply an attempt to provide intuition regarding orbifolds of the Reshetikhin-Turaev defect TQFT. If we consider the orbifold data for the 2-dimensional defect TQFT and the Reshetikhin-Turaev defect TQFT it is possible to see some similarities (in fact the orbifold data for n-dimensional defect TQFTs are similar for all n due to the recursive nature of their definitions [Definitions 2.4 and 3.5, CRS19]). In particular, Frobenius algebras appear in both sets of data. As we have seen above, in the 2-dimensional case, these Frobenius algebras arise naturally from the structure of the lax-oplax functor $\underline{\underline{G}} \to \mathcal{D}_{\mathcal{Z}}$, and so it seems reasonable to suspect that a generalisation of such a functor to the Gray category setting may produce similar results, encapsulating much of the orbifold data for the Reshetikhin-Turaev defect TQFT. Assuming such a generalisation is possible, then the definition of the orbifold of the Reshetikhin-Turaev defect TQFT would proceed as it has done in the bicategory setting above.

We end this chapter by stating a result due to Carqueville, Runkel and Schaumann that provides part of the motivation for considering defect TQFTs in the context of error-correction, and the foundation of the following chapter:

Theorem 4.3.1. *[Theorem 4.5, CRS18] For any spherical fusion category $\mathcal{S}$ there is a natural isomorphism between the Turaev-Viro-Barrett-Westbury TQFT based on $\mathcal{S}$ and the $\mathcal{A}_{\mathcal{S}}$-orbifold of the Reshetikhin-Turaev defect TQFT based on* $\mathrm{vect}_{\mathbb{C}}$.

In the next chapter we will see how to actually compute the orbifold of the Reshetikhin-Turaev defect TQFT via a specific example, the orbifold of a defect torus, but we pre-empt some of those details here in order to round out our intuition as to why the orbifold produced something similar to a state sum. Recalling the comments made at the start of Section 3.3, the Turaev-Viro-Barrett-Westbury TQFT evaluates a manifold by triangulating it and averaging over the states assigned to each component of the triangulation. In practice, the orbifolding of the Reshetikhin-Turaev defect TQFT proceeds in a similar fashion: the orbifold data is assigned to the Poincaré dual of a triangulation of a 3-manifold, and then evaluated by the TQFT, which is paramount to "averaging" over this data.

Chapter 5

The TQFT Picture for the Toric Code

The entire basis for this thesis rests upon a known result relating the toric code and the Turaev-Viro-Barrett-Westbury TQFT: the Turaev-Viro-Barrett-Westbury TQFT over the spherical fusion category $\mathbb{Z}_2\text{-}\operatorname{vect}_{\mathbb{C}}$ evaluated on the torus produces the code subspace of the toric code (this result was first encountered in the development of this thesis in [KKR10] but the introduction of [BK12] provides a clear overview of the relationship between Kitaev's models and the Turaev-Viro-Barrett-Westbury TQFT). This result is written succinctly as the following theorem, the proof of which is the topic of Section 5.1.

Theorem 5.0.1. *We have*

$$|(\Sigma, A)|_{\mathbb{Z}_2\text{-}\operatorname{vect}_{\mathbb{C}}} \cong H_{\text{code}}$$

where $\Sigma \in \boldsymbol{Bord}_3^{\operatorname{col}(\mathbb{Z}_2\text{-}\operatorname{vect}_{\mathbb{C}})}$ *is the torus,* A *is empty and* H_{code} *is the code subspace for the toric code.*

However, as Chapter 2 attests, there is more to quantum error-correction than just the code subspace, in particular knowledge of the projection map onto that subspace is vital. Unfortunately, there does not seem to be any natural way of formulating this projection mapping within the confines of the Turaev-Viro-Barrett-Westbury TQFT, that is, from a morphism in $\mathbf{Bord}_3^{\operatorname{col}(\mathbb{Z}_2\text{-}\operatorname{vect}_{\mathbb{C}})}$ that contains enough structure to describe the projection mapping for the toric code defined on a specific lattice. So in order to model quantum error-correction via a topological quantum field theory, we need to search further afield. Firstly, the Turaev-Viro-Barrett-Westbury TQFT generalises slightly to the Turaev-Viro graph TQFT but this generalisation is regarding *how* the TQFT is evaluated and rather than *what* it evaluates, so is equivalent to the Turaev-Viro-Barrett-Westbury TQFT and hence still not powerful enough for our needs (though the generalisation does simplify the proof of Theorem 5.0.1 slightly). Now, it is known that the Turaev-Viro-Barrett-Westbury TQFT based on a modular tensor category $\mathcal{C}$ and evaluated on a closed oriented 3-manifold M is equivalent to the following product involving the Reshetikhin-Turaev TQFT, also based on $\mathcal{C}$ [Theorem VII.4.1.1, Tur16]

$$|M|_{\mathcal{C}} = \mathcal{Z}_{RT,\mathcal{C}}(M)\mathcal{Z}_{RT,\mathcal{C}}(-M)$$

where $-M$ denotes the manifold M with opposite orientation. This result speaks to the fact that the Reshetikhin-Turaev TQFT is the more fundamental of the two TQFTs. The relationship between the Reshetikhin-Turaev TQFT and Turaev-Viro graph TQFT is strengthened by the more general equivalence between the Turaev-Viro graph TQFT based on a spherical fusion category $\mathcal{C}$ and the Reshetikhin-Turaev TQFT based on the modular tensor category $Z(\mathcal{C})$ (the centre of $\mathcal{C}$) [Theorem 17.1, TV17]. So it seems prudent to consider the Reshetikhin-Turaev TQFT as a candidate model for error-correction with the toric code. This investigation proceeds by making use of the Reshetikhin-Turaev defect TQFT, which extends the Reshetikhin-Turaev TQFT and, utilising the result from the end of the preceding chapter, leads us to the main theorem of this thesis:

Theorem 5.0.2. *Let* $\Sigma^{t^*,\mathcal{A}_{\mathbb{Z}_2\text{-}\mathrm{vect}_\mathbb{C}}} \in \boldsymbol{Bord}_3^{\mathrm{df}}(\mathbb{D})$ *be the* $\mathbb{D}$*-decorated torus with stratification arising from the dual of the triangulation* t *of the torus as defined in Figure 2.1 and labelled by the orbifold datum* $\mathcal{A}_{\mathbb{Z}_2\text{-}\mathrm{vect}_\mathbb{C}}$*. Then*

(i) $\mathrm{Im}(\mathcal{Z}^{\mathrm{df}}_{RT,\mathrm{vect}_\mathbb{C}}(C_\Sigma^{t^*,\mathcal{A}_{\mathbb{Z}_2\text{-}\mathrm{vect}_\mathbb{C}}})) = H_{\mathrm{code}}$*, and*

(ii) $\mathcal{Z}^{\mathrm{df}}_{RT,\mathrm{vect}_c}(C_\Sigma^{t^*,\mathcal{A}_{\mathbb{Z}_2\text{-}\mathrm{vect}_\mathbb{C}}}) = P_{\mathrm{vert}} \circ f$*,*

where $C_\Sigma^{t^*,\mathcal{A}_{\mathbb{Z}_2\text{-}\mathrm{vect}_\mathbb{C}}} \in \boldsymbol{Bord}_3^{\mathrm{df}}(\mathbb{D})$ *is the morphism used to define the* $A_{\mathbb{Z}_2\text{-}\mathrm{vect}_\mathbb{C}}$*-orbifold of* $\mathcal{Z}^{\mathrm{df}}_{RT,\mathrm{vect}_c}$ *on the undecorated torus,* f *is a projection from the domain of* $\mathcal{Z}^{\mathrm{df}}_{RT,\mathrm{vect}_c}(C_\Sigma^{t^*,\mathcal{A}_{\mathbb{Z}_2\text{-}\mathrm{vect}_\mathbb{C}}})$ *to* $\mathrm{Im}(P_{\mathrm{plaq}})$*,* H_{code} *is the code subspace of the toric code defined on* t^**, and* P_{vert} *is the component of the projection map* P_{code} *defined on the plaquettes of* t^**.*

The structure of this chapter is as follows. Section 5.1 is devoted to proving Theorem 5.0.1 and discussing the links to the projection map P_{code} of the toric code. This proof proceeds in two parts, written in Section 5.1.1 and Section 5.1.2. Section 5.1.1 relates the domain of the map $|\,\mathrm{id}_{(\Sigma,A)}, G, G|^\circ$ (recall Section 3.3.2) for Σ the torus, A the empty set and G a skeleton of Σ, to the vector space $\mathrm{Im}(P_{\mathrm{plaq}})$ where P_{plaq} is defined as the product of P_p projectors for $p \in G^{(0)}$ (recall Section 2.2 for the definitions of P_{plaq} and P_p). The remainder of the proof is completed in Section 5.1.2 by showing that $|\,\mathrm{id}_{(\Sigma,A)}, G, G|^\circ$ is precisely the projection P_{vert}, where P_{vert} is defined by the projectors P_v of Section 2.2 also defined from G. Section 5.1.3 makes some concluding remarks about Theorem 5.0.1 and highlights the key features that are also present in the proof of Theorem 5.0.2.

Section 5.2 is concerned with the proof of Theorem 5.0.2, with Section 5.2.1 laying some foundation for the bulk of the proof which is contained in Section 5.2.2. This proof has many similarities with that of Theorem 5.0.1, however the domain of the map $\mathcal{Z}^{\mathrm{df}}_{RT,\mathrm{vect}_c}(C_\Sigma^{t^*,\mathcal{A}_{\mathbb{Z}_2\text{-}\mathrm{vect}_\mathbb{C}}})$ differs to that of $|\,\mathrm{id}_{(\Sigma,A)}, G, G|^\circ$ in that it contains $\mathrm{Im}(P_{\mathrm{plaq}})$ as a proper subset (it is partly this feature that supports the choice of the defect TQFT over the Turaev-Viro graph TQFT as a model for error-correction). Section 5.2.1 outlines how the domain $|\,\mathrm{id}_{(\Sigma,A)}, G, G|^\circ$, and hence $\mathrm{Im}(P_{\mathrm{plaq}})$ can be recovered in the defect TQFT framework, and Section 5.2.2 relates the morphism $\mathcal{Z}^{\mathrm{df}}_{RT,\mathrm{vect}_c}(C_\Sigma^{t^*,\mathcal{A}_{\mathbb{Z}_2\text{-}\mathrm{vect}_\mathbb{C}}})$ to P_{vert}. Section 5.3 concludes this chapter with a discussion of the advantages and disadvantages of an error-correction model based on TQFTs in general, and the Reshetikhin-Turaev defect TQFT in particular.

5.1 The Turaev-Viro Graph TQFT and the Toric Code Subspace

Let $(\Sigma, A) \in \mathbf{Bord}_3^{\mathrm{col}(\mathbb{Z}_2\text{- vect}_{\mathbb{C}})}$ be the coloured surface where Σ is the torus and A is empty. Recall from Section 3.3.2 that the Turaev-Viro graph TQFT evaluates (Σ, A) by considering the isomorphism

$$|(\Sigma, A)|_{\mathbb{Z}_2\text{- vect}_{\mathbb{C}}} \cong \mathrm{Im}(|\,\mathrm{id}_{(\Sigma,A)}, G_A, G_A|^{\circ}) \tag{5.1}$$

where G_A is a graph defined from a skeleton G of Σ that interacts with A in a specific way (see Definition 3.3.2). In this case, since A is empty, $G_A = G$. The specific choice of G can be interpreted as a choice of lattice for defining the toric code as in Section 2.2. For example, one could take G to be the Poincaré dual (in red) of the triangulation t of the torus shown in black in Figure 5.1. Doing so would make the links between the proof of Section 5.1 and the toric code as in Example 2.2.3 most clear.

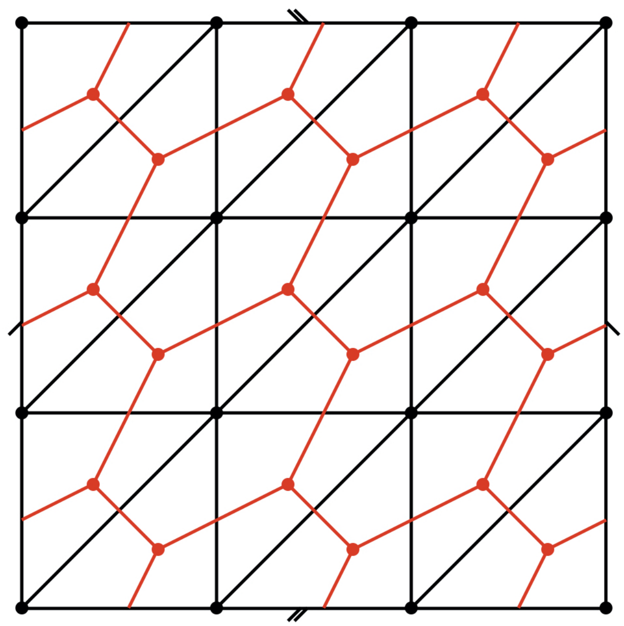

Figure 5.1: A skeleton G of the torus is denoted in red.

Remark 5.1.1. Neither the definition of the toric code in Section 2.2 nor the Turaev-Viro graph TQFT in Section 3.3 (and Appendix B) is required to be defined using a triangulation (or its dual), but can instead be defined on any cellulation of the torus. We will take G to be an arbitrary skeleton of Σ throughout this section, however it is necessary to note that the orbifold of the defect TQFT *is* defined via the Poincaré dual of a triangulation, and Theorem 5.0.2 is stated and proved for the specific t and t^* in Figure 5.1, so it may be useful to keep this example skeleton in mind.

Let us recall two things. Firstly, the map $|\,\mathrm{id}_{(\Sigma,A)}, G, G|^{\circ}$ is a map from $\bigoplus_{c\in\mathrm{col}(G)} \mathcal{H}(G^c)$ to itself (Section 3.3.1), and secondly the code subspace H_{code} for the toric code in Section 2.2 can be defined to be the image of the P_{vert} acting on $\mathrm{Im}(P_{\mathrm{plaq}})$. In consideration of these points and Equation (5.1), we state the following two propositions that constitute the proof of Theorem 5.0.1:

Proposition 5.1.1. *The vector spaces* $\bigoplus_{c\in\mathrm{col}(G)}\mathcal{H}(G^c)$ *and* $\mathrm{Im}(P_{\mathrm{plaq}})$ *are isomorphic, where* $P_{\mathrm{plaq}} = \prod_{p\in G^{(0)}} P_p$.

Proposition 5.1.2. *The map* $|\,\mathrm{id}_{(\Sigma,A)}, G, G|^{\circ}$ *is equal to* $P_{\mathrm{vert}} = \frac{1}{|\mathfrak{A}|}\sum_{g\in\mathfrak{A}} g$ *where* $\mathfrak{A}$ *is the group generated by operators* A_v *(see Definition 2.2.1) with* $v \in G^{(2)}$.

Recall that operators A_v and projectors P_p from Equation (2.7) and Equation (2.4) respectively. The notation $G^{(2)}$ is incorrect but useful; we take it to mean the set of connected components of $\Sigma \setminus G$, that is, the "plaquettes" of G. The proof of these propositions is precisely the proof Theorem 5.0.1 since H_{code} and $|(\Sigma, A)|_{\mathbb{Z}_2\text{-}\mathrm{vect}_{\mathbb{C}}}$ are then computed by the image of the same map from the same domain vector space.

5.1.1 The Domain of $|\,\mathrm{id}_{(\Sigma,A)}, G, G|^{\circ}$

The proof of Proposition 5.1.1 commences by analysing $\bigoplus_{c\in\mathrm{col}(G)}\mathcal{H}(G^c)$. Recall Equation (3.13):

$$\mathcal{H}(G^c) = \bigotimes_{p\in G^{(0)}} H_p$$

where H_p is as in Section 3.3.1 (though in that subsection, the subscript used was v) and c is a colouring of G. Since A is empty, G has no distinguished vertices (distinguished vertices were defined in Definition 3.3.2), and so we can write

$$\mathcal{H}(G^c) \cong \bigotimes_{p\in G^{(0)}} \mathrm{Hom}_{\mathbb{Z}_2\text{-}\mathrm{vect}_{\mathbb{C}}}(\mathbb{1}, c(e_1^p)^{\epsilon(e_1^p)} \otimes ... \otimes c(e_{|p|}^p)^{\epsilon(e_{|p|}^p)})$$

where the e_i^p are the incident edges of $p \in G^{(0)}$, $|p|$ is the valence of p and ϵ encodes the orientation of these edges towards or away from p (we are using 'p' instead of 'v' for the vertices of G in order to be consistent with the notation for P_{plaq}; recall the comments made in Remark 2.2.2). The isomorphism in the above equation is a specific cone isomorphism which is related to the projective system that is used to remove any dependence on the choice of cyclic ordering of edges when defining H_p as discussed in Remark 3.3.4 and in more detail in Appendix B. Now, the simple objects of $\mathbb{Z}_2\text{-}\mathrm{vect}_{\mathbb{C}}$ are $\mathbb{C}_0 = \mathbb{1}$ and $\mathbb{C}_1$ which we know are isomorphic to their duals, so we can ignore the $\epsilon(e_i^p)$ and write

$$\mathrm{Hom}_{\mathbb{Z}_2\text{-}\mathrm{vect}_{\mathbb{C}}}(\mathbb{1}, c(e_1^p)^{\epsilon(e_1^p)} \otimes ... \otimes c(e_{|p|}^p)^{\epsilon(e_{|p|}^p)}) \cong \mathrm{Hom}_{\mathbb{Z}_2\text{-}\mathrm{vect}_{\mathbb{C}}}(\mathbb{C}_0, \mathbb{C}_{i_1} \otimes ... \otimes \mathbb{C}_{i_{|p|}})$$

where the $i_k^p \in \{0,1\}$ for $k = 1, ..., |p|$ are defined by $c(e_k^p) \cong \mathbb{C}_{i_k^p}$ and again the superscript p is to emphasise the relation to $p \in G^{(0)}$. The claim here is that these hom-spaces associated to vertices enforce the same conditions as the plaquette projectors P_p for the toric code.

Recall from Example 3.1.15 the fusion rules of $\mathbb{Z}_2\text{-}\mathrm{vect}_{\mathbb{C}}$ and the definition of morphisms as being degree 0 maps. The fusion rules produce an isomorphism

$$\mathrm{Hom}_{\mathbb{Z}_2\text{-}\mathrm{vect}_{\mathbb{C}}}(\mathbb{C}_0, \mathbb{C}_{i_1^p} \otimes ... \otimes \mathbb{C}_{i_{|p|}^p}) \cong \mathrm{Hom}_{\mathbb{Z}_2\text{-}\mathrm{vect}_{\mathbb{C}}}(\mathbb{C}_0, \mathbb{C}_{i_1^p + ... + i_{|p|}^p \mod 2})$$

where $\mathbb{C}_{i_1^p+...+i_{|p|}^p \mod 2}$ is the result of sequential applications of the fusion rules to $\mathbb{C}_{i_1}\otimes...\otimes\mathbb{C}_{i_n}$ (this follows from Equation (3.12) and by noting that the result of successive application of the fusion rules of $\mathbb{Z}_2\text{-}\mathrm{vect}_{\mathbb{C}}$ is independent of the order in which they are applied). Now, by the definition of hom-spaces fpr $\mathbb{Z}_2\text{-}\mathrm{vect}_{\mathbb{C}}$ as being degree 0 maps, for $\mathrm{Hom}_{\mathbb{Z}_2\text{-}\mathrm{vect}_{\mathbb{C}}}(\mathbb{C}_0, \mathbb{C}_{i_1^p+...+i_{|p|}^p \mod 2})$ to be non-zero we require $i_1^p + ... + i_{|p|}^p = 0 \mod 2$. If we denote by $i \in \{0,1\}^{|G^{(1)}|}$ the vector with entries i_k defined by $c(e_{i_k}) \cong \mathbb{C}_{i_k}$ for all $e_{i_k} \in G^{(1)}$, and denote by $l_p \in \{0,1\}^{|G^{(1)}|}$ the vector with entries with value 1 correpsonding to the edges incident to p and 0's everywhere else, we get that $i \cdot l_p = i_1^p + ...i_{|p|}^p$ and so the condition $i_1^p + ...i_{|p|}^p = 0 \mod 2$ is precisely the condition $i \cdot l_p = 0 \mod 2$ imposed by P_p (see the discussion surrounding Equation (2.8)).

Using i defined from the colouring c as in the preceding paragraph, we can write

$$\begin{aligned}\bigoplus_{c\in\mathrm{col}(G)} \mathcal{H}(G^c) &= \bigoplus_{c\in\mathrm{col}(G)} \bigotimes_{p\in G^{(0)}} \mathrm{Hom}_{\mathbb{Z}_2\text{-}\mathrm{vect}_{\mathbb{C}}}(\mathbb{C}_0, c(e_1^p)^{\epsilon(e_1^p)} \otimes ... \otimes c(e_n^p)^{\epsilon(e_n^p)}) \\ &\cong \bigoplus_{i\in\{0,1\}^{|G^{(1)}|}} \bigotimes_{p\in G^{(0)}} \mathrm{Hom}_{\mathbb{Z}_2\text{-}\mathrm{vect}_{\mathbb{C}}}(\mathbb{C}_0, \mathbb{C}_{i_1^p} \otimes ... \otimes \mathbb{C}_{i_{|p|}^p})\end{aligned}$$

Applying the reasoning above regarding the conditions requried for these hom-spaces to be non-zero, we get

$$\bigoplus_{i\in\{0,1\}^{|G^{(1)}|}} \bigotimes_{p\in G^{(0)}} \mathrm{Hom}_{\mathbb{Z}_2\text{-}\mathrm{vect}_{\mathbb{C}}}(\mathbb{C}_0, \mathbb{C}_{i_1^p} \otimes ... \otimes \mathbb{C}_{i_{|p|}^p}) \cong \bigoplus_{\substack{i\in\{0,1\}^{|G^{(1)}|},\\ i\cdot l_p=0 \mod 2, \forall p\in G^{(0)}}} \bigotimes_{p\in G^{(0)}} \mathrm{Hom}_{\mathbb{Z}_2\text{-}\mathrm{vect}_{\mathbb{C}}}(\mathbb{C}_0, \mathbb{C}_{i_1^p} \otimes ... \otimes \mathbb{C}_{i_{|p|}^p})$$

since for all other values of i, at least one factor $\mathrm{Hom}_{\mathbb{Z}_2\text{-}\mathrm{vect}_{\mathbb{C}}}(\mathbb{C}_0, \mathbb{C}_{j_1^p} \otimes ... \otimes \mathbb{C}_{j_{|p|}^p})$ will be zero. By observing that $\mathrm{Hom}_{\mathbb{Z}_2\text{-}\mathrm{vect}_{\mathbb{C}}}(\mathbb{C}_0, \mathbb{C}_0) \cong \mathbb{C}_0$, and applying the fusion rules to each tensor product $\bigotimes_{p\in G^{(0)}} \mathrm{Hom}_{\mathbb{Z}_2\text{-}\mathrm{vect}_{\mathbb{C}}}(\mathbb{C}_0, \mathbb{C}_{i_1^p} \otimes ... \otimes \mathbb{C}_{i_{|p|}^p})$ we get

$$\bigoplus_{c\in\mathrm{col}(G)} \mathcal{H}(G^c) \cong \bigoplus_{\substack{i\in\{0,1\}^{|G^{(1)}|},\\ i\cdot l_p=0 \mod 2, \forall p\in G^{(0)}}} \bigotimes_{p\in G^{(0)}} \mathbb{C}_0 \cong \bigoplus_{\substack{i\in\{0,1\}^{|G^{(1)}|},\\ i\cdot l_p=0 \mod 2, \forall p\in G^{(0)}}} \mathbb{C}_0 \tag{5.2}$$

This vector space is precisely that of $\mathrm{Im}(P_{\mathrm{plaq}})$ from Section 2.2. This completes the proof of Proposition 5.1.1.

Remark 5.1.2. Let us emphasise the importance of the convention of relating $i \in \{0,1\}^{|G^{(1)}|}$ to the colours of edges that results in Equation (5.2) since it used throughout this chapter. Writing the basis vector for the factor $\mathbb{C}_0$ corresponding to $i \in \{0,1\}^{|G^{(1)}|}$ such that $i \cdot l_p = 0 \mod 2$ for all $p \in G^{(0)}$ by $\mathbf{e}_i$, the equivalence between colourings of G and the basis vectors of $\mathrm{Im}(P_{\mathrm{plaq}})$. In the next subsection, this equivalence is extended to include colourings of faces of the 3-skeleton of the cylinder over Σ representing $|\,\mathrm{id}_{(\Sigma,A)}, G, G|^\circ$ incident to edges of G. This extended equivalence also features in Section 5.2.

5.1.2 The Maps $|\,\mathrm{id}_{(\Sigma,A)}, G, G|^\circ$ and P_{vert}

The analysis of the map $|\,\mathrm{id}_{(\Sigma,A)}, G, G|^\circ$ relies heavily on Appendix B, particularly Appendix B.2, and partially upon Appendix A, so the reader may find it useful to peruse those appendices in parallel to the proof of Proposition 5.1.2 in this subsection.

The map $|\operatorname{id}_{(\Sigma,A)}, G, G|^\circ : \bigoplus_{c_0\in\operatorname{col}(G)} \mathcal{H}(G^{c_0}) \to \bigoplus_{c_1\in\operatorname{col}(G)} \mathcal{H}(G^{c_1})$ is computed by considering the restriction to each summand in the domain and codomain. These component maps, denoted $|\operatorname{id}_{(\Sigma,A)}, G^{c_0}, G^{c_1}|^\circ : \mathcal{H}(G^{c_0}) \to \mathcal{H}(G^{c_1})$ for $c_0, c_1 \in \operatorname{col}(G)$, are computed from bordisms (C_Σ, R, h) where C_Σ is the 3-manifold arising from the cylinder over Σ, R is a ribbon graph internal to C_Σ defined by $A\times[0,1]$ (so is the empty ribbon in the present case), and h is a homeomorphism

$$h : (-\Sigma, -A) \sqcup (\Sigma, A) \to (\partial C_\Sigma, \partial R)$$

Here $-\Sigma$ is the torus with opposite orientation and $-A$, and hence ∂R, is empty. It is understood that G^{c_0} induces a coloured skeleton $(G^{c_0})^{\mathrm{op}}$ on $-\Sigma$ and G^{c_1} is a coloured skeleton on Σ. Recall from Section 3.3.2, the map $|\operatorname{id}_{(\Sigma,A)}, G^{c_0}, G^{c_1}|^\circ \in \operatorname{Hom}_{\mathrm{Vect}_{\mathbb{C}}}(\mathcal{H}(G^{c_0}), \mathcal{H}(G^{c_1}))$ is computed by the formula

$$|\operatorname{id}_{(\Sigma,A)}, G^{c_0}, G^{c_1}|^\circ = \frac{\dim(\mathbb{Z}_2\text{- vect}_{\mathbb{C}})^{\#(\Sigma\setminus G)-\#(C_{\Sigma\setminus P})}}{\dim(c_1)} \sum_{c\in\operatorname{col}(P,d)} \dim(c)(V_c \otimes \operatorname{id}_{\mathcal{H}((G^{c_0})^{\mathrm{op}})\otimes\mathcal{H}(G^{c_1})})(*_c) \tag{5.3}$$

where (P,d) is a choice of coloured neat positive diagram for C_Σ (see Definition B.2.10, Definition B.2.11, and Definition B.2.17) that extends $(G^{c_0})^{\mathrm{op}}$ and G^{c_1} on the boundary, and all the components of the equation are recalled as they are discussed below.

Let us first make a choice of neat positive diagram (P,d) for (C_Σ, R). Since R is the empty ribbon, we actually only require $P = (P,d)$ to be a 3-skeleton of $(C_\Sigma, (G^{c_0})^{\mathrm{op}} \sqcup G^{c_1})$ (see Definition B.2.6, noting that, for G taken as in Figure 5.1, $(G^{c_0})^{\mathrm{op}} \sqcup G^{c_1}$ does indeed satisfy the required criteria, in particular that each vertex has valence greater than or equal to 2). We define P by considering three copies of G in $C_\Sigma = \Sigma\times[0,1]$: one in $\Sigma\times\{0\}$ corresponding to $(G^{c_0})^{\mathrm{op}}$, one in $\Sigma\times\{1/2\}$ and one at $\Sigma\times\{1\}$ corresponding to G^{c_1}. The copy of G in $\Sigma\times\{\frac{1}{2}\}$ is considered without any orientations. A portion of the 3-skeleton so defined for the choice of G in Figure 5.1 is shown in Figure 5.2 where the red edges at the base and top of the figure denote incidence with edges of $(G^{c_0})^{\mathrm{op}}$ and G^{c_1} respectively.

We specify P by detailing its sets of vertices, edges and faces, denoted $P^{(0)}$, $P^{(1)}$ and $P^{(2)}$. Only the elements of $P^{(2)}$ are given orientations at this stage (orientations aren't shown in Figure 5.2). Orientations of edges in $P^{(1)}$ are considered later in defining the contraction vector $*_c$. We take the set $P^{(0)}$ to be the set of vertices of each copy of G:

$$P^{(0)} = \left\{G^{(0)}\times\{0\}\right\} \cup \left\{G^{(0)}\times\{1/2\}\right\} \cup \left\{G^{(0)}\times\{1\}\right\}$$

We make special note here of the set of vertices $\{G^{(0)}\times\{1/2\}\}$ as these are the internal nodes of P (see Definition B.2.12) and are required in defining the map V_c in Equation (5.3). We denote this set of internal nodes by $\widehat{P}^{(0)}$. The set of edges of P, which are currently viewed as unoriented, is

$$P^{(1)} = \left\{G^{(1)}\times\{0\}\right\} \cup \left\{G^{(1)}\times\{1/2\}\right\} \cup \left\{G^{(1)}\times\{1\}\right\} \cup \left\{G^{(0)}\times[0,1/2]\right\} \cup \left\{G^{(0)}\times[1/2,1]\right\}$$

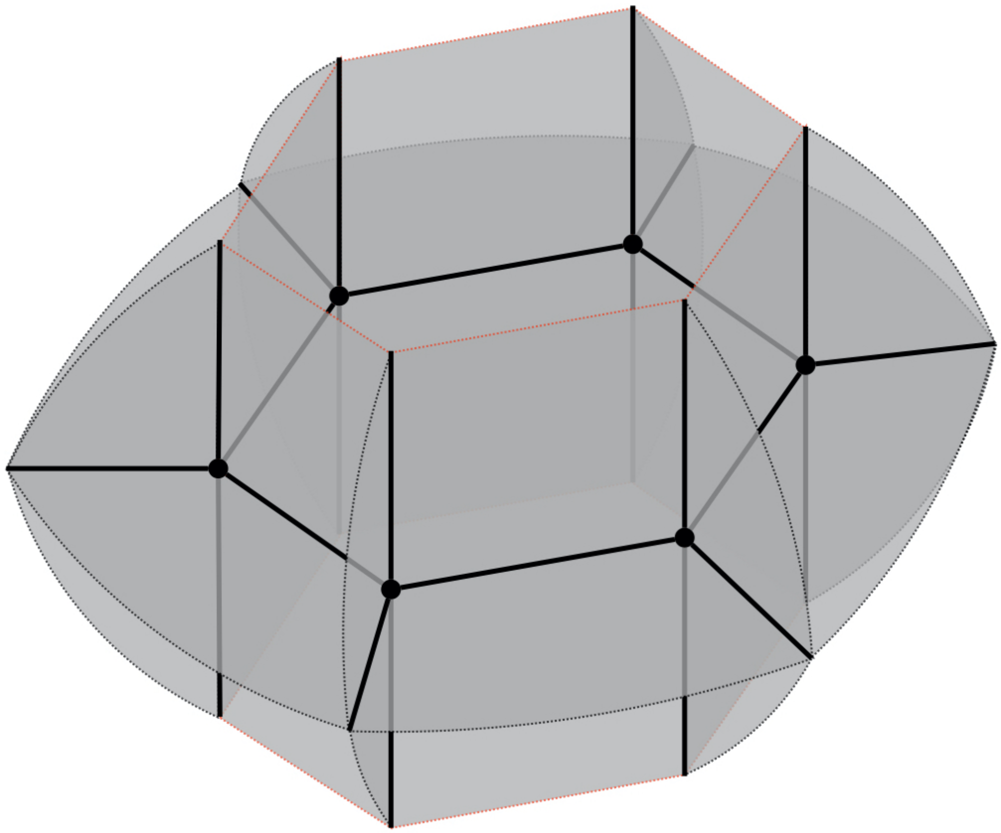

Figure 5.2: A portion of the 3-skeleton P that extends t^* in Figure 5.1.

In words, the edges of P are the edges of each copy of G, as well as edges joining each vertex in one copy of G with the corresponding vertex in the next copy of G. Finally, the set of faces of P is

$$P^{(2)} = \left\{G^{(1)} \times [0, 1/2]\right\} \cup \left\{G^{(1)} \times [1/2, 1]\right\} \cup \left\{G^{(2)} \times \{1/2\}\right\}$$

where again we slightly misuse notation and take $G^{(2)} \times \{1/2\}$ to mean the connected components of $\Sigma \times \{1/2\} \setminus G \times \{1/2\}$. Note that the connected components of $(-\Sigma) \setminus (G^{c_0})^{\mathrm{op}}$ and $\Sigma \setminus G^{c_1}$ are <u>not</u> included in the set of faces of P (this can be seen in Figure 5.2 since there is no face connecting the red edges in either boundary). The polyhedron P so defined is indeed a 3-skeleton since P is ∂-cylindrical (see Definition B.2.4) and since $\partial P = (G^{c_0})^{\mathrm{op}} \sqcup G^{c_1}$ and $C_\Sigma \setminus P$ is homeomorphic to $\big(\partial C_\Sigma \setminus ((G^{c_0})^{\mathrm{op}} \sqcup G^{c_1})\big) \times [0, 1)$ (as per Definition B.2.6).

We can now start to simplify Equation (5.3). The dimension of $\mathbb{Z}_2\text{-}\operatorname{vect}_{\mathbb{C}}$ is 2 and the notation $\#(\cdot)$ counts the connected components of the argument so the numerator of the first term of Equation (5.3) is

$$\dim(\mathbb{Z}_2\text{-}\operatorname{vect}_{\mathbb{C}})^{\#(\Sigma \setminus G) - \#(C_\Sigma \setminus P)} = 2^{\#(\Sigma \setminus G) - 2\#(\Sigma \setminus G)} = \frac{1}{2^{|G^{(2)}|}}$$

since for our choice of P, $C_\Sigma \setminus P$ has has twice the number of connected components as $\Sigma \setminus G$. Next, the denominator $\dim(c_1)$ is defined to be

$$\dim(c_1) = \prod_{e \in G^{(1)}} \dim(c_1(e)) = 1$$

since $\dim(\mathbb{C}_0) = \dim(\mathbb{C}_1) = 1$. Thus, the first term of Equation (5.3) is $\frac{1}{2^{|G^{(2)}|}} = \frac{1}{|\mathfrak{A}|}$ (recall the definition of $\mathfrak{A}$ from Definition 2.2.1), so we can already start to see the resemblance between the maps $|\operatorname{id}_{(\Sigma,A)}, G^{c_0}, G^{c_1}|^{\circ}$ and the projection map P_{vert} of Section 2.2.

Similarly to $\dim(c_1)$, $\dim(c)$, where c is a colouring of (P,d), is defined to be

$$\dim(c) = \prod_{r \in P^{(2)}} \dim(c(r))^{\chi(r)} = 1$$

where $\chi(r)$ denotes the Euler characteristic of the face r. The product is again equal to 1 by the same reasoning as above regarding the dimensions of the simple objects of $\mathbb{Z}_2\text{-}\operatorname{vect}_{\mathbb{C}}$. All that remains to complete the computation from Equation (5.3) is to understand the contraction vector $*_c$ and its image under the map $V_c \otimes \operatorname{id}_{\mathcal{H}((G^{c_0})^{\text{op}}) \otimes \mathcal{H}(G^{c_1})}$. This represents the key step that relates $|\operatorname{id}_{(\Sigma,A)}, G, G|^{\circ}$ to P_{vert} (recall Equation (2.5)).

The claim is as follows:

$$\sum_{c \in \operatorname{col}(P,d)} (V_c \otimes \operatorname{id}_{\mathcal{H}((G^{c_0})^{\text{op}}) \otimes \mathcal{H}(G^{c_1})})(*_c) = \sum_{g \in \mathfrak{A}} g$$

To prove this claim we first need to understand what is meant by a colouring c of (P,d). As outlined in Definition B.2.17, c is a map from the faces of (P,d) to the set of simple objects of $\mathbb{Z}_2\text{-}\operatorname{vect}_{\mathbb{C}}$, that is, $c : P^{(2)} \to I$, with the added constraint that for the faces $f \in P^{(2)}$ incident to edges e of $(G^{c_0})^{\text{op}}$ (respectively G^{c_1}), $c(f) = c_0(e)$ (respectively $c(f) = c_1(e)$). By the definition of $P^{(2)}$, for given colourings c_0 and c_1 of G, the colouring c is only able to freely colour the faces in $G^{(2)} \times \{1/2\}$.

Next, we extend the convention from Section 5.1.1 as per the comments made in Remark 5.1.2. We call the elements of the subset $\{G^{(0)} \times [0,1/2]\} \cup \{G^{(0)} \times [1/2,1]\} \cup \{G^{(1)} \times \{1/2\}\} \subset P^{(1)}$ internal edges. Let an internal edge be denoted by $\hat{e}$. Note that this subset excludes edges of P that lie entirely in the boundary of C_Σ, but does include edges that have one vertex in the a copy of G. Denote by $\mathcal{E}$ the set of all internal edges equipped with orientations, and denote by $\mathcal{E}_\partial \subset \mathcal{E}$ those oriented internal edges that have one vertex p in the boundary of C_Σ and are oriented away from that vertex.

Recalling the hom-spaces H_p from the previous subsection, we have the following for a given $c \in \operatorname{col}(P,d)$ and for each $\hat{e} \in \mathcal{E}_\partial$:

$$H_p \cong \operatorname{Hom}_{\mathbb{Z}_2\text{-}\operatorname{vect}_{\mathbb{C}}}(\mathbb{C}_0, c(f_1^{\hat{e}}) \otimes ... \otimes c(f_{|p|}^{\hat{e}})) =: H_{\hat{e}} \tag{5.4}$$

where the $f_j^{\hat{e}}$ are the faces of P incident to the edge $\hat{e}$. This isomorphism is guaranteed by the definition of P and the fact that the colouring of c is required to be consistent with the colouring of the of G in the boundary. That is, $\hat{e}$ also has valence $|p|$ and $c(f_j)$ is isomorphic to the object assigned to the edge of G to which f_j is incident. We are once again are able to ignore the influence of the relative orientations of the f_j and internal edge $\hat{e}$ due to the isomorphism between the simple objects of $\mathbb{Z}_2\text{-}\mathrm{vect}_{\mathbb{C}}$ and their duals (please note a more thorough treatment of these hom-spaces and internal edges resides in Appendix B.2 which in particular accounts for the choice of cyclic ordering of faces around $\hat{e}$).

Let us denote by $\mathcal{E}^0_\partial \subset \mathcal{E}_\partial$ the set of internal edges with source vertex in $(G^{c_0})^{\mathrm{op}}$. It then follows from Proposition 5.1.1 and Equation (5.4) that

$$\mathrm{Im}(P_{\mathrm{plaq}}) \cong \sum_{c\in \mathrm{col}(P,d)} \bigotimes_{\hat{e}\in\mathcal{E}^0_\partial} H_{\hat{e}}.$$

An equivalent statement can be made for $\mathcal{E}^1_\partial$ defined as the internal edges with souce vertex in G^{c_1}. This means that we can consider a colouring c of P restricted to the faces incident to the inwardly oriented and outwardly oriented boundary components of the boundary of C_Σ respectively as vectors $\mathbf{e}_{\mathrm{in}}$ and $\mathbf{e}_{\mathrm{out}}$ in $\mathrm{Im}(P_{\mathrm{plaq}})$. This perspective will be useful in discussing the map V_c below.

We can use Equation (5.4) to write, for a given $c \in \mathrm{col}(P,d)$ that extends the colourings c_0 and c_1 of copies of G on the boundary,

$$\bigotimes_{\hat{e}\in\mathcal{E}} H_{\hat{e}} \cong \Big(\bigotimes_{\hat{e}\in\mathcal{E}\setminus\mathcal{E}_\partial} H_{\hat{e}}\Big) \otimes \Big(\mathcal{H}(G^{c_0})^* \otimes \mathcal{H}(G^{c_1})\Big)$$

In this form, it is clear that the map V_c acts on $\mathcal{E}\setminus\mathcal{E}_\partial$. This set of oriented internal edges consists of precisely those with source vertex an internal node of P. The map V_c is defined be evaluating link graphs associated to these internal nodes (see Appendix B.2 for the definition of a link graph). Figure 5.3 depicts an internal node (red vertex) and its incident faces and edges for the 3-skeleton over $G = t^*$. The sphere used to produce the link graph Γ_v is shown in Figure 5.4a, and its planar equivalent is shown in Figure 5.4b.

For the purposes of evaluation, we can simply consider the link graph in $\mathbb{R}^2$ instead of in S^2 due to the fact that the evaluation of the graph is up to isotopy and since we are working over a spherical category $\mathbb{Z}_2\text{-}\mathrm{vect}_{\mathbb{C}}$ (see Theorem A.2.2 specifically and Appendix A more generally).

By Appendix A, we evaluate Γ_v via the function $\mathbb{F}_v : \bigotimes_{u\in\Gamma_v^{(0)}} H_u \to \mathrm{End}_{\mathbb{Z}_2\text{-}\mathrm{vect}_{\mathbb{C}}}(\mathbb{1}) \cong \Bbbk$, where H_u is the vector space assigned to vertex u of Γ_v by the usual hom-space of incident edges. There is once again a correspondence between the vector spaces assigned to vertices u of Γ_v and those assigned to the internal oriented edges of (P,d) they correspond to. The map V_c is then defined to be the image of $\bigotimes_{v\in\widehat{P}^{(0)}} \mathbb{F}_v$ under this correspondence (see the end of Appendix B.2 for a more rigorous treatment of the map V_c).

Next, we consider V_c localised to the internal nodes bounding a face in (P,d) corresponding to a plaquette in $G\times\{1/2\}$, such as in the example in Figure 5.3. We label faces in $G\times\{1/2\}$ by k and label vertical faces these systematically: for a vertical face incident to an edge e_l from above is labelled by f_{j_l} and a vertical face incident from below is labelled f_{i_l}. We proceed by analysing V_c in the case shown in this figure since it is sufficient to discuss the conceptual points and the extension to the general case is simple.

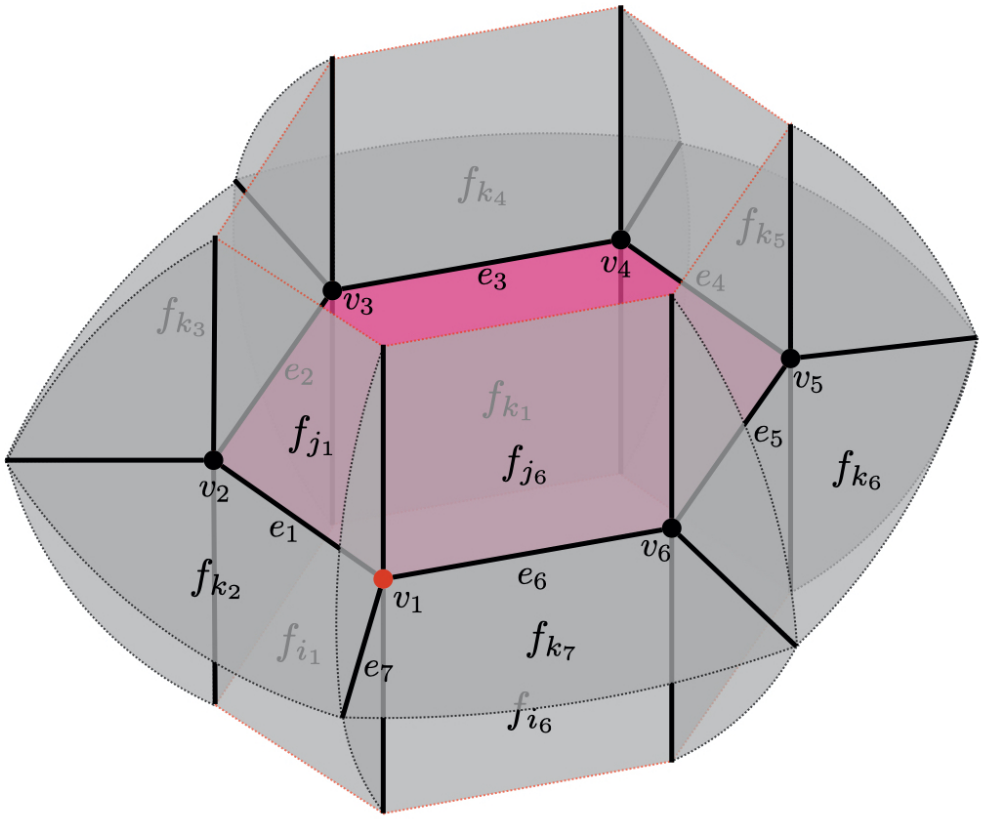

Figure 5.3: The 3-skeleton of C_Σ localised to an element of $G^{(2)} \times \{1/2\}$ (in pink) corresponding to a plaquette v of the skeleton G.

For our choice of skeleton P, every internal node v produces the same (uncoloured) graph Γ_v, where the labelling of edges is produced by the colouring c localised to the faces incident to v. The only influence of the choice of skeleton G is with regard to the number of vertices u of the graph that correspond to edges in $G \times \{1/2\}$, and each such vertex is treated the same way. Thus, in the analysis of the link graph for v_1 in Figure 5.3, which is the link graph in Figure 5.4b, we make special note of the vertices u_1, u_2 and u_3 as these are the vertices coresponding to edges incident to horizontal faces.

For the map V_c to be non-zero, we require $\mathbb{F}_v$ to be non-zero for all internal nodes v, which in turn requires all of the H_u for $u \in \Gamma_v^{(0)}$ to be non-zero. Since these H_u are hom-spaces of tensor products of simple objects of $\mathbb{Z}_2$- $\mathrm{vect}_{\mathbb{C}}$, we know precisely when they are non-zero from the fusion rules detailed in Example 3.1.15. The requirement that the hom spaces $H_{u_0}, H_{u_1}, H_{u_2}, H_{u_3}$ and H_{u_4} be non-zero imposes the following conditions

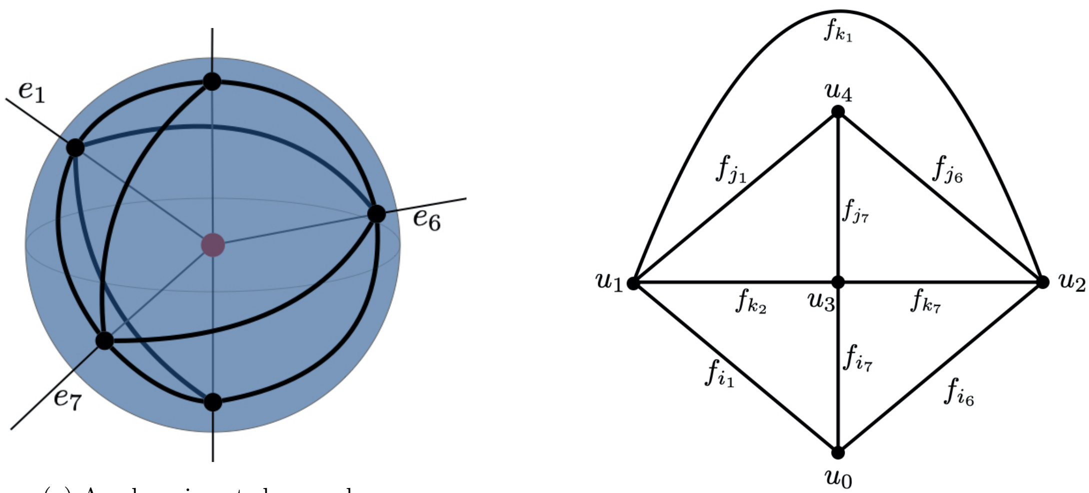

(a) A sphere inserted around v_1.

(b) The link graph Γ_{v_1}.

Figure 5.4

on the colouring c:

$$c(f_{i_1}) \otimes c(f_{i_7}) \otimes c(f_{i_6}) \cong \mathbb{C}_0$$
$$c(f_{j_1}) \otimes c(f_{k_1}) \otimes c(f_{i_1}) \otimes c(f_{k_2}) \cong \mathbb{C}_0$$
$$c(f_{j_6}) \otimes c(f_{k_7}) \otimes c(f_{i_6}) \otimes c(f_{k_1}) \cong \mathbb{C}_0$$
$$c(f_{j_7}) \otimes c(f_{k_2}) \otimes c(f_{i_7}) \otimes c(f_{k_7}) \cong \mathbb{C}_0$$

By writing $c(f_{i_l}) = \mathbb{C}_{i_l}$ and similarly for the j and k indices, we can recast these conditions as

$$i_1 + i_6 + i_7 = 0 \mod 2$$
$$j_1 = k_1 + k_2 + i_1 \mod 2$$
$$j_6 = k_1 + k_7 + i_6 \mod 2$$
$$j_7 = k_2 + k_7 + i_7 \mod 2$$

Note that the vector space H_{u_4} is guaranteed to be non-zero if the above criteria are satisfied since

$$j_1 + j_6 + j_7 = i_1 + i_6 + i_7 \mod 2$$

and $i_1 + i_6 + i_7 = 0 \mod 2$ by assumption. At the moment we are interested in just the conditions related to the face k_1 in Figure 5.3. By a similar process for the link graphs for v_2 through v_6, and by ignoring the conditions that do not include the term k_1, we arrive at the following list of conditions:

$$
\begin{aligned}
j_1 &= k_1 + k_2 + i_1 \mod 2 \\
j_2 &= k_1 + k_3 + i_2 \mod 2 \\
j_3 &= k_1 + k_4 + i_3 \mod 2 \\
j_4 &= k_1 + k_5 + i_4 \mod 2 \\
j_5 &= k_1 + k_6 + i_5 \mod 2 \\
j_6 &= k_1 + k_7 + i_6 \mod 2
\end{aligned}
$$

In the case of a general skeleton G, the number of conditions produced by similar analysis is equal to the number of edges bounding the plaquette. By the identification $c(f_{i_l}) = \mathbb{C}_{i_l}$, let us write $i \in \{0,1\}^{|G^{(1)}|}$ for the vector with entries i_l arising from all vertical faces incident to edges e_l in $G \times \{1/2\}$ from below. By Remark 5.1.2 and the proof given in the previous section more generally, we can identify the colouring c_0 with this vector i and thus with a copy of $\mathbb{C}_0$ as in Equation (5.2) (we are assuming c_0 is such that $\mathcal{H}(G^{c_0})$ is non-zero). Let us denote the basis vector of this copy of $\mathbb{C}_0$ as $\mathbf{e}_i$ (this is also a basis vector in $\mathrm{Im}(P_{\mathrm{plaq}})$).

Denoting by j the vector in $\{0,1\}^{|G^{(1)}|}$ corresponding to the faces f_{j_l} by a similar process, our aim is to analyse which vectors j survive under the map V_c localised to the face $f_{k_1}$for a given input vector i. That is, we rewrite j in terms of i and k_1 by using the rules produced above by the evaluation of link graphs of the internal nodes of f_{k_1} (we ignore the influence from the other horizontal faces for the time being, by taking the values $k_2, ..., k_6$ to be zero in the above equations). We can see that $j = i$ if $k_1 = 0$ (i.e. if $c(f_{k_1}) = \mathbb{C}_0$) and $j = i + l_{k_1}$ when $k_1 = 1$ (i.e. when $c(f_{k_1}) = \mathbb{C}_1$), where $l_{k_1} \in \{0,1\}^{|G^{(1)}|}$ is the vector with 1's in the entries corresponding to the edges bounding f_{k_1} and 0's elsewhere. Thus, the colouring of face f_{k_1} by the simple object $\mathbb{C}_1$ produces conditions that look very similar to those imposed by the vertex operators A_{v_1} (where we take A_{v_1} to be short hand for the vertex operator corresponding to the plaquette k_1 and recall the discussion of the vertex operators in Section 2.2).

This reasoning can be extended to all other the faces in $G^{(2)} \times \{1/2\}$, and by recalling Equation (3.14) we can take the following perspective. For a given colouring c of (P, d), the map $V_c \otimes \mathrm{id}_{\mathcal{H}((G^{c_0})^{\mathrm{op}}) \otimes \mathcal{H}(G^{c_1})}$ is from $\left(\bigotimes_{\hat{e} \in \mathcal{E} \setminus \mathcal{E}_\partial} H_{\hat{e}}\right) \otimes \left(\mathcal{H}((G^{c_0})^{\mathrm{op}}) \otimes \mathcal{H}(G^{c_1})\right)$ to $\mathbb{C} \otimes \mathrm{Hom}_{\mathrm{Vect}_{\mathbb{C}}}(\mathcal{H}(G^{c_0}), \mathcal{H}(G^{c_1}))$ whose image is the set of maps that are proportional to the action of the element $\prod_{r=1}^{|G^{(2)}|} A_{v_r}^{k_r}$ of $\mathfrak{A}$ where $k_r \in \{0,1\}$ is such that $c(f_{k_r}) = \mathbb{C}_{k_r}$, $A_{v_r}^0$ is the identity map, and we are again using the short hand for vertex operators A_{v_r}. To select precisely the map with proportionality equal to 1, we are required to evaluate $V_c \otimes \mathrm{id}_{\mathcal{H}((G^{c_0})^{\mathrm{op}}) \otimes \mathcal{H}(G^{c_1})}$ on the contraction vector $*_c$.

To define $*_c$ (see Definition B.2.19 and surrounding theory) we note that the vector space $\bigotimes_{\hat{e} \in \mathcal{E}} H_{\hat{e}}$ contains two factors related to each (unoriented) internal edge $\hat{e}$, namely $H_{\hat{e}}$ and $H_{-\hat{e}}$, where the minus sign denotes the opposite orientation. These vector spaces are dual to one another, and hence induce a non-degenerate pairing (see Appendix B.2) and hence has an inverse. The contraction vector is constructed from the image of $1 \in \mathbb{C}$ under these inverses, namely as the tensor product of such images for all internal edges e.

Now, we know from the fusion rules and the definition of duality in $\mathbb{Z}_2\text{-}\operatorname{vect}_{\mathbb{C}}$ that for each internal edge $\hat{e}$, either $H_{\hat{e}}$ is the zero vector space or $H_{\hat{e}}$ is isomorphic to $\mathbb{C}_0$. Clearly, any contraction vector $*_c$ defined from a colouring c that produces $H_{\hat{e}} = 0$ for one or more edges $\hat{e}$, will be 0, and so is evaluated to 0 by $V_c \otimes \mathrm{id}_{\mathcal{H}((G^{c_0})^{\mathrm{op}})\otimes\mathcal{H}(G^{c_1})}$. For colourings c such that all $H_{\hat{e}}$ are isomorphic to $\mathbb{C}_0$, then the non-degenerate pairings are $\mathrm{ev}_{\mathbb{C}_0}$ (or $\widetilde{\mathrm{ev}}_{\mathbb{C}_0}$, but these are equivalent in this case) and so $*_c$ is the image of 1 under $\mathrm{coev}_{\mathbb{C}_0}$ (equivalently $\widetilde{\mathrm{coev}}_{\mathbb{C}_0}$) for each edge e. Thus, $*_c$ is a tensor product of basis elements of $H_{\hat{e}}$ for each e.

Thus, we have that $(V_c \otimes \mathrm{id}_{\mathcal{H}((G^{c_0})^{\mathrm{op}})\otimes\mathcal{H}(G^{c_1})})(*_c)$ is the map defined by the action $g = \prod_{r=1}^{|G^{(2)}|} A_{v_r}^{k_r}$. Returning to Equation (5.3), we can write

$$
\begin{aligned}
|\,\mathrm{id}_{(\Sigma,A)}, G, G|^\circ &= \sum_{c_0,c_1\in\mathrm{col}(G)} \frac{\dim(\mathbb{Z}_2\text{-}\operatorname{vect}_{\mathbb{C}})^{\#(\Sigma\setminus G)-\#(C_{\Sigma\setminus P})}}{\dim(c_1)} \sum_{c\in\mathrm{col}(P,d)} \dim(c)(V_c \otimes \mathrm{id}_{\mathcal{H}((G^{c_0})^{\mathrm{op}})\otimes\mathcal{H}(G^{c_1})})(*_c) \\
&= \frac{1}{|\mathfrak{A}|} \sum_{c\in\mathrm{col}(P,d)} (V_c \otimes \mathrm{id}_{\mathcal{H}((G^{c'_0})^{\mathrm{op}})\otimes\mathcal{H}(G^{c'_1})})(*_c) \\
&= \frac{1}{|\mathfrak{A}|} \sum_{g\in\mathfrak{A}} g
\end{aligned}
$$

where c'_0 and c'_1 in the second line denote the only valid colouring of G in the inward and outward boundary components of C_Σ for a given c such that $\mathcal{H}(G^{c'_0})$ and $\mathcal{H}(G^{c'_1})$ are both non-zero. This completes the proof of Proposition 5.1.2.

5.1.3 A Summary of the Key Points

It seems worthwile to provide a quick summary of some of the key components of the above proofs that will also appear in Section 5.2. Firstly, we saw that the starting point for evaluation of the Turaev-Viro graph TQFT was a vector space equivalent to $\mathrm{Im}(P_{\mathrm{plaq}})$ and moreover, this vector space was produced by considering hom-spaces of objects assigned to edges incident to vertices. This vector space also appears in the context of the Reshetikhin-Turaev defect TQFT albeit under slightly modified circumstances, as seen in the proof of Proposition 5.2.1 below. Next, we saw a correspondence between the objects assigned to faces incident to the edges of the skeletons in the boundary components of the cylinder and the objects assigned to those edges, allowing us to identify the labels for the faces with the vector space $\mathrm{Im}(P_{\mathrm{plaq}})$. The action of the projection P_{vert} was implemented at the vertices of faces "parallel" to plaquettes in the boundary surface, and the labelling of such faces were related to the elements of the group $\mathfrak{A}$. This phenomenon appears in the proof of Proposition 5.2.2 in Section 5.2.2, however this proof is required to consider the dual of a triangulation of the cylinder rather than a nice choose of cellular decomposition like the 3-skeleton P above, which slightly alters the treatment of the projections corresponding to the elements of $\mathfrak{A}$.

5.2 The $\mathcal{A}_{\mathbb{Z}_2\text{-}\operatorname{vect}_{\mathbb{C}}}$-Orbifold and P_{vert}

In this section, we prove Theorem 5.0.2 which is restated here:

Theorem 5.0.2. *Let* $\Sigma^{t^*,\mathcal{A}_{\mathbb{Z}_2\text{-}\mathrm{vect}_\mathbb{C}}} \in \boldsymbol{Bord}_3^{\mathrm{df}}(\mathbb{D})$ *be the* $\mathbb{D}$*-decorated torus with stratification arising from the dual of the triangulation* t *of the torus as defined in Figure 2.1 and labelled by the orbifold datum* $\mathcal{A}_{\mathbb{Z}_2\text{-}\mathrm{vect}_\mathbb{C}}$*. Then*

(i) $\mathrm{Im}(\mathcal{Z}^{\mathrm{df}}_{RT,\mathrm{vect}_\mathbb{C}}(C_\Sigma^{t^*,\mathcal{A}_{\mathbb{Z}_2\text{-}\mathrm{vect}_\mathbb{C}}})) = H_{\mathrm{code}}$*, and*

(ii) $\mathcal{Z}^{\mathrm{df}}_{RT,\mathrm{vect}_c}(C_\Sigma^{t^*,\mathcal{A}_{\mathbb{Z}_2\text{-}\mathrm{vect}_\mathbb{C}}}) = P_{\mathrm{vert}} \circ f$*,*

where $C_\Sigma^{t^*,\mathcal{A}_{\mathbb{Z}_2\text{-}\mathrm{vect}_\mathbb{C}}} \in \boldsymbol{Bord}_3^{\mathrm{df}}(\mathbb{D})$ *is the morphism used to define the* $A_{\mathbb{Z}_2\text{-}\mathrm{vect}_\mathbb{C}}$*-orbifold of* $\mathcal{Z}^{\mathrm{df}}_{RT,\mathrm{vect}_c}$ *on the undecorated torus,* f *is a projection from the domain of* $\mathcal{Z}^{\mathrm{df}}_{RT,\mathrm{vect}_c}(C_\Sigma^{t^*,\mathcal{A}_{\mathbb{Z}_2\text{-}\mathrm{vect}_\mathbb{C}}})$ *to* $\mathrm{Im}(P_{\mathrm{plaq}})$*,* H_{code} *is the code subspace of the toric code defined on* t^**, and* P_{vert} *is the component of the projection map* P_{code} *defined on the plaquettes of* t^**.*

Most of the work presented here is regarding part (ii) of the thereom, since part (i) is a direct consequence of Theorem 5.0.1, Theorem 4.3.1 and the definition of the orbifold of the Reshetikhin-Turaev defect TQFT [Construction 3.8, CRS19] (this is elaborated upon shortly).

The proof of Theorem 5.0.2 (ii) proceeds in two parts, which we again present as two propositions where $C_\Sigma^{t^*,\mathcal{A}_{\mathbb{Z}_2\text{-}\mathrm{vect}_\mathbb{C}}}$ is as in the statement of Theorem 5.0.2 above:

Proposition 5.2.1. $\mathcal{Z}^{\mathrm{df}}_{RT,\mathrm{vect}_c}(C_\Sigma^{t^*,\mathcal{A}_{\mathbb{Z}_2\text{-}\mathrm{vect}_\mathbb{C}}}) = \pi \circ f$ *where* π *is a projection and* f *is as in the statement of Theorem 5.0.2.*

Proposition 5.2.2. *The projection* π *is* P_{vert} *restricted to* $\mathrm{Im}(P_{\mathrm{plaq}})$*.*

Before commencing the proofs of these propositions, let us give a description of $C_\Sigma^{t^*,\mathcal{A}_{\mathbb{Z}_2\text{-}\mathrm{vect}_\mathbb{C}}}$, which will be elaborated upon in Section 5.2.2. The underlying 3-manifold is the cylinder C_Σ over the torus (which mirrors the underlying manifold for the identity bordism in the Turaev-Viro case above), but given we are now working in the context of $\mathbf{Bord}_3^{\mathrm{df}}(\mathbb{D})$, this cylinder is provided with extra structure. We take $C_\Sigma^{t^*}$ to be C_Σ equipped with the stratification arising from τ^*, where τ is a triangulation of the C_Σ that extends the triangulation t of Σ, supplemented by 0-strata in the interior of each 2- and 3-stratum. Then $C_\Sigma^{t^*,\mathcal{A}_{\mathbb{Z}_2\text{-}\mathrm{vect}_\mathbb{C}}}$ is the defect bordism obtained from $C_\Sigma^{t^*}$ by labelling its 3-, 2-, 1- and 0-strata by the orbifold datum $\mathcal{A}_{\mathbb{Z}_2\text{-}\mathrm{vect}_\mathbb{C}}$. We recall from Definition 4.3.1 that this data consists of:

- $\mathcal{A}_3 = \mathrm{vect}_\mathbb{C}$ assigned to 3-strata;
- $\mathcal{A}_2 = \mathbb{C}^2$ as a Frobenius algebra (with multiplication and pairing assigned from the direct sum of trivial Frobenius algebras $\mathbb{C}$), assigned to 2-strata;
- $\mathcal{A}_1 = \bigoplus_{i,j,k\in I} \mathrm{Hom}_{\mathbb{Z}_2\text{-}\mathrm{vect}_\mathbb{C}}(i\otimes j, k)$, where I is a representative set of simple objects for $\mathbb{Z}_2\text{-}\mathrm{vect}_\mathbb{C}$. This is an object of $\mathrm{vect}_\mathbb{C}$ by the fact that $\mathbb{Z}_2\text{-}\mathrm{vect}_\mathbb{C}$ is spherical fusion, and moreover, is a $\mathbb{C}^2$-$(\mathbb{C}^2\otimes\mathbb{C}^2)$-bimodule (for more on multi-modules, see [Section 2, CRS17]). This object $T := \mathcal{A}_1$ labels 1-strata.

- $\mathcal{A}_0^{\pm}$, ψ and ϕ, which label 0-strata in the interior of C_Σ. The maps $\mathcal{A}_0^{\pm}$ are maps in $\mathrm{Hom}_{\mathrm{vect}_{\mathbb{C}}}(T \otimes_{\mathbb{C}^2} T, T \otimes_{\mathbb{C}^2} T)$ and will be relabelled as α (for $\mathcal{A}_0^+$) and $\overline{\alpha}$ (for $\mathcal{A}_0^-$) for consistency with the referenced literature (e.g. [CRS18]).

By [Construction 3.8, CRS19] and Theorem 4.3.1 (which is [Theorem 4.5, CRS18]) we have that

$$\mathrm{Im}(\mathcal{Z}^{\mathrm{df}}_{RT,\mathrm{vect}_c}(C_\Sigma^{t^*,\mathcal{A}_{\mathbb{Z}_2\text{-}\mathrm{vect}_{\mathbb{C}}}})) \cong |(\Sigma, A)|_{\mathbb{Z}_2\text{-}\mathrm{vect}_{\mathbb{C}}}$$

where A is empty, and so by applying Theorem 5.0.1 we have shown part (i) of Theorem 5.0.2.

Throughout this section, we will refer to $\mathcal{Z}^{\mathrm{df}}_{RT,\mathrm{vect}_c}(C_\Sigma^{t^*,\mathcal{A}_{\mathbb{Z}_2\text{-}\mathrm{vect}_{\mathbb{C}}}})$ as 'the orbifold morphism'.

5.2.1 The Orbifold Morphism as a Composition of Projections

The proof of Proposition 5.2.1 relies on the manipulation of ribbon graphs, in particular regarding the vertical composition of ribbon graphs corresponding to composition of the morphisms represented by these graphs. Before we elaborate on these points, let us consider the following lemma:

Lemma 5.2.3. *For $\Sigma^{t^*,\mathcal{A}_{\mathbb{Z}_2\text{-}\mathrm{vect}_{\mathbb{C}}}} \in \boldsymbol{Bord}_3^{\mathrm{df}}(\mathbb{D})$ the decorated torus with 2-, 1- and 0-strata given by $(t^*)^{(2)}$, $(t^*)^{(1)}$ and $(t^*)^{(0)}$ and labelled by $\mathcal{A}_3$, $\mathcal{A}_2$ and $\mathcal{A}_1$ respectively, we have*

$$\mathcal{Z}^{\mathrm{df}}_{RT,\mathrm{vect}_{\mathbb{C}}}(\Sigma^{t^*,\mathcal{A}_{\mathbb{Z}_2\text{-}\mathrm{vect}_{\mathbb{C}}}}) \cong \bigoplus_{c\in\mathrm{col}(t^*)} \mathcal{H}((t^*)^c)$$

where the vector space on the right is that of Section 5.1.1 for the skeleton $G = t^*$ (where t^* is shown in red in Figure 5.1).

The vector space $\mathcal{Z}^{\mathrm{df}}_{RT,\mathrm{vect}_{\mathbb{C}}}(\Sigma^{t^*,\mathcal{A}_{\mathbb{Z}_2\text{-}\mathrm{vect}_{\mathbb{C}}}})$ is *not* the domain of $\mathcal{Z}^{\mathrm{df}}_{RT,\mathrm{vect}_c}(C_\Sigma^{t^*,\mathcal{A}_{\mathbb{Z}_2\text{-}\mathrm{vect}_{\mathbb{C}}}})$, however the domain of the latter and the domain of the morphism used to define $\mathcal{Z}^{\mathrm{df}}_{RT,\mathrm{vect}_{\mathbb{C}}}(\Sigma^{t^*,\mathcal{A}_{\mathbb{Z}_2\text{-}\mathrm{vect}_{\mathbb{C}}}})$ (see below) are the same which motivates the consideration of Lemma 5.2.3. The morphism used to define $\mathcal{Z}^{\mathrm{df}}_{RT,\mathrm{vect}_{\mathbb{C}}}(\Sigma^{t^*,\mathcal{A}_{\mathbb{Z}_2\text{-}\mathrm{vect}_{\mathbb{C}}}})$ will become the projection f in the statement of Proposition 5.2.1. To the proof of the lemma.

Proof. We know from Section 3.4.2 and Appendix C.2 how to evaluate the decorated surface $\Sigma^{t^*,\mathcal{A}_{\mathbb{Z}_2\text{-}\mathrm{vect}_{\mathbb{C}}}}$. Since it has 2-, 1- and 0-strata labelled by $\mathrm{vect}_{\mathbb{C}}$, $\mathbb{C}^2$ (as a Frobenius algebra) and T respectively, we evaluate $\Sigma^{t^*,\mathcal{A}_{\mathbb{Z}_2\text{-}\mathrm{vect}_{\mathbb{C}}}}$ by considering a (different) defect cylinder $\widehat{C}$ over $\Sigma^{t^*,\mathcal{A}_{\mathbb{Z}_2\text{-}\mathrm{vect}_{\mathbb{C}}}}$ with 3-, 2- and 1-strata also labelled by $\mathrm{vect}_{\mathbb{C}}$, $\mathbb{C}^2$ and T respectively. These strata 3-, 2- and 1-strata arise from the 2-, 1- and 0-strata of $\Sigma^{t^*,\mathcal{A}_{\mathbb{Z}_2\text{-}\mathrm{vect}_{\mathbb{C}}}}$ as per the discussion of the cylinder over Σ in Section 3.4.2. Thus, we note that $\widehat{C}$ differs from $C_\Sigma^{t^*,\mathcal{A}_{\mathbb{Z}_2\text{-}\mathrm{vect}_{\mathbb{C}}}}$ in that the latter has 0-strata in the interior where as the former doesn't.

The ribbon graph associated to $\widehat{C}$ is prescribed as follows. The 2-strata in $\widehat{C}_\Sigma$ are triangulated, and ribbons and coupons labelled by the algebra $\mathbb{C}^2$ and its multiplication and comultiplication respectively, are associated to the duals of these triangulations. Since the result of the evaluation is independent of the choice of triangulation of each 2-stratum (see [Section 5, CRS17] in particular Lemma 5.6 and the discussion surrounding Equation (5.16)), we take the simplest one (such as that shown in black on the the left hand side of Figure 5.5). Next the 1-strata are thickened to ribbons labelled T, and the $\mathbb{C}^2$-ribbons from the 2-strata meet these T-ribbons at coupons labelled by the action of $\mathbb{C}^2$ on T (the left and right actions of $\mathbb{C}^2$ on T are denoted ρ_L and ρ_R respectively in Figure 5.5). Each 2-stratum then produces a piece of ribbon graph as seen on the right in Figure 5.5 (the boundary circles of the cylinder in this figure are meant to be interpreted as a patch of the surface $\Sigma^{t^*,\mathcal{A}_{\mathbb{Z}_2\text{-}\mathrm{vect}_{\mathbb{C}}}}$ and not its entirety).

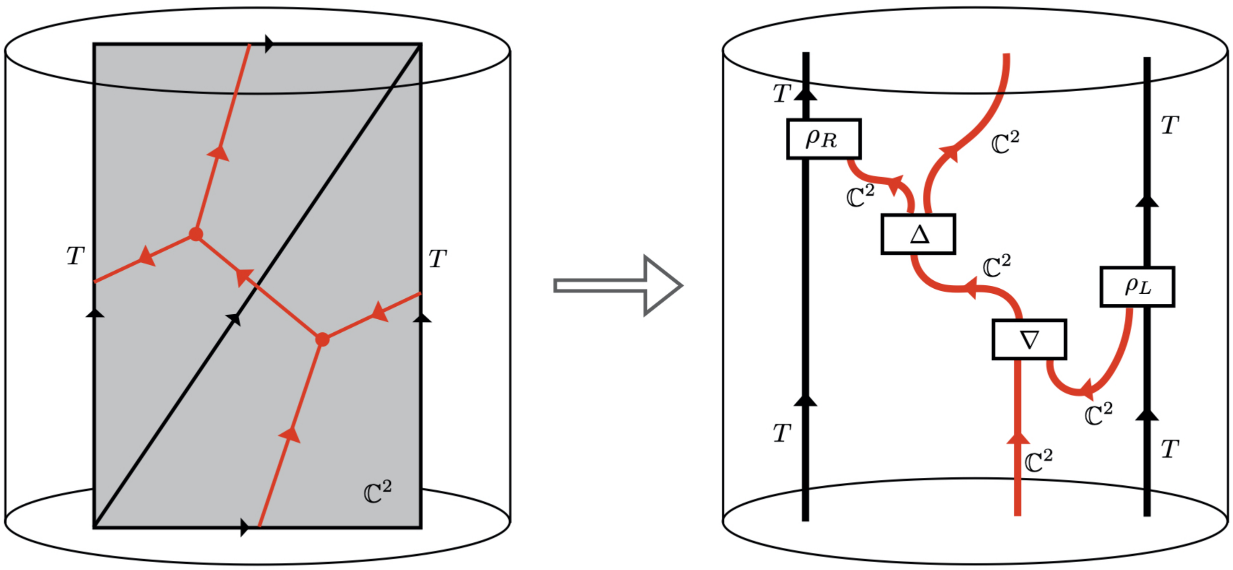

Figure 5.5: The ribbon graph from a 2-stratum.

Due to the regularity of the decorations on $\Sigma^{t^*,\mathcal{A}_{\mathbb{Z}_2\text{-}\mathrm{vect}_{\mathbb{C}}}}$, and hence the ribbon graph induced in $\widehat{C}$, we can proceed by evaluating the cylinder $\widehat{C}$ with just one 2-stratum labelled by $\mathbb{C}^2$ bounded by two 1-strata labelled by T. This analysis then generalises to the full case of $\widehat{C}$. By denoting the weighted extended manifold corresponding to $\widehat{C}$ with ribbon graph for one 2-stratum by $\overline{C}$, and the extended surface corresponding to the base of the cylinder by $\overline{\Sigma}$, we have

$$\mathcal{Z}^{\mathrm{df}}_{RT,\mathrm{vect}_{\mathbb{C}}}(\Sigma^{t^*,\mathcal{A}_{\mathbb{Z}_2\text{-}\mathrm{vect}_{\mathbb{C}}}}) \cong \mathrm{Im}\left(\mathcal{Z}_{RT,\mathrm{vect}_{\mathbb{C}}}(\overline{C}) : \mathcal{Z}_{RT,\mathrm{vect}_{\mathbb{C}}}(\overline{\Sigma}) \to \mathcal{Z}_{RT,\mathrm{vect}_{\mathbb{C}}}(\overline{\Sigma})\right)$$

From Section 3.4.1 and Appendix C.1, we can write down the vector space $\mathcal{Z}_{RT,\mathrm{vect}_{\mathbb{C}}}(\overline{\Sigma})$:

$$\begin{aligned}\mathcal{Z}_{RT,\mathrm{vect}_{\mathbb{C}}}(\overline{\Sigma}) &\cong \mathrm{Hom}_{\mathrm{vect}_{\mathbb{C}}}(\mathbb{1}, T\otimes\mathbb{C}^2\otimes T\otimes(\mathbb{C}\otimes\mathbb{C}^*)) \\ &\cong T\otimes\mathbb{C}^2\otimes T\end{aligned}$$

where the T and $\mathbb{C}^2$ factors correspond to the marked points in $\overline{\Sigma}$ and the $(\mathbb{C}\otimes\mathbb{C}^*)$ term arises from the genus of the underlying manifold of $\overline{\Sigma}$. The reduction to $T\otimes\mathbb{C}^2\otimes T$ follows since $\mathbb{C}$ is the unit of $\mathrm{vect}_{\mathbb{C}}$.

The claim now is that $\mathrm{Im}\left(\mathcal{Z}_{RT,\mathrm{vect}_{\mathbb{C}}}(\overline{C})\right)$ is $T\otimes_{\mathbb{C}^2}T$, that is, the tensor product of two $\mathbb{C}^2$-$(\mathbb{C}^2\otimes\mathbb{C}^2)$-bimodules

T over a common algebra $\mathbb{C}^2$ (see [Section 3.1, CRS18] for more details). The proof of this claim follows from [Lemma 5.10, CRS17]:

Lemma 5.2.4. *[Lemma 5.10, CRS17] We have*

$$\mathcal{Z}^{\mathrm{df}}_{RT,\mathrm{vect}_c}(S_{M,N}) \cong \mathrm{Hom}_{A_1\otimes\ldots\otimes A_n}(M,N)$$

where $S_{M,N}$ is a sphere with two 0-strata labelled by multi-modules $A_1...A_nM$ and $A_1...A_nN$ connected by n 1-strata labelled by the algebras $A_1,...,A_n$.

The notation $\mathrm{Hom}_{A_1\otimes\ldots\otimes A_n}(M,N) \subseteq \mathrm{Hom}_{\mathrm{vect}_c}(M,N)$ denotes the space of multi-module maps (we are taking the multi-modules M and N, and algebras A_i, to be internal to vect_c as this is relevant to our case, but in general they can be internal to any modular category; for more details on multi-modules and multi-module maps see [Section 2, CRS17] in particular Definitions 2.2 and 2.3). For our purposes, M and N are copies of T and we take just one 1-stratum and hence one algebra $A = \mathbb{C}^2$. The proof of Lemma 5.2.4 [Lemma 5.10, CRS17] proceeds by analysing the ribbon graph that is used to evaluate the Reshetikhin-Turaev defect TQFT on the surface $S_{M,N}$. By the comments made in Remark 3.4.1, the evaluation of this ribbon graph is precisely the same as the evaluation of the ribbon graph in the interior of $\overline{C}_\Sigma$ despite Σ and S being different (non-homeomorphic) surfaces. Thus, we have $\mathcal{Z}^{\mathrm{df}}_{RT,\mathrm{vect}_c}(\Sigma) \cong \mathrm{Hom}_{\mathbb{C}^2}(T,T)$, which is then isomorphic to $T \otimes_{\mathbb{C}^2} T$ by the definition of multi-module maps in $\mathrm{vect}_{\mathbb{C}}$.

The proof of Lemma 5.2.4 can be extended to determine the evaluation of the decorated surface $\Sigma^{t^*,\mathcal{A}_{\mathbb{Z}_2\text{-}\mathrm{vect}_{\mathbb{C}}}}$ (see [Lemma 3.2, CRS18] and the remarks preceding it). In particular, we get

$$\mathcal{Z}^{\mathrm{df}}_{RT,\mathrm{vect}_{\mathbb{C}}}(\Sigma^{t^*,\mathcal{A}_{\mathrm{vect}_{\mathbb{C}}}}) \cong T \otimes_{\mathbb{C}^2} \ldots \otimes_{\mathbb{C}^2} T \tag{5.5}$$

where each pair of bimodules T that label 0-strata joined by a 1-stratum of $\Sigma^{t^*,\mathcal{A}_{\mathbb{Z}_2\text{-}\mathrm{vect}_{\mathbb{C}}}}$, appear in the tensor product on the right hand side of Equation (5.5) as a tensor product over the algebra $\mathbb{C}^2$ labelling the shared 1-stratum.

Writing T as the direct sum $T = \bigoplus_{i,j,k\in I} \mathrm{Hom}_{\mathbb{Z}_2\text{-}\mathrm{vect}_{\mathbb{C}}}(i\otimes j,k)$ we note that

$$T \otimes_{\mathbb{C}^2} T = \bigoplus_{i,j,k,l,m\in I} \mathrm{Hom}_{\mathbb{Z}_2\text{-}\mathrm{vect}_{\mathbb{C}}}(i\otimes j,k) \otimes \mathrm{Hom}_{\mathbb{Z}_2\text{-}\mathrm{vect}_{\mathbb{C}}}(k\otimes l,m)$$

by the definition of the action of $\mathbb{C}^2$ (see [Definition 4.2, CRS18]). By extending this reasoning to the full tensor product in Equation (5.5), we can write

$$\mathcal{Z}^{\mathrm{df}}_{RT,\mathrm{vect}_{\mathbb{C}}}(\Sigma^{t^*,\mathcal{A}_{\mathrm{vect}_{\mathbb{C}}}}) \cong \bigotimes_{x\in(t^*)^{(0)}} \bigoplus_{i_x,j_x,k_x\in I} \mathrm{Hom}_{\mathbb{Z}_2\text{-}\mathrm{vect}_{\mathbb{C}}}(i_x\otimes j_x,k_x) \tag{5.6}$$

where we are taking as in implicit in this tensor product the compatibility of the objects between copies of T joined by 1-strata. This compatiblity across the entire stratification t^* allows us to rewrite the right hand side of Equation (5.6) to sum over possible assignments of objects to the 1-strata of $(t^*)^{(1)}$:

$$\bigotimes_{x\in(t^*)^{(0)}} \bigoplus_{i_x,j_x,k_x\in I} \mathrm{Hom}_{\mathbb{Z}_2\text{- vect}_{\mathbb{C}}}(i_x\otimes j_x, k_x) \cong \bigoplus_{(i_1,i_2,\ldots,i_{|(t^*)^{(1)}|})\in I^{|(t^*)^{(1)}|}} \bigotimes_{x\in(t^*)^{(0)}} \mathrm{Hom}_{\mathbb{Z}_2\text{- vect}_{\mathbb{C}}}(i^x_{s_1}\otimes i^x_{s_2}, i^x_{s_3})$$

where the objects $i^x_{s_1}$, $i^x_{s_2}$ and $i^x_{s_3}$ are the objects of $(i_1, i_2, ..., i_{|(t^*)^{(1)}|})$ corresponding to the 1-strata incident to the 0-strata x. By noting that $\mathrm{Hom}_{\mathbb{Z}_2\text{- vect}_{\mathbb{C}}}(i\otimes j, k) \cong \mathrm{Hom}_{\mathbb{Z}_2\text{- vect}_{\mathbb{C}}}(\mathbb{1}, k\otimes i\otimes j)$ for simple objects i, j and k, and that each $(i_1, i_2, ..., i_{|(t^*)^{(1)}|}) \in I^{|(t^*)^{(1)}|}$ is equivalent to a choice of map $c : (t^*)^{(1)} \to I$, we recover precisely the space

$$\bigoplus_{c\in\mathrm{col}(t^*)} \mathcal{H}((t^*)^c)$$

from Section 5.1.1 where t^* is consider as a skeleton of the torus. □

We now prove Proposition 5.2.1 by considering the $\mathcal{Z}^{\mathrm{df}}_{RT,\mathrm{vect}_{\mathbb{C}}}(C^{t^*,\mathcal{A}_{\mathbb{Z}_2\text{- vect}_{\mathbb{C}}}}_{\Sigma})$ as a composition of morphisms, one of which arises from the cylinder $\widehat{C}$. Recall that $C^{t^*,\mathcal{A}_{\mathbb{Z}_2\text{- vect}_{\mathbb{C}}}}_{\Sigma}$ differs from $\widehat{C}$ by the presence of the 0-strata in the interior of the cylinder, namely at the intersection of 1-strata and in the interior of 2- and 3-strata. Now, by the definition of $C^{t^*,\mathcal{A}_{\mathbb{Z}_2\text{- vect}_{\mathbb{C}}}}_{\Sigma}$ with stratification arising from τ^*, there is a neighbourhood of the boundary component $\Sigma^{t^*,\mathcal{A}_{\mathbb{Z}_2\text{- vect}_{\mathbb{C}}}}$ that is homeomorphic to $\Sigma^{t^*,\mathcal{A}_{\mathbb{Z}_2\text{- vect}_{\mathbb{C}}}}\times[0,1] = \widehat{C}$ (this neighbourhood cannot contain any internal 0-strata at the intersection of 1-strata). Since the Reshetikhin-Turaev defect TQFT is anomaly free, and by the properties of the the ribbon graphs used to evaluate it, we can write

$$\mathcal{Z}^{\mathrm{df}}_{RT,\mathrm{vect}_{\mathbb{C}}}(C^{t^*,\mathcal{A}_{\mathbb{Z}_2\text{- vect}_{\mathbb{C}}}}_{\Sigma}) = \mathcal{Z}^{\mathrm{df}}_{RT,\mathrm{vect}_{\mathbb{C}}}(C') \circ \mathcal{Z}^{\mathrm{df}}_{RT,\mathrm{vect}_{\mathbb{C}}}(\widehat{C})$$

where $C' \in \mathbf{Bord}^{\mathrm{df}}_3(\mathbb{D})$ is such that the gluing of C' to $\widehat{C}$ is homeomorphic to $C^{t^*,\mathcal{A}_{\mathbb{Z}_2\text{- vect}_{\mathbb{C}}}}_{\Sigma}$.

Now from [Construction 3.8, CRS19] we have that $\mathcal{Z}^{\mathrm{df}}_{RT,\mathrm{vect}_{\mathbb{C}}}(C^{t^*,\mathcal{A}_{\mathbb{Z}_2\text{- vect}_{\mathbb{C}}}}_{\Sigma})$ is a projection, and from [Construction 5.5, CRS17] that $\mathcal{Z}^{\mathrm{df}}_{RT,\mathrm{vect}_{\mathbb{C}}}(\widehat{C})$ is too, so it follows that $\mathcal{Z}^{\mathrm{df}}_{RT,\mathrm{vect}_{\mathbb{C}}}(C')$ must be a projection. Writing $\pi = \mathcal{Z}^{\mathrm{df}}_{RT,\mathrm{vect}_{\mathbb{C}}}(C')$ and $f = \mathcal{Z}^{\mathrm{df}}_{RT,\mathrm{vect}_{\mathbb{C}}}(\widehat{C})$, and applying Lemma 5.2.3 completes the proof of Proposition 5.2.1.

We conclude this subsection with a few comments regarding Lemma 5.2.3 and its consequences for the analysis of the projection π in Section 5.2.2. We saw in the proof of Lemma 5.2.3 that the effect of the components of the ribbon graph corresponding to the 2-strata of $\widehat{C}$ is to enforce the copies of T bounding the 2-strata to share simple objects in their constituent hom-spaces. This holds more generally for the components of the ribbon graph corresponding to $C^{t^*,\mathcal{A}_{\mathbb{Z}_2\text{- vect}_{\mathbb{C}}}}_{\Sigma}$. In Section 5.2.2, we will be analysing this ribbon graph more closely, and this analysis is made much simpler by omitting the ribbons corresponding to the 2-strata of $C^{t^*,\mathcal{A}_{\mathbb{Z}_2\text{- vect}_{\mathbb{C}}}}_{\Sigma}$ and instead keep track of the common labels between copies of T.

5.2.2 The Projections π and P_{vert}

We now turn to the proof of Proposition 5.2.2 which proceeds by a close analysis of the ribbon graph associated to $C^{t^*,\mathcal{A}_{\mathbb{Z}_2\text{- vect}_{\mathbb{C}}}}_{\Sigma}$.

Let us consider a specific stratification τ^* for $C_\Sigma^{t^*,\mathcal{A}_{\mathbb{Z}_2\text{-}\mathrm{vect}_\mathbb{C}}}$ that extends t^* which is reproduced below in Figure 5.6 in red. We require t^* to be oriented so we consider the triangulation t (in black) with a total ordering on its vertices, and with edges oriented accordingly. The dual t^* is then oriented such that the orientation of the edge of t followed by the orientation of the corresponding edge in t^* produces the standard orientation of $\mathbb{R}^2$. The labels u_1 through u_8 are used for discussion regarding the ribbon graph associated to the plaquette 5 below.

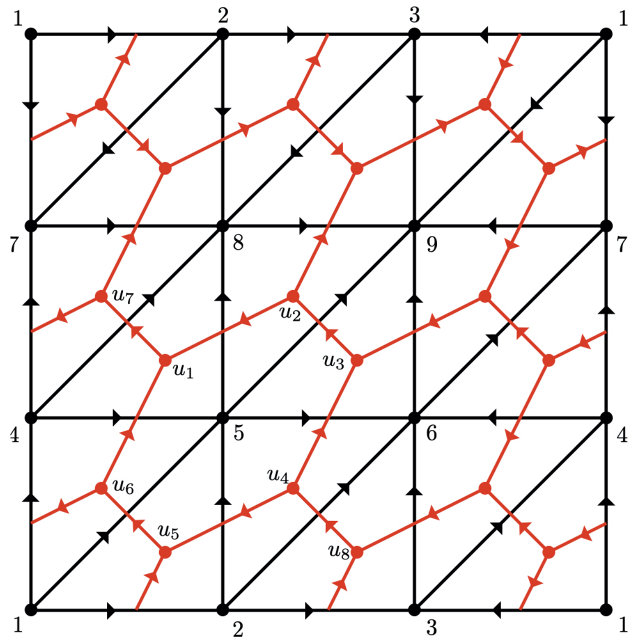

Figure 5.6: An oriented and ordered triangulation of a torus.

To define τ^* we extend the triangulation t of Σ to a triangulation τ of $C_\Sigma^{t^*,\mathcal{A}_{\mathbb{Z}_2\text{-}\mathrm{vect}_\mathbb{C}}}$, and consider its dual. We will construct τ and τ^* piece by piece, with each piece corresponding to a black square in Figure 5.6. We notice that there are four different occurrences of square as determined by the orientations of their edges, as shown in Figure 5.7a. Their relative locations in the torus are shown by Figure 5.7b.

We then consider cylinders over each of these four squares, and triangulate them in a compatible way so that all vertices of τ are vertices of the triangulations of the boundary components of $C_\Sigma^{t^*,\mathcal{A}_{\mathbb{Z}_2\text{-}\mathrm{vect}_\mathbb{C}}}$, and so that when considered together they produce a valid cylinder over $\Sigma^{t^*,\mathcal{A}_{\mathbb{Z}_2\text{-}\mathrm{vect}_\mathbb{C}}}$. We take the triangulation of the outgoing boundary copy of $\Sigma^{t^*,\mathcal{A}_{\mathbb{Z}_2\text{-}\mathrm{vect}_\mathbb{C}}}$ to have total ordering $10,...,18$ such that vertex n of the incoming copy of t lies directly below vertex $n+9$ in the outgoing copy of t for all $n = 1,...,9$. This means that all edges of τ in the interior of $C_\Sigma^{t^*,\mathcal{A}_{\mathbb{Z}_2\text{-}\mathrm{vect}_\mathbb{C}}}$ will be oriented from incoming boundary to outgoing. The diagonally vertical edges of τ in the interior mirror the orientations of the corresponding edges of each copy of t, that is, for an edge oriented from vertex n to vertex m in the incoming copy of t (and equivalent edge from $n+9$ to $m+9$ in the outgoing copy of t), the diagonally vertical edge is oriented from n to $m+9$. The triangulations of the cylinders over the four types of square constructed in this fashion are compatible, and are shown in Figure 5.8.

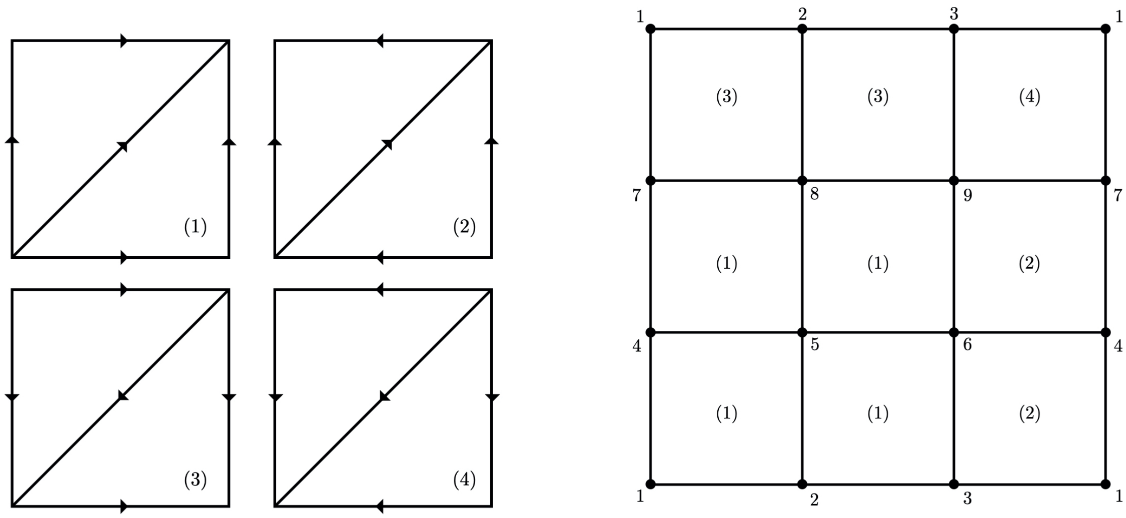

(a) The types of squares in the triangulation.

(b) The location of the different types of squares in the triangulation.

Figure 5.7

For the purposes of brevity and clarity, from this point onwards, we will only treat the cylinder over square (1) since we will calculate the portion of the ribbon graph associated to the plaquette labelled 5 (that is, the plaquette in $(t^*)^{(2)}$ corresponding to the vertex labelled 5 in $t^{(0)}$). The analysis of the other squares and other plaquettes follows via similar methods and reasoning.

The next step is to start to analyse τ^* for the portion corresponding to Figure 5.8a. We need to label the 3-, 2-, 1- and 0-strata of τ^*, which in particular requires us to be able to systematically assign α or $\overline{\alpha}$ to each 0-strata corresponding to a tetrahedron of τ based on its orientation (the other strata are fixed to a single choice of label). The maps α and $\overline{\alpha}$ are elements of the vector spaces that $\mathcal{Z}^{\mathrm{df}}_{RT,\mathrm{vect}_{\mathbb{C}}}$ assigns to specific decorated spheres, namely those in Figure 5.9, where the sphere Figure 5.9a corresponds to α and Figure 5.9b to $\overline{\alpha}$ (see also [Equation 2.16, CRS18]).

We comment here on the 0-strata that do not explictly arise from the dual τ^* but reside in the interior of 3- and 2-strata disjoint from all other strata. These 0-strata are called point insertions and are labelled by ϕ for those 0-strata within 3-strata, and ψ for those within 2-strata. The factor contributed by each ψ to the evaluation of the defect TQFT is the product of the dimensions of simple objects of $\mathbb{Z}_2\text{-}\mathrm{vect}_{\mathbb{C}}$, which we know from Section 5.1.2 also features in the calculation of the Turaev-Viro invariant, but is equal to 1 so we will relieve it of any further consideration in this section. The factor contributed by ϕ is $\frac{1}{\dim \mathbb{Z}_2\text{-}\mathrm{vect}_{\mathbb{C}}} = \frac{1}{2}$ for each 3-stratum, which we also saw in the Turaev-Viro case. In fact, the factor ϕ is only for each full 3-stratum in $C_{\Sigma}^{t^*,\mathcal{A}_{\mathbb{Z}_2\text{-}\mathrm{vect}_{\mathbb{C}}}}$, and instead a factor $\phi^{\frac{1}{2}}$ is present for each 3-stratum that is "cut-off" by the boundary.

We can relate the defect spheres Figure 5.9a and Figure 5.9b to the tetrahedra of τ as follows. By considering the boundary of a tetrahedron as a triangulated sphere, we can orient the edges so that the defect sphere

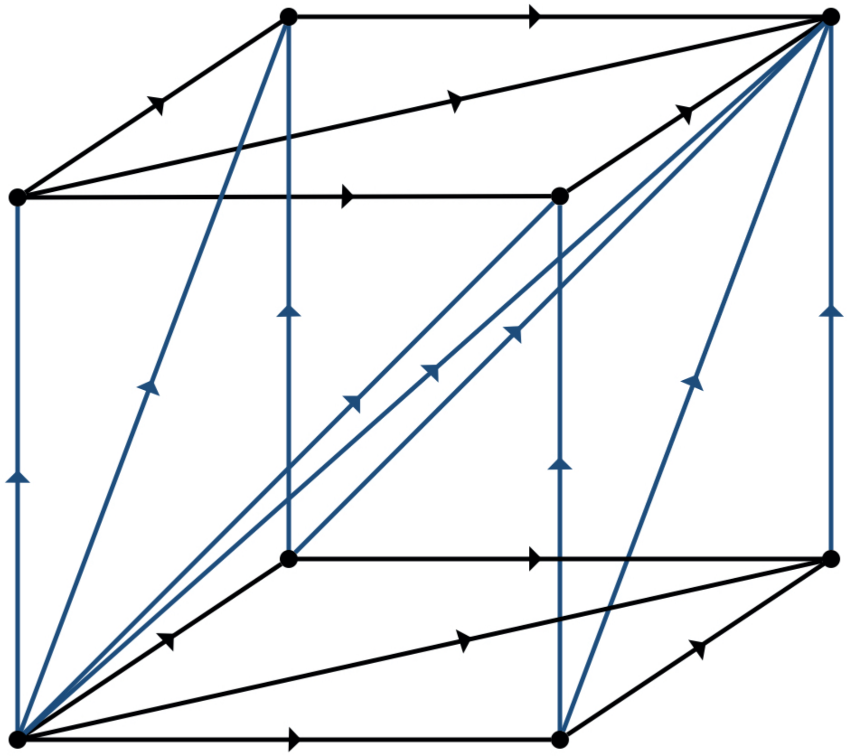

(a) The cylinder of the square (1).

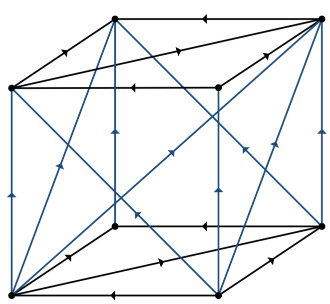

(b) The cylinder over the square (2).

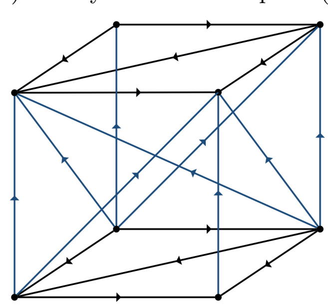

(c) The cylinder over the square (3).

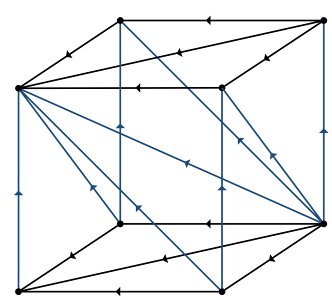

(d) The cylinder over the square (4).

Figure 5.8: The cylinders of the squares of the triangulation.

is stratified by the dual of the triangulated sphere, using the same rule regarding orientations as for t and t^*. This process is shown diagrammatically in Figure 5.10. This figure gives us a reference by which we can assign α and $\overline{\alpha}$ to the tetrahedron of the cylinder over square (1), and hence to the corresponding 0-strata of τ^* in this cylinder, an assignment which is denoted by a rectangular tag in Figure 5.11 (this tag names the 0-strata first, by u or u' with subscripts, the denotes the associated label).

The next task is to catalogue all the 2-cells of τ^* corresponding to the cylinder over square (1), which is done in Figure 5.12. This figure denotes the 1-strata of τ^* in red (where the 0-strata for each half of the

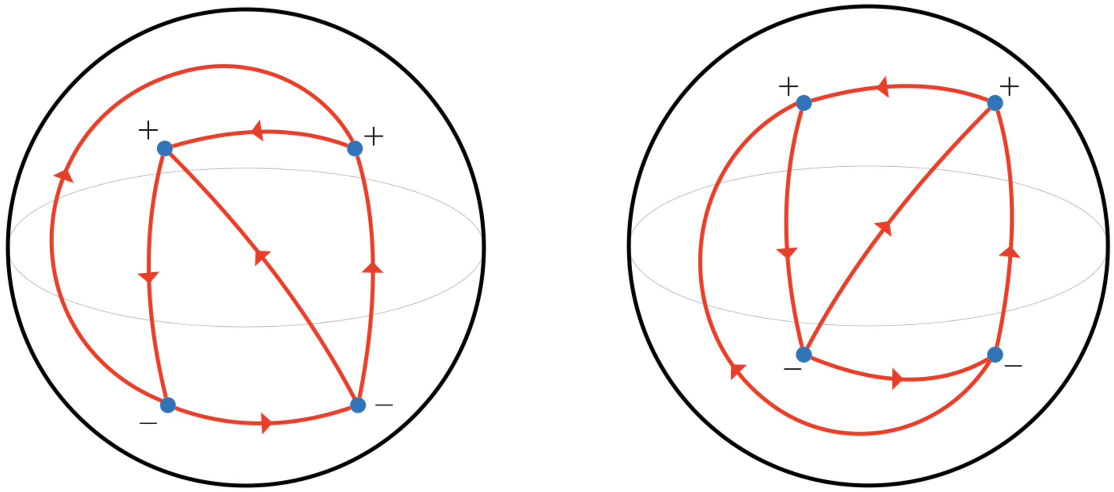

(a) The defect sphere associated to α. (b) The defect sphere associated to $\overline{\alpha}$

Figure 5.9

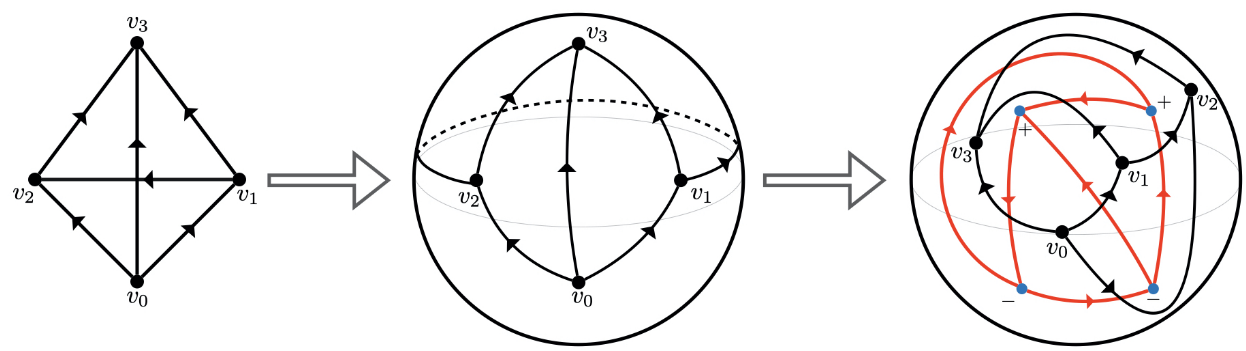

(a) The correspondence between α and the orientation of a tetrahedron.

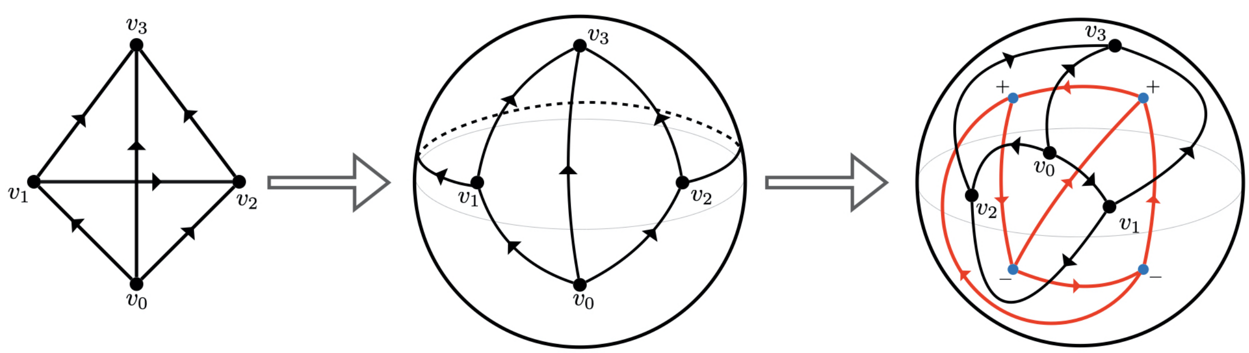

(b) The correspondence between $\overline{\alpha}$ and the orientation of a tetrahedron.

Figure 5.10

cylinder have been denoted as being colinear for diagrammatic simplicity) and the constituent 2-strata in black. These 2-strata are oriented accordingly with respect to the modified stratification and located in the

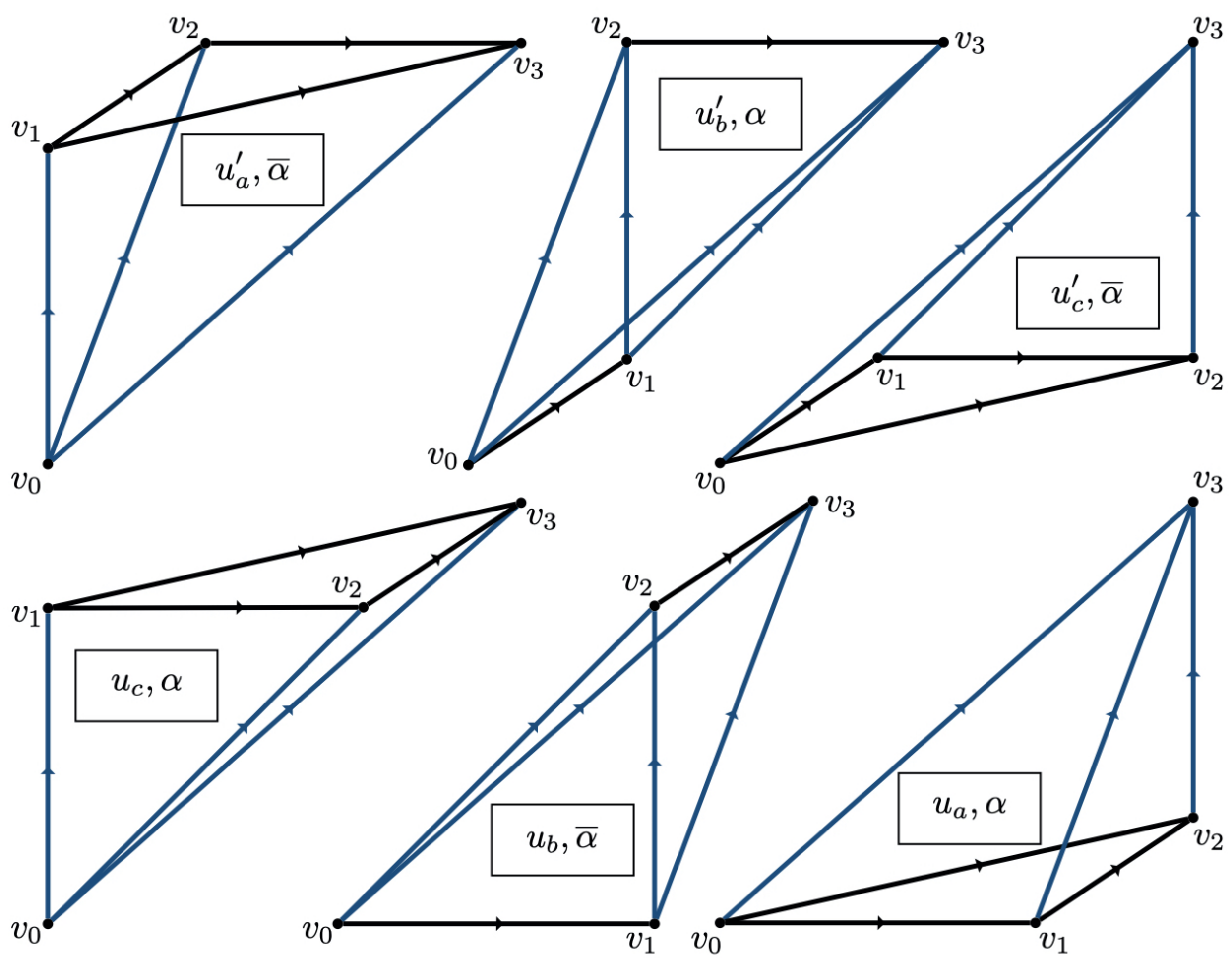

Figure 5.11: The components of the triangulation of the cylinder over square (1) and their associated labels.

diagram close to their location in the stratification. The labels BF, FF, RF, and LF stand for Back Face, Front Face, Right Face and Left Face respectively and indicate where the 1-strata join other squares.

Recall the comments made at the end of the previous subsection regarding how keeping track of how 2-strata connect 1-strata labelled by T relates to the removal of the ribbons associated with those 2-strata. With this in mind, we can present the reduced ribbon graph of just the T-ribbons associated to the cylinder over square (1), shown in Figure 5.13. The same notation is used regarding connections to other squares.

By referring back to Figure 5.6 and Figure 5.7b if needed in order to get straight how these pieces of ribbon graph connect, we can present the (reduced) ribbon graph associated to the plaquette labelled 5, as in Figure 5.15. Again this ribbon graph just shows the T-ribbons; the role played by the $\mathbb{C}^2$-ribbons is filled by the cataloguing of faces, which is presented in Appendix D. The diagram in Figure 5.14 simply shows the 1- and 0-strata of τ^* associated to the plaquette 5 and is meant to be used alongside Appendix D to identify which faces are incident to which 1-strata.

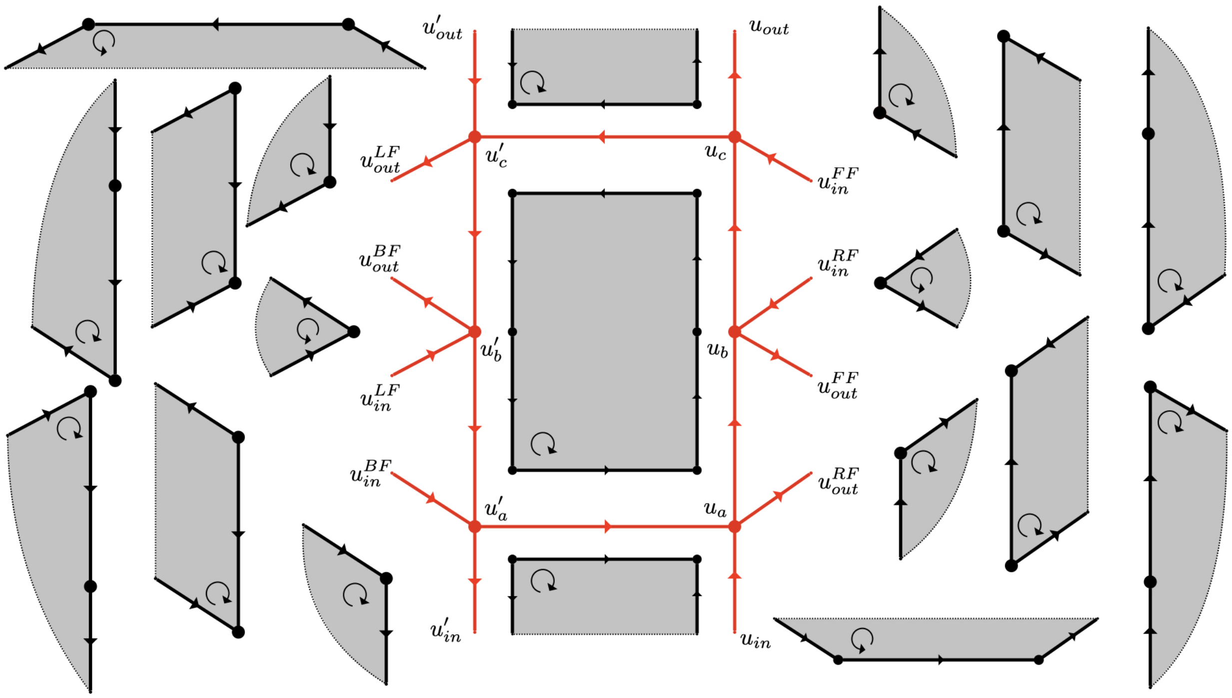

Figure 5.12: A catalogue of the faces of τ^* for the cylinder over square (1).

Note: The labels of faces in Appendix D are capital Latin letters supplemented by captial Latin letters with an overline. There is no relationship between a letter and the same letter with an overline. An alphabet of 43 letters was required to label all faces and this seemed like a valid way of producing one. Any occurence of labels with same base letter on faces that are incident to the same edge is simply coincidence.

We are now close to being able to evaluate the ribbon graph in Figure 5.15, but it will be useful to make a few comments first. Notice that some vertical strands between coupons are oriented downwards and some oriented upwards. In our calculations below, we will reverse the orientations of the downward strands by assigning T^* to them instead of T (see Appendix A.2 for the rules on manipulating ribbon graphs). The big ribbon graph in Figure 5.15 will be computed in pieces, one piece for each vertex u_i of the plaquette 5 (as depicted in Figure 5.6). By invoking the isomorphism $T \cong T^*$ (objects of $\mathrm{vect}_{\mathbb{C}}$ are isomorphic to their duals), we will orient all strands for each ribbon graph piece to be generally upwards, where all strands for a piece are labelled either by T or T^* (this becomes clearer in the Figure 5.16 through Figure 5.21). The pieces of ribbon graph will be evaluated by analysing how the corresponding piece of the morphism acts on basis element of T and T^*, denoted by $\lambda_{ABC} \in \mathrm{Hom}_{\mathbb{Z}_2\text{-}\mathrm{vect}_{\mathbb{C}}}(A \otimes B, C)$ and $\hat{\lambda}_{ABC} \in \mathrm{Hom}_{\mathbb{Z}_2\text{-}\mathrm{vect}_{\mathbb{C}}}(C, A \otimes B)$ respectively (these basis vectors are identified under the isomorphism). We will use the capitalised letters to denote both the label for a given 2-cell of τ^* as well as the simple object corresponding to it in a hom-space of T.

With this notation, we then write down formula for the maps α and $\overline{\alpha}$ for both T and T^*, which make use of the F-tensor (and its inverse) for $\mathbb{Z}_2\text{-}\mathrm{vect}_{\mathbb{C}}$ (see Example 3.1.15), and allows for straightforward calculations

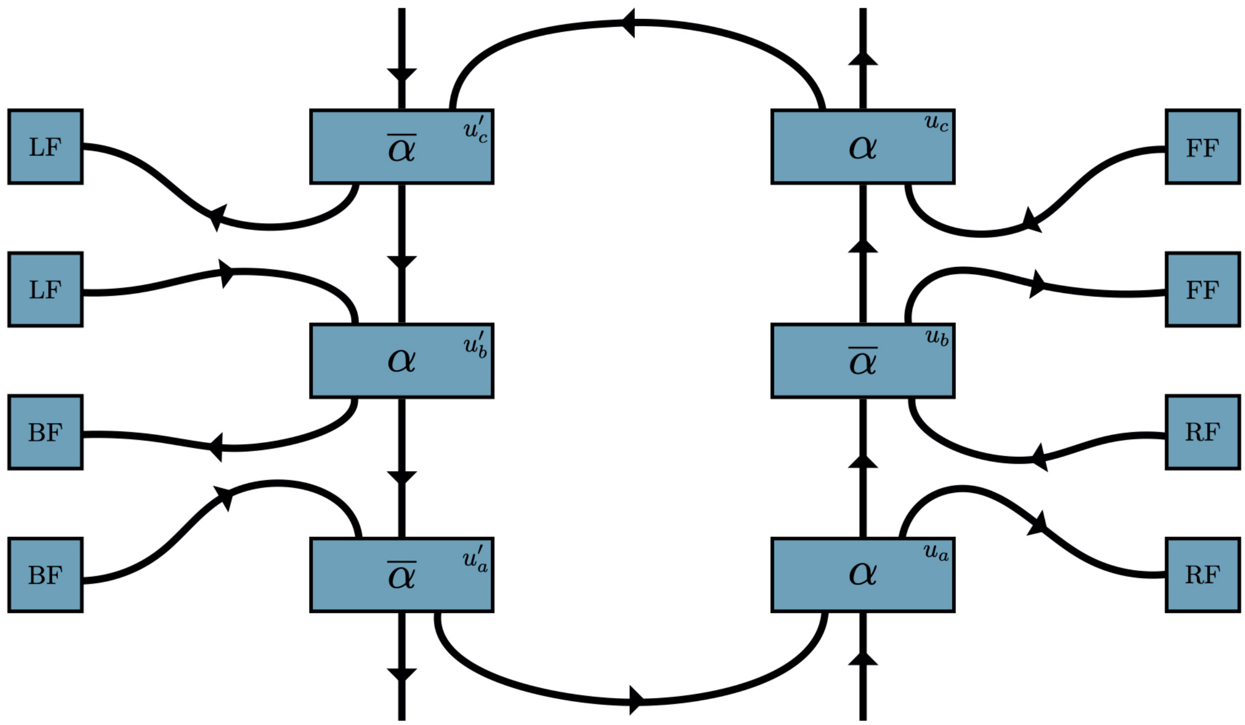

Figure 5.13: The reduced ribbon graph corresponding to τ^* over square (1).

below. We have

$$\begin{aligned} \alpha : T \otimes_C T &\to T \otimes_F T \\ \lambda_{ABC} \otimes_C \lambda_{CDE} &\mapsto \mathbf{F}^{\lambda_{ABC},\lambda_{CDE}}_{\lambda_{AFE},\lambda_{BDF}} \, \lambda_{AFE} \otimes_F \lambda_{BDF} \end{aligned} \tag{5.7}$$

$$\begin{aligned} \overline{\alpha} : T \otimes_C T &\to T \otimes_F T \\ \lambda_{ACE} \otimes_C \lambda_{BDC} &\mapsto \mathbf{F}^{-1} \, \lambda_{ABF} \otimes_F \lambda_{FDE} \end{aligned} \tag{5.8}$$

$$\begin{aligned} \alpha : T^* \otimes_C T^* &\to T^* \otimes_F T^* \\ \lambda_{ACE} \otimes_C \lambda_{BDC} &\mapsto \mathbf{F}^{-1} \, \lambda_{ABF} \otimes_F \lambda_{FDE} \end{aligned} \tag{5.9}$$

$$\begin{aligned} \overline{\alpha} : T^* \otimes_C T^* &\to T^* \otimes_F T^* \\ \lambda_{ABC} \otimes_C \lambda_{CDE} &\mapsto \mathbf{F} \, \lambda_{AFE} \otimes_F \lambda_{BDF} \end{aligned} \tag{5.10}$$

where the F-tensor here has been boldified to distinguish it from the label F (and the sub- and super-scripts dropped after the first occurence). We notice that α and $\overline{\alpha}$ for T^* are equivalent to $\overline{\alpha}$ and α for T respectively (with λ's replaced by $\hat{\lambda}$'s). These maps are defined in [Equations (4.37) and (4.38), CRS18] where the image of each map is summed over all possible simple objects F, but for the case at hand, there will always be exactly one simple object of $\mathbb{Z}_2\text{-}\mathrm{vect}_{\mathbb{C}}$ that satisfies the F-tensor. The role of the F-tensor is to ensure that the hom-spaces that the λ generate are non-zero in both the domain and codomain of the maps α and $\overline{\alpha}$. That is, for $\alpha : T \otimes_C T \to T \otimes_F T$ above, the F-tensor enforces that $\mathrm{Hom}_{\mathbb{Z}_2\text{-}\mathrm{vect}_{\mathbb{C}}}(A \otimes B, C)$, $\mathrm{Hom}_{\mathbb{Z}_2\text{-}\mathrm{vect}_{\mathbb{C}}}(C \otimes D, E)$, $\mathrm{Hom}_{\mathbb{Z}_2\text{-}\mathrm{vect}_{\mathbb{C}}}(A \otimes F, E)$ and $\mathrm{Hom}_{\mathbb{Z}_2\text{-}\mathrm{vect}_{\mathbb{C}}}(B \otimes D, F)$ are all non-zero (where A, B, C, D, E, F are all simple

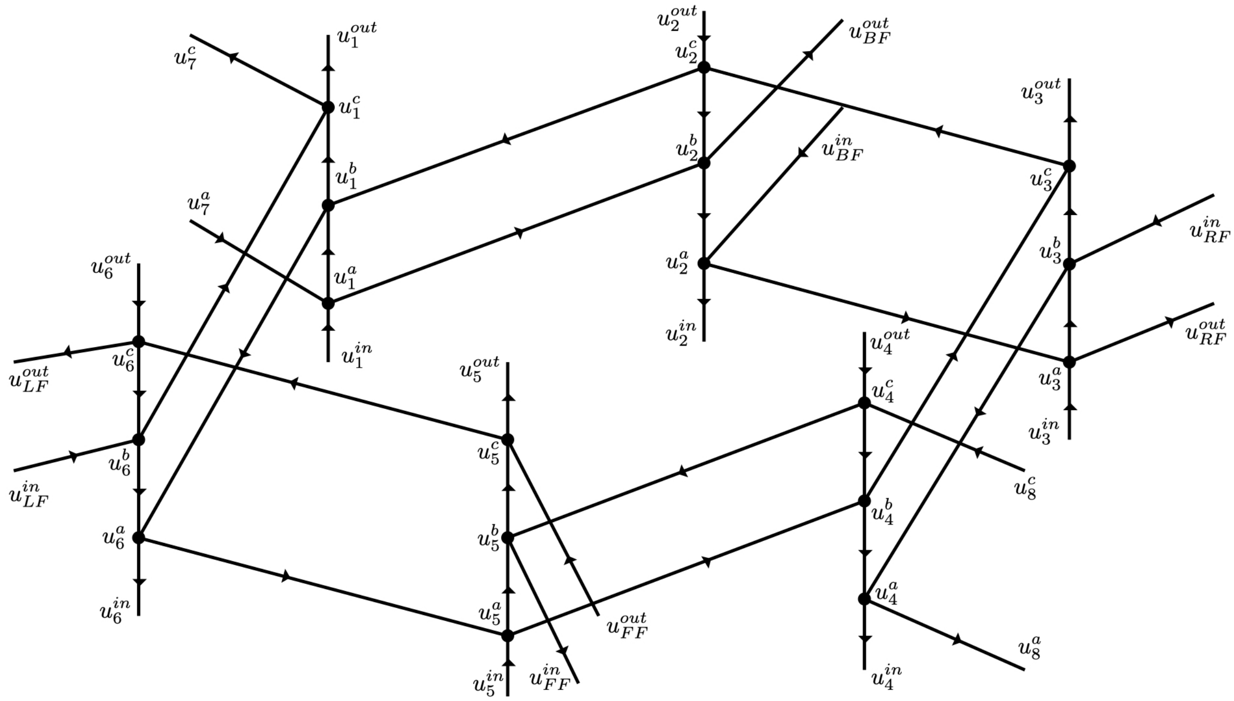

Figure 5.14: A diagram of the 1-strata of τ^* for the plaquette 5.

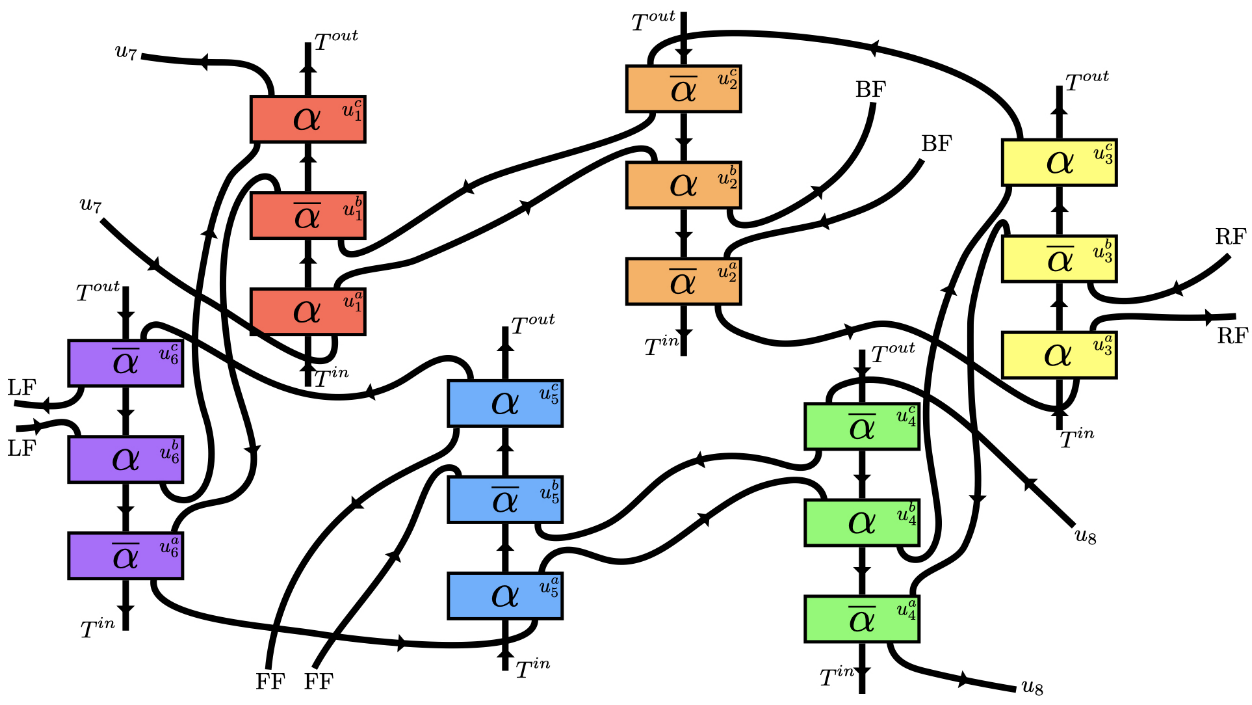

Figure 5.15: The reduced ribbon graph for the plaquette 5.

objects). Just as in Example 3.1.15 we can write

$$\mathbf{F}^{\lambda_{ABC},\lambda_{CDE}}_{\lambda_{AFE},\lambda_{BDF}} := \delta_{(A+B=C \mod 2)}\,\delta_{(C+D=E \mod 2)}\,\delta_{(A+F=E \mod 2)}\,\delta_{(B+D=F \mod 2)}$$

where the equations defining the Kronecker deltas arise from the fusion rules of $\mathbb{Z}_2$- $\mathrm{vect}_{\mathbb{C}}$.

We analyse the ribbon graph by considering a tensor product of basis vectors of each of the copies of T (or T^*), that is λ_{ABC} (or $\hat{\lambda}_{ABC}$) which are labelled by the superscript 'in' in Figure 5.15. The labels of these basis elements are constrained by the tensoring of the T over $\mathbb{C}^2$, meaning that basis elements of copies of T that share an incident 2-stratum, will share the label corresponding to that 2-stratum.

We now analyse the piece of ribbon graph corresponding to u_1. This piece of the graph is shown in Figure 5.16 and the corresponding diagram chase is as follows, where we are making use of the formula for α and $\overline{\alpha}$ from Equation (5.7) through Equation (5.10) (note that the ribbon depicted in Figure 5.16 indicates which 2-strata is common between the T-ribbons incident to a coupon by the subscript on the '$\bigotimes$' symbol between ribbons). The following equations describe the path of the basis vector $\lambda^{\text{in}}_{IH\overline{J}}$ through the ribbon graph:

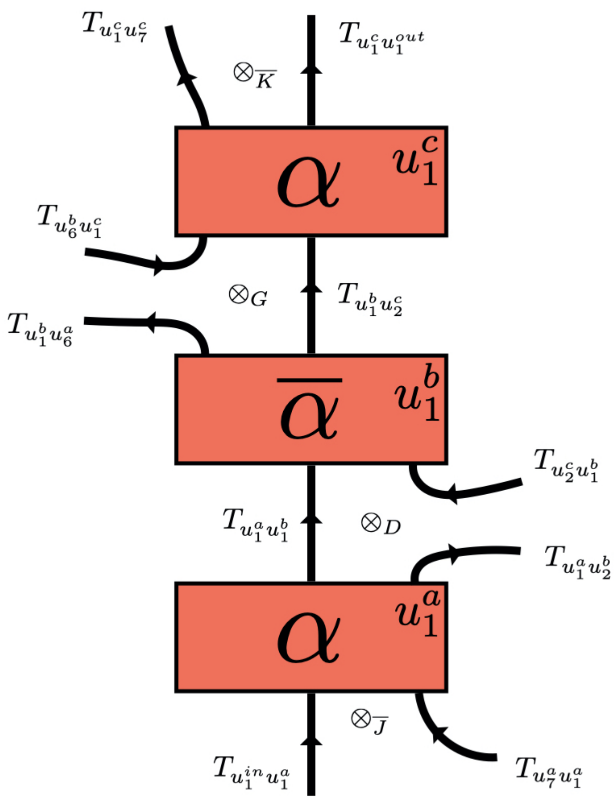

Figure 5.16: The reduced ribbon graph localised at u_1.

$$\lambda^{\text{in}}_{IH\overline{J}} \otimes_{\overline{J}} \lambda_{\overline{J}RJ} \overset{\alpha}{\mapsto} \delta_{H+I=\overline{J}}\, \delta_{\overline{J}+R=J}\, \delta_{H+R=D}\, \delta_{I+D=J}\, \lambda_{IDJ} \otimes_D \lambda_{HRD}$$
$$\lambda_{IDJ} \otimes_D \lambda_{AKD} \overset{\overline{\alpha}}{\mapsto} \delta_{I+D=J}\, \delta_{A+K=D}\, \delta_{I+A=G}\, \delta_{G+K=J}\, \lambda_{IAG} \otimes_G \lambda_{GKJ}$$
$$\lambda_{SLG} \otimes_G \lambda_{GKJ} \overset{\alpha}{\mapsto} \delta_{L+S=G}\, \delta_{G+K=J}\, \delta_{L+K=\overline{K}}\, \delta_{S+\overline{K}=J}\, \lambda_{S\overline{K}J} \otimes_{\overline{K}} \lambda^{\text{out}}_{LK\overline{K}}$$

The subscripts on the δ are still regarded modulo two, the notation was dropped for simplicity. For $\lambda_{LK\overline{K}}$ to be non-zero, the following have to be satisfied (not all of the equations pertain directly to the labels $L, K, \overline{K}$; the list below represents all the constraints enforced by the graph at u_1):

$$H + I = \overline{J} \tag{5.11}$$
$$\overline{J} + R = J$$
$$H + R = D \tag{5.12}$$
$$I + D = J$$
$$A + K = D \tag{5.13}$$
$$I + A = G \tag{5.14}$$
$$G + K = J$$
$$L + S = G \tag{5.15}$$
$$L + K = \overline{K} \tag{5.16}$$
$$S + \overline{K} = J$$

The analysis of the vertices $u_2, ..., u_6$ proceeds in exactly the same fashion, whilst noting that for u_2, u_4 and u_6 the ribbons are labelled with T^* instead of T. The portion of the ribbon graphs associated to u_2 through u_6 are depicted in Figure 5.17 through Figure 5.21 (where the same convention for denoting which labels are common between ribbons T as Figure 5.16 is used) and the corresponding calculations are below.

The diagram chase for the ribbon graph at u_2 (Figure 5.17) is:

$$\hat{\lambda}^{\text{in}}_{H\overline{L}T} \otimes_T \hat{\lambda}_{TUB} \overset{\overline{\alpha}}{\mapsto} \delta_{H+\overline{L}=T}\, \delta_{T+U=B}\, \delta_{H+V=B}\, \delta_{\overline{L}+U=V}\, \hat{\lambda}_{HVB} \otimes_V \hat{\lambda}_{\overline{L}UV}$$
$$\hat{\lambda}_{HVB} \otimes_V \hat{\lambda}_{RWV} \overset{\alpha}{\mapsto} \delta_{H+V=B}\, \delta_{R+W=V}\, \delta_{H+R=D}\, \delta_{D+W=B}\, \hat{\lambda}_{HRD} \otimes_D \hat{\lambda}_{DWB}$$
$$\hat{\lambda}_{AKD} \otimes_D \hat{\lambda}_{DWB} \overset{\overline{\alpha}}{\mapsto} \delta_{A+K=D}\, \delta_{D+W=B}\, \delta_{A+X=B}\, \delta_{K+W=X}\, \hat{\lambda}_{AXB} \otimes_X \hat{\lambda}^{\text{out}}_{KWX}$$

which produces the conditions (any redundancy of conditions imposed with regard to the current portion of the ribbon graph or to previously analysed portions of the ribbon graph is accounted for by only listing new

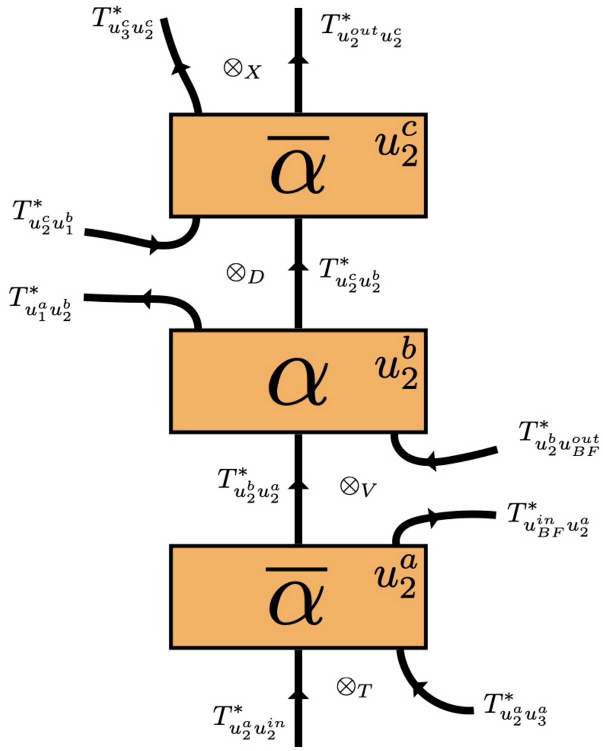

Figure 5.17: The reduced ribbon graph localised at u_2.

conditions):

$$
\begin{aligned}
H + \bar{L} &= T \\
T + U &= B && (5.17) \\
H + V &= B \\
\bar{L} + U &= V && (5.18) \\
R + W &= V && (5.19) \\
D + V &= B \\
A + X &= B && (5.20) \\
K + W &= X
\end{aligned}
$$

The diagram chase at u_3 (Figure 5.18) is:

$$
\begin{gathered}
\lambda^{in}_{M\overline{M}T} \otimes_T \lambda_{TUB} \overset{\alpha}{\mapsto} \delta_{M+\overline{M}=T}\, \delta_{T+U=B}\, \delta\overline{M} + U = Y\, \delta_{M+Y=B}\, \lambda_{MYB} \otimes_Y \lambda_{\overline{M}UY} \\
\lambda_{MYB} \otimes_Y \lambda_{Z\overline{A}Y} \overset{\overline{\alpha}}{\mapsto} \delta_{M+Y=B}\, \delta_{Z+\overline{A}=Y}\, \delta_{M+Z=E}\, \delta_{E+\overline{A}=B}\, \lambda_{MZE} \otimes_E \lambda_{E\overline{E}B} \\
\lambda_{NAE} \otimes_E \lambda_{E\overline{A}B} \overset{\alpha}{\mapsto} \delta_{N+A=E}\, \delta_{E+\overline{A}=B}\, \delta_{A+X=B}\, \delta_{N+\overline{A}=X}\, \lambda_{AXB} \otimes_X \lambda^{\text{out}}_{N\overline{A}X}
\end{gathered}
$$

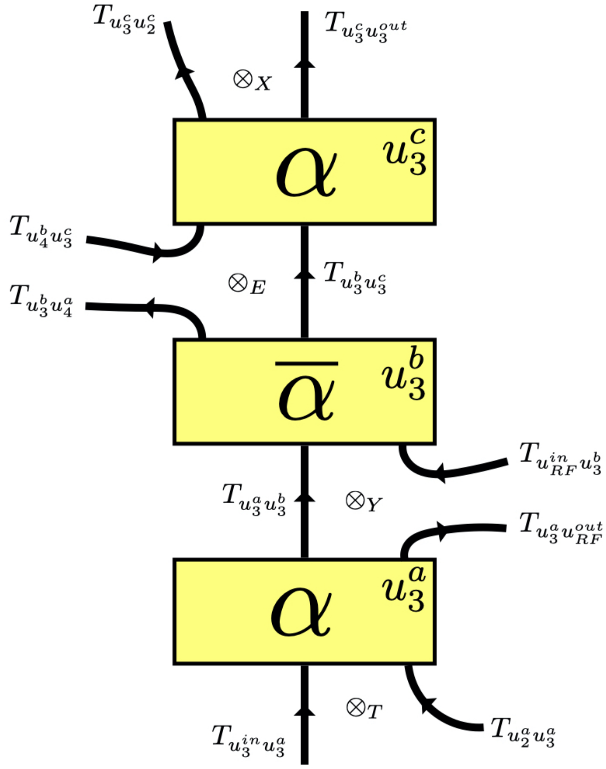

Figure 5.18: The reduced ribbon graph localised at u_3.

which produced the (new) conditions:

$$\begin{aligned} M + \bar{M} &= T \qquad (5.21)\\ \bar{M} + U &= Y \\ M + Y &= B \\ Z + \bar{A} &= Y \\ E + \bar{A} &= B \\ N + A &= E \qquad (5.22)\\ N + \bar{A} &= X \qquad (5.23)\\ M + Z &= E \qquad (5.24) \end{aligned}$$

The diagram chase at u_4 (Figure 5.19) is:

$$\hat{\lambda}^{\text{in}}_{OM\overline{N}} \otimes_{\overline{N}} \hat{\lambda}_{\overline{N}ZP} \overset{\overline{\alpha}}{\longmapsto} \delta_{O+M=\overline{N}}\, \delta_{\overline{N}+Z=P}\, \delta_{O+E=P}\, \delta_{M+Z=E}\, \hat{\lambda}_{OEP} \otimes_E \hat{\lambda}_{MZE}$$
$$\hat{\lambda}_{OEP} \otimes_E \hat{\lambda}_{ANE} \overset{\alpha}{\longmapsto} \delta_{O+E=P}\, \delta_{A+N=E}\, \delta_{O+A=F}\, \delta_{F+N=P}\, \hat{\lambda}_{OAF} \otimes_F \hat{\lambda}_{FNP}$$
$$\hat{\lambda}_{\overline{B}QF} \otimes_F F\hat{N}P \overset{\overline{\alpha}}{\longmapsto} \delta_{\overline{B}+Q=P}\, \delta_{F+N=P}\, \delta_{\overline{B}+\overline{O}=P}\, \delta_{N+Q=\overline{O}}\, \hat{\lambda}_{\overline{BO}P} \otimes_{\overline{O}} \hat{\lambda}^{\text{out}}_{QN\overline{O}}$$

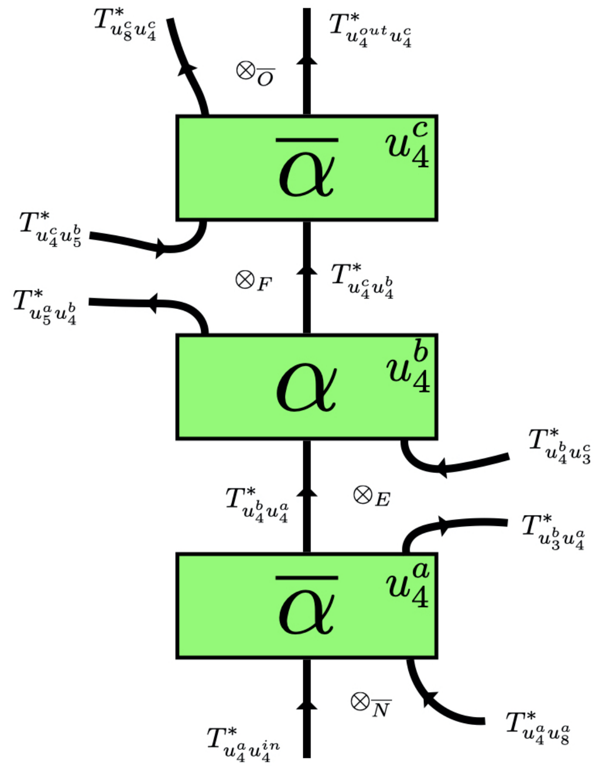

Figure 5.19: The reduced ribbon graph localised at u_4.

which produces the conditions:

$$\begin{aligned} O + M &= \bar{N} \\ \bar{N} + Z &= P \qquad (5.25) \\ O + E &= P \\ O + A &= F \qquad (5.26) \\ F + N &= P \\ \bar{B} + Q &= F \qquad (5.27) \\ \bar{B} + \bar{O} &= P \qquad (5.28) \\ N + Q &= \bar{O} \end{aligned}$$

The diagram chase for u_5 (Figure 5.20) is:

$$\lambda^{\text{in}}_{\overline{D}O\overline{C}} \otimes_{\overline{C}} \lambda_{\overline{C}AC} \xmapsto{\alpha} \delta_{\overline{D}+O=\overline{C}}\, \delta_{\overline{C}+A=C}\, \delta_{\overline{D}+F=C}\, \delta_{O+A=F}\, \lambda_{\overline{D}FC} \otimes_F \lambda_{OAF}$$

$$\lambda_{\overline{D}FC} \otimes_F \lambda_{\overline{B}QF} \xmapsto{\overline{\alpha}} \delta_{\overline{D}+F=C}\, \delta_{\overline{B}+Q=F}\, \delta_{\overline{D}+\overline{B}=\overline{E}}\, \delta_{\overline{E}+Q=C}\, \lambda_{\overline{DBE}} \otimes_{\overline{E}} \lambda_{\overline{E}QC}$$

$$\lambda_{\overline{GPE}} \otimes_{\overline{E}} \lambda_{Q\overline{E}C} \xmapsto{\alpha} \delta_{\overline{G}+\overline{P}=\overline{E}}\, \delta_{Q+\overline{E}=C}\, \delta_{\overline{G}+\overline{F}=C}\, \delta_{\overline{P}+Q=\overline{F}}\, \lambda_{\overline{GF}C} \otimes_{\overline{F}} \lambda^{\text{out}}_{\overline{P}Q\overline{F}}$$

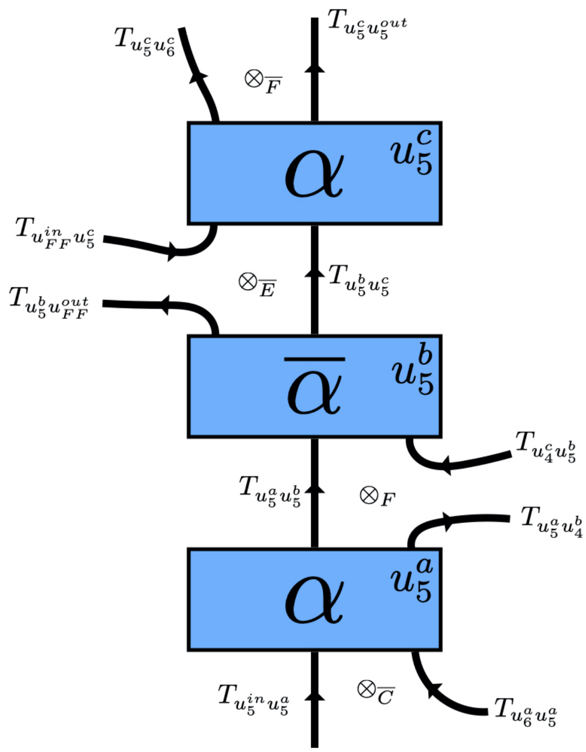

Figure 5.20: The reduced ribbon graph localised at u_5.

which produces the conditions:

$$\bar{D} + O = \bar{C} \tag{5.29}$$

$$\bar{C} + A = C \tag{5.30}$$

$$\bar{D} + F = C$$

$$\bar{D} + \bar{B} = \bar{E} \tag{5.31}$$

$$\bar{E} = Q = C$$

$$\bar{G} + \bar{P} = \bar{E} \tag{5.32}$$

$$\bar{G} + \bar{F} = C \tag{5.33}$$

$$\bar{P} + Q = \bar{F} \tag{5.34}$$

Finally, the diagram chase for u_6 (Figure 5.21) is:

$$\hat{\lambda}^{\text{in}}_{\overline{H}I\overline{C}} \otimes_{\overline{C}} \hat{\lambda}_{\overline{C}AC} \xmapsto{\overline{\alpha}} \delta_{\overline{H}+I=\overline{C}}\, \delta_{\overline{C}+A=C}\, \delta_{\overline{H}+G=C}\, \delta_{I+A=G}\, \hat{\lambda}_{\overline{H}GC} \otimes_G \hat{\lambda}_{IAG}$$

$$\hat{\lambda}_{\overline{H}GC} \otimes_G \hat{\lambda}_{SLG} \xmapsto{\delta}_{\overline{H}+G=C}\ \delta_{S+L=G}\, \delta_{\overline{H}+S=\overline{I}}\, \delta_{\overline{I}+L=C}\, \hat{\lambda}_{\overline{H}S\overline{I}} \otimes_{\overline{I}} \hat{\lambda}_{\overline{I}LC}$$

$$\hat{\lambda}_{\overline{GQI}} \otimes_{\overline{I}} \hat{\lambda}_{\overline{I}LC} \xmapsto{\overline{\alpha}} \delta_{\overline{G}+\overline{Q}=\overline{I}}\, \delta_{\overline{I}+L=C}\, \delta_{\overline{G}+\overline{F}=C}\, \delta_{\overline{Q}+L=F}\, \hat{\lambda}_{\overline{GF}C} \otimes_{\overline{F}} \hat{\lambda}^{\text{out}}_{\overline{Q}L\overline{F}}$$

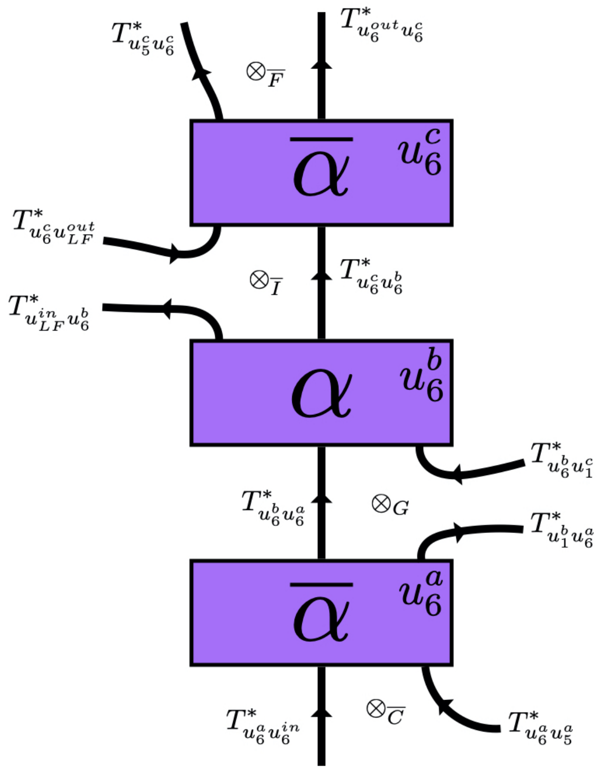

Figure 5.21: The reduced ribbon graph localised at u_6.

which produces the conditions:

$$\bar{H} + I = \bar{C} \tag{5.35}$$
$$\bar{H} + G = C$$
$$\bar{H} + S = \bar{I}$$
$$\bar{I} + L = C$$
$$\bar{G} + \bar{Q} = \bar{I}$$
$$\bar{Q} + L = \bar{F} \tag{5.36}$$

Let us now discuss how to interpret the results of these calculations. Recall from the proof of Proposition 5.1.2 that the labels of faces incident to the inward boundary component and the labels of faces incident to the outward boundary component were identifed with the labels of edges of the coloured skeletons G^{c_0} and G^{c_1} respectively, and from there related to basis vectors of $\mathrm{Im}(P_{\mathrm{plaq}})$. Moreover, the labels of the "horizontal faces" were identified with the elements of $\mathfrak{A}$. By Lemma 5.2.3, the domain of π is also $\mathrm{Im}(P_{\mathrm{plaq}})$ and we can interpret the labels of the 2-strata of τ^* in precisely the same way. Let us denote by $\mathbf{e}_j$ the vector in $\mathrm{Im}(P_{\mathrm{plaq}})$ where $j \in \{0,1\}^{|(t^*)|^{(1)}}$ has entries determined by the values of the labels of 2-strata incident to the inward boundary component $\Sigma^{t^*, \mathcal{A}_{\mathbb{Z}_2\text{-}\mathrm{vect}_{\mathbb{C}}}}$.

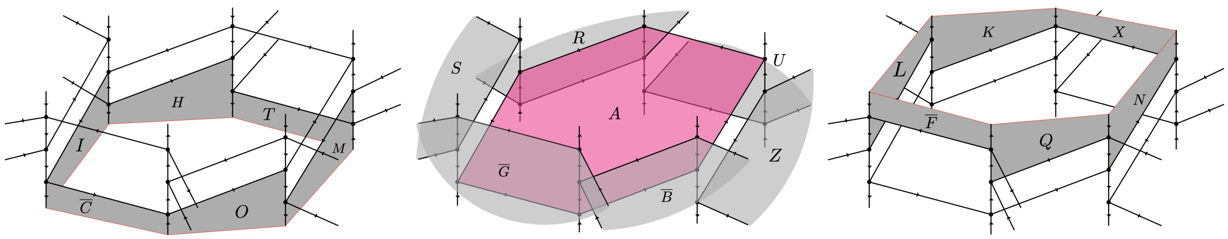

(a) (b) (c)

Figure 5.22: The key labels for relating the ribbon graph to the projector P_{v_5}.

Since we are only considering the piece of the ribbon graph that evaluates to π corresponding to the plaquette 5, we aim to show that morphism represented by this piece of ribbon graph, which we denote π_5, is the component of P_{vert} corresponding to the same plaquette, namely P_{v_5}. By recalling the definition of the projectors P_v from Equation (2.3), our aim is to show that

$$\pi_5(\mathbf{e}_j) = \frac{1}{2}(\mathbf{e}_j + \mathbf{e}_{j+k_{v_5}})$$

where $k_{v_5} \in \{0,1\}^{|(t^*)^{(0)}|}$ is the vector with 1's for the entries corresponding to the edges bounding the plaquette 5, and 0's elsewhere. In terms of labels, this means we aim to write the labels incident to the output boundary component of $C_\Sigma^{t^*, \mathcal{A}_{\mathbb{Z}_2\text{-}\mathrm{vect}_\mathbb{C}}}$ in terms of the input labels, and the label corresponding to the plaquette 5 using the constraints enforced by the ribbon graph. Figure 5.22 portrays a diagram displaying all such labels as well as the labels corresponding to the plaquettes neighbouring plaquette 5. So by using the rules established by the analysis of the ribbon graph at u_1 through u_6, we get

$$\begin{aligned}
L &\overset{5.15}{=} G + S \overset{5.14}{=} A + I + S \\
K &\overset{5.13}{=} A + D \overset{5.12}{=} A + H + R \\
X &\overset{5.20}{=} A + B \overset{5.17}{=} A + U + T \\
N &\overset{5.22}{=} A + E \overset{5.24}{=} A + Z + M \\
Q &\overset{5.27}{=} F + \overline{B} \overset{5.26}{=} A + O + \overline{B} \\
\overline{F} &\overset{5.33}{=} C + \overline{G} \overset{5.30}{=} A + \overline{C} + \overline{G}
\end{aligned}$$

As per Figure 5.22 the labels S, R, U, Z, $\overline{B}$ and $\overline{G}$ correspond to the plaquettes neighbouring plaquette 5. In terms of analyising π_5, we take these to have value 0. In doing so, and by writing the output labels and input labels as the tuples $(L, K, X, N, Q, \overline{F})$ and $(I, H, T, M, O, \overline{C})$ respectively, we get

$$(L, K, X, N, Q, \overline{F}) = (A + I, A + H, A + T, A + M, A + O, A + \overline{C})$$

So for fixed choice of values for the input labels $(I, H, T, M, O, \overline{C})$ and by summing over all other labels, we see that the only tuples $(L, K, X, N, Q, \overline{F})$ that survive are $(I, H, T, M, O, \overline{C})$ when A takes value 0 and $(1 + I, 1 + H, 1 + T, 1 + M, 1 + O, 1 + \overline{C})$ when A takes value 1. By identifiying the fixed input labels with the vector $\mathbf{e}_j$, the tuple $(1+I, 1+H, 1+T, 1+M, 1+O, 1+\overline{C})$ is identified with $\mathbf{e}_{j+k_{v_5}}$ since no other output labels depend on A. Thus, it only remains to note that that the factor of $\frac{1}{2}$ arises from the half point insertions corresponding to the two half 3-strata above and below the 2-strata A.

The same reasoning as has been presented above can be extended to all other plaquettes. The cylinders over the squares (2), (3) and (4) produce similar dual stratifications and hence ribbon graphs consisting of T ribbons passing through two α maps and one $\overline{\alpha}$, or T^* passing through two $\overline{\alpha}$ maps and one α, just as is the case for the square (1). Writing π_{v_i} for the morphisms represented by these ribbon graphs for each plaquette $v_1, ..., v_9$, we can write the morphism represented by the full ribbon graph as $\pi = \pi_{v_1} \circ \pi_{v_2} \circ ... \pi_{v_9}$. The morphism has domain isomorphic to $\mathrm{Im}(P_{\text{plaq}})$ and consists of components equivalent to $P_{v_1}, ..., P_{v_9}$, hence π is equivalent to P_{vert} with domain restricted to $\mathrm{Im}(P_{\text{plaq}})$. This concludes the proof of Proposition 5.2.2.

5.3 Conclusions

The purpose of this section is to provide an evaluation of the proposed model of quantum error-correction using the Reshetikhin-Turaev defect TQFT, and to outline some of the potential steps for further developing this model. We begin by first detailing some of the advantages that a TQFT approach to topological error-correction has over other approaches, then compare the benefits of an approach based on the defect TQFT with those of an approach based on the Turaev-Viro graph TQFT. This is followed by some discussion on the shortcomings of both approaches. Finally, Section 5.3.1 puts forward some possible areas for future work in pursuing a TQFT model of error-correction.

Advantages of a TQFT approach:

Due to the topological nature of topological quantum error-correction, a topological quantum field theory seems like a reasonable place to search for a generalisable model. The primary advantage of this approach is the ability to handle different anyon models with the same machinery. It could well prove true that some general structure is present in topological quantum error-correcting codes that exists for all anyon models, and can be used to direct a search for new and better codes. It may be that the defect TQFT is an ideal lens by which to see this structure. The other key bastion of the TQFT approach is the potential to formulate maps between different codes, either by mapping between TQFTs, or by considering different models internal to the same TQFT, as is the case for the Reshetikhin-Turaev defect TQFT.

Advantages of the Reshetikhin-Turaev defect TQFT over the Turaev-Viro graph TQFT:

Many of the advantages of the Reshetikhin-Turaev defect TQFT have been recounted already, but we reiterate them here. Firstly, the Reshetikhin-Turaev defect TQFT naturally retains more of the structure of the toric code than the Turaev-Viro graph TQFT due to the ability to represent qubits by defects in the surface and morphisms of the bordism category $\mathbf{Bord}_3^{\mathrm{df}}(\mathbb{D})$. It may also be possible to represent logical operations on the code subspace by analysing certain morphisms of $\mathbf{Bord}_3^{\mathrm{df}}(\mathbb{D})$ that are endomorphisms of the surface Σ that produces the codespace via the orbifold. This may be true in the Turaev-Viro case also, however the Reshetikhin-Turaev defect TQFT still plays favourite since the the ability to analyse the defects of such endomorphisms may allow easier generalisation of the component operations on the physical system that produce the logical operations to different anyon models. The fact that the orbifold data is generated internal to $\mathrm{vect}_{\mathbb{C}}$ for any spherical fusion category is also an advantage since the ability to have surfaces labelled by different orbifold data, and hence producing different codes, within the same bordism category and be evaluated by the same functor, provides a much more natural framework to map between codes than for the Turaev-Viro graph TQFT which would require maps between different theories. Analysing the bordisms that encode these maps between codes in $\mathbf{Bord}_3^{\mathrm{df}}(\mathbb{D})$ may also shed light on how to implement these maps practically.

Advantages of the Turaev-Viro graph TQFT:

The primary advantage of the Turaev-Viro graph TQFT is the relative ease of its use and the resultant ease of relating it to the toric code. In comparison to the calculation of the orbifold morphism in Section 5.2.2, the evaluation of $|(\Sigma, A)|^{\circ}$ was relatively straight forward as it required a much simpler choice of cellular decomposition of the cylinder. This advantage may be short-lived since it may soon be the case that the orbifold data for the Reshetikhin-Turaev defect TQFT is adapted to apply to any cell decomposition rather than specifically the dual of a triangulation.

Disadvantages of the TQFT approach:

At the present time, the two largest drawbacks of an approach to quantum error-correction via topological field theories seem to be: the difficulty of use relative to gain in comparison to other models, and the apparent inability to represent operations on physical qubits to a granular enough level. At the moment, the Turaev-Viro and Reshetikhin-Turaev defect TQFTs can produce the code subspace of the toric code and get only part of the way towards representing the projector P_{code}, which can be done much more directly via the stabiliser formalism for quantum error-correction as introduced in Chapter 2. The stabiliser formalism can also describe many more error-correcting codes, topological and otherwise, which have yet to be represented by a TQFT. Moreover, the part of P_{code} that is represented in the TQFT setting, specfically P_{vert}, is not yet done so in a fashion that makes very clear how to interpret the components of the ribbon graph in the orbifold morphism as the action of the Pauli X operation on physical qubit for example. It may well be that with future work done in this area, in particular using the defect TQFT, that these apparent disadvantages will disappear.

5.3.1 Future Work

The immediate areas of future work in developing the error-correction model via the Reshetikhin-Turaev defect TQFT are largely related to completing the translation of the projector P_{code} into this setting. More specifically, the a study of the potential bordisms that replicate the projector P_{plaq} could be undertaken. It would then be necessary to properly investigate how to consider this bordism and the orbifold morphism as a product of commuting projectors which would likely amount to manipulating the resultant ribbon graphs in an appropriate way.

Currently the formalism of the Reshetikhin-Turaev defect TQFT considers only 2-manifolds without boundary, which limits the applicability of this model to physically realisable architectures. However, it does seem possible to extend the Reshetikhin-Turaev TQFT and hence also the defect TQFT to consider surface with boundary [Remark III.1.6, Tur16]. This would then likely allow one to modify the analysis for the toric code to the surface code and its variants.

Finally, the model based on the Reshetikhin-Turaev defect TQFT would start proving its worth if more and more codes could be formulated with it. A possible place to start could be by trying to reproduce the colour code by considering the orbifold data corresponding to the category of $\mathbb{Z}_2 \times \mathbb{Z}_2$-graded vector spaces [Section V, BB19].

Appendix A

Evaluating Graphs and Ribbon Graphs

Underlying both the Turaev-Viro graph TQFT and the Reshetikhin-Turaev TQFT (and hence also the Reshetikhin-Turaev defect TQFT, see either Section 3.4.2 or Appendix C) is the necessity to evaluate graphs, including ribbon graphs, that are labelled with objects and morphisms of a given category $\mathcal{C}$. As will be expanded upon below, to evaluate a labelled graph means to assign a morphism of $\mathcal{C}$ to the graph. In particular, in computing the Turaev-Viro graph TQFT on a given morphism of $\mathbf{Bord}_3^{\mathrm{col}(\mathcal{C})}$, it is necessary to evaluate graphs on spheres surrounding internal nodes of the morphism, and in computing the Reshetikhin-Turaev defect TQFT, it is necessary to compute a morphism associated to a given ribbon graph representing a morphism in $\mathbf{Bord}_3^{\mathrm{df}}(\mathbb{D})$. This appendix is included here for completeness, so provides only the details necessary for earlier chapters. There are many resources that provide far more detail regarding this graphical calculus, for example [JS91]. The details provided below follow the theory outlined in the first four chapters of [TV17].

A.1 Graphs and Ribbon Graphs

Throughout this chapter, we take the term 'graph' to be quite general, as defined below, which may contrast slightly with the use of the term in other chapters (for example when talking about the graph G_A arising from a skeleton G in Section 3.3.1). We take 'graph' to have the following definition, which essentially corresponds to a Reidemeister diagram ([Section 3.2.1, TV17]), which is an extension of a Penrose diagram ([Section 2.2.2, TV17]).

Definition A.1.1. A **graph** is a finite collection of coupons and strands in $\mathbb{R} \times [0, 1] \subset \mathbb{R}^2$ where a **coupon** is a rectangle with sides parallel to the horizontal and vertical axes where one horizontal side is distinguished and called the bottom base, and **strands** are oriented lines that either have endpoints in $\mathbb{R} \times \{0\}$, $\mathbb{R} \times \{1\}$ or the top or bottom bases of a coupon, or form closed loops. The coupons are required to be pairwise disjoint and lie entirely in $\mathbb{R} \times (0, 1)$. If a graph has strands with endpoints in $\mathbb{R} \times \{0\}$ or $\mathbb{R} \times \{1\}$, then it is said to have **free ends**.

Remark A.1.2. (i). The usual notion of graph consisting of edges and vertices can be recovered from the above definition by contracting coupons to a point, and by inserting a vertex into every loop and at every free end.

(ii). In the above definition, there is no restriction placed on strands being able to cross. In particular, the case where crossings are forbidden corresponds to a Penrose diagram, and the case where crossings are allowed to a Reidemeister diagram (see references above). We won't need to make much distinction between the two cases other than in the definition of coloured graphs below.

We take the definition of a ribbon graph almost exactly the same as the definition for graph above, except that each strand now has a framing (so becomes what visually looks like a ribbon), and the ribbon graph is considered in $\mathbb{R}^3$:

Definition A.1.3. A **ribbon graph** is a finite collection of coupons and ribbons in $\mathbb{R} \times [0, 1] \times [0, 1] \subset \mathbb{R}^3$ where a coupon is the same as above, and a **ribbon** is a topological space homeomorphic to either $[0, 1] \times [0, 1]$ or an annulus. Each ribbon homeomorphic to $[0, 1] \times [0, 1]$ must have bases $[0, 1] \times \{0\}$ and $[0, 1] \times \{1\}$ lying in $\mathbb{R} \times \{0\} \times [0, 1]$, $\mathbb{R} \times \{1\} \times [0, 1]$ or in the bottom or top base of a coupon.

Remark A.1.4. It is possible to produce a graph in $\mathbb{R}^2$ from a ribbon graph with only one slight complication. By identifying a ribbon with its 'centreline', that is with $[0, 1] \times \{\frac{1}{2}\}$ or equivalent for the annulus, we can produce strands, and by projecting to $\mathbb{R} \times [0, 1] \times \{0\}$ such that all coupons are disjoint from each other and from $\mathbb{R} \times \{0\} \times \{0\}$ and $\mathbb{R} \times \{1\} \times \{0\}$, we can produce a graph as per Definition A.1.1. The only complication arises in the case where a ribbon is twisted, as this feature is lost when producing a strand from its centreline. This problem is rectified below when coloured graphs are introduced. It is also prudent to make a comment that the projection to $\mathbb{R} \times [0, 1] \times \{0\}$ satisfying the desired criteria can always be taken, but may requires isotoping the ribbon graph. For our ultimate purposes of evaluating a ribbon graph, this does not change the evaluation as it is invariant up to isotopy (more on this later).

For the following definition $\mathcal{C}$ is a tensor category with extra structure as specified.

Definition A.1.5. A **$\mathcal{C}$-coloured graph** (respectively **$\mathcal{C}$-coloured ribbon graph**) is a graph (resp. ribbon graph) such that every strand (resp. ribbon) is labelled by an object of $\mathcal{C}$ and each coupon is labelled by a morphism of $\mathcal{C}$ such that if the the objects labelling strands (ribbons) incident to the bottom base of the coupon are $X_1, ..., X_n$ and the objects labelling the strands (ribbons) incident to the top edge are $Y_1, ..., Y_m$, then the morphism is in $\mathrm{Hom}_{\mathcal{C}}(X_1 \otimes ... \otimes X_n, Y_1 \otimes ... \otimes Y_m)$. The following caveats are also imposed:

- the colouring of a graph containing crossings must be by a braided tensor category $\mathcal{C}$;
- the colouring of a ribbon graph must be by a ribbon category $\mathcal{C}$.

Remark A.1.6. Following on from the comments of the previous remark, a $\mathcal{C}$-coloured graph can be produced from a $\mathcal{C}$-coloured ribbon graph by introducing a new coupon inserted at every twist in a ribbon, labelled by the appropriate twist θ_X where X is the object labelling the ribbon, and then following the same procedure as above. Similarly, it is possible to produce a $\mathcal{C}$-coloured graph without crossings from a $\mathcal{C}$-coloured graph with crossings, by inserting a new coupon at each crossing point which is labelled by the appropriate braiding map. For the purposes of this thesis, we will essentially be considering $\mathcal{C}$-coloured ribbon graphs as $\mathcal{C}$-coloured graphs, sometimes with and sometimes without the crossings replaced by coupons labelled with braiding maps. Consequently, we may, from time to time, drop the term 'ribbon' from our discourse and use 'strand' to mean both ribbon and strand as per the definitions above. Furthermore, since we will be taking either $\mathcal{C} = \mathrm{vect}_{\mathbb{C}}$ or $\mathcal{C} = \mathbb{Z}_2\text{-}\,\mathrm{vect}_{\mathbb{C}}$, much of the time any twists or crossings can be removed due to the corresponding twist and braiding maps of $\mathrm{vect}_{\mathbb{C}}$ and $\mathbb{Z}_2\text{-}\,\mathrm{vect}_{\mathbb{C}}$ being trivial.

A.2 Evaluating Graphs

This section commences by listing the rules for manipulating graphs, and then details how graphs are evaluated. The graphs encountered in this thesis are typically not too complex, so the rules stated below do not necessarily exhaust all possible rules for the graphical calculus. We let $\mathcal{C}$ be a pivotal category, and consider extra structure for particular rules. Let objects and morphisms of $\mathcal{C}$ be denoted by uppercase and lower case Latin letters respectively. All graphs will be read from bottom to top.

Rules for manipulating graphs:

An object X is represented by a strand with label X, and the direction of the strand determines whether the object appears in the domain or codomain of a morphism ψ as X or X^*. A strand with no coupon labelled by X^* is equivalent to a strand with oppposite orientation labelled by X. For a strand labelled X incident to a coupon labelled by f that connects to the bottom base of the coupon, then the domain of f contains X if the strand is oriented towards the coupon, and X^* if the strand is oriented away from the coupon. Conversely, if a strand labelled by X is incident to the top edge of a coupon labelled by f, then the codomain of f contains X if the strand is oriented away from the coupon and X^* otherwise. The morphism id_X can be represented by either strands labelled by X incident to a coupon labelled by id_X with appropriate orientations, or just by a single strand labelled by X. The composition of morphisms $g : X \to Y$ and $f : Y \to Z$ is represented by a strand X oriented towards the bottom edge of a coupon g with strand Y from the top edge of the coupon g to the coupon f, and a strand Z oriented from the top of the coupon f upwards. Graphically, these rules are shown in Figure A.1 through **??**.

A strand labelled by the unit of $\mathcal{C}$, $\mathbb{1}$, is equivalent to the absence of a strand. So a coupon with just a single strand can be viewed as a morphism with domain (or codomain) the unit object, as shown in Figure A.4. In particular, we will see that this means that a graph with no free ends represents a morphism in $\mathrm{End}_{\mathcal{C}}(\mathbb{1})$.

The horizontal juxtaposition of two strands labelled by X and Y represents the object $X \otimes Y$, which can also be represented as a single strand labelled by $X \otimes Y$. Similarly, the tensor product of two morphisms

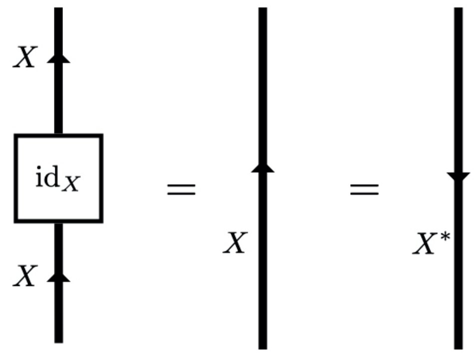

Figure A.1: The equivalence of ribbons labeled by X and X^*.

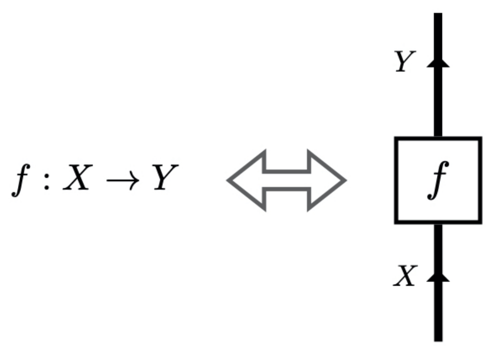

Figure A.2: A coupon depicting a morphism f.

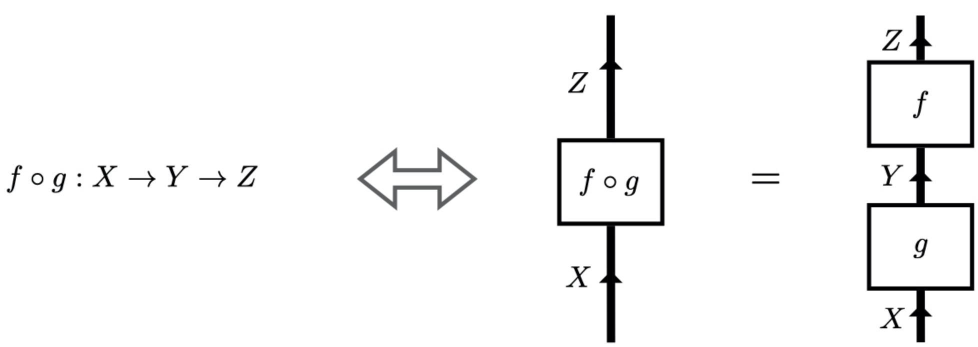

Figure A.3: The composition of morphisms f and g.

$f : X \to Y$ and $g : X' \to Y'$ are given by horizontal juxtaposition. The tensor product $f \otimes g$ can be represented in equivalent ways by manipulating the relative 'heights' of the coupons on each strand (these graphs are all isotopic). These features are shown in Figure A.5 and Figure A.6.

If $\mathcal{C}$ is a rigid category, we can represent the ev, coev, $\widetilde{\mathrm{ev}}$ and $\widetilde{\mathrm{coev}}$ maps either as curved strands or equivalently as two strands incident to either the bottom or top base of the coupon as below. Recalling the

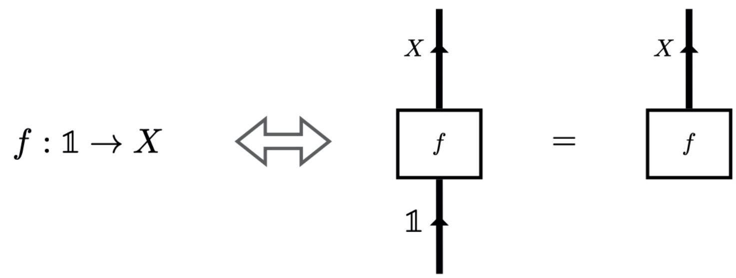

Figure A.4: The ribbon associated to the unit object.

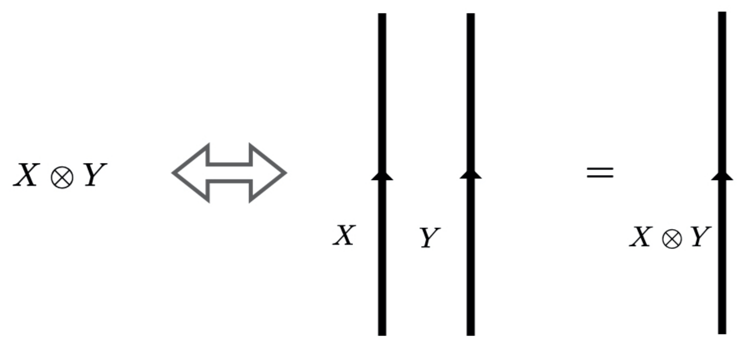

Figure A.5: The tensor product of objects.

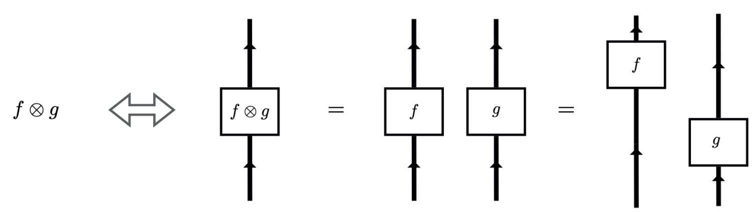

Figure A.6: The tensor product of morphisms.

comments above regarding the unit $\mathbb{1}$, a strand labelled by $\mathbb{1}$ may or may not be present.

Accordingly, it is possible to express both the (left and right) traces and (left and right) dimensions of morphisms and objects respectively in this graphical calculus, shown in Figure A.8. For $\mathcal{C}$ a braided category, as mentioned earlier, a crossing of two strands can be replaced by a coupon labelled by an appropriate braiding map and with appropriately ordered strands, as in Figure A.9.

There are further moves, called Reidemeister moves, that will not be written here explicitly as they are not directly needed for any computation within this thesis, which may be used to manipulate graphs without altering the evaluation of the graph (see Theorem A.2.2 below).

Now we can define by what is meant by evaluating a $\mathcal{C}$-coloured graph G. Using the rules listed above, it is possile to reduce any graph G to a graph G' of the form in Figure A.10.

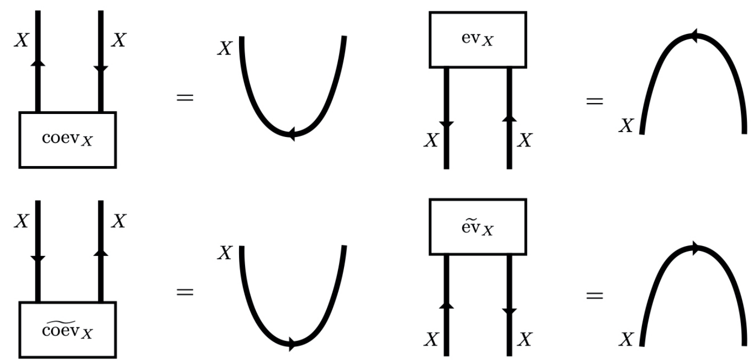

Figure A.7: The coevaluation and evaluation maps for $\mathcal{C}$.

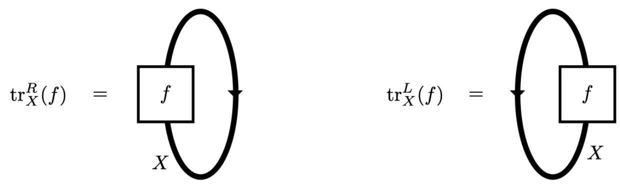

Figure A.8: Left and right trace evaluated on morphism f

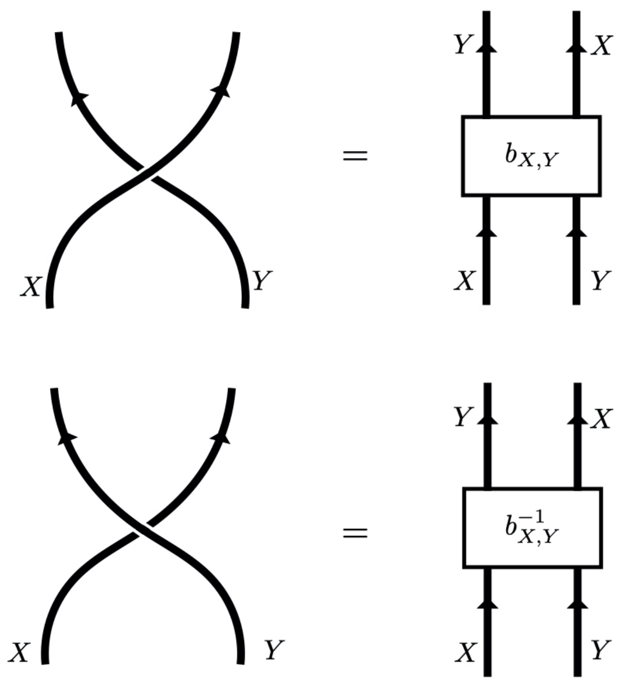

Figure A.9

The evaluation of G is then just the morphism labelling the single coupon of G'. We denote this evaluation by $\mathbb{F}(G)$. At times, in particular when the objects of the category $\mathcal{C}$ can be considered as consisting of a

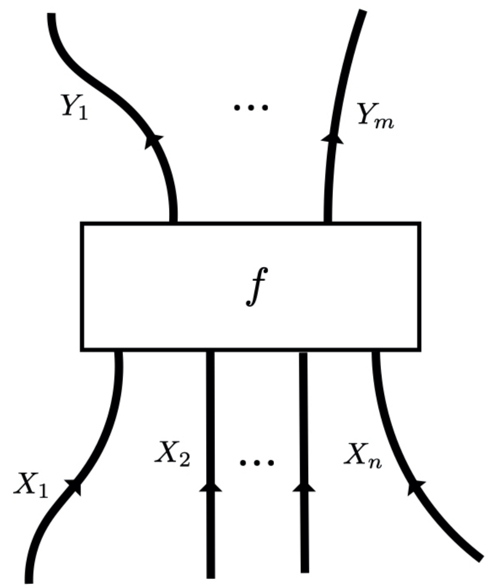

Figure A.10: Any ribbon graph can be reduced to a graph with one coupon.

family of elements (such as a vector space), a graph will be investigated simply by 'diagram-chasing' the object from the bottom of the graph to the top. It will also sometimes be useful to consider a graph G that has objects of $\mathcal{C}$ labelling strands, but no morphisms labelling coupons. In this case, we can consider the tensor product over all coupons v of the relevant hom-spaces H_v associated to each coupon, denoted $\bigotimes_v H_v$, and then define $\mathbb{F}(G)$ as a map

$$\mathbb{F}(G) : \bigotimes_v H_v \to \mathrm{Hom}_{\mathcal{C}}(X_{\mathrm{in}}, X_{\mathrm{out}})$$

where X_{in} is the object (or tensor product of objects) associated to free ends on the bottom of the graph G and X_{out} is the object (or tensor product of objects) associated to the free ends at the top of the graph. In particular, the case where G has no free ends, the map $\mathbb{F}(G)$ has codomain $\mathrm{End}(\mathbb{1})$. This case is relevant to the discussion of the Turaev-Viro graph TQFT in Appendix B.

We conclude this chapter with some key results that are important for use of $\mathbb{F}(\cdot)$ for computations in this thesis, as well as that formalise some comments made above. The first theorem relates the invariance of $\mathbb{F}$ under isotopy and the application of the rules above and is modified slightly from Theorem 3.3 in [TV17].

Theorem A.2.1. *If two $\mathcal{C}$-coloured graphs G and G' are related by isotopy or by any of the rules above (possibly including the Reidemeister rule) relevant to $\mathcal{C}$, then $\mathbb{F}(G) = \mathbb{F}(G')$.*

Here, the phrase 'relevant to $\mathcal{C}$' is to be understood as enforcing only the rules that are applicable for a $\mathcal{C}$-coloured graph can be applied. That is, if $\mathcal{C}$ is a pivotal category without any braiding structure, then the rules associated to crossings cannot be applied. The above theorem was written this way instead of writing out many similar theorems for coloured graphs for each type of category considered.

The next theorem is specific to when $\mathcal{C}$ is a spherical category, and is used when evaluating the Turaev-Viro graph TQFT.

Theorem A.2.2. *[Lemma 2.9, TV17] Let $\mathcal{C}$ be a spherical category and let G and G' be $\mathcal{C}$-coloured graphs. Then if G and G' are related by isotopies on S^2, then $\mathbb{F}(G) = \mathbb{F}(G')$.*

This theorem is useful since we can isotope a graph G on $S^2 = \mathbb{R}^2 \cup \{\infty\}$ away from the pole corresponding to $\{\infty\}$ and so we can consider the graph as residing in $\mathbb{R}^2$.

Appendix B

Supplementary Material for the Turaev-Viro graph TQFT

This appendix has been included to provide a rigorous supplement to the discussion of the Turaev-Viro graph TQFT in Section 3.3. This appendix also provides support to Chapter 5 in which the graph TQFT is used to explicitly compute vector spaces. The material presented here represents a collation of the necessary information from [TV17] and largely follows their terminology, although some notation is changed to match that presented in Section 3.3 and in Chapter 5. Throughout we take $\mathcal{C}$ to be a spherical fusion category over a base field $\Bbbk$.

B.1 Vector Spaces for Coloured Surfaces

Recall from Section 3.3 the definition of a skeleton G of a $Z(\mathcal{C})$-coloured surface (Σ, A), the induced graph G_A, and the definition of the naive vector space

$$|G;(\Sigma,A)|^{\circ} = \bigoplus_{c\in\mathrm{col}(G_A)} \bigotimes_{v\in G_A^{(0)}} H_v.$$

Here we define the vector spaces H_v properly by introducing the necessary theory to define the inverse limit by which these spaces are constructed.

Definition B.1.1. For $X, Y \in \mathcal{C}$, define the **permutation map** $\pi_{X,Y}$ by

$$\begin{aligned}\pi_{X,Y} : \mathrm{Hom}_{\mathcal{C}}(\mathbb{1}, X\otimes Y) &\to \mathrm{Hom}_{\mathcal{C}}(\mathbb{1}, Y\otimes X)\\ f &\mapsto (\mathrm{ev}_X \otimes \mathrm{id}_{Y\otimes X})\circ(\mathrm{id}_{X^*}\otimes f\otimes \mathrm{id}_X)\circ\widetilde{\mathrm{coev}}_X\end{aligned}$$

For any $X, Y \in \mathcal{C}$, $\pi_{X,Y}$ is $\Bbbk$-linear and $\{\pi_{X,Y}\}_{X,Y\in\mathcal{C}}$ is natural for any morphisms $g : X \to X'$, $h : Y \to Y'$.

Moreover, we have the following lemma:

Lemma B.1.1. *[Lemma 12.1, TV17] For any $X, Y \in \mathcal{C}$, $\pi_{X,Y}$ is an isomorphism and $\pi_{X,Y}^{-1} = \pi_{Y,X}$. Furthermore, $\pi_{X,\mathbb{1}} = \pi_{\mathbb{1},X} = \mathrm{id}_{\mathrm{Hom}_{\mathcal{C}}(\mathbb{1},X)}$.*

Let $((X_1, \epsilon_1), ..., (X_n, \epsilon_n))$ be a tuple, where $X_i \in \mathcal{C}$ and $\epsilon_i \in \{+, -\}$, that determines an object $X = X_1^{\epsilon_1} \otimes ... \otimes X_n^{\epsilon_n}$, where $X_i^+ = X_i$ and $X_i^- = X_i^*$. It follows from the definition of $\mathcal{C}$ as spherical fusion that $\mathrm{Hom}_{\mathcal{C}}(\mathbb{1}, X)$ is a $\mathbb{k}$-vector space, which is preserved up to isomorphism via a permutation map for the object arising from the tuple $((X_1, \epsilon_1), ..., (X_n, \epsilon_n))$, as shall be seen below. The signed objects $X_i^{\epsilon_i}$ will be assigned at different times in Chapter 5 to edges incident to a vertex of a graph and to faces incident to edges, so to deal with the general case we make the following definition.

Definition B.1.2. A **cyclic $\mathcal{C}$-set** is a tuple (E, c, ϵ) where E is a finite, non-empty set with a chosen cyclic ordering on its elements, and $c : E \to \mathrm{Ob}(\mathcal{C})$ and $\epsilon : E \to \{+, -\}$ are maps.

For a cyclic $\mathcal{C}$-set (E, c, ϵ) with cyclic ordering $e = e_1 < e_2 < ... < e_n < e_1$, we define the $\mathbb{k}$-vector space

$$H_e = \mathrm{Hom}_{\mathcal{C}}(\mathbb{1}, c(e_1)^{\epsilon(e_1)} \otimes c(e_2)^{\epsilon(e_2)} \otimes ... \otimes c(e_2)^{\epsilon(e_n)}).$$

For some $e' = e_i$ with $i \neq 1$, we define

$$[e, e'] = c(e_1)^{\epsilon(e_1)} \otimes ... \otimes c(e_{i-1})^{\epsilon(e_{i-1})}$$
$$[e', e] = c(e_i)^{\epsilon(e_i)} \otimes ... \otimes c(e_n)^{\epsilon(e_n)}$$

We can then write H_e and $H_{e'}$ in terms of $[e, e']$ and $[e', e]$, like so

$$H_e = \mathrm{Hom}_{\mathcal{C}}(\mathbb{1}, [e, e'] \otimes [e', e])$$
$$H_{e'} = \mathrm{Hom}_{\mathcal{C}}(\mathbb{1}, [e', e] \otimes [e, e'])$$

Having written H_e and $H_{e'}$ in this way, we can define a family of isomorphisms $f_{e,e'}$ for all $e, e' \in E$ where $f_{e,e} = \mathrm{id}_{H_e, H_e}$ and $f_{e,e'} = \pi_{[e,e'],[e',e]} : H_e \to H_{e'}$. For any $e, e', e'' \in E$ where (without loss of generality) $e = e_1 < e_2 < ... < e' = e_i < ... < e'' = e_j < ... < e_n < e_1$, we have that the composite $f_{e',e''} f_{e,e'}$ is the map

$$\begin{aligned}
&\mathrm{Hom}_{\mathcal{C}}(\mathbb{1}, c(e_1)^{\epsilon(e_1)} \otimes c(e_2)^{\epsilon(e_2)} \otimes ... \otimes c(e_{i-1})^{\epsilon(e_{i-1})} \otimes c(e_i)^{\epsilon(e_i)} \otimes ... \otimes c(e_n)^{\epsilon(e_n)}) \\
&\to \mathrm{Hom}_{\mathcal{C}}(\mathbb{1}, c(e_i)^{\epsilon(e_i)} \otimes ... \otimes c(e_{j-1})^{\epsilon(e_{j-1})} \otimes c(e_j)^{\epsilon(e_j)} \otimes ... \otimes c(e_{i-1})^{\epsilon(e_{i-1})}) \\
&\to \mathrm{Hom}_{\mathcal{C}}(\mathbb{1}, c(e_j)^{\epsilon(e_j)} \otimes ... \otimes c(e_n)^{\epsilon(e_n)} \otimes c(e_1)^{\epsilon(e_1)} \otimes ... \otimes c(e_{j-1})^{\epsilon(e_{j-1})})
\end{aligned}$$

and is equal to $f_{e,e''}$. This with the above Lemma B.1.1 is sufficient for $\big(\{H_e\}_{e \in E}, \{f_{e,e'}\}_{e,e' \in E}\big)$ to be a projective system of $\mathbb{k}$-vector spaces and vector space isomorphisms. We then define

$$H(E) = \lim_{\leftarrow} H_e.$$

Since this inverse limit is over a system of isomorphisms, we can define a family, called **cone isomorphisms**, $\{\tau_e : H(E) \to H_e\}_{e\in E}$.

So, for the vector space $|G;(\Sigma, A)|^\circ$ we produce a cyclic $\mathcal{C}$-set for each non-distinguished vertex v (recall the definition of distinguished vertices in Definition 3.3.2) by taking the set of edges incident to v to be E with a choice of ordering, the map $c : E \to \mathrm{Ob}(\mathcal{C})$ is given by the colouring of the graph G_A and the map ϵ encodes whether an edge $e \in E$ is oriented towards v, where $\epsilon(e) = -$, or away from v, where $\epsilon(e) = +$. For a distinguished vertex v_a, the cyclic $\mathcal{C}$-set is defined as follows: $E = \{e_{\text{out}}, v_a, e_{\text{in}}\}$; the map c evaluates e_{in} and e_{out} to be the objects assigned by the colouring of the graph G_A and evaluates v_a to be the object of $\mathcal{C}$ $F(X_a)$ where F is the forgetful functor $F : Z(\mathcal{C}) \to \mathcal{C}$; and the map ϵ is defined by

$$\epsilon(e_{\text{out}}) = +$$
$$\epsilon(e_{\text{in}}) = -$$
$$\epsilon(v_a) = \epsilon(a)$$

where, with a slight abuse of notation, $\epsilon(a)$ is used to denote the sign associated to $a \in A$. In both the distinguished and non-distinguished cases, we take $H_v = H(E)$.

As alluded to in Section 3.3.1, in practice, we invoke the use of a cone isomorphism $\tau_e : H(E) \to H_e$ in order to compute $H(E)$.

B.2 Vector Space Homomorphism Assigned to $\mathrm{id}_{(\Sigma,A)}$

Recall that $|(\Sigma, A)|_{\mathcal{C}}$ is defined via

$$|(\Sigma, A)|_{\mathcal{C}} := \lim_{\leftarrow} \mathrm{Im}(|\,\mathrm{id}_{(\Sigma,A)}, G_A, G_A|^\circ)$$

where

$$|\,\mathrm{id}_{(\Sigma,A)}, G_A, G_A|^\circ = \sum_{c_0, c_1 \in \mathrm{col}(G_A)} |\,\mathrm{id}_{(\Sigma,A)}, G_A^{c_0}, G_A^{c_1}|^\circ$$

and

$$|\,\mathrm{id}_{(\Sigma,A)}, G_A^{c_0}, G_A^{c_1}|^\circ = \frac{\dim(\mathcal{C})^{\#(\Sigma\setminus G) - \#(C_\Sigma \setminus P)}}{\dim(c_1)} \sum_{c \in \mathrm{col}(P,d)} \dim(c)(V_c \otimes \mathrm{id}_{\mathcal{H}(G_R)})(*_c) \tag{B.1}$$

Also recall that the morphism $\mathrm{id}_{(\Sigma,A)}$ is represented by a bordism (C_Σ, R, h), where C_Σ is the cylinder over Σ, R is the ribbon in C_Σ that is defined to be $R = A \times [0, 1]$ (the framing arising from the tangent directions for each $a \in A$), and h is a homeomorphism of $Z(\mathcal{C})$-coloured surfaces:

$$h : (-\Sigma, -A) \sqcup (\Sigma, A) \to (\partial C_\Sigma, \partial R)$$

Here we unpack these formulae and present the required theory to understand them. A number of preliminary definitions are required, which motivates much of the reasoning behind why they are presented here as an appendix.

We first formalise the definition of a 3-skeleton which is denoted by the P in the neat positive diagram (P, d) in Equation (B.1).

Definition B.2.1. A 2**-polyhedron** P is a topological space that can be triangulated using a finite number of simplices of dimension less than or equal to 2 such that all 0-simplices and 1-simplices are faces of 2-simplices. A **stratification** of a 2-polyhedron P is an unoriented graph G_P embedded in P such that $P \setminus \mathrm{Int}(P) \subset G_P$. A **stratified polyhedron** is a 2-polyhedron P endowed with a stratification G_P. The edges and vertices of G_P are denoted $P^{(1)}$ and $P^{(0)}$ respectively.

Definition B.2.2. A **branch of a vertex** $x \in P^{(0)}$ of a stratified 2-polyhedron P is a homotopy class of paths $[0,1] \to P$ starting at x and such that $(0,1]$ is mapped to $P \setminus P^{(1)}$. A **branch of an edge** $e \in P^{(1)}$ is the homotopy class of paths $[0,1] \to P$ starting at the interior of e and mapping $(0,1]$ to $P \setminus P^{(1)}$. The number of branches of a vertex or an edge is called the **valence** of that vertex or edge.

It is the branches of an edge e that can be used to produce a cyclic $\mathcal{C}$-set associated to e as mentioned above.

Definition B.2.3. The **boundary graph** ∂P of a stratified 2-polyhedron P consists of all edges of P with valence 1, and their vertices.

Definition B.2.4. A stratified 2-polyhderon P is ∂**-cylindrical** if for each vertex x in ∂P, there is a unique edge in $P^{(1)} \setminus \partial P$ such that this edge is adjacent to all branches of x and the second endpoint is distinct from x.

Remark B.2.5. If P is ∂-cylindrical, then there is a neighbourhood of ∂P in P that is homeomorphic to $\partial P \times [0,1]$. It is the feature of ∂-cylindricality that ensures compatibility of 3-skeletons (see definition below) with bordisms with collars, and hence the gluing of two 3-skeletons to produce a new 3-skeleton.

Definition B.2.6. Let G be an oriented graph in the boundary ∂M of a compact 3-manfiold M such that all vertices of G have valence greater than or equal to 2. A **3-skeleton** of the pair (M, G) is an oriented ∂-cylindrical stratified 2-polyhedron P embedded in M such that:

1. $\partial P = G$ as oriented graphs and $P \setminus \partial P \subset M \setminus \partial M$;
2. $M \setminus P$ is a disjoint union of open 3-balls and a 3-manifold homeomorphic to $(\partial M \setminus G) \times [0, 1)$.

For any pair (M, G) with G satisfying the above criteria, a 3-skeleton is guaranteed to exist [Theorem 11.5, TV17].

In Equation (B.1), we are taking $M = C_\Sigma$ and $G = G_A^{\mathrm{op}} \sqcup G_A$. We now formalise the definition of a neat positive diagram, which also depends on a number of preliminary definitions.

Definition B.2.7. A **plexus** is a topological space d obtained from a disjoint union of a finite number of oriented circles, oriented arcs and coupons by gluing the endpoint of some arcs to the bases of the coupons. A **coupon** is a rectangle (2-manifold with corners homeomorphic to $[0,1] \times [0,1]$) with a distinguished base, the bottom base. The endpoints of arcs not glued to coupons are called **free ends**. A plexus is $Z(\mathcal{C})$**-coloured** if each circle and arc is labelled with an object of $Z(\mathcal{C})$ and each coupon is labelled with a morphism $f \in \mathrm{Hom}_{Z(\mathcal{C})}(X, Y)$ where X and Y are objects of $Z(\mathcal{C})$ representing the arcs glued to the bottom base and top base of the coupon respectively.

Definition B.2.8. A **knotted plexus** d in an oriented stratified 2-polyhedron P is a plexus d immersed in P such that:

1. all coupons of d are embedded in $P \setminus P^{(1)}$ preserving orientation;
2. all points of d where arcs cross lie in $P \setminus P^{(1)}$ and one of the two strands is distinguished. Arcs may only cross at interior points of each arc;
3. the plexus d is disjoint from $P^{(0)}$ and $d \cap \partial P = \partial d$;
4. the strands of d meet edges in $P^{(1)}$ transversally.

The intersection of strands of d and edges of $P^{(1)}$ not lying in ∂P are called **switches**. A knotted plexus is $Z(\mathcal{C})$**-coloured** if the underlying plexus d is $Z(\mathcal{C})$-coloured.

Each switch w of d lies on an edge e_w in $P^{(1)}$. The strand of d corresponding to the switch w lies in two branches of e_d. Since P is oriented, each of these branches has an orientation.

Definition B.2.9. A switch w is **positive** if the branches of e_d containing d have compatible orientations.

Definition B.2.10. A **positive diagram** is a pair (P, d) where P is a 3-skeleton of a pair (M, G) and d is a knotted plexus in P such that each switch of d is positive.

Definition B.2.11. A positive diagram (P, d) is **neat** if d has no circle strand embedded in $\mathrm{Int}(P)$ and disjoint from the rest of d.

Again, we are guaranteed existence:

Theorem B.2.1. *[Thm 14.4, TV17] All ribbon graphs in (M, G) can be represented by neat positive diagrams.*

Thus, we know a neat positive diagram (P, d) exists for the manifold C_Σ with ribbon graph R and boundary graph $G = G_R = h((G_A^{c_0})^{\mathrm{op}} \sqcup G_A^{c_1})$ for the specific case examined in Chapter 5. The ribbon in that case is empty, so in fact (P, d) is merely a 3-skeleton, but we cover the case where A is non-empty and $R = A \times [0,1]$ in this appendix since this is required to nderstand how the Turaev-Viro graph TQFT evaluates a general coloured surface. For a neat positive diagram corresponding to C_Σ with $R = A \times [0,1]$, we have that (P, d) is $Z(\mathcal{C})$-coloured, with the colouring of d arising from the labelling of the ribbon R by objects of $Z(\mathcal{C})$.

We require yet more terminology before we are able to fully compute Equation (B.1) for the case where R is non-empty. Let (P, d) be a neat positive diagram throughout the following.

Definition B.2.12. A **node** of (P, d) is a vertex of P (i.e. element of $P^{(0)}$), or a switch, crossing, coupon or free end of d. A node is **internal** if it lies in $\mathrm{Int}(M)$.

Remark B.2.13. Pursuant to the comment made above, in the case presented in this thesis, the only nodes we encounter are vertices of P, and the nodes associated to crossings and coupons only occur for analysing the evaluation of the Turaev-Viro graph TQFT on a general morphism, and hence are omitted from this appendix.

Definition B.2.14. Let $\tilde{d} = d \cup P^{(1)} \subset P$. The complement of nodes in $\tilde{d}$ are open intervals. The closure of any such open interval in $\mathrm{Int}(M)$ is called a **rim** of (P, d). Let $\mathcal{E}$ denote the set of all oriented rims of (P, d) and let $\mathcal{E}_\partial$ denote the set of all oriented rims with tail endpoint in ∂M.

Remark B.2.15. In particular, this means that the edges of the graph G_R in ∂M are *not* rims of (P, d). Later, the definition of contraction vectors relies on a tensor product over all rims of (P, d), hence the extra emphasis on what is and is not a rim here. The tensor product is over oriented rims, and we note here that each (unoriented) rim features twice in $\mathcal{E}$, once with each possible orientation.

Definition B.2.16. A **face** of (P, d) is a connected component of $P \setminus \tilde{d}$. The set of faces is denoted $\mathrm{Fac}(P, d)$. Each face has orientation arising from the orientation of the 2-cell of P from which it originates.

Definition B.2.17. A **colouring** of (P, d) is a map $c : \mathrm{Fac}(P, d) \to I$ such that the colouring of all faces adjacent to edges of G_R are consistent with the colouring of those edges.

Remark B.2.18. Recall from the definition of ∂-cylindricality that each edge of G_R has precisely one face adjacent to it. This also ensures that each vertex v of G_R has precisely one (unoriented) rim of (P, d) incident to v (as a node of (P, d)), a point that is relevant below.

Recall from the previous section that a cyclic $\mathcal{C}$-set can be constructed out of both edges incident to a vertex in a graph, as well as from 2-cells incident to an edge, or rather in the case here, faces incident to a rim. We construct these cyclic sets slightly differently for rims of (P, d) corresponding to strands of d and edges of P, as follows.

Let $e \in \mathcal{E}$ be a rim that is an edge of P (i.e. $e \in P^{(1)}$). Then we can consider the cyclic $\mathcal{C}$-set (P_e, c, ϵ) where $P_e = \{f_1, ..., f_n\}$ is the set of branches of (faces incident to) e, with a chosen cyclic ordering, $c : P_e \to I$ is the map induced by the colouring of (P, d) and $\epsilon : P_e \to \{+, -\}$ evaluates to $+$ on a face f_i if the orientation of f_i and the orientation of e are compatible, and $-$ otherwise. As per the previous section, $H(P_e)$ denotes the inverse limit over the hom-spaces

$$\mathrm{Hom}_{\mathcal{C}}(\mathbb{1}, c(f_1)^{\epsilon(f_1)} \otimes ... \otimes c(f_n)^{\epsilon(f_n)}).$$

For a rim $e \in \mathcal{E}$ that corresponds to a strand of d, we define the $\mathcal{C}$-set (P_e, c, ϵ) analogously to the case of distinguished vertices in a graph G_A (and in fact this analogy will be made more explicit shortly). The set

$P_e = \{f_-, e, f_+\}$ where f_- is the face incident to e whose orientation is incompatible with that of e, and f_+ is the face whose orientation is compatible (note that f_- and f_+ have the same orientation since they arise from the same 2-cell of P). Consequently, $\epsilon(f_\pm) = \pm$. The map c assigns to $f_\pm$ their respective colours under the colouring of (P, d) and to e the image of the colour of the strand of d under the forgetful functor $F : Z(\mathcal{C}) \to \mathcal{C}$. The map ϵ evaluates e to $+$ if the orientation of e corresponds to that of its associated strand in d , and $-$ otherwise. Again, $H(P_e)$ denotes the inverse limit over hom-spaces

$$\mathrm{Hom}_{\mathcal{C}}(\mathbb{1}, c(f_-)^* \otimes F(X)^{\epsilon(e)} \otimes c(f_+))$$

where X is the colour of the strand of d corresponding to e.

Now, let us consider the rims in $\mathcal{E}_\partial$. By the comments made regarding ∂-cylindricality earlier, we know that each $e \in \mathcal{E}_\partial$ corresponds to a vertex (distinguished and non-distinguished) of G_R and the edges of G_R correspond to precisely one face of (P, d). We thus get canonical isomorphisms $H(P_e) \cong H(E_v)$ for all e, where e is incident to $v \in G_R$. The spaces $H(P_e)$ where e is a rim corresponding to a strand of d is isomorphic to $H(E_v)$ when v is disinguished. These isomorphisms induce an isomorphism on the tensor product

$$\bigotimes_{e \in \mathcal{E}_\partial} H(P_e) \cong \mathcal{H}(G_R) = \bigotimes_{v \in G_R^{(0)}} H(E_v)$$

which then allows us to write

$$\bigotimes_{e \in \mathcal{E}} H(P_e) \cong \bigotimes_{e \in \mathcal{E} \setminus \mathcal{E}_\partial} H(P_e) \otimes \mathcal{H}(G_R)$$

This starts to provide some context for the term $(V_c \otimes \mathrm{id}_{\mathcal{H}(G_R)})(*_c)$ in Equation (B.1), where the map V_c acts upon $\bigotimes_{e \in \mathcal{E} \setminus \mathcal{E}_\partial} H(P_e)$. The contraction vector $*_c$ is also defined via consideration of the $H(P_e)$, which we turn our attention to next.

We can once more rearrange the tensor product $\bigotimes_{e \in \mathcal{E}} H(P_e)$ to produce

$$\bigotimes_{\hat{e}} H(P_e) \otimes H(P_{-e})$$

where $\hat{e}$ denotes the rim e considered without any orientation and signifies that the tensor product is over all unoriented rims, and where $-e$ denotes the rim e with the opposite orientation. By invoking the cone isomorphisms, we get

$$\begin{aligned} H(P_e) &\cong \mathrm{Hom}_{\mathcal{C}}(\mathbb{1}, X_1^{\epsilon_1} \otimes X_2^{\epsilon_2} \otimes ... \otimes X_n^{\epsilon_n}) \\ H(P_{-e}) &\cong \mathrm{Hom}_{\mathcal{C}}(\mathbb{1}, X_n^{-\epsilon_n} \otimes X_{n-1}^{-\epsilon_{n-1}} \otimes ... \otimes X_1^{-\epsilon_1}) \\ &\cong \mathrm{Hom}_{\mathcal{C}}(X_1^{\epsilon_1} \otimes X_2^{\epsilon_2} \otimes ... \otimes X_n^{\epsilon_n}, \mathbb{1}) \end{aligned}$$

In particular, this allows us to see that $H(P_e)$ and $H(P_{-e})$ are dual to each other, and hence defines a pairing $\omega_e : H(P_e) \otimes H(P_{-e}) \to \Bbbk$. A contraction vector for this pairing is the image of $1_\Bbbk$ under the inverse pairing to ω_e, denoted $\Omega_e : \Bbbk \to H(P_{-e}) \otimes H(P_e)$. Before we proceed any further, let us demonstrate why such an inverse is guaranteed to exist.

According to [Section 4.3.1, TV17], a tensor $\Bbbk$-category $\mathcal{D}$ is **non-degenerate** if it has simple unit object and for each non-degenerate pairing $X \otimes Y \to \mathbb{1}$ in $\mathcal{D}$ the induced pairing

$$\mathrm{Hom}_{\mathcal{D}}(\mathbb{1}, X) \otimes_{\Bbbk} \mathrm{Hom}_{\mathcal{D}}(\mathbb{1}, Y) \to \Bbbk$$

is non-degenerate in $\mathrm{Vect}_{\Bbbk}$. Furthermore, all pre-fusion $\Bbbk$-categories are non-degenerate [Lemma 4.3, TV17]. Here a **pre-fusion $\Bbbk$-category** is a $\Bbbk$-category $\mathcal{D}$ such that there is a set of representative simple objects I satisfying the following:

1. $\mathbb{1} \in I$;
2. $\mathrm{Hom}_{\mathcal{D}}(i, j) = 0$ for any $i \neq j \in I$;
3. every object in $\mathcal{D}$ can be written as a direct sum of a finite number of elements of I.

Clearly, our spherical fusion category $\mathcal{C}$ is pre-fusion and hence is non-degenerate in terms of the definition above. Moreover, we can write down a pairing

$$(X_1^{\epsilon_1} \otimes ... \otimes X_n^{\epsilon_n}) \otimes (X_n^{-\epsilon_n} \otimes ... \otimes X_1^{-\epsilon_1}) \to \Bbbk$$

based on the evaluation maps ev_{X_i} and $\widetilde{\mathrm{ev}}_{X_i}$ which are non-degenerate since their inverses coev_{X_i} and $\widetilde{\mathrm{coev}}_{X_i}$ respectively. Thus, we can find an inverse $\Omega_e : \Bbbk \to H(P_{-e}) \otimes H(P_e)$ for every pairing $\omega_e : H(P_e) \otimes H(P_{-e}) \to \Bbbk$.

Definition B.2.19. A **contraction vector** $*_e$ of a non-degenerate pairing ω_e is defined to be

$$*_e = \Omega_e(1_{\Bbbk})$$

where Ω_e is inverse to ω_e.

We then take the tensor product over all unoriented rims of all contraction vectors:

$$\bigotimes_{\hat{e}} *_e \in \bigotimes_{e \in \mathcal{E}} H(P_e)$$

where again the tensor product over $\hat{e}$ signifies the tensor product over all unoriented rims. Recalling from above that we have a canonical isomorphism

$$\bigotimes_{e \in \mathcal{E}} H(P_e) \cong \bigotimes_{e \in \mathcal{E} \setminus \mathcal{E}_\partial} H(P_e) \otimes \mathcal{H}(G_R),$$

we take $*_c$ to be the image of $\bigotimes_{\hat{e}} *_e$ under this isomorphism.

We finally come to the last piece of the formula (B.1): the map V_c. This map acts on $\bigotimes_{e\in\mathcal{E}\setminus\mathcal{E}_\partial}$ and is defined by even more rearranging of this tensor product and by once again relating faces incident to rims and nodes, to a graph.

Every rim in $\mathcal{E}\setminus\mathcal{E}_\partial$ has a tail eindpoint at an internal node of (P,d). As mentioned a couple of times, there is only one type of nodes relevant to this thesis, namely vertices of P, but we cover the case of switches also. We deal with each case separately in the following discussion, and a similar process can be done for the other types of internal nodes that can occur in the general case (for details see [Section 15.5.1, TV17]).

Let x be an internal node of (P,d) corresponding to a vertex of P. There exists a closed ball neighbourhood of x, B_x such that B_x contains no other node of (P,d). We then define the **link graph** Γ_x of x to be the graph embedded in ∂B_x with vertices corresponding to $e\cap\partial B_x$ for all rims e incident to x, and with edges corresponding to $f\cap\partial B_x$ for all faces (branches) incident to x. The orientation of these edges arise from the orientation of the faces.

If x is an internal node corresponding to a switch, then a neigbourhood of x in P looks like a series of half-planes intersecting the edge of P through which the strand of d passes, as depicted in [Figure 14.2, TV17], which also shows another closed ball neighbourhood that does not enclose any other node.

The graph (with crossings) Γ_x associated to this node is constructed via a slightly different method, where the vertices of Γ_x are the points of intersection of the edge of P containing the switch with ∂B_x and also the intersection of the strand of d defining the switch and ∂B_x. The faces incident to the edge of P containing the switch that do not contain any strand of d (i.e. faces corresponding to 2-cells of P) induce edges of Γ_x the same as above via the intersection of the face with ∂B_x. These edges are coloured black in [Section 15.5, TV17] and join two black vertices. The two 2-cells of P containing the strand of d correspond to four faces of (P,d) and consequently correspond to four edges of Γ_x, again where each face intersects ∂B_x. These edges are still coloured black, but join one black vertex to one red vertex. Finally, the strand of d, which runs through the interior of B_x, corresponds to a red edge in Γ_x via projection to ∂B_x. This red edge joins the two red vertices.

In both the above cases, the link graph has no free ends, so we can apply $\mathbb{F}$ from the Appendix A to produce a map $\mathbb{F}(\Gamma_x):\mathcal{H}(\Gamma_x)\to\mathrm{End}(\mathbb{1})=\Bbbk$. Taking the tensor product over all internal nodes x we have the map

$$\bigotimes_x \mathbb{F}(\Gamma_x):\bigotimes_x \mathcal{H}(\Gamma_x)\to\mathrm{End}(\mathbb{1}).$$

Now $\mathcal{H}(\Gamma_x)=\bigotimes_{v\in\Gamma_x^{(1)}} H_v(\Gamma_x)\cong\bigotimes_{e_v\in P^{(1)}} H(P_e)$ where e_v is the rim of P corresponding to the vertex v in Γ_x by definition of the link graph, and so the extends to

$$\bigotimes_x \mathcal{H}(\Gamma_x)\cong\bigotimes_{e\in\mathcal{E}\setminus\mathcal{E}_\partial} H(P_e)$$

and so the map $V_c:\bigotimes_{e\in\mathcal{E}\setminus\mathcal{E}_\partial} H(P_e)\to\mathrm{End}(\mathbb{1})$ is defined to be the image of $\bigotimes_x\mathbb{F}(\Gamma_x)$ under this isomorphism. The tensor products over x here are understood to be over the internal nodes of (P,d).

This concludes the required theory regarding the evaluation of the Turaev-Viro graph TQFT on coloured surface. The evaluation on a general morphism is similar, with a greater variety of types of nodes in the neat positive diagram representing the morphism.

Appendix C

Supplementary Material for the Reshetikhin-Turaev Defect TQFT

Similarly to the previous appendix, this appendix serves the purpose of providing more rigour to the discussion in Sections 3.4.1 and 3.4.2. In particular, the source bordism category for the Reshetikhin-Turaev TQFT, $\mathbf{Bord}^{\mathcal{C}}_{\mathrm{wt}}$, is more closely analysed, how $\mathcal{Z}_{RT,\mathcal{C}}$ and $\mathcal{Z}^{\mathrm{df}}_{RT,\mathcal{C}}$ evaluate surfaces and morphisms is investigated, and why both TQFTs are anomaly-free is discussed more closely. The material in Appendix C.1 regarding the Reshetikhin-Turaev TQFT is largely drawn from [Chapter IV, Tur16] and the material in Appendix C.2 regarding the the defect TQFT comes from [CRS17; CRS18]. The aim throughout this chapter is to provide as much generality as is reasonably possible within the constraints of this thesis, however there are instances where full generality is dropped and the discussion is restricted to the case of interest, that is the Reshetikhin-Turaev TQFT over $\mathrm{vect}_{\mathbb{C}}$, in order to help facilitate clarity of the key points.

C.1 The Reshetikhin-Turaev TQFT

Recall from Section 3.4.1 that the Reshetikhin-Turaev TQFT evaluates both extended surfaces and weighted extended manifolds from $\mathbf{Bord}^{\mathcal{C}}_{\mathrm{wt}}$ by evaluating ribbon graphs inside 3-manifolds. This section aims to provide the necessary details to make this more precise. We reproduce certain definitions from Section 3.4.1 here for convenience, before complementing them with the required theory that was omitted in Chapter 3. Throughout let $\mathcal{C}$ be a modular tensor category with representative set of simple objects I, with the aim that this be ultimately replaced by the specific modular tensor category $\mathrm{vect}_{\mathbb{C}}$.

The Reshetikhin-Turaev TQFT has a fundamental dependence on the invariant assigned to a closed 3-manifold with a $\mathcal{C}$-coloured ribbon graph residing in its interior. This section commences with a description of this invariant, then proceeds to define how the Reshetikhin-Turaev TQFT evaluates extended surfaces and weighted extended manifolds based upon this invariant.

C.1.1 Invariants of $\mathcal{C}$-coloured Ribbons in 3-manifolds

A known result states that any given closed, connected, oriented 3-manifold can be obtained via surgery on a given link L in the 3-sphere S^3 [Lic62; Wal60] . Roughly speaking, surgery on a link means removing a closed neighbourhood B_L of link L in S^3, and then re-gluing that neighbourhood in a particular way to produce a closed manifold M. A brief outline of how to compute the invariant of a given closed 3-manifold with internal ribbon graph R is as follows:

1. Consider the manifold M as the result of surgery on a link L in S^3;
2. After applying an isotopy if necessary (the invariant is up to isotopy), we can consider the ribbon R as disjoint from B_L in M;
3. The ribbon R can then be considered as a ribbon in S^3, and produces a new ribbon graph by union with the link L;
4. Again, by isotoping if need be, the ribbon $R \cup L$ can be considered as a ribbon in $S^3 \setminus \{\infty\} = \mathbb{R}^3$;
5. The invariant is then given, along with a few extra terms, by summing the evaluations of the ribbon graph $R \cup L$ in $\mathbb{R}^3$ over all $\mathcal{C}$-colourings of L.

The details relating to the surgery procedure to produce the manifold M from a link L with n components $L_1, ..., L_n$ are not provided here. For the fully general discussion of the invariant of a ribbon R in a closed 3-manifold M, some knowledge of the 4-manifold $\widetilde{M}_L$ that produces M by $M = \partial \widetilde{M}_L$ is required, in particular the sign $\sigma(L)$ of the intersection pairing on $H_2(\widetilde{M}_L; \mathbb{R})$. However, we may avoid discussion of this 4-manifold and intersection pairing in the case of the invariant based on $\mathrm{vect}_{\mathbb{C}}$ as shall be seen below.

Recalling that $\dim(\mathcal{C}) = \sum_{i \in I} \dim(X_i)^2$, we can define a similar scalar from knowledge of the twist θ associated to the modular tensor category $\mathcal{C}$:

$$\Theta_C := \sum_{i \in I} \theta_i^{-1} \dim(X_i)^2$$

where θ_i is the invertible scalar in $\Bbbk$ associated to the twist $\theta_i : X_i \to X_i$, where X_i is a simple object. The final required piece before we can write down the invariant $\tau(M, R)$ of ribbon R in closed manifold M, is to state that a $\mathcal{C}$-colouring of link L, similarly to a $\mathcal{C}$-colouring of any ribbon graph, is a map $c : L \to I$, and the set of colouring of L is denoted $\mathrm{col}(L)$. Then, we define $\tau(M, R)$ as

$$\tau(M, R) := \Theta_{\mathcal{C}}^{\sigma(L)} \sqrt{\dim(\mathcal{C})}^{-\sigma(L)-n-1} \sum_{c \in \mathrm{col}(L)} \big(\prod_{i=1}^{n} \dim(c(L_i)) \big) \mathbb{F}(L_c \cup R) \tag{C.1}$$

where $\mathbb{F}$ denotes the evaluation of the coloured ribbon graph as per Appendix A and L_c denotes the link L as a coloured ribbon graph.

As mentioned above, for the case of the invariant $\tau(M,R)$ defined over modular category $\mathrm{vect}_{\mathbb{C}}$, we have $\dim(\mathrm{vect}_{\mathbb{C}}) = \Theta_{\mathrm{vect}_{\mathbb{C}}} = 1$ so all dependence on the intersection pairing disappears, and we simply have

$$\tau(M,R) = \prod_{i=1}^{n} \dim(c(L_i))\mathbb{F}(L_c \cup R)$$

since there is exactly one colouring $c : L \to I$ as I has a single element. Much of the intermediate theory required in defining the anomaly-free Reshetikhin-Turaev TQFT also have factors relying on $\dim(\mathcal{C})$ and $\Theta_{\mathcal{C}}$ which will also be removed in the case of $\mathrm{vect}_{\mathbb{C}}$.

C.1.2 A Precursor to the Reshetikhin-Turaev TQFT

The next character to be introduced to this plot is a TQFT $\overline{\mathcal{Z}}^{\mathcal{C}}_{RT} : \mathbf{Bord}^{\mathcal{C}}_{\mathrm{dec}} \to \mathrm{Vect}_{\Bbbk}$. This TQFT is typically not anomaly-free (depending on the specific modular category $\mathcal{C}$), but provides the basis for the anomaly-free TQFT $\mathcal{Z}_{RT,\mathcal{C}}$ that is our current focus. This TQFT makes fundamental use of the 2-manifold invariant discussed above, and the rest of the work required to produce $\mathcal{Z}_{RT,\mathcal{C}}$ from $\overline{\mathcal{Z}}^{\mathcal{C}}_{RT}$ is related to removing anomalies. The precursor TQFT $\overline{\mathcal{Z}}^{\mathcal{C}}_{RT}$ evaluates decorated surfaces and decorated manifolds (i.e. the objects and representatives of morphisms of $\mathbf{Bord}^{\mathcal{C}}_{\mathrm{dec}}$) by producing and evaluating ribbon graphs in $\mathbb{R}^3$ and closed 3-manfiolds respectively.

We first define decorated surfaces and decorated manifolds, which will be called d-surfaces and d-manifolds respectively in order to distinguish them from the decorated surfaces of Section 3.2.2 (though they are closely related), and hence define $\mathbf{Bord}^{\mathcal{C}}_{\mathrm{dec}}$.

Definition C.1.1. A ***d*-surface** Σ is a closed oriented surface with a finite, totally ordered family of disjoint, simple, oriented arcs labelled with objects of $\mathcal{C}$ and signs $\{+,-\}$. The **type** of a d-surface Σ, denoted $\Sigma(T)$, is a tuple $(g;(X_1,\epsilon_1),\ldots,(X_n,\epsilon_n))$ where g is the genus of Σ and the (X_i,ϵ_i) are the labels of the marked arcs in the given ordering. A **homeomorphism of *d*-surface** $f : \Sigma \to \Sigma'$ is a homeomorphism of the underlying surfaces that preserve the orientation, label and order of the marked arcs.

Definition C.1.2. A **standard *d*-surface** Σ^{std}_T is a canonical choice of d-surface of type T.

Definition C.1.3. A **parametrisation of a *d*-surface** Σ is a pair $(\Sigma^{\mathrm{std}}_T, f : \Sigma^{\mathrm{std}}_T \to \Sigma)$ where Σ^{std}_T is a standard d-surface and f is a homeomorphism of d-surfaces.

Definition C.1.4. A ***d*-manifold** is a tuple $(M,\partial_+M,\partial_-M,R)$ where M is a 3-manifold with boundary consisting of parametrised d-surfaces ∂_+M and ∂_-M, and a $\mathcal{C}$-coloured ribbon graph R in the interior, where R meets the boundary at precisely the oriented arcs in ∂_+M and ∂_-M. A **homeomorphism of *d*-manifolds** is a homeomorphism of the underlying 3-manifolds that restricts to a homeomorphism of d-surfaces on the boundary, and preserves the ribbon graph on the interior.

Definition C.1.5. The bordism category $\mathbf{Bord}^{\mathcal{C}}_{\mathrm{dec}}$ has objects as d-surfaces and morphisms as representatives of homeomorphism classes of d-manifolds. Composition of morphisms is via gluing of d-manifolds along a homeomorphism of d-surfaces on the boundary and the tensor product is given by disjoint union.

For more details regarding gluing of bordisms, see [Section III.4.1, Tur16].

The TQFT $\overline{\mathcal{Z}}^{\mathcal{C}}_{RT}$ evaluates a d-surface Σ by considering a particular ribbon graph in $\mathbb{R}^3$ based on the type T of Σ. This ribbon graph consists of coloured and uncoloured strands and a single coupon. The evaluation of the ribbon graph gives the vector space arising from the hom-spaces associated to the coupon by summing over the colourings of the uncoloured strands. More precisely, let Σ be a d-surface of type $T = (g; (X_1, \epsilon_1), ..., (X_n, \epsilon_n))$ and consider the graph R_T consisting of a single coupon with the first n strands (from left to right) labelled by the $X_i^{\epsilon_i}$ attached on one end to the coupon and with the other end free, and the remaining g strands have both ends attached to the coupon (with no crossings) and are uncoloured. It will be useful for the definition of $\overline{\mathcal{Z}}^{\mathcal{C}}_{RT}$ to consider this graph as being embedded in a 3-manifold M_T with boundary $\partial M_T = \Sigma$, that, is M_T can be viewed as a morphism $\emptyset \to \Sigma$ (see Figure 3.6).

The evaluation $\overline{\mathcal{Z}}^{\mathcal{C}}_{RT}(\Sigma)$ proceeds by evaluating the graph R_T by summing over the simple objects in I on the g uncoloured strands. We write this as

$$\overline{\mathcal{Z}}^{\mathcal{C}}_{RT}(\Sigma) := \bigoplus_{(V_1,...,V_g)\in I^g} \mathrm{Hom}_{\mathcal{C}}(\mathbb{1}, X_1^{\epsilon_1} \otimes ... \otimes X_n^{\epsilon_n} \otimes \bigotimes_{r=1}^{g} (V_r \otimes V_r^*))$$

where for each $r = 1, ..., g$, both V_r and its dual V_r^* appear since the uncoloured strands attach to the coupon twice with opposite orientations.

Now let us consider how $\overline{\mathcal{Z}}^{\mathcal{C}}_{RT}$ evaluates a d-manifold $(M, \partial_+ M, \partial_- M, R)$. Let $(\Sigma_T^{\mathrm{std}}, f : \Sigma_T^{\mathrm{std}} \to \partial_+ M)$ and $(\Sigma_{T'}^{\mathrm{std}}, f' : \Sigma_{T'}^{\mathrm{std}} \to \partial_- M)$ be parametrisations of the boundary of M by standard d-surfaces. Let M_T and $M_{T'}$ denote the 3-manifolds representing morphisms $\emptyset \to \Sigma_T^{\mathrm{std}}$ and $\emptyset \to \Sigma_{T'}^{\mathrm{std}}$ with ribbon graphs R_T and $R_{T'}$ as in Figure 3.6. We can produce a closed 3-manifold $\widetilde{M}$ with internal ribbon graph $\widetilde{R}$ by gluing M_T and $M_{T'}$ to M along the given parametrisations $f : \partial M_T = \Sigma_T^{\mathrm{std}} \to \partial_+ M$ and $f' : \partial M_{T'} = \Sigma_{T'}^{\mathrm{std}} \to \partial_- M$. The ribbon graph $\widetilde{R}$ is partially uncoloured, namely in the components of the graph corresponding to the uncoloured portions of R_T and $R_{T'}$.

C.1.3 The Reshetikhin-Turaev TQFT on Extended Surfaces

We are now at a stage where the evaluation of the Reshetikhin-Turaev TQFT can be defined for extended surfaces, which are d-surfaces with extra data, namely a choice of Lagrangian subspace of the first homology group of the d-surface. This extra data allows any influence from the gluing anomalies to be removed. First, we recall some definitions from Section 3.4.1.

Definition C.1.6. A **extended surface** is a pair $(\Sigma, \mathcal{L})$ where Σ is a closed oriented surface with a finite family of disjoint, simple oriented arcs labelled by objects of $\mathcal{C}$ and signs $\{+, -\}$ (called marked arcs), and

$\mathcal{L}$ is a Lagrangian space of $H_1(\Sigma;\mathbb{R})$ (considered as a symplectic vector space with the intersection pairing) where Σ here denotes the underlying manifold of the d-surface Σ.

Definition C.1.7. A **homeomorphism of extended surfaces** $f:(\Sigma,\mathcal{L})\to(\Sigma',\mathcal{L}')$ is a homeomorphism of the underlying unmarked surfaces that preserves orientations and arcs (including their labels and signs), and induces an isomorphism $f_\#: H_1(\Sigma;\mathbb{R})\to H_1(\Sigma';\mathbb{R})$ such that $f_\#(\mathcal{L})=\mathcal{L}'$.

An extended surface $(\Sigma,\mathcal{L})$ can be viewed as a d-surface by forgeting the Lagrangian space $\mathcal{L}$. In fact, the terminology 'extended' refers to extending the definition of d-surface. The parametrisation of an extended surface is then defined to be the parametrisation of the underlying d-surface as in the previous section:

Definition C.1.8. A **parametrisation of an extended surface** $(\Sigma,\mathcal{L})$ is a pair $(\Sigma_T^{\mathrm{std}}, f:\Sigma_T^{\mathrm{std}}\to\Sigma)$ where Σ_T^{std} is a standard d-surface and f is a d-surface homeomorphism to the d-surface Σ.

To this point, this subsection has not presented any extra material to that in Section 3.4.1, but that now changes with the formalisation of the maps $\phi(f_0,f_1):\overline{\mathcal{Z}}^{\mathcal{C}}_{RT}(\Sigma^{\mathrm{std}}_{T_0})\to\overline{\mathcal{Z}}^{\mathcal{C}}_{RT}(\Sigma^{\mathrm{std}}_{T_1})$. This requires some theory that is necessary for an understanding these maps and the role that the Lagrangian plays in the eradication of anomalies in the general case, as well as for understanding of the evaluation of $\mathcal{Z}_{RT,\mathcal{C}}$ on bordisms. For the case where $\mathcal{C}=\mathrm{vect}_{\mathbb{C}}$ much of this theory becomes redundant.

Definition C.1.9. Let (H,ω) be a symplectic vector space. An **isotropic** subspace $\ell\subset H$ is a linear subspace such that $\ell\subset\mathrm{Ann}(\ell)=\{h\in H|\omega(h,\ell)=0\}$.

Recall from Definition 3.2.12 that the Lagrangian subspace $\mathcal{L}$ is a maximal isotropic subspace of H.

Definition C.1.10. The **Maslov index** $\mu(\ell_1,\ell_2,\ell_3)$ for isotropic spaces $\ell_1,\ell_2,\ell_3\subset H$ is the signature of the bilinear form $\widetilde{\omega}(\cdot,\cdot)$ on $(\ell_1+\ell_2)\cap\ell_3$ defined as follows. For $x,y\in(\ell_1+\ell_2)\cap\ell_3$ with $x=x_i\in\ell_i$ for $i=1,2$, we define $\widetilde{\omega}$ by

$$\widetilde{\omega}(x,y):=\omega(x_2,y).$$

We also need the notion of a Lagrangian relation:

Definition C.1.11. A **Lagrangian relation** between symplectic vector spaces (H_1,ω_1) and (H_2,ω_2) is a Lagrangian subspace of $(-H_1)\oplus H_2$ where $-H_1$ denotes the symplectic vector space $(H_1,-\omega_1)$.

Denoting the set of all Lagrangian subspaces of a symplectic vector space (H,ω) by $\mathrm{Lag}(H)$, for any Lagrangian relation $L\subset(-H_1)\oplus H_2$ we can produce two maps $L_*:\mathrm{Lag}(H_1)\to\mathrm{Lag}(H_2)$ and $L^*:\mathrm{Lag}(H_2)\to\mathrm{Lag}(H_1)$. These maps are defined as follows:

$$\begin{aligned}
L_*:\mathrm{Lag}(H_1)&\to\mathrm{Lag}(H_2)\\
\ell_1&\mapsto L_*(\ell_1)=\{h_2\in H_2|\text{ there exists a } h_1\in\ell_1 \text{ such that } (h_1,h_2)\in L\}\\
L^*:\mathrm{Lag}(H_2)&\to\mathrm{Lag}(H_1)\\
\ell&\mapsto L^*(\ell_2)=\{h_1\in H_1|\text{ there exists a } h_2\in\ell_2 \text{ such that } (h_1,h_2)\in L\}
\end{aligned}$$

For a proof that $L_*(\ell_1)$ and $L^*(\ell_2)$ are indeed Lagrangian subspaces of their respective symplectic vector spaces, see [Section IV.3.4, Tur16]. We now turn to the symplectic vector spaces that we are most concerned with: the symplectic vector spaces $H_1(\Sigma;\mathbb{R})$ for closed oriented surfaces Σ, along with antisymmetric bilinear form given by the intersection pairing.

We can produce a Lagrangian subspace of $H_1(\Sigma;\mathbb{R})$ by considering a bordism M such that $\Sigma = \partial M$, and the inclusion map $H_1(\Sigma;\mathbb{R}) \to H_1(M;\mathbb{R})$ induced by the inclusion $\Sigma \to M$. The Lagrangian subspace associated to Σ is then the kernel of the inclusion map $H_1(\Sigma;\mathbb{R}) \to H_1(M;\mathbb{R})$. In particular, this provides a method for assigning a Lagrangian subspace to a d-surface Σ. For example, the Lagrangian subspace assigned to a standard d-surface Σ_T^{std} is the kernel of the inclusion map $H_1(\Sigma_T^{\mathrm{std}};\mathbb{R}) \to H_1(M_T;\mathbb{R})$ where M_T is a bordism with boundary homeomorphic to Σ_T^{std}. Denote this Lagrangian subspace by $\ell(\Sigma_T^{\mathrm{std}})$. We also note that a parametrisation $f : \Sigma_T^{\mathrm{std}} \to \Sigma$ induces a Lagrangian relation, which we also denote by f.

We can now define the maps $\phi(f_0, f_1)$ for parametrisations $(\Sigma_{T_0}^{\mathrm{std}}, f_0)$ and $(\Sigma_{T_1}^{\mathrm{std}}, f_1)$ of $(\Sigma, \mathcal{L})$ as follows:

$$\phi(f_0,f_1) = (\sqrt{\dim\mathcal{C}}\Theta_{\mathcal{C}}^{-1})^{\mu\left((f_0)_*(\ell(\Sigma_{T_0}^{\mathrm{std}})),\ell(\Sigma),(f_1^{-1})_*^{-1}(\ell(\Sigma_{T_1}^{\mathrm{std}}))\right)-\mu\left((f_0)_*(\ell(\Sigma_{T_0}^{\mathrm{std}})),\mathcal{L},(f_1)_*(\ell(\Sigma_{T_1}^{\mathrm{std}}))\right)}\overline{\mathcal{Z}}_{RT}^{\mathcal{C}}(M_1)\circ\overline{\mathcal{Z}}_{RT}^{\mathcal{C}}(M_0)$$

where M_0 and M_1 are bordisms representing $f_0 : \Sigma_{T_0}^{\mathrm{std}} \to \Sigma$ and $f_1^{-1} : \Sigma \to \Sigma_{T_1}^{\mathrm{std}}$ respectively. The composition via gluing is over $f_1^{-1}f_0$ and the compatibility of the gluing is encoded in the factors of $(f_0)_*$ and $(f_1)_*$.

It can then be shown, using the properties of the Maslov indices [Section IV.3, Tur16], that for any parametrisations f_0, f_1, f_2 of Σ that the following hold:

- $\phi(f_0, f_0) = \mathrm{id}$;
- $\phi(f_1, f_2) \circ \phi(f_0, f_1) = \phi(f_0, f_2)$;
- $\phi(f_0, f_1)$ and $\phi(f_1, f_0)$ are inverse to each other.

Thus, the family $\left\{\{\overline{\mathcal{Z}}_{RT}^{\mathcal{C}}(\Sigma_T^{\mathrm{std}})\}_{(\Sigma_T^{\mathrm{std}}, f:\Sigma_T^{\mathrm{std}}\to\Sigma)}, \{\phi(f_0,f_1)\}_{f_0,f_1}\right\}$ is an inverse system. We define $\mathcal{Z}_{RT,\mathcal{C}}((\Sigma,\mathcal{L}))$ as the limit over this system:

$$\mathcal{Z}_{RT,\mathcal{C}}(\Sigma) := \lim_{\leftarrow} \overline{\mathcal{Z}}_{RT}^{\mathcal{C}}(\Sigma_T^{\mathrm{std}}).$$

As with every TQFT seen so far in this thesis, the result of taking the limit is isomorphic to any one of the component vector spaces of the inverse system, so we typically consider

$$f_\# : \mathcal{Z}_{RT,\mathcal{C}}((\Sigma,\mathcal{L})) \xrightarrow{\cong} \overline{\mathcal{Z}}_{RT}^{\mathcal{C}}(\Sigma_T^{\mathrm{std}}) \tag{C.2}$$

for some standard d-surface Σ_T^{std} and parametrisation $f : \Sigma_T^{\mathrm{std}} \to \Sigma$.

Recalling that in our specific case of interest, the Reshetikhin-Turaev TQFT defined over $\mathrm{vect}_{\mathbb{C}}$, we have $\dim(\mathrm{vect}_{\mathbb{C}}) = \Theta_{\mathrm{vect}_{\mathbb{C}}} = 1$ so we are considering the inverse system over maps

$$\phi(f_0,f_1) = \overline{\mathcal{Z}}_{RT}^{\mathrm{vect}_{\mathbb{C}}}(M_1)\circ\overline{\mathcal{Z}}_{RT}^{\mathrm{vect}_{\mathbb{C}}}(M_0).$$

C.1.4 The Reshetikhin-Turaev TQFT on Weighted Extended Manifolds

Let us write down the definition of a weighted extended manifold which is essentially the same as that from Section 3.4.1:

Definition C.1.12. A **weighted extended manifold** (M, m) consists of a compact, oriented 3-manifold M with boundary ∂M an extended surface and a $\mathcal{C}$-coloured ribbon graph in the interior, and $m \in \mathbb{Z}$ satisfies the condition that if $M = \emptyset$ then $m = 0$. A **homeomorphism of weighted extended manifolds** (M, m) and (M', m') such that $m = m'$, is a homeomorphism of the underlying 3-manifolds that preserves the ribbon graph, and restricts to a homeomorphism of extended surfaces on the boundary.

The evaluation of Reshetikhin-Turaev TQFT on a weighted extended manifold depends heavily on the TQFT $\overline{\mathcal{Z}}^{\mathcal{C}}_{RT}$ defined previously, as well as the isomorphisms from Equation (C.2). That is, $\mathcal{Z}_{RT,\mathcal{C}}$ is evaluated on a weighted extended bordism (M, m) by considering a scalar $\zeta_{\mathcal{C}}(M, m)$ depending on $\dim(\mathcal{C})$, $\Theta_{\mathcal{C}}$ and m multiplying the following composition:

$$\mathcal{Z}_{RT,\mathcal{C}}(\partial_- M) \xrightarrow{(f_0)^{-1}_{\#}} \overline{\mathcal{Z}}^{\mathcal{C}}_{RT}(\Sigma^{\mathrm{std}}_{T_0}) \xrightarrow{\kappa_{\mathcal{C}}(M,m)\overline{\mathcal{Z}}^{\mathcal{C}}_{RT}(M')} \overline{\mathcal{Z}}^{\mathcal{C}}_{RT}(\Sigma^{\mathrm{std}}_{T_1}) \xrightarrow{(f_1)^{-1}_{\#}} \mathcal{Z}_{RT,\mathcal{C}}(\partial_+ M)$$

where $\kappa_{\mathcal{C}}(M, m)$ is a scalar depending on $\dim(\mathcal{C}), \Theta_{\mathcal{C}}$ and Maslov indices related to the extended surfaces $\partial_-(M)$ and $\partial_+(M)$, $\Sigma^{\mathrm{std}}_{T_0}$ and $\Sigma^{\mathrm{std}}_{T_1}$ are standard d-surfaces parametrising $\partial_- M$ and $\partial_+ M$, and M' is a d-manifold corresponding to M between the d-surfaces $\Sigma^{\mathrm{std}}_{T_0}$ and $\Sigma^{\mathrm{std}}_{T_1}$.

Essentially all that is required to make this rigorous, is to specify what the scalars $\zeta_{\mathcal{C}}$ and $\kappa_{\mathcal{C}}$ are (both of which are trivial for $\mathcal{C} = \mathrm{vect}_{\mathbb{C}}$ as per the previous subsections). The first, $\zeta_{\mathcal{C}}(M, m)$, is very straightforward:

$$\zeta_{\mathcal{C}}(M, m) = (\sqrt{\dim(\mathcal{C})}\Theta^{-1}_{\mathcal{C}})^{-m}$$

For $\kappa_{\mathcal{C}}(m, m)$, we need to do a little more work. Let $\ell(\partial_+ M)$ and $\ell(\partial_- M)$ denote the chosen Lagrangian subspaces, of $H_1(\partial_+ M; \mathbb{R})$ and $H_1(\partial_- M; \mathbb{R})$ respectively, defining the extended surfaces $\partial_+ M$ and $\partial_- M$. Let $f_0 : \Sigma^{\mathrm{std}}_{T_0} \to \partial_+ M$ and $f_1 : \Sigma^{\mathrm{std}}_{T_1} \to \partial_- M$ be parametrisations as above. Recalling Definition C.1.4, we can then consider M as a d-manifold M'. We can also consider the Lagrangian relation $L_M \subset (-H_1(\partial_- M; \mathbb{R})) \oplus H_1(\partial_+ M; \mathbb{R}) = H_1(\partial M; \mathbb{R})$ induced by the inclusion $H_1(\partial M; \mathbb{R}) \to H_1(M; \mathbb{R})$ (see [Section IV.4.2, Tur16]). We can now define $\kappa_{\mathcal{C}}(M, m)$:

$$\kappa_{\mathcal{C}}(M, m) := (\sqrt{\dim(\mathcal{C})}\Theta^{-1}_{\mathcal{C}})^{\mu\left((L_M)^*((f_0)_*(\ell(\Sigma^{\mathrm{std}}_{T_0}))),\ell(\partial_- M),(f_1)_*(\ell(\Sigma^{\mathrm{std}}_{T_1}))\right)-\mu\left((L_M)_*((f_1)_*(\ell(\Sigma^{\mathrm{std}}_{T_1}))),\ell(\partial_+ M),(f_0)_*(\ell(\Sigma^{\mathrm{std}}_{T_0}))\right)}$$

So, putting it all together, we define $\mathcal{Z}_{RT,\mathcal{C}}$ evaluated on (M, m) to be

$$\mathcal{Z}_{RT,\mathcal{C}}(M, m) := \zeta_{\mathcal{C}}(M, m)\left((f_1)^{-1}_{\#} \circ (\kappa_{\mathcal{C}}(M, n)\overline{\mathcal{Z}}^{\mathcal{C}}_{RT}(M')) \circ (f_0)_{\#}\right)$$

For the case $\mathcal{C} = \mathrm{vect}_{\mathbb{C}}$, this simplifies to

$$\mathcal{Z}_{RT,\mathrm{vect}_{\mathbb{C}}}(M, m) = (f_1)^{-1}_{\#} \circ \overline{\mathcal{Z}}^{\mathcal{C}}_{RT}(M') \circ (f_0)_{\#}$$

which elucidates the fact that $\overline{\mathcal{Z}}_{RT}^{\mathrm{vect}_{\mathbb{C}}}$ represents the key computational component for evaluating $\mathcal{Z}_{RT,\mathrm{vect}_{\mathbb{C}}}$.

For any modular tensor category $\mathcal{C}$, we have the following result:

Theorem C.1.1. *[Theroem 9.2.1, Tur16] The TQFT $\mathcal{Z}_{RT,\mathcal{C}}$ is anomaly-free and non-degenerate.*

C.2 The Defect TQFT

In order to properly define the defect TQFT, we need to define how it evaluates $\mathbb{D}$-decorated surfaces (recall Definition 3.2.10) which then allows us to define the defect data D_0 associated to 0-strata in the interior of bordisms, a necessary step in being able to define the evaluation of the TQFT on arbirtary $\mathbb{D}$-defect bordisms. The evaluation of surfaces proceeds in a similar fashion the the evaluation of surfaces in the Turaev-Viro graph TQFT that is, by evaluating a cylinder over the surface and considering its image. Throughout this section let $\mathbb{D}$ be a set of defect data arising from a modular tensor category $\mathcal{C}$ (recall Definition 3.4.2). The material of the following subsection is drawn from [Section 5, CRS17].

C.2.1 The Defect TQFT on Decorated Surfaces

Let Σ_{df} be an object in $\mathbf{Bord}_3^{\mathrm{df}}(\mathbb{D})$. In particular this means that any 2-, 1-, and 0-strata of Σ_{df} are labelled from elements from D_3, D_2 and D_1 respectively, subject to the compatibility requirements of the maps s, t, and j. The cylinder over Σ_{df}, denoted $C_{\Sigma_{\mathrm{df}}}$, is defined to be $\Sigma_{\mathrm{df}} \times [0,1]$ with $\partial C_{\Sigma_{\mathrm{df}}} = \Sigma_{\mathrm{df}} \sqcup (-\Sigma_{\mathrm{df}})$ where $-\Sigma_{\mathrm{df}}$ is the decorated surface Σ_{df} with opposite orientation but same label for all strata. The stratification of $C_{\Sigma_{\mathrm{df}}}$ arises from Σ_{df} as follows: each 2-, 1- and 0-strata of Σ_{df} is crossed with the interval $[0,1]$ to produce 3-, 2- and 1-strata respectively. The orientations of the induced 3-strata are that of the 3-manifold underlying $C_{\Sigma_{\mathrm{df}}}$, the orientations of the induced 2-strata are such that they are compatible with the orientations of the corresponding 1-strata in Σ_{df} and $-\Sigma_{\mathrm{df}}$, and the orientations of the induced 1-strata are compatible with the orientations of the corresponding 0-strata in Σ_{df}.

Importantly, this process does not produce any 0-strata in the interior of $C_{\Sigma_{\mathrm{df}}}$ so the defect data already supplied is sufficient for the evaluation of $C_{\Sigma_{\mathrm{df}}}$. The 3-, 2- and 1-strata of $C_{\Sigma_{\mathrm{df}}}$ are labelled with the same elements of D_3, D_2 and D_1 as the corresponding 2-, 1- and 0-strata of Σ_{df}. Since D_3 is a singleton set, it is essentially ignored, so we consider $C_{\Sigma_{\mathrm{df}}}$ as a defect bordism with only line and surface defects.

This evaluation of $C_{\Sigma_{\mathrm{df}}}$ essentially proceeds by transforming $C_{\Sigma_{\mathrm{df}}}$, in a systematic way, into a weighted extended 3-manifold with $\mathcal{C}$-coloured ribbon in the interior, then evaluating it via the pure Reshetikhin-Turaev TQFT. This procedure is made more formal below and follows closely [Construction 5.5 CRS17] but restricted to the cases relevant for this thesis.

Recalling that D_2 is the set of Δ-separable Frobenius algebras in $\mathcal{C}$ (denoted $(A_i, \nabla_i, \Delta_i)$ for succinctness) and D_1 is the union of sets of tuples $((A_1, \epsilon_1), ..., (A_n, \epsilon_n), M)$ where the A_i are from D_2, the ϵ_i are signs, and M is a cyclic multi-module over $A_1^{\epsilon_1} \otimes ... \otimes A_n^{\epsilon_n}$, the first step in evaluating $C_{\Sigma_{\mathrm{df}}}$ is by associating ribbons labelled with M to 1-strata and ribbons labelled with the A_i to 2-strata.

Remark C.2.1. Due to the cyclicity of M, a choice needs to be made regarding the orientation of the framing of the ribbon M with regard to the A_i, a choice that may introduce a twist to the ribbon M. Since we will ultimately be taking $\mathcal{C} = \mathrm{vect}_{\mathbb{C}}$ which has a trivial twist, we suppress this choice in the present discussion. See [Section 5 CRS17] for details.

The evaluation of $C_{\Sigma_{\mathrm{df}}}$ proceeds as follows:

1. Choose a triangulation t_i of each 2-stratum of $C_{\Sigma_{\mathrm{df}}}$ assigning a total order to the vertices of the triangulation, and assigning orientations to all edges of t_i consistent with the total ordering;

2. Consider the Poincaré dual of t_i, again with each edge oriented such that the orientation of the edge of t_i followed by the orientation of the corresponding edge in the dual, give the orientation of the 2-stratum;

3. Decorate each edge of the Poincaré dual with the Frobenius algebra A_i associated to the 2-stratum, and decorate each vertex of the dual with either ∇_i or Δ_i depending on the orientations of the adjacent edges (i.e. a vertex with two incoming edges and one outgoing edge is labelled by the multiplication ∇_i, and vice versa);

4. Thicken each line labelled by M and by A_i into a ribbon, where the framing of the ribbons A_i is that of the 2-stratum to which it is associated, and the framing of the ribbon M is consistent with the choice discussed in Remark C.2.1. Each vertex of the dual becomes a coupon labelled with the corresponding maps (∇_i or Δ_i);

5. The vertices of the Poincaré dual of t_i that lie on the line that becomes an M-ribbon correspond to coupons labelled by the action of $A_i^{\epsilon_i}$ on the multi-module M, denotes $\beta_i : A_i^{\epsilon_i} \times M \to M$ (where $A_i^{+} = A_i$ and $A_i^{-} = A_i^{\mathrm{op}}$);

6. Considering the underlying surface of Σ_{df} decorated with the arcs corresponding to the intersection of the A_i and M ribbons and $\Sigma_{\mathrm{df}} \subset \partial C_{\Sigma_{\mathrm{df}}}$, and coloured with A_i and M, and similarly for $-\Sigma_{\mathrm{df}} \subset \partial C_{\Sigma_{\mathrm{df}}}$, we have two extended surfaces $\widetilde{\Sigma}$ and $\widetilde{\Sigma'}$ and a weighted extended bordism between them, $\widetilde{C}_{\Sigma_{\mathrm{df}}}$ (the cylinder $C_{\Sigma_{\mathrm{df}}}$ considered with internal ribbon graph as above only and no stratification). The notation $\widetilde{\Sigma'}$ has been used rather than $-\widetilde{\Sigma}$ since, depending on the triangulations t_i of 2-strata, $\widetilde{\Sigma'}$ may not be equal to $-\widetilde{\Sigma}$;

7. Applying $\mathcal{Z}_{RT,\mathcal{C}}$ to this bordism produces a vector space homomorphism

$$\mathcal{Z}_{RT,\mathcal{C}}(\widetilde{C}_{\Sigma_{\mathrm{df}}}) : \mathcal{Z}_{RT,\mathcal{C}}(\widetilde{\Sigma}) \to \mathcal{Z}_{RT,\mathcal{C}}(\widetilde{\Sigma'})$$

The above construction relies upon the choices of triangulations made of the 2-strata, and in particular, the effects of these triangulations on the boundary surface, which produce the extended surface $\widetilde{\Sigma}$ and $\widetilde{\Sigma'}$. It can be shown that there is in fact no dependence on the triangulation away from the boundary [Lemma 5.6 CRS17]. The effects of the triangulation on the boundary are removed by an inverse limit, reminiscent of that used in defing the Turaev-Viro graph TQFT. The evaluation of $\mathcal{Z}^{\mathrm{df}}_{RT,\mathcal{C}}$ on Σ_{df} is then defined to be this inverse limit. Again, with stark similarities to the Turaev-Viro graph TQFT, we can in practice compute $\mathcal{Z}^{\mathrm{df}}_{RT,\mathcal{C}}(\Sigma_{\mathrm{df}})$ by computing the image of $\mathcal{Z}_{RT,\mathcal{C}}(\tilde{C}_{\Sigma_{\mathrm{df}}})$ in the case where $\widetilde{\Sigma'} = -\widetilde{\Sigma}$, that is, when the triangulation t_i for each 2-stratum induces equivalent triangulations of the corresponding boundary 1-strata in Σ_{df} and $-\Sigma_{\mathrm{df}}$ (see the discussion preceding Theorem 5.8 in [CRS17]). Since any valid triangulation of 2-strata that satisfy this reqiurement will do, we will in practice take the simplest triangulation possible.

Having defined the evaluation of the defect TQFT on surface decorated with labelled 1- and 0-strata, we can now produce the data D_0 required for labelling 0-strata in the interior of defect bordisms, and also demonstrate the equivalences between extended surfaces in $\mathbf{Bord}^3_{\mathrm{wt}}$ and $\mathbb{D}$-decorated surfaces in $\mathbf{Bord}^{\mathrm{df}}_3(\mathbb{D})$. We turn first to the D_0 defect data.

C.2.2 D_0-defect Data and Point Insertions

The approach taken in this subsection regarding defining the set D_0 of valid labels for 0-strata in interiors of bordism of $\mathbf{Bord}^{\mathrm{df}}_3(\mathbb{D})$, is somewhat backward. We commence by presenting a result that states that every defect TQFT factors through D_0-complete defect TQFT, then assume that the defect Reshetikhin-Turaev TQFT is D_0-complete and show how to compute the set D_0.

Consider the following proposition, which is written for defect TQFTs of arbitrary dimension $n \geq 1$:

Proposition C.2.1. *[Proposition 2.17, CRS19] For a given defect TQFT $\mathcal{Z} : \boldsymbol{Bord}^{\mathrm{df}}_n(\mathbb{D}) \to \mathrm{Vect}_{\Bbbk}$, there exist defect data $\mathbb{D}^\bullet$, a map of defect data $h : \mathbb{D} \to \mathbb{D}^\bullet$ and a defect TQFT $\mathcal{Z}^\bullet : \boldsymbol{Bord}^{\mathrm{df}}_n(\mathbb{D}^\bullet) \to \mathrm{Vect}_{\Bbbk}$ such that $\mathcal{Z}^\bullet$ is D_0-complete and*

$$\mathcal{Z} = \mathcal{Z}^\bullet \circ h_*$$

where $h_* : \boldsymbol{Bord}^{\mathrm{df}}_n(\mathbb{D}) \to \boldsymbol{Bord}^{\mathrm{df}}_n(\mathbb{D}^\bullet)$ is a functor induced by the map h.

For our present purposes, we ignore any consideration of the map of defect data and the functor it induces (see [CRS19] for details), and define what it means for a defect TQFT to be D_0-complete. We restrict to the case of $n = 3$ as is relevant to this thesis.

Definition C.2.2. A defect TQFT $\mathcal{Z} : \mathbf{Bord}^{\mathrm{df}}_3(\mathbb{D}) \to \mathrm{Vect}_{\Bbbk}$ is **D_0-complete** if

$$D_0 = \cup_{\Sigma \in \Lambda} V_\Sigma$$

where $\Lambda \subset \mathbf{Bord}^{\mathrm{df}}_3(\mathbb{D})$ is the set of all objects of $\mathbf{Bord}^{\mathrm{df}}_3(\mathbb{D})$ that have underlying surface as a sphere, and V_Σ is the subspace of invariant states of Σ.

Next we need to understand what is meant by invariant states of Σ, which is a subspace of $\mathcal{Z}(\Sigma)$, and will be defined rather informally. Consider the cone over Σ, $C(\Sigma)$ (not to be confused with the notation of a cylinder over Σ, which has Σ as a subscript) viewed as a decorated sratified manifold, where the central 0-stratum is unlabelled, but all other labels extend that of $\Sigma = \partial C(\Sigma)$. We then consider the bordisms $f : \Sigma \to \Sigma$ in $\mathbf{Bord}_3^{\mathrm{df}}(\mathbb{D})$ defined as

$$H_f : C(\Sigma) \setminus \bar{f}(C(\mathring{\Sigma}))$$

where $C(\mathring{\Sigma})$ denotes the interior of $C(\Sigma)$ and $\bar{f}$ is an embedding of $C(\Sigma)$ into itself (see [Section 2.4, CRS19] for details). Then the **invariant states** of Σ is

$$V_\Sigma = \{v \in \mathcal{Z}(\Sigma) | \mathcal{Z}(f)(v) = v \text{ for all embeddings } f\}$$

In our particular case of interest, where $\mathcal{Z} = \mathcal{Z}_{RT,\mathrm{vect}_\mathbb{C}}$, V_Σ is precisely equal to $\mathcal{Z}_{RT,\mathrm{vect}_\mathbb{C}}(\Sigma)$ (see remark 2.1 in [CRS18]).

In this thesis, we only come across three specific scenarios of defect data for 0-strata, namely those specified in the orbifold data $\mathcal{A}$ associated to a given spherical fusion category (see Section 4.3). These 0-strata arise as either the intersection point of four 1-strata (labelled appropriately by the orbifold data), or as a 0-strata lying in the interior of either a 3-stratum or 2-stratum. The latter cases are called point insertions and are what we turn to next.

The point insertions associated to 3- and 2-strata are labelled by ϕ and ψ respectively. Since a small enough spherical neighbourhood around a 0-stratum in a given 3-stratum intersects no 2- or 1-strata, the labels ϕ can be any element of $\mathcal{Z}^{\mathrm{df}}_{RT,\mathrm{vect}_\mathbb{C}}(S^2)$ where S^2 is the undecorated sphere. This means that $\phi \in \mathbb{C}$ (in fact for ϕ to be a valid component of an orbifold datum, ϕ is required to be invertible) since $\mathcal{Z}^{\mathrm{df}}_{RT,\mathrm{vect}_\mathbb{C}}(S^1)$ is evaluated as the image of the identity map $\mathcal{Z}_{RT,\mathrm{vect}_\mathbb{C}}(S^1) \to \mathcal{Z}_{RT,\mathrm{vect}_\mathbb{C}}(S^1)$. Similarly, a small enough spherical neighbourhood around a 0-stratum in the interior of a 2-stratum only intersects the 2-stratum in which the point lies, so ψ is an element of the Reshetikhin-Turaev defect TQFT evaluated on a sphere with a single 1-stratum and no other strata (ψ is also required to be invertible). This 1-stratum is labelled consistently with the labelling of the 2-stratum on which the point insertion lies.

As seen in Section 4.3, the specific choices of ϕ and ψ for the orbifold data associated to a spherical fusion category $\mathcal{C}$, are $\phi = \frac{1}{\dim(\mathcal{C})}$ (we know that $\dim(\mathcal{C})$ is invertible in $\mathbb{C}$ by definition of spherical fusion category over $\mathbb{C}$) and ψ is a choice of square root of ths diagonal matrix with entries as dimensions of the simple objects of $\mathcal{C}$. For $\mathcal{C} = \mathbb{Z}_2\text{-}\mathrm{vect}_\mathbb{C}$, we get that $\phi = \frac{1}{2}$ and ψ is simply the 2×2 identity matrix (and consequently we drop ψ from further discussion of the $\mathbb{Z}_2\text{-}\mathrm{vect}_\mathbb{C}$ orbifolding of $\mathcal{Z}_{RT,\mathrm{vect}_\mathbb{C}}$).

The allowed labels for 0-strata residing at the intersection of four 1-strata labelled by $\mathcal{A}_1$ are computed by applying the Reshetikhin-Turaev defect TQFT to the spheres shown in Figure C.1

This evaluates to $\mathrm{Hom}_{\mathrm{vect}_\mathbb{C}}(\mathcal{A}_1 \otimes_{\mathcal{A}_2} \mathcal{A}_1, \mathcal{A}_1 \otimes_{\mathcal{A}_2} \mathcal{A}_1)$ (see [Lemma 3.2, CRS18]). Since $\mathcal{A}_1$ is defined via the direct sum of hom-spaces of the spherical fusion category $\mathcal{C}$, which are $\mathbb{C}$-vector spaces as per the definition

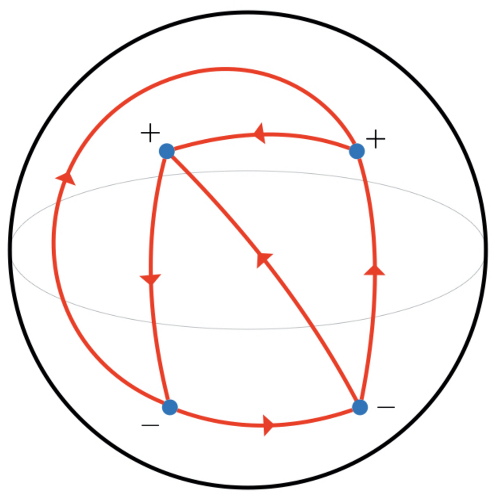

(a) The defect sphere associated to α.

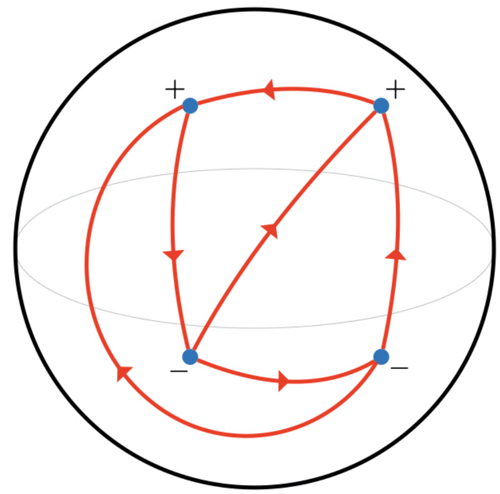

(b) The defect sphere associated to $\overline{\alpha}$

Figure C.1

of spherical fusion category, it is important to note that $\mathcal{A}_1$ can be viewed as a morphism in $\mathrm{vect}_{\mathbb{C}}$, and hence can be used to label coupons in a ribbon graph (as we shall see in the next subsection).

C.2.3 The Defect TQFT on $\mathbb{D}$-Defect Bordisms

Just as in the case for evaluating a defect bordism with just line and surface defects, the Reshetikhin-Turaev defect TQFT over $\mathrm{vect}_{\mathbb{C}}$ evaluates a general bordism by producing a vect_c-coloured ribbon graph, which is then evaluated via $\mathbb{F}$ as per Appendix A. Since a general bordism may contain 0-strata in the bulk, we need to make use of the previous subsection to understand how exactly producing this ribbon graph proceeds. This is the purpose of this subsection, and largely manifests itself as a summary of the preceding two subsections. Let M be a arbitrary bordism in $\mathbf{Bord}_3^{\mathrm{df}}(\mathbb{D})$.

As was seen in Appendix C.2.1, the first step is to triangulate every 2-stratum of M, assign a total ordering of vertices to determine an orientation for each edge of this triangulation and then consider the Poincaré dual of this triangulation, where the edges of the dual acquire orientations in a systematic way from the orientations of the triangulation (same as earlier). Importantly, the edges of the Poincaré dual meet the 1-strata that bound the 2-strata away from any 0-strata. If the 2-stratum of M being triangulated contains 0-strata in its interior, then the Poincaré dual must be such that for each 0-stratum, there is an edge with this 0-stratum residing in its interior.

The next step is to turn the Poincaré dual of the 2-strata and the 1-strata of M into ribbons same as in Appendix C.2.1, except now there is an extra coupon for each 0-stratum in the interior of the 2-strata which is labelled by an appropriate morphism $\mathrm{Hom}_{\mathrm{vect}_{\mathbb{C}}}(A, A)$ where A is the label of the 2-stratum of M (and hence the label of the ribbons arising from the Poincaré dual).

Appendix D

Supplementary Material for Section 5.2.2

The proof of Proposition 5.2.2 in Section 5.2.2 requires keeping track of the 2-strata of a dual of a triangulation τ, their orientations, and the 1-strata to which they are incident. Figure D.1, which is spread over multiple pages, catalogues these 2-strata and the required information for each stratum. This figure is meant to be consulted alongside Figure 5.14 since the 2-strata as shown here have the same diagrammatic orientation as in that figure. The 2-strata were catalogued from those with the greatest number of edges visible in Figure 5.14 to least, and starting with those incident to 1-strata corresponding to u_1, following by those incident to u_2 and so on. The 2-strata shown below are not scaled consistently, but rather relative sizes are adjusted to better fit the diagram.

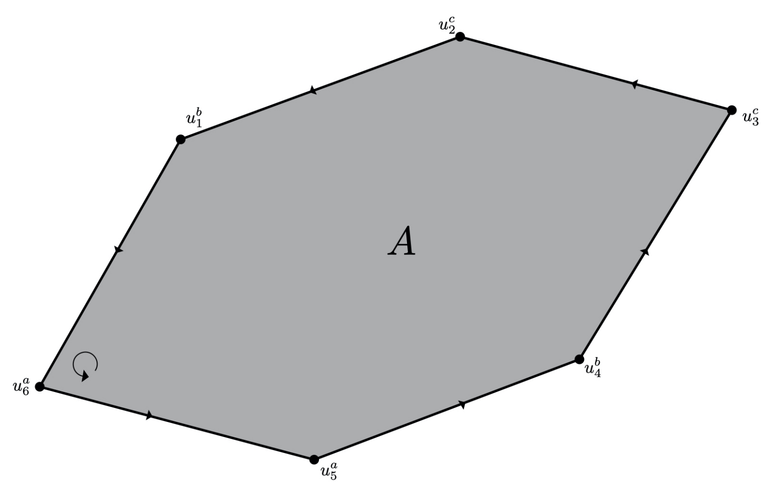

Figure D.1: A catalogue of all the 2-strata of the dual stratification related to the plquette 5 (see ??). Catalogue continues below.

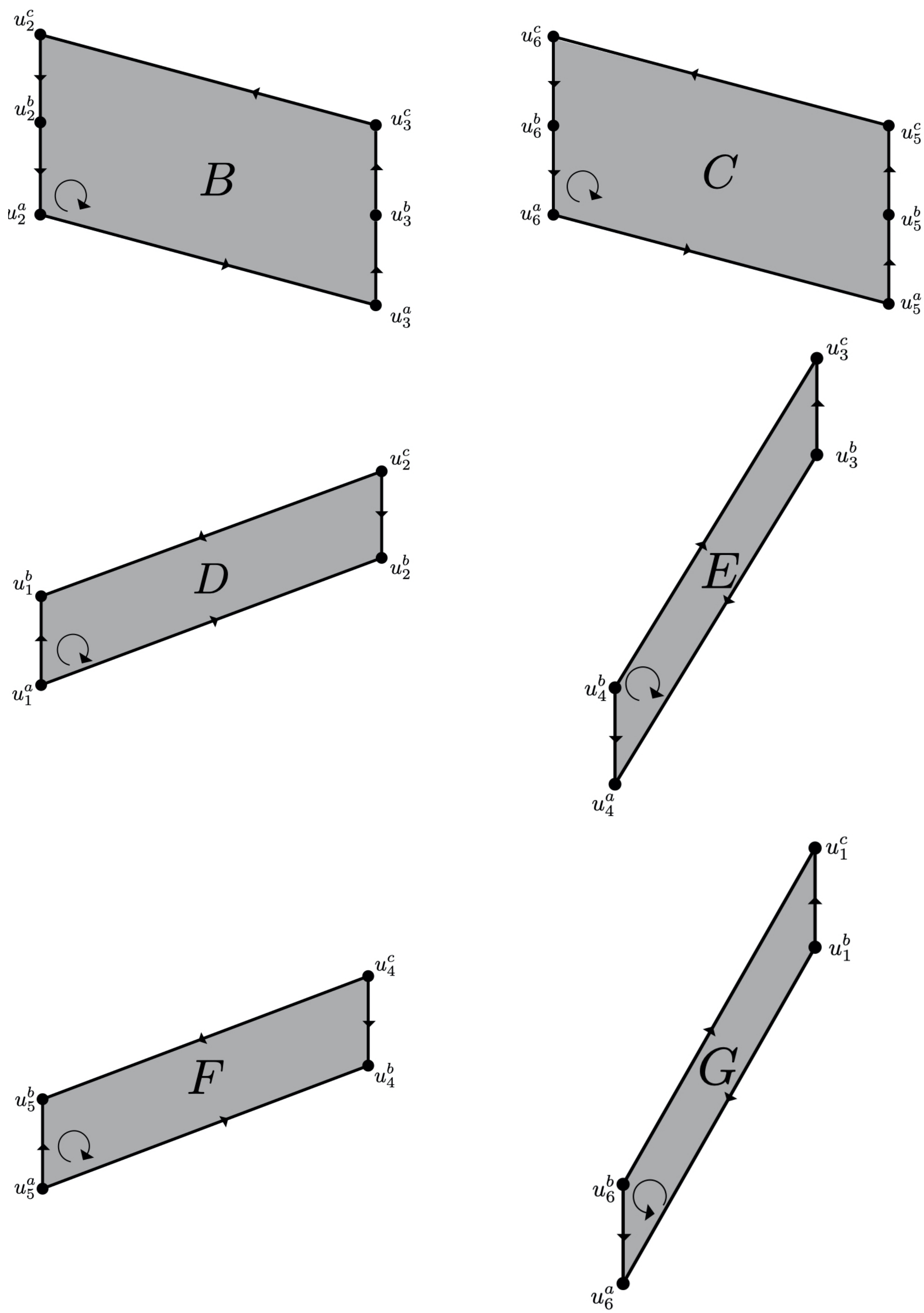

Figure D.1: The catalogue continued.

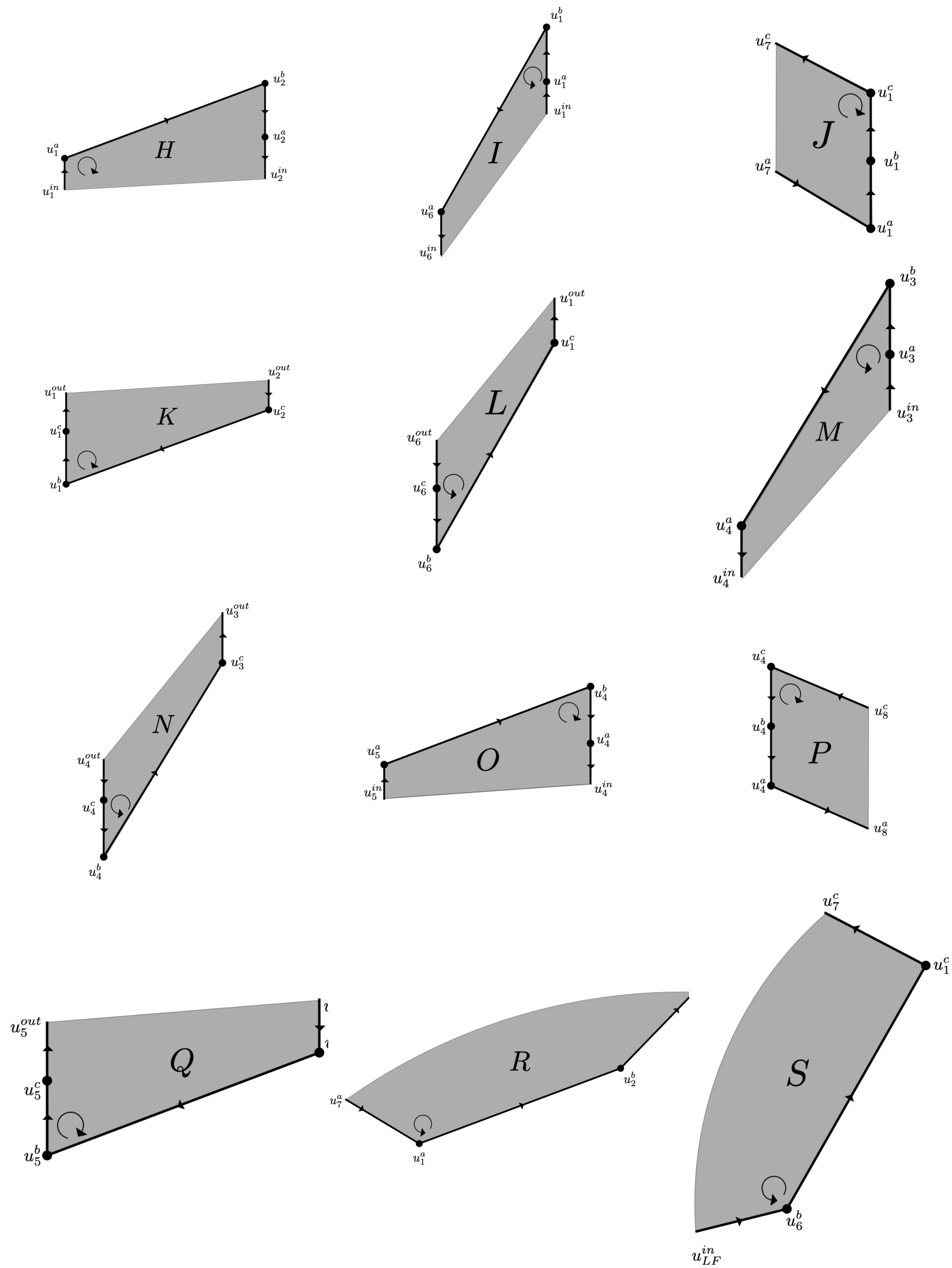

Figure D.1: The catalogue continued.

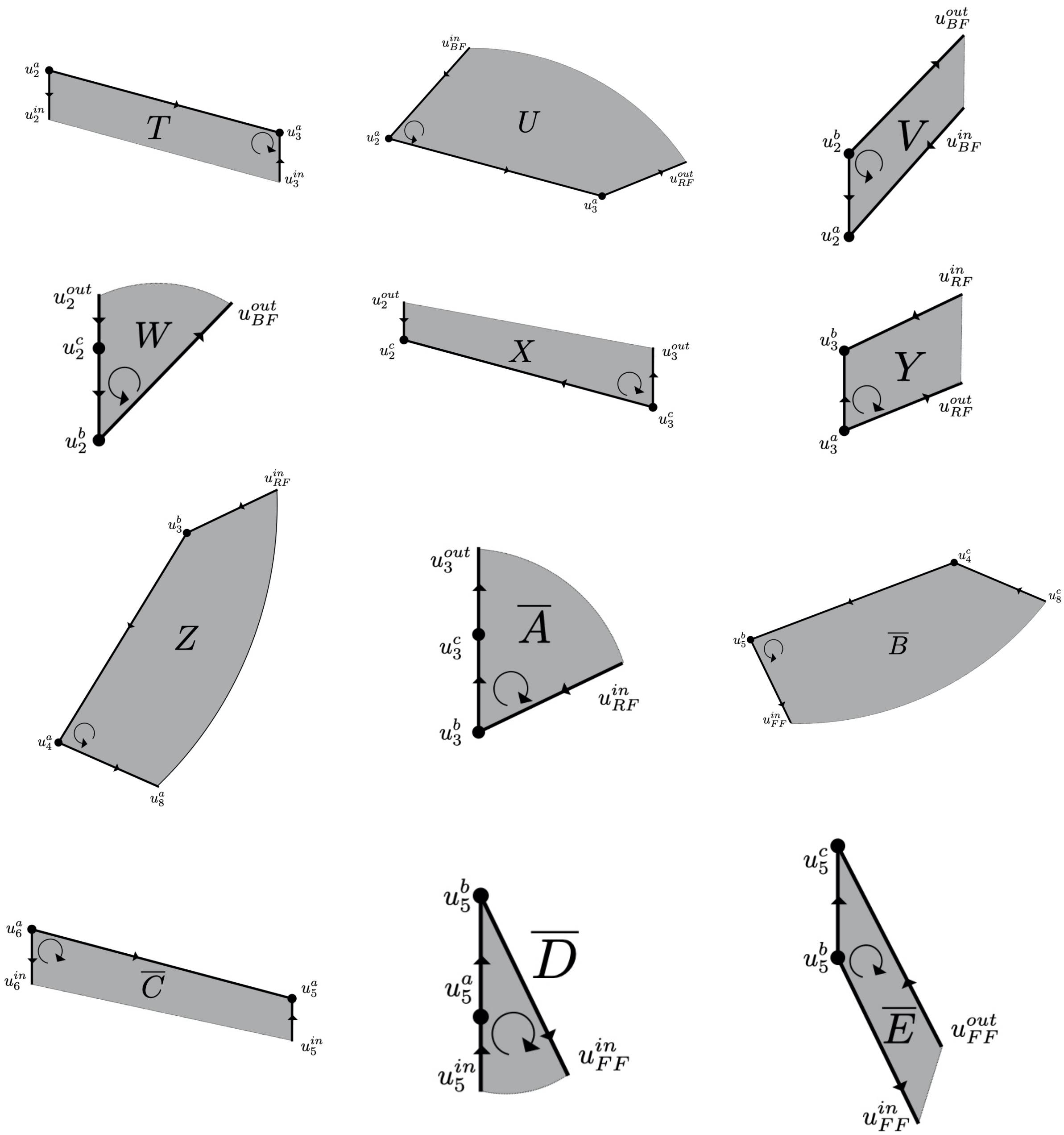

Figure D.1: The catalogue continued.

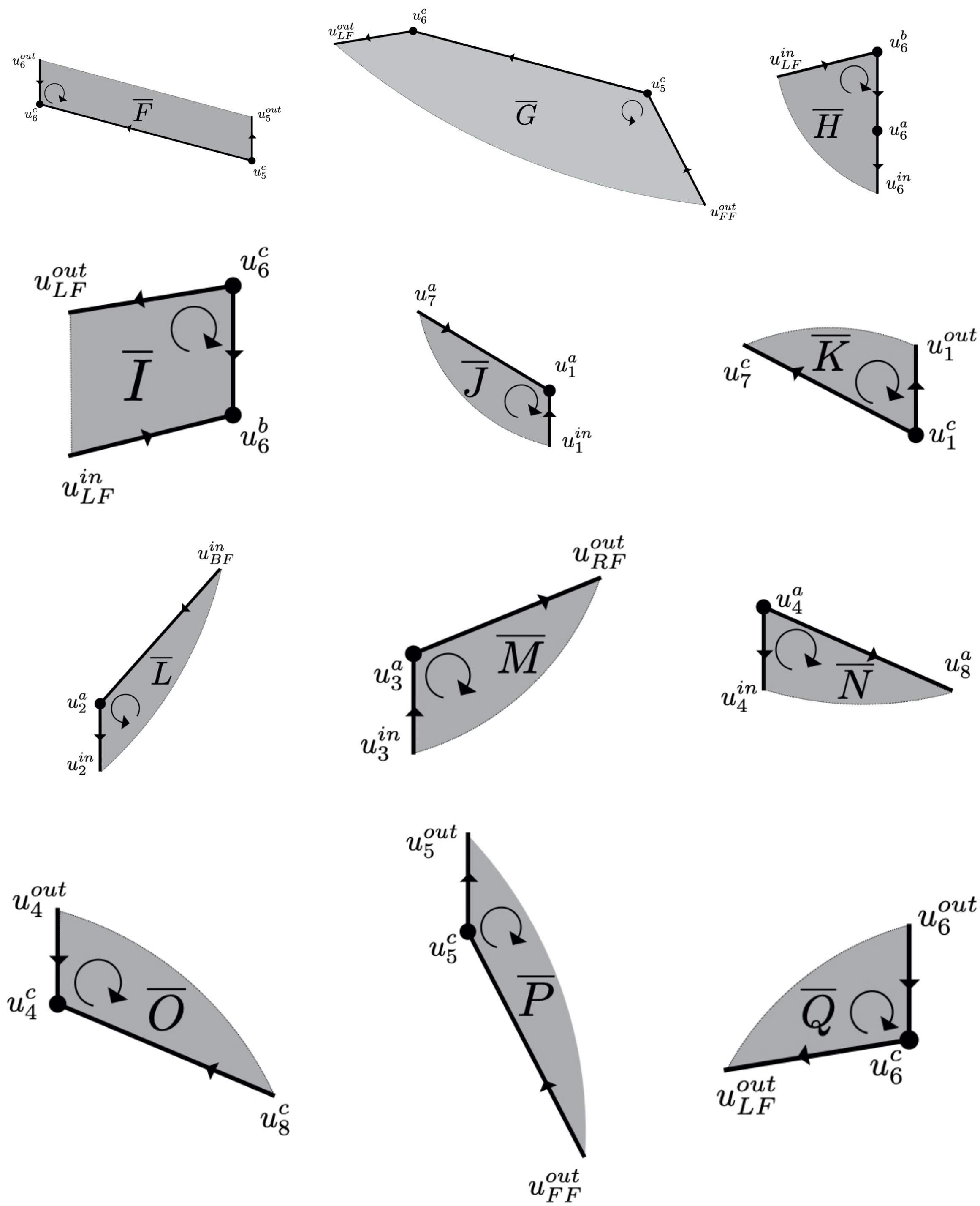

Figure D.1: The catalogue concluded.

Bibliography

[AB08] Dorit Aharonov and Michael Ben-Or. “Fault-tolerant quantum computation with constant error rate”. In: *SIAM Journal on Computing* (2008).

[BB19] Jacob C Bridgeman and Daniel Barter. “Computing data for Levin-Wen with defects”. In: *arXiv preprint arXiv:1907.06692* (2019).

[BK12] Benjamin Balsam and Alexander Kirillov Jr. “Kitaev’s lattice model and Turaev-Viro TQFTs”. In: *arXiv preprint arXiv:1206.2308* (2012).

[Bor94] Francis Borceux. *Handbook of categorical algebra: volume 1, Basic category theory*. Vol. 1. Cambridge University Press, 1994.

[BW96] John Barrett and Bruce Westbury. “Invariants of piecewise-linear 3-manifolds”. In: *Transactions of the American Mathematical Society* 348.10 (1996), pp. 3997–4022.

[CMS16] Nils Carqueville, Catherine Meusburger, and Gregor Schaumann. “3-dimensional defect TQFTs and their tricategories”. In: *arXiv preprint arXiv:1603.01171* (2016).

[CR12] Nils Carqueville and Ingo Runkel. “Orbifold completion of defect bicategories”. In: *arXiv preprint arXiv:1210.6363* (2012).

[CRS17] Nils Carqueville, Ingo Runkel, and Gregor Schaumann. “Line and surface defects in Reshetikhin-Turaev TQFT”. In: *arXiv preprint arXiv:1710.10214* (2017).

[CRS18] Nils Carqueville, Ingo Runkel, and Gregor Schaumann. “Orbifolds of Reshetikhin-Turaev TQFTs”. In: *arXiv preprint arXiv:1809.01483* (2018).

[CRS19] Nils Carqueville, Ingo Runkel, and Gregor Schaumann. “Orbifolds of n–dimensional defect TQFTs”. In: *Geometry & Topology* 23.2 (2019), pp. 781–864.

[CS96] A Robert Calderbank and Peter W Shor. “Good quantum error-correcting codes exist”. In: *Physical Review A* 54.2 (1996), p. 1098.

[ENO05] Pavel Etingof, Dmitri Nikshych, and Viktor Ostrik. “On fusion categories”. In: *Annals of Mathematics* (2005), pp. 581–642.

[Fey99] Richard P Feynman. “Simulating physics with computers”. In: *Int. J. Theor. Phys* 21.6/7 (1999).

[FKW02] Michael H Freedman, Alexei Kitaev, and Zhenghan Wang. "Simulation of topological field theories by quantum computers". In: *Communications in Mathematical Physics* 227.3 (2002), pp. 587–603.

[FLW02] Michael H Freedman, Michael Larsen, and Zhenghan Wang. "A Modular Functor Which is Universal for Quantum Computation". In: *Communications in Mathematical Physics* 227.3 (2002), pp. 605–622.

[FSG09] Austin G Fowler, Ashley M Stephens, and Peter Groszkowski. "High-threshold universal quantum computation on the surface code". In: *Physical Review A* 80.5 (2009), p. 052312.

[Got97] Daniel Gottesman. "Stabilizer codes and quantum error correction". In: *arXiv preprint quant-ph/9705052* (1997).

[JS91] André Joyal and Ross Street. "The geometry of tensor calculus, I". In: *Advances in mathematics* 88.1 (1991), pp. 55–112.

[Kit03] A Yu Kitaev. "Fault-tolerant quantum computation by anyons". In: *Annals of Physics* 303.1 (2003), pp. 2–30.

[KKR10] Robert Koenig, Greg Kuperberg, and Ben W Reichardt. "Quantum computation with Turaev–Viro codes". In: *Annals of Physics* 325.12 (2010), pp. 2707–2749.

[Lic62] WB Raymond Lickorish. "A representation of orientable combinatorial 3-manifolds". In: *Annals of Mathematics* (1962), pp. 531–540.

[Llo96] Seth Lloyd. "Universal quantum simulators". In: *Science* (1996), pp. 1073–1078.

[LW05] Michael A Levin and Xiao-Gang Wen. "String-net condensation: A physical mechanism for topological phases". In: *Physical Review B* 71.4 (2005), p. 045110.

[Mac] S MacLane. *Categories for the Working Mathematician. 1972.*

[Müg03] Michael Müger. "From subfactors to categories and topology II: The quantum double of tensor categories and subfactors". In: *Journal of Pure and Applied Algebra* 180.1-2 (2003), pp. 159–219.

[NC02] Michael A Nielsen and Isaac Chuang. *Quantum computation and quantum information.* 2002.

[NM+19] Engineering National Academies of Sciences, Medicine, et al. *Quantum computing: progress and prospects.* National Academies Press, 2019.

[RW18] Eric Rowell and Zhenghan Wang. "Mathematics of topological quantum computing". In: *Bulletin of the American Mathematical Society* 55.2 (2018), pp. 183–238.

[Sat57] Ichirô Satake. "The Gauss-Bonnet theorem for V-manifolds". In: *Journal of the Mathematical Society of Japan* 9.4 (1957), pp. 464–492.

[Ste96] Andrew Steane. "Multiple-particle interference and quantum error correction". In: *Proceedings of the Royal Society of London. Series A: Mathematical, Physical and Engineering Sciences* 452.1954 (1996), pp. 2551–2577.

[Thu79] William P Thurston. *The geometry and topology of three-manifolds.* Princeton University Princeton, NJ, 1979.

[Tur16] Vladimir G Turaev. *Quantum invariants of knots and 3-manifolds*. Vol. 18. Walter de Gruyter GmbH & Co KG, 2016.

[TV17] Vladimir G Turaev and Alexis Virelizier. *Monoidal categories and topological field theory*. Vol. 322. Springer, 2017.

[TV92] Vladimir G Turaev and Oleg Ya Viro. "State sum invariants of 3-manifolds and quantum 6j-symbols". In: *Topology* 31.4 (1992), pp. 865–902.

[Wal60] Andrew H Wallace. "Modifications and cobounding manifolds". In: *Canadian Journal of Mathematics* 12 (1960), pp. 503–528.

[Wit89] Edward Witten. "Quantum field theory and the Jones polynomial". In: *Communications in Mathematical Physics* 121.3 (1989), pp. 351–399.